CRANFIELD INSTITUTE OF TECHNOLOGY

DEPARTMENT OF MATERIALS

Ph.D THESIS

PEDRO EDUARDO LEAL BARBOSA RODRIGUES

# The Relationship between the Welding Conditions Thermal Cycles, Microstructure and Toughness of Weld Metal in C.-Mn Steels.

Supervisor J.H. Rogerson.

February, 1978.

ABSTRACT

Submerged arc weld deposits were produced using a 40 mm thick low Sulphur, low Phosphorous, Carbon Manganese microalloyed steel to B.S. 4360 : 50D. The welding consumables used were a 4 mm diameter C. 1½% Mn Wire (SD3) in conjunction with the OP 41 TT 'fully basic' flux.

Two series of three welds were made at three different calculated heat inputs of 5.8 KJ/mm, 3.9 KJ/mm and 2.9 KJ/mm. For the first series the welding current was kept constant at 650 amp and the welding speed was varied from 200 mm/min to 400 mm/min. For the second series the welding speed was kept constant at 300 mm/min, but the welding current varied from 850 amp to 480 amp.

For both the sub-surface and root regions of each weld the relationship between weld metal post solidification cooling cycle, transformation temperature, weld metal microstructure and toughness was examined and it was shown primarily that there is not a simple relationship between heat input as conventionally measured and the weld metal cooling cycle.

The weld metal cooling cycle was found to be dependent upon various factors such as :

1. The actual heat input, measured in terms of weld metal bead volume.

2. Weld bead shape measured in terms of width to depth ratio.

3. Flux consumption measured in weight of the slag removed per unit volume of weld bead.

4. The relationship between the size of the weld bead and the geometry of the immediately surrounding plate.

5. The post solidification thermal effects imposed by the subsequent weld runs.

From the thermal analysis measurements made whilst welding was in progress, two transformation reactions were identified. A high temperature transformation occuring at approximately 850°C identified by subsequent metallographic examinations as the pro-eutectoid ferrite transformation, and a low temperature transformation occuring at approximately 650°C identified as the acicular ferrite phase transformation.

The thermal analysis results also showed that the weld metal cooling rate had an effect on the weld metal transformation temperatures. For each transformation an increase in the weld cooling rate lead to a depression of the transformation temperature.

The present results indicate that the most desirable welding condition from a toughness point of view, should give a weld metal cooling cycle which was "slow" for the 1400°C - 900°C temperature

range, but "fast" below the temperature of 900°C. This would lead to a microstructure formed of large columnar grains, but with a high acicular ferrite volume fraction.

All welds showed a through thickness toughness variation. These differences in the through thickness properties were mainly attributed to the large differences in the thermal history between the sub-surface and the root beads which in turn lead to different microstructures, the sub-surface beads were formed by a larger columnar grain and a higher volume fraction of acicular ferrite than the root beads. The root beads Charpy V specimens also contained some refined equiaxed ferrite grains while the sub-surface Charpy V specimens contained solely as deposited weld metal. These differences in the microstructure features between the sub-surface and the root beads in turn appear to be, for the present welds, the main cause for the differences in the through thickness properties.

The overall conclusion from the present work is therefore that the weld metal deposits made at the same calculated heat input do not necessarily show the same toughness properties. This results from the fact that the cooling cycle, transformation temperature and amount of weld metal reheated by the subsequent runs are determined by the precise welding conditions.

CONTENTS

TABLES

FIGURES

20. Continuous cooling curve and subsequent thermocycles for the seventh sub-surface bead of the weld deposit made at 650 amp - 200 mm/min.

21. Continuous cooling curve and subsequent thermocycles for the nineth sub-surface bead of the weld deposit made at 650 amp - 300 mm/min.

22. Continuous cooling curve and subsequent thermocycles for the first root bead of the weld deposit made at 650 amp - 400 mm/min.

23. Continuous cooling curve and subsequent thermocycles for the second root bead of the weld deposit made at 650 amp - 400 mm/min.

24. Continuous cooling curve and subsequent thermocycles for the third root bead of the weld deposit made at 650 amp. - 400 mm/min.

25. Continuous cooling curve and subsequent thermocycles for the eleventh sub-surface bead of the weld deposit made at 650 amp - 400 mm/min.

26. Continuous cooling curve and subsequent thermocycles for the fourteenth sub-surface bead of the weld deposit made at 650 amp - 400 mm/min.

27. Continuous cooling curve and subsequent thermocycles for the first root bead of the weld deposit made at 850 amp - 300 mm/min.

28. Continuous cooling curve and subsequent thermocycles for the second bead of the weld deposit made at 850 amp - 300 mm/min.

29. Continuous cooling curve and subsequent thermocycles for the third bead of the weld deposit made at 850 amp. - 300 mm/min.

30. Continuous cooling curve and subsequent thermocycles for the sixth sub-surface bead of the weld deposit made at 850 amp - 300 mm/min.

31. Continuous cooling curve and subsequent thermocycles for the eighth sub-surface bead of the weld deposit made at 850 amp - 300 mm/min.

32. Continuous cooling curve and subsequent thermocycles for the first root bead of the weld deposit made at 480 amp. - 300 mm/min.

33. Continuous cooling curve and subsequent thermocycles for the second root bead of the weld deposit made at 480 amp. - 300 mm/min.

34. Continuous cooling curve and subsequent thermocycles for the third root bead of the weld deposit made at 480 amp. - 300 mm/min.

35. Continuous cooling curve and subsequent thermocycles for the eleventh sub-surface bead of the weld deposit made at 480 amp. - 300 mm/min.

36. Continuous cooling curve and subsequent thermocycles for the fourteenth sub-surface bead of the weld deposit made at 480 amp. - 300 mm/min.

37. Continuous cooling curves for the first, second, third and sub-surface beads for the weld deposit made at 650 amp - 200 mm/min.

38. Continuous cooling curve for the first, second, third and sub-surface beads of the weld deposit made at 650 amp - 300 mm/min.

39. Continuous cooling curve for the first, second, third and sub-surface beads of the weld deposit made at 650 amp - 400 mm/min.

40. Continuous cooling curve for the first, second, third and sub-surface beads of the weld deposit made at 850 amp. - 300 mm/min.

41. Continuous cooling curve for the first, second, third and sub-surface beads of the weld deposit made at 480 amp. - 300 mm/min.

42. Continuous cooling curve for the sub-surface beads of the weld deposits made at 650 amp - 200 mm/min and 850 amp - 300 mm/min. (5.8 KJ/mm).

43. Continuous cooling curve for the first root beads of the weld deposits made at 650 amp - 200 mm/min and 850 amp - 300 mm/min. (5.8 KJ/mm).

44. Continuous cooling curve for the sub-surface beads of the weld deposits made at 650 amp - 400 mm/min and 480 amp - 300 mm/min. (2.9 KJ/mm).

45. Continuous cooling curve for the first root bead of the weld deposits made at 650 amp - 400 mm/min and 480 amp - 300 mm/min. (2.9 KJ/mm).

46. Typical thermal analysis result for the 650 amp - 200 mm/min. weld.

47. Typical thermal analysis trace for the 650 amp - 400 mm/min weld.

48. Weld 650 amp - 200 mm/min. Sub-Surface $\delta$ Ferrite Structure x 50.

49. Weld 650 amp - 200 mm/min. Sub-Surface Columnar Structure x 50.

50. Weld 650 amp - 200 mm/min. Sub-Surface as deposited structure x 200.

51. Weld 650 amp - 200 mm/min. Sub-Surface as deposited structure x 500.

52. Weld 650 amp - 200 mm/min. Sub-Surface Charpy V fracture path x 200

53. Weld 650 amp - 200 mm/min. Sub-Surface M.A. Microphases x 2000.

54. Weld 650 amp - 200 mm/min. Root δ Ferrite Structure x 50.

55. Weld 650 amp - 200 mm/min. Root Columnar Structure x 50.

56. Weld 650 amp - 200 mm/min. Root as deposited structure x 200.

57. Weld 650 amp - 200 mm/min. Root as deposited structure x 500.

58. Weld 650 amp - 200 mm/min. Root Charpy V fracture path x 200.

59. Weld 650 amp - 200 mm/min. Root M.A. Microphases x 2000.

60. Weld 650 amp - 300 mm/min. Sub-Surface δ ferrite Structure x 50.

61. Weld 650 amp - 300 mm/min. Sub-Surface Columnar Structure x 50.

62. Weld 650 amp - 300 mm/min. Sub-Surface as deposited structure x 200.

63. Weld 650 amp - 300 mm/min. Sub-Surface as deposited structure x 500.

64. Weld 650 amp - 300 mm/min. Sub-Surface Charpy V fracture path x 200.

65. Weld 650 amp - 300 mm/min. Sub-Surface M.A. Microphases x 2000.

66. Weld 650 amp - 300 mm/min. Root δ Ferrite Structure x 50.

67. Weld 650 amp - 300 mm/min. Root Columnar Structure x 50.

68. Weld 650 amp - 300 mm/min. Root as deposited structure x 200.

69. Weld 650 amp - 300 mm/min. Root as deposited structure x 500.

70. Weld 650 amp - 300 mm/min. Root Charpy V fracture path x 200.

71. Weld 650 amp - 300 mm/min. Root M.A. Microphases x 2000.

72. Weld 650 amp - 400 mm/min. Sub-Surface δ Ferrite Structure x 50.

73. Weld 650 amp - 400 mm/min. Sub-Surface Columnar Structure x 50.

74. Weld 650 amp - 400 mm/min. Sub-Surface as deposited structure x 200.

75. Weld 650 amp - 400 mm/min. Sub-Surface as deposited structure x 500.

76. Weld 650 amp - 400 mm/min. Sub-Surface Charpy V fracture path x 200.

77. Weld 650 amp - 400 mm/min. Sub-Surface M.A. Microphases x 2000.

78. Weld 650 amp - 400 mm/min. Root δ Ferrite Structure x 50.

79. Weld 650 amp - 400 mm/min. Root Columnar Structure x 50.

80. Weld 650 amp - 400 mm/min. Root as deposited structure x 200.

81. Weld 650 amp - 400 mm/min. Root as deposited structure x 500.

82. Weld 650 amp - 400 mm/min. Root Charpy V fracture path x 200.

83. Weld 650 amp - 400 mm/min. Root M.A. Microphases x 2000.

84. Weld 850 amp - 300 mm/min. Sub-Surface δ Ferrite Structure x 50.

85. Weld 850 amp - 300 mm/min. Sub-Surface Columnar Structure x 50.

86. Weld 850 amp - 300 mm/min. Sub-Surface as deposited structure x 200.

87. Weld 850 amp - 300 mm/min. Sub-Surface as deposited structure x 500.

88. Weld 850 amp - 300 mm/min. Sub-Surface Charpy V fracture path x 200.

89. Weld 850 amp - 300 mm/min. Sub-Surface M.A. Microphases x 2000.

90. Weld 850 amp - 300 mm/min. Root δ Ferrite Structure x 50.

91. Weld 850 amp - 300 mm/min. Root Columnar Structure x 50.

92. Weld 850 amp - 300 mm/min. Root as deposited structure x 200.

93. Weld 850 amp - 300 mm/min. Root as deposited structure x 500.

94. Weld 850 amp - 300 mm/min. Root Charpy V fracture path x 200.

95. Weld 850 amp - 300 mm/min. Root M.A. Microphases x 2000.

96. Weld 480 amp - 300 mm/min. Sub-Surface Ferrite Structure x 50.

97. Weld 480 amp - 300 mm/min. Sub-Surface Columnar Structure x 50.

98. Weld 480 amp - 300 mm/min. Sub-Surface as deposited structure x 200.

99. Weld 480 amp - 300 mm/min. Sub-Surface as deposited structure x 500.

100. Weld 480 amp - 300 mm/min. Sub-Surface Charpy V fracture path x 200.

101. Weld 480 amp - 300 mm/min. Sub-Surface M.A. Microphases x 2000.

102. Weld 480 amp - 300 mm/min. Root δ Ferrite Structure x 50.

103. Weld 480 amp - 300 mm/min. Root Columnar Structure x 50.

104. Weld 480 amp - 300 mm/min. Root as deposited structure x 200.

105. Weld 480 amp - 300 mm/min. Root as deposited structure x 500.

106. Weld 480 amp - 300 mm/min. Root charpy V fracture path x 200.

107. Weld 480 amp - 300 mm/min. Root M.A. Microphases x 2000.

108. Weld metal impact properties for the sub-surface regions of the 650 amp - 200 mm/min, 300 mm/min and 400 mm/min welds.

109. Weld Metal impact properties for the root regions of the 650 amp - 200 mm/min, 300 mm/min and 400 mm/min welds.

110. Weld metal impact properties for the sub-surface regions of the 850 amp, 650 amp and 480 amp - 300 mm/min welds.

111. Weld metal impact properties for the root regions of the 850 amp, 650 amp, 480 amp - 300 mm/min welds.

112. Weld metal impact properties for the sub-surface and root regions of the 650 amp - 200 mm/min weld.

113. Weld metal impact properties for the sub-surface and root regions of the 650 amp - 300 mm/min weld.

114. Weld metal impact properties for the sub-surface and root regions of the 650 amp - 400 mm/min weld.

115. Weld metal impact properties for the sub-surface and root regions of the 850 amp - 300 mm/min weld.

116. Weld metal impact properties for the sub-surface and root regions of the 480 amp - 300 mm/min weld.

117. Weld metal impact properties for the sub-surface regions of the 650 amp - 200 mm/min and 850 amp - 300 mm/min welds. (5.8 KJ/mm).

118. Weld metal impact properties for the Root regions of the 650 amp - 200 mm/min and 850 amp - 300 mm/min welds. (5.8 KJ/mm).

119. Weld metal impact properties for the sub-surface regions of the 650 amp - 400 mm/min and 480 amp - 300 mm/min welds. (2.9 KJ/mm).

120. Weld metal impact properties for the root regions of the 650 amp - 400 mm/min and 480 amp - 300 mm/min welds. (2.9 KJ/mm).

121. C.C.T. diagram for HSLA Steel containing Nb (85). 0.10%C, 1.33% Mn, 0.33% Si, 0.04% Nb and C.C.T. diagram for the sub-surface welds, using an austenitising temperature of 1400°C.

122. C.C.T. diagram for HSLA Steel containing Nb (85). 0.10% C, 1.33% Mn, 0.33% Si, 0.04% Nb and C.C.T. diagram for the sub-surface welds, using an austenitising temperature of 1000°C.

## INTRODUCTION

The submerged arc welding process was independently developed in the U.S.A. and U.S.S.R. in 1935 (1). In this welding process the arc is formed between a continuously fed bare wire electrode and the work piece. The welding arc is completely submerged under a granulated flux which provides arc shielding and a protective slag. For most applications the welding current used varies between 250 amp. and 1000 amp. D.C. But welding currents of up to 2,000 amp. can be used however in this case A.C. is used to prevent arc blow (1).

The main attraction of this welding process is its high deposition rate, but since this is a fully automatic process it can only be used in the down-hand position or if the work piece is rotated so as to get the joint in the down-hand position.

In order to use submerged arc welding for the most critical structural applications it is necessary to ensure that this process can deposit weld metal capable of meeting the requirements stipulated by the relevant codes of practice, e.g.: BS 5500.

The necessity of meeting this requirement lead to an extensive development of welding consumables and operating procedures. Although the correlation between operating procedure and weld metal properties is now generally well established there are still some aspects of this relationship which require further investigation.

In order to clarify some of these aspects in micro alloy carbon manganese steels, the following work was carried out using a carbon manganese welding consumable in conjunction with a basic flux. The aims of this particular work are :-

1. The effect of weld metal heat imput on weld metal fracture toughness.

2. The difference in fracture toughness of the weld metals produced at the same calculated heat imput but at different welding condition.

3. The variation in toughness through the thickness of weld metals in thick sections.

## LITERATURE SURVEY

### Introduction

The fracture resistance of weld metals is determined by a large number of factors which are closely related and interdependant but for convenience these factors will be examined independently in the following order :-

Weld Metal Microstructure
Weld Metal Chemical Composition
Weld Metal Inclusions
Weld Metal Stress Field
Welding Procedure
Welding Flux composition
Welding Electrode Composition.

### Weld Metal Microstructure

As the weld pool cools down the solidification structure in carbon manganese microalloyed steels is formed by a series of $\delta$ ferrite columnar grains. This phase subsequently transforms into an autensite phase which in turn will again transform into a number of other metallurgical phases according with the weld metal chemical composition and cooling rate.

### Solidification Structure

In carbon manganese weld metal this structure consists of a series of $\delta$ ferrite columnar grains stretching inwards from the fusion boundary. These columnar grains generally develop with a common crystallographic direction along their axis and are separated by high-angle boundaries. In some cases the columnar grains meet at the weld centre line, but in other cases independently nucleated grains form at the weld centre (2). This structure is therefore the starting point and consequently may play a significant role in the subsequent transformation structures. For this reason the solidification mechanism will be examined. But since very little work has been done in the solidification structure of submerged arc welds, the solidification pattern will have to be deduced largely from other processes and materials.

Calvo et al (3) reported that the growth made in solidificating weld metals varied according to the degree of supercooling. The initial thermal gradient at the fusion boundary led to a cellular solidification mode. The decrease in thermal gradient towards the centre of the weld pool led to a transition from cellular to dendritic growth. In the centre of the weld pool dendrites can nucleate ahead of the solidification front.

Savage et al (4) found using H-Y 80 and gas tungsten arc welds as well as spot welds in Monel and auto body (mild steel plate) and Hostelloy 'N' that during solidification the nucleation event was insignificant and that epitaxial growth occured from the unmelted base metal. The growth mode being determined by the resulting fusion

zone structure.

In a subsequent work Savage et al (5) has shown that the orientation of the individual grains at the edge of the fusion zone in an arc weld are epitaxially related to that of the adjacent incompletely melted grains at the edge of the heat-affected zone, and that the process of competitive growth causes a tendency for preferred crystallographic orientation of the grains in the fusion zone. These authors noted that the shape of the weld puddle can profoundly influence the type of preferred orientation produced during solidification since competitive growth favours those grain with an easy growth direction aligned in the direction of maximum temperature gradient.

The solidification structure can therefore be controlled through the welding parameters as these will affect the thermal condition during solidification. One of the important aspects of controlling the solidification process would be to influence the subsequently transformed microstructures. This would be possible if as suggested by Garland (7) the austenite columnar grains revealed by a continuous band of ferrite related closely to the δ ferrite grain which have formed during solidification. However recent investigation (8) has shown that this is not necessarily so.

Widgery (8) noted that only a proportion of the continuous ferrite bands which are pro-eutectoid in origin in deposits which solidify as δ ferrite correspond to the original columnar solidification boundaries. The same author suggested that two processes operate in the transformation of the δ ferrite to austenite. (2)

Firstly the austenite grains already present in the parent material grow epitaxially into the weld metal as it cools. This growth will tend to produce austenite columnar grains because of the steep thermal gradient from edge to centre of the weld, and it is also possible for the austenite grains to grow across ferrite boundaries. Secondly, nucleation and growth of austenite can occur ahead of the grains growing from the weld edge and in this situation the nuclei form on the high angle δ ferrite boundaries. If a nucleus grows into only one adjacent grain the δ ferrite boundary is preserved as an austenite boundary but if the nucleus grows into both grains the δ ferrite boundary is lost.

Similar results to Wedgery (8) were also found by Bernard et al (9) using a carbon manganese steel and a submerged arc welding process. These authors noted that the δ ferrite columnar grains had a distinctly different orientation to that of the austenite grain structure and therefore concluded that the austenite grain orientation occured independently of the δ ferrite orientation, the austenite grain boundaries crossing the δ ferrite grain boundaries without apparent difficulty.

These authors suggested that the austenite grain structure is not dependent on the δ ferrite structure but on the thermal gradient which existed during the formation of this structure.

Therefore as shown by Widgery (8) and Bernard et al (9) it seems unlikely to be possible to control the subsequent austenite microstructure by means of the $\delta$ ferrite structure as these two structures do not necessarily have a close relationship. With the possible exception that the initial cooling rate which affects the $\delta$ ferrite solidification structure may also affect the microsegregation of alloying elements such as carbon, which in turn may lead to regions of retained austenite and martensitic phases as noted by Biss et al (27) in hot rolled bainitic steels.

Micro Segregation during Solidification

Micro segregation of the solute elements is caused by solubility differences in the solid and molten phases of one component in another in a given alloy system (10).

This segregation of impurity elements can lead to the formation of solid impurity films which may crack under the contracting stress due to solidification. (11)

Borland (12) found that the tendency for solidification cracking in welds depended on the quantity and distribution of liquid around grain boundaries during freezing though a critical solidification range. In this temperature range the crystal network is extensive and therefore the liquid mobility restricted to such an extent that if crack occurs, they can no longer "heal". This author suggested that if almost continuous films of liquid were present high stresses would build up and the narrow bridges between dendrites and micro-crack were likely to occur but with less continuous films higher stresses are required to cause cracking. This author also correlated the liquid distribution during cooling with of the interphase (solid - liquid) and grain boundary energies and noted that

$$\tau = \frac{\gamma_{LS}}{\gamma_{SS}} = \frac{1}{2 \cos \frac{\theta}{2}}$$

$\gamma_{LS}$ - liquid solid interfacial energy

$\gamma_{SS}$ - grain boundary energy

$\theta$ = dehedral angle.

Low values of $\tau$ (slightly above 0.5) are extremely harmful while high ratios (0.57) are beneficial since the liquid is restricted to train edge and corners.

These results were also confirmed by Rogerson et al (6) using Al-Su, and Al Cd and Al-In alloys. These authors noted that alloys which gave the lowest dehedral angles also showed the greatest severity to cracking in both welds and castings. Alloying additions which lead to an increase in the dehedral angle also lead to a reduction in cracking. These authors concluded that the shape of the intergranular liquid regions present during solidification of welds and castings is one of the metallurgical factors determining the tendency to hot cracking.

However for binary alloys where the dehedral angle $\theta$ is only likely to attain values just above $0^{o}$ this author has shown that the severity of the crack is mainly related to the extent of the freezing range and therefore for iron binary alloy elements which have a long either delta or gamma freezing range even when present in small amounts cause solidification cracking. This is the case for such elements as sulphur and boron which are consequently undesirable in weld metal deposits. For more complex alloys large chemical composition differences between the solid phase and the liquid can develop and therefore the dehedral angle will assume a more important role.

Segregation effects were also examined by Bernard et al (9) using a scanning microscope analysis in carbon-manganese steel submerged arc weld deposits. These authors noted that some weak segregation of manganese occured, and that the concentration of this element increased at the inter dendritic spaces. However a less significant variation was found for silicon. Similar analysis were also carried out for other elements which were present in the weld deposit but no significant effect of segregation was found. These authors concluded that neither macro or micro segregations occured to a significant level, this fact being attributed to the fast solidification rates of these welds.

Therefore presumably microsegregation does not have a significant effect on the weld metal deposits examined by the above authors, although martensitic and retained austenite phases have been reported ( 15, 19, 62 ) to be present in weld metal deposits, and the presence of these phases are associated (18) with microsegregation of alloying elements.

## Transformation Structures

### Pro-eutectoid Ferrite

As the austenite transforms, the first structure (9) to form is generally termed pro-eutectoid ferrite. This structure is soft and not inherently brittle and it has been suggested (2) that because this phase is often present in the form of thin veins surrounding areas of harder transformation products, strain concentrates in this phase and therefore cleavage cracks often initiate in this phase. This structure is therefore considered to lower the cleavage resistance.

Taylor (13) attributed the poor toughness of this phase partly to its coarse grain size (200 - 300 um).

Tuliani et al (14) comparing the weld metal toughness of three different submerged arc weld deposits of similar composition but made at different flux compositions which caused a variation in the weld metal cooling rate, found that weld metal with the highest transition temperature showed the largest amount of pro-eutectoid ferrite with relatively big almost polygonal grains. The transition temperature was lower in weld metal showing smaller pro-eutectoid ferrite veins.

These authors concluded that this structure had a negative effect on the notch toughness properties. This conclusion is generally accepted by most workers in this field. (2, 13, 14, 15).

Pearlite Structures

Pearlite structures are not generally produced in significant amounts in directly cooled weld metal, except in the case of high heat imput weld deposits. Tuliani et al (14) have reported the presence of lamellar cementite-ferrite structures which were observed using a T.E.M. in submerged arc weld deposits made at a heat imput value of 3.54 KJ/mm. The presence of this structure at the boundaries of the pro-eutectoid ferrite is considered detrimental to toughness (13) as this structure offers a low resistance path to propagating cracks. The size of the pearlite colony is also important since the colony boundaries can act as crack arresters and therefore large colonies are less desirable from a weld metal toughness point of view than small ones. (13)

Bainitic Structures

Bainitic structures can form in the interior of the austenite grains during cooling. A bainitic transformation involves a structure change followed by a redistribution of carbon which precipitates out in the form of carbides (16, 17). There are two types of bainitic structures. Upper and lower bainite. Upper bainite forms at lower cooling rates than lower bainite.

Upper Bainite

This phase has an acicular structure appearance, and in this phase the ferrite plates grow out into the austenite pushing the carbon atoms away from them until carbide particles are nucleated in the carbon rich regions between the ferrite plates (16, 17). The distinction between this structure and transformation product having a ferrite side plate morphology can be extremely difficult although different characteristic features exist between these two structures (2, 18).

Cochrane (18) noted that one characteristic feature of upper bainite is that it is always grain-boundary nucleated, and therefore where a similar structure is formed originating from an allotriomorph it is reasonable to assume that this structure developed from secondary side plates. A second characteristic of upper bainite is that in the classical upper bainite generally there are cementite plates between the laths. This is an indication of some degree of co-operation during growth. In the sideplate morphologies carbon rich regions are formed between ferrite lath due to carbon rejection into the remaining austenite. These regions may transform into a variety of structures ranging from pearlite to martensite.

A third characteristic is the dislocation density which is higher for the upper bainite than for the secondary side plates morphologies because upper bainite forms at a lower temperature.

Widgery (2) also noted that a transformation product which this author named "ferrite side plates" is often referred to as upper bainite. Though careful examination by the author showed that in mild steel weld metals this structure tended to show a plate rather than a lath type morphology.

Although there is clearly some difficulty in distinguishing between these two structures, it is generally accepted (2, 13, 14, 18) that the presence of these structures is undesirable, because brittle fractures are often found to originate in these areas (2).

Lower Bainite

Another form of bainite is termed lower bainite. This structure forms at a lower temperature than upper bainite, as well divided plates crystalographically orientated in relation to the austenite matrix speckled with fine carbide particles (17).

In lower bainite structures a moving crack has to intersect, propagate around or fracture a large number of dispersed carbides, and therefore tends to be arrested. When a moving crack is arrested some deformation and ductile tearing will occur prior to the initiation of a new cleavage crack, consequently the transition temperature in this range is extended (13).

Pickering (20) has shown that the impact properties of bainitic structures is related to their tensile strength. The transition temperature increased with tensile strength. A discontinuity in the impact transition temperature and tensile strength curve exists corresponding to a change of structure from upper to lower bainite. However lower bainite structures have not been generally reported to be present in weld metal structures.

Acicular Ferrite

The interior of the austenite grains in most weld metals used in structural steels is formed by a fine acicular structure, commonly known as acicular ferrite. (2)

Cochrane (18) notes that the mode of formation of this structure is not firmly established. This author suggested that these ferrite laths could be described as interpenetrating ferrite crystals growing from the same parent austenite and thus similar in crystallography to intergranular ferrite plates.

The same author (18) also notes that the diffusion of carbon is necessary to form these structures since identical structures can be formed from coarse grained austenites by rapid cooling ($1 - 10^{\circ}C/sec$) with a transformation temperature range of $640^{\circ}C - 540^{\circ}C$ consistent with the temperature range over which intergranular ferrite plates can form.

This is contradictory to what has been suggested by Farrar et al (25) who consider the acicular ferrite structure to be a low carbon martensite, and have termed this phase massive martensite.

The acicular ferrite structure is generally (2, 13, 14, 15, 19, 23, 25) considered to have good notch toughness properties and this fact has been partially attributed to (25), the small grain size of this structure in the order of 0.1 to 1 $\mu$m and to the high angle grain boundaries of this phase.

Microphases

During the formation of the ferrite structures described previously, with exception of the upper bainite phase, a certain degree of carbon segregation to the parent austenite occurs. (18) The way in which this carbon rich austenite region decomposes is a function of the prevailing cooling rate and therefore retained austenite and martensitic phases can be present as the weld metal cools down.

Due to the small size of these micro phases (approx. 2 $\mu$m) their identification was found to be quite difficult (18) and T.E.M. examinations are necessary, although using a light microscope and a picral etch Cochrane (18) suggested that the nature of these microphases may be revealed by three distinct colourations. Light brown colouration indicates a lath martensite structure; a yellow-brown colouration indicates twinned martensite and a grey-white colouration indicates retained austenite. However other authors, such as Biss et al (27) and Fick et al (62) did not discriminate between the retained austenite and the martensite phases, because of the difficulty involved in identifying these phases. The presence and nature of these microphases have been shown to affect the properties of low carbon steels (27) as well as weld metals (15, 19).

Wheatley et al (28) using M.M.A. process and different electrode size, and hence varying the weld metal cooling rate, noted the presence of retained austenite and the absence of carbides in rapidly cooled weld metals. These authors suggest that the presence of austenite appears to be potentially deleterious since it occurs as lamellae between the ferrite grains.

Blocky martensitic structures were noted in weld metal deposits by Garland et al (19). These authors concluded that coarse blocky lath martensite together with varying proportions of bainitic carbides had a deleterious influence upon the weld metal impact properties. Regions of high carbon twined martensite were also found, but these regions had a much less marked effect in lowering the cleavage crack resistance than the phases previously considered.

Effect of Grain Size on Weld Metal Properties

The effect of grain refinement in the reheated regions of multipass weld metals on the toughness and tensile properties has been reported by various authors (21, 25, 28, 31).

Tuliani et al (21) found a straight line relationship between the average grain diameter in the refined weld metal regions of submerged arc weld deposits and a 40 ft lb. transition temperature.

These refined regions had a beneficial effect on weld metal properties.

Farrar et al (25) studied the weld metal toughness properties of submerged arc weld deposits produced using the same plate and wire composition, but different fluxes which lead to different weld metal cooling rates. These authors concluded that the improvement in the weld metal toughness of the welds produced at higher cooling rates could be partially attributed to the smaller grain size of the reheated regions.

Fick et al (31) using a submerged arc welding process showed that refining the weld metal by subsequent weld runs substantially lowered the transition temperature. This improvement was ascribed to the formation of an "independent" relationship between ferrite grains in the refined condition. It seems therefore that the grain size of the refined regions of weld metal deposits have an important role to play on the overall weldments properties.

## Weld Metal Chemical Composition

The chemical composition of most of the material used in welding low-carbon structural steels is composed of less than 0.2% carbon, and varying quantities of other alloying elements, such as manganese, nickel, chromium etc. These alloying additions are made in order to obtain the desirable mechanical properties, low cost being the general criteria in choosing between alloying elements which give similar weld metal properties.

## Effect of Carbon

Tensile strength, and notch toughness are considerably affected by small variations in carbon levels. Carbon can be present in the ferritic matrix in the form of an interstitial solid solution thus distorting the lattice and therefore increasing the tensile strength. Carbon can also be present in the form of precipitates forming iron carbides $Fe_3C$ or combined with other elements such as Mo, Cr, V if they are present. (26, 27)

The carbon content in steel plates was found (26) to effect the upper and lower shelf energy as well as the shape of the transition curve and using a Charpy V notch specimen a 15 ft lb transition temperature was raised by about 14°C for each increase of 0.1% of carbon.

Garland et al (19) found that lowering the carbon content level had a beneficial effect on the as-welded properties. This was attributed to the fact that during cooling twinned martensite was formed at the expense of lath martensite and bainitic carbides which have a lower notch toughness.

Cochrane (66) also noted that at a given cooling rate for a low carbon manganese niobium steel increasing the carbon and silica levels produced a classical upper bainite structure instead of an acicular ferrite structure. This change in microstructure has detrimental effects on the toughness properties.

Carbon in the weld metal was also found to have an important deoxidant effect and a minimum weld metal carbon content of 0.05% was necessary to obtain optimum low oxygen values. (33)

## Effect of Manganese

The principal role of manganese in weld metals is to provide sufficient hardness to achieve an adequately strong microstructure as well as to act as a deoxidant (24).

Colving et al (32) using a weld metal deposit with the same carbon composition of 0.075% to 0.089% and varying the manganese percentage from 1.13% to 2.12% found that the increase in manganese produced an increase in yield and ultimate tensile strength but a decrease in elongation. An increase from 1% to 1.5% in manganese also resulted in an improvement of Charpy V notch values for low temperatures.

Similar beneficial effects of manganese were noted by Farrar et al (25). These authors reported that a small increase of 0.2% in manganese content of the weld metal from 0.81% to 1.02% corresponded to a decrease of the transition temperature.

Results from Colvin et al (44) on single pass welds using a carbon manganese wire consumable (SD3) in conjunction with two different edge preparations giving 80% and 40% dilutions have shown that weld metal with higher manganese levels of 1.28% to 1.49% giving a manganese to silicon ratio of 4 to 1 had better impact properties than lower manganese welds of 1.01% to 0.64% giving a manganese to silicon ratio of 6 to 1 and 10 to 1 respectively.

The beneficial effects of manganese are generally attributed (37) to the fact that manganese is a promoter of fine acicular ferrite as well as producing a reduction in the proportion of pro-eutectoid ferrite.

Effect of Silicon

Silicon is added to weld metal to act as a deoxidant and is present in the electrode wire, or as a compound in the flux to effectively deoxidise the weld metal and prevent porosity (38).

Sakaki (46) found using a manual metal arc process that small quantities of silicon raise the upper shelf energy, and lower the transition temperature. However values of silicon in excess of approximately 0.4% tend to decrease the upper shelf energy values and increase the transition temperature.

Similar results were also found by Dorschu et al (45). These authors, reported that silicon in amounts between 0.35% and 0.8% caused a deterioration of the impact properties in manual metal arc deposits. Using a submerged arc welding process the authors again found that additions of silicon above 0.5% increased the transition temperature.

Tuliani et al (21) using submerged arc welding at a fixed heat imput found that a decrease in silicon, and therefore an increase in the manganese silicon ratio corresponded to a grain refinement of the reheated regions. A relationship was found to exist between the lower shelf energy values and the manganese silicon ratios. An increase in manganese silicon ratio from 3 to 5 corresponded to a lower shelf Charpy V energy increase from 5 ft lb to 25 ft lb.

Tuliani et al (38) used commercial submerged arc welding wires of different silicon content to study the effects of a progressive decrease in the metal silicon content. These authors found that a decrease in silicon from 0.4% to 0.09% also caused a decrease in the solid solution hardening and hardenability of the matrix and therefore affected both the tensile and impact properties. This decrease in silicon also lead to an increase in the amount of manganese used in the deoxidation reaction, as well as leading to an increase in the weld metal carbon content. These authors concluded that for structural applications the silicon levels of 0.18 to 0.20% should be recommended.

Effect of Niobium

The demand by the structural industry of high strength low alloy steels with good impact toughness and good weldability led to the use of niobium as an alloying element. This is because this element has good grain refining and hardenability properties, the latter promoting the formation of an accicular ferrite structure during cooling after roling, and as previously discussed this type of micro structure has high strength and good toughness properties (82).

The mechanism by which niobium promotes the formation of a fine grain structure has been discussed by Duckworth (29) and this author noted that in normalised steels niobium carbides and carbonitrides which disolve at 1050°C precipitate on cooling as a fine precipitate. On heating above 700°C these precipitates coarsen and when the steel is normalised at 900°C - 950°C a precipitate capable of pinning the austenite grain is formed therefore restricting grain growth.

For the as rolled condition niobium also acts as a grain refining element but through a slightly different way than in normalised steels. In this case niobium precipitates during rolling at the austenite sub-grain boundaries formed by recovery at each rolling pass. These sub-grains are therefore pinned and recrystalization by sub-grain growth is therefore restricted. Due to subsequent rolling passes these precipitates coarsen and help to limit grain boundary migration, therefore reducing the overall rate of recrystalization.

If sufficient niobium is left in solution then on cooling precipitation hardening occurs in the ferrite matrix which leads to an increase in strength. (39).

The precipitation of niobium carbides is closely dependent on the steels rolling procedures and therefore cooling rates as found by Malcolm Gray et al (39) when evaluating the response of a proposed arctic pipe line steel to changes in rolling schedule and cooling rates after rolling. These authors found that because of the supression of niobium carbides precipitation the hot rolled strength decreased with an increase in cooling rate from 79.5 ksi at 2°F/sec to 66 ksi at 45°F/sec.

Due to the dilution between the steel parent plate and the weld metal niobium can be introduced into the weld metal. In weld metals the different mechanisms through which niobium can affect the weld metal toughness have been noted by Garland et al (19) and are as follows :-

1. Niobium increases the hardenability of the weld metal and hence the proportion of acicular ferrite in the microstructure.

2. Niobium promotes the formation of lath martensite in association with coarse bainitic carbides in the transformed microstructure. Niobium also favours the potential segregation of these phases to both the transformation and solidification boundaries. These phases decrease toughness and lower the yield stress and ultimate stress ratios.

3. Niobium can also precipitate in the form of pre-precipitation clustering either during cooling of the acicular ferrite matrix after welding or during subsequent stress relief. This may or may not have a detrimental influence on toughness depending on the other microstructural changes accompanying this precipitation.

The relative importance of these three effects are influenced by the welding procedure, since niobium carbides precipitation is closely related to the steel cooling rate, as found by Malcolm Gray et al (39). The niobium precipitation effects may not be very significant in H.L.A. weld metals as suggested by Sawhill et al (47) because a significant amount of precipitation hardening can not occur due to the low transformation temperatures and fast weld metal cooling rates.

For submerged arc welds Colvin et al (44) have noted that niobium levels in the weld metal above 0.039% had a marked lowering effect on the toughness impact values while niobium values up to 0.02% did not seem to effect significantly the weld metal toughness properties. These authors therefore suggested that high levels of niobium in weld metals was undesirable.

Effect of Vanadium

In a similar way to Niobium, Vanadium is often added in small amounts to grain-refine C.Mn structural steels, to achieve a combination of high strength, and toughness. In steels containing roughly equal amounts of Niobium (0.04%) and Vanadium (0.04%) the Niobium is most effective in retarding the austenite grain growth, while Vanadium precipitates in the ferrite matrix and provides additional age hardening (48). Low levels of vanadium in weld metal deposits (less than 0.1%) were found to be beneficial (49). The negative effect of vanadium additions was attributed to nitride precipitation while the beneficial effect was not clearly explained.

In order to clarify the effects of vanadium on the weld metals properties a series of investigations were conducted by Kirkood et al (50). These authors reported that additions of vanadium to the weld bead promoted the formation of an acicular ferrite structure. This would lead to an improvement in the weld metal properties, however vanadium also increases the total number of retained martensitic microphase and also promotes the segregation of these microphases to the solidification and transformation boundaries. This effect would lower the weld metal toughness properties and therefore the overall net results of the vanadium additions will be the balance between these two effects.

On stress relief the retained martensitic phases degenerate into a ferrite carbide aggregate and the full potential of the original acicular ferrite microstructure can be achieved, providing that the detremental effect of precipitation hardening does not occur. Therefore for low vanadium welds (0.032%) the precipitation hardening due to vanadium carbon nitrides is not sufficiently large to offset the improvement in properties caused by the degeneration of the retained microphases and an overall size in properties occurs.

At higher vanadium values (0.12%) the precipitation hardening negative effect appears to be larger than the beneficial effects caused by the degeneration of the microphases and therefore the overall properties are similar to vanadium free welds with much less acicular ferrite present.

Again the same authors also looked at the combined effect of vanadium with niobium and found that individual additions of niobium (0.024%) and vanadium (0.05%) only had minor effects on the weld metal toughness, while the combination of the two elements lead to a marked improvement in the toughness properties.

As the overall microstructure was similar for all these welds, the difference in toughness behaviour of the niobium/vanadium welds was attributed to the fact that these welds contained less lath martensite, however no precise explanation of the niobium/vanadium inter-action was given.

Effect of Titanium.

Titanium is generally used as a deoxident in $CO_2$ welding wires, but is not commonly used in submerged arc weld consumables. Boniszewski et al (40) found that for $CO_2$ welding additions of 0.14% to 0.2% of titanium gave some improvement in the toughness properties but higher titanium values led to increased solid solution hardenability of the matrix with inevitable detrimental consequences on the toughness properties.

Again Boniszewki (41) has suggested that titanium has the effect of binding carbon, oxygen and nitrogen removing these elements from solid solution which in turn lead to an improvement in the weld metal properties.

Effect of Aluminium

Aluminium like titanium is also used as a deoxidant but generally only in $CO_2$ and self-shielded welding consumables.

In self-shielded electrodes aluminium is used to prevent the nitrogen introduced into the weld pool during welding from ovoluting during solidification. This ovolution of nitrogen can lead to weld metal porosity.

In this case aluminium is used as a nitride former and thus preventing the nitrogen bubble nucleation (51).

Aluminium was found to be, by Kaplan et al (51), the most desirable method of preventing porosity in a self-shielded welding process. These authors noted however that nitrogen as aluminium nitride was the main source of weld embrittlement, and high levels of aluminium in solid solution also degrades the weld metal toughness properties. Similar results have been found by Koteck et al (43) which have noted that self-shielded arc deposits showing aluminium in the chemical composition had lower impact properties than weld deposits without aluminium.

Masubuchi et al (42) noted that small aluminium additions of (0.05% to 0.1%) appear to improve the weld metal toughness properties, and these authors attributed the beneficial effects of aluminium to its deoxidizing effects.

Effects of Sulphur

Sulphur is present in weld metal as a residual element and if this element is allowed to segregate to grain boundaries, inter-granular brittleness can occur.

Colvin et al (44) correlated manganese to sulphur ratio with impact properties, and found that weld metal with ratios of 80 to 1, 60 to 1, and 30 to 1 respectively showed a decrease in impact properties corresponding to a decrease in manganese sulphur ratio.

The manganese, sulphur interaction in solid solution may lead to give precipitates on dislocations which can cause an increase of work-hardening rate and therefore increase the transition temperature. (21)

Effect of Phosphorus

Phosphorus, like sulphur, is also a residual element and has a strong effect in raising the transition temperature. The 15 ft lb Charpy V notch transition temperature is raised by $7^{o}C$ for each 0.01% of phosphorus (26). Phosphorus has also been reported (14) to form weld metal inclusions, and therefore low levels of phosphorus are desirable.

Effect of Nitrogen

Nitrogen in steels can be present in various forms. These have been summarized by Jenkins et al (53) as :-

1. Interstitial nitrogen which may be dispersed or collected around lattice defects.

2. Combined nitrogen present as nitrides which may consist of either simple or complex precipitated phases.

3. Occulded nitrogen present in the molecular gaseous state and contained in pores within the metal.

The interstitial nitrogen has an important role in the strain ageing mechanism, since removing nitrogen and carbon from steel eliminated both initial discontinuous yielding as well as strain ageing (52).

The combined nitrogen in the form of nitrides can act as precipitation hardening elements which are therefore detrimental to notch toughness properties (51).

Nitrogen in the molecular gaseous state can be present in weld metal as "pores" and consequently unacceptable. (51).

Jenkins et al (55) noted that in submerged arc welding the effects of nitrogen have not been given much attention, and attributed this to the fact of the relatively small nitrogen variation encountered. (0.007% to 0.012%).

Effect of Oxygen

Generally the oxygen content in weld metal is used as an indicator of the inclusion level. Taylor et al (13) analysing the results of various workers, concluded that high concentration of inclusions corresponding to oxygen contents above 600 ppm control the upper shelf energy values and have an effect on the ductile to brittle transition temperature but their influence on the lower shelf energy was not clear. For oxygen concentrations below 300 ppm the inclusion seems to have little effect on the toughness and the microstructural features dominate. In the 600 to 300 ppm the situation is more complex and the toughness may be influenced by both the microstructure and inclusion level.

However it is important to note that the correlation between oxygen analysis values obtained by vacuum fusion process may not always be accurate as found by Widgery (8). This author used an alternative analysing method of fast neutron activation analysis. Another important aspect is the possible role of oxygen in controlling the weld metal microstructure. Kirkwood (54) has suggested that the number of small inclusions created by high oxygen levels act as potential nucleation sites for upper transformation products during continuous cooling and therefore weld deposits with high oxygen levels ( 440 ppm) will tend to show upper bainite structure while lower oxygen levels will lead to an acicular ferrite structure.

Weld Metal Inclusions

Impurity elements may be trapped in the weld metal during solidification. In the elastic region the principle effect of these particles is to increase the stress of the local areas of stress concentration, and therefore alter the uniaxiality of the stress field (55).

The role of these second-phase particles is particularly significant in the ductile failure mode as void initiation may occur either by cracking of the second-phase particules or by decohesion of the inter phase between the particles and the matrix. Once the voids have initiated they may grow by plastic deformation until they impinge upon one another when void coalescence takes place and the metal fractures. (56)

Since the microvoid growth and coalescence depends strongly on the properties of the matrix surrounding the void, particularly the localized yield stress and strain hardening ability the fracture toughness values can be varied only by altering the matrix properties and maintaining a constant but low inclusion content (13). Therefore if the inclusion content is below a certain critical value (56) the number of inclusions are insufficient at a given matrix yield stress to influence the fracture process and voids must be nucleated at grain boundaries, carbides and dislocation pile-ups.

The fact that the matrix properties have an important role at low inclusion levels, is clearly shown in the following figure (13). In this figure the oxygen level is used as an indicator of inclusion level, and it can be observed that at low oxygen levels, and therefore low inclusion levels, a large variation in weld metal toughness can be obtained.

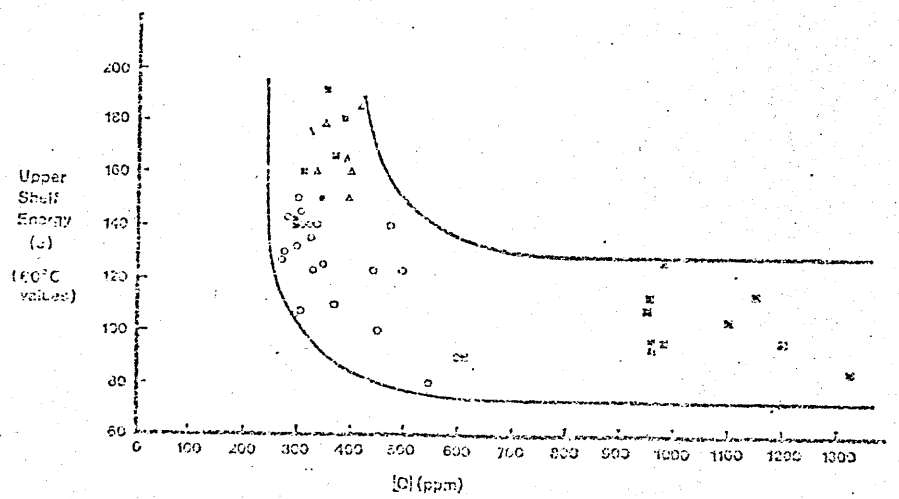


o Δ □ Represent results from different authors.

Relationship between Charpy Upper Shelf Energy and Oxygen contents of S.A. Weld Metals, (13).

The correlation between fracture toughness and inclusion level has been examined by various workers using the oxygen level as an indicator of the inclusion level.

Hanmerz et al (34) using a metal inert gas welding process found a straight line relationship between Charpy V notch values and oxygen levels in the weld metal. This author concluded that to an oxygen increase in the weld metal corresponded a lower fracture toughness value.

A similar conclusion was also reached by Tuliani et al (21) using a submerged arc welding process. These authors found that an increase in oxygen content corresponded to a decrease in the upper shelf energy. A correlation between reduction of area and oxygen levels was also reported. Sulphur generally in the form of $Mn_1S$, also contributed to the total number of inclusions present.

The effects of sulphur on the inclusion volume fracture Vv has been established by Widgery (64) in a "Rule of Thumb" formula produced by this author as shown below :=

$$Vv = 5.5 \text{ (Wt \% O + Wt \% S)}.$$

Weld Metal Stress Field

In weld metals strain ageing embrittlement is thought to occur as a result of welding thermal strain and subsequent ageing or by simultaneous straining and ageing known as dynamic strain ageing (57).

Strain ageing is a type of behaviour in which the strength of a metal is increased and the ductility decreased on heating at relatively low temperatures ($100^{o}C$ - $250^{o}C$) after cold work. (26) Other properties besides strength and ductility may also be affected by strain ageing such as the ductile to brittle transition temperature, high temperature strength, fatigue strength and electrical and magnetic properties (58).

Strain ageing is dependent on the metal chemical composition. Strain ageing can only occur if carbon and nitrogen atoms are present, since it is the atoms of these elements which migrate to dislocations locking them, and therefore causing discontinuous yielding and strain ageing. (58) Aluminium also affects the strain ageing behaviour of steels, as noted by Burdekin et al (59). These authors noted that in contrast with a carbon manganese steel, the aluminium treated steel showed only relatively little susceptibility to effects of strain ageing embrittlement. This behaviour was attributed to the fact that aluminium had combined with nitrogen therefore preventing the strain ageing effects of this element.

In multipass carbon manganese weld deposits strain ageing effects may play an important role in the relative variation in weld metal toughness between the root runs and the sub-surface.

Nicholson et al (37) using a carbon manganese steel weld deposit produced by a manual metal arc process found that the toughness of the root areas was lower than that of the sub-surface. These authors could not attribute the low toughness of the root areas to either variations in the microstructure or chemical composition and therefore suggested that strain ageing effects could be a possible explanation.

Cochrane et al (60) also examining the root-run toughness of multi-pass manual metal arc welds suggested, as Nicholson et al (37), that the low root-run toughness was caused by dynamic strain ageing produced by the thermo-mechanical effect of subsequent weld runs necessary to complete the weld joint.

Recent work on the problem of weld root areas of multi-pass manual metal arc welds was reported by Robinson (61) and this author again attributed the root run toughness drop mainly to strain ageing effects.

The effects of strain ageing on the root run toughness of carbon manganese microalloyed in submerged arc welds was examined by Fick et al (62). These authors found that although strain ageing may have played a part in the weld metal through thickness toughness variation it did not appear to be the sole mechanism and in some cases was not even a significant mechanism.

From the literature it seems therefore that dynamic strain ageing has an effect on the weld metal toughness properties although it is difficult to establish the magnitude of this effect.

Welding Procedure

The welding procedure has an effect on the weld metal toughness properties, because the welding arc conditions partly control the weld cooling cycle which in turn determines the type of transformation reaction taking place during the cooling of the solidified weld metal.

Both mathematical and empirical studies of the rapid thermal cycles associated with welding have been made by a number of workers (65, 66, 67, 68, 69, 70, 71) with the aim of estimating, from the welding conditions and plate thickness, the weld metal cooling cycle, and subsequently, predicting the weld metal properties.

Generally to use mathematical methods the values of a number of variables must be known, such as thermal conductility of the plate material and energy input to the plate, or in the case of empirical methods, values of plate dimensions and arc heat input must be entered into empirical graphs from which the value of constants which are used in subsequent calculations are obtained.

However, due to the relative complexity of these calculating methods, a simple heat input formula is most commonly used to correlate the parameters with weld properties. In this formula the arc heat input is measured in terms of arc energy as follows :-

$$E = \frac{V \times A \times 60}{1000 \times S}$$

E = Energy in KJ/mm

V = Welding voltage

A = Welding current

S = Welding speed in mm/min.

Bennett (72) used this formula to correlate weld metal heat input and the properties of a low carbon manganese submerged arc weld.

This author found that an initial increase in heat input from 2 KJ/mm to 3.6 KJ/mm lead to an improvement of the toughness properties of approximately 27 J at 0°C but a subsequent increase in heat input from 3.6 KJ/mm to 7.2 KJ/mm lead to a decrease in weld metal toughness of approximately 30 J at 0°C. In this work however, no attempt is made to correlate weld metal heat input and microstructural features.

Clark et al (73) also examined the effect of two different heat inputs on the weld metal toughness of low carbon manganese submerged arc welds. The low heat input weld was made at "ideal" conditions with a maximum heat input of 3.8 KJ/mm and a low interpass temperature of 100°C while the high heat input weld was made at "commercial" conditions with a maximum heat input of 6.1 KJ/mm and a maximum interpass temperature of 300°C.

The results showed that the impact properties of the low heat input welds were markedly better than those of the high heat input welds. The difference in Charpy V notch energy observed was approx. 40 J at - 20°C. Again as in Bennett's work (72) no correlation is made between weld metal heat input and microstructural features.

Garland et al (74) examined the effects of three different heat inputs (7.6 KJ/mm, 3.3 KJ/mm and 1.9 KJ/mm) on the weld metal toughness using a carbon manganese welding wire but in conjunction with two different welding fluxes, a fully basic flux OP41TT marketed by Oerlikon Electrode Ltd., and an amphoteric flux BX200 marketed by BOC/Murex.

The increase in heat input from 3.3 KJ/mm to 7.6 KJ/mm severely reduced the as welded impact strength of the OP41TT weld to a very low level of 8 J at - 20°C, but the properties of the BX200 welds were found to be only slightly impaired giving energy values of 35 J at - 20°C.

For both high heat input welds the reduction in fracture toughness was partially attributed to the reduction of the area fraction occupied by the acicular ferrite phase. The lower properties of the OP41TT weld in comparison with the BX200 weld were attributed to the higher carbon (0.04%) and lower manganese (0.15%) values of the OP41TT welds, which in turn lead to a 10% increase of the area occupied by the upper bainite phase which has poor notch toughness properties.

The OP41TT welds also had a significant concentration of lath martensite and partially degenerated lath martensite while the BX200 welds showed predominantly twinned martensite. These authors consider that the presence of lath martensite has a greater deliterious effect on the notch toughness than twinned martensite.

A reduction in heat input from 3.3KJ/mm to 1.9 KJ/mm lead to an increase in the as welded impact strength for both weld deposits, OP41TT and BX200 but this increase was greater in the case of the OP41TT weld.

The increase in toughness of these welds was not attributed to a variation in the fraction area of the acicular ferrite phase but on differences in the amount and distribution of the lath and twinned martensitic phases in each of these two weld deposits.

Wilson et al (75) examined the influence of the number of runs required to fill the same welded joint on the properties of submerged arc welds using a welding wire and flux of "normal commercial quality". These authors did not specify the flux bassisity but the welding wire was of a high manganese content (approx. 2%).

The results showed that the Charpy V impact values decreased and the transition curve also became shallower with an increase in the number of weld runs. The increase in the number of weld runs also lead to a decrease in the scatter of Charpy V impact values.

The optical observations of the microstructure showed that an increase in the number of weld runs (decrease in heat input) lead to an increase in the acicularity of the microstructure. These authors suggested that this microstructural change was responsible for the increase in strength at the expense of ductility of these low heat input welds.

From the work previously described it is clear that a general relationship between weld metal heat imput and properties cannot be found, since in some cases an increase in heat input lead to a decrease in the weld metal toughness values and in other cases had the opposite effect.

The difficulty in correlating weld metal heat input with weld metal properties is attributed (76) to the fact that for a fixed weld heat input in KJ/mm but at different welding parameters, various weld metal cooling cycles can be obtained which in turn will produce different microstructures which affect the weld properties.

Shultz et al (76) therefore suggested that instead of using the weld metal heat imput to predict the weld metal cooling rate, the weld nugget area would be more appropriate since this area correlates closely to the weld calorific heat content. These authors using a 5 Ni - Cr - Mo - V steel and a manual metal arc welding process concluded that the weld nugget area was a useful indication of the weld metal mechanical properties which are influenced by the cooling rate. These authors also reported that the arc voltage had no significant effect on the weld nugget area the weld metal cooling rate being determined by the arc current and travel speed.

However one of the limitations of using the weld nugget area method to predict weld properties is that this method does not accurately take into account the way in which the heat flows away from the weld nugget, which will vary according to the size of the surrounding plate material nor does it account for the effects on the cooling cycle of weld beads of the same area but different aspect ratios. These limitations are of some importance since Strunck et al (77) found that the cooling rates of individual passes were sensitive to their location relative to the bottom and side walls of the groove. The average cooling rate of the weld joint upper half being approximately 25% less than that of the corresponding welds lower half.

The increased cooling rates of the root areas was attributed to an increase in the weld nugget area in contact with the metal through which heat was conducted.

It appears that there is no simple and accurate method for predicting the weld metal cooling rate and therefore microstructure and properties from the arc parameters. This difficulty has lead to the actual measurement of the weld pool cooling cycle by means of thermocouple implant.

This measuring technique lends itself to the possibility of "in situ" thermal analysis, of the transformation reaction taking place during cooling, and Grangon et al (78) used this method of thermal analysis to examine the effect of welding conditions on the H.A.Z. properties of a medium carbon (0.34% c) steel.

This technique consists basically of a differentiating circuit, using a capacitor, the electromotive force being supplied by the thermocouple which was subjected to the thermal cycle during welding. The differentiated current, which is proportional to the derivative of the voltage and therefore to the rate of change of the temperature was amplified and recorded using a multichannel recorder, so that the temperature/time and the rate of change of the temperature were plotted simultaneously. The same apparatus could also record the welding current and arc voltage.

In a subsequent report Grangon et al (79) described how these authors measure the transformation temperatures of Manual Metal arc electrodes using a similar "in situ" thermal analysis method. From measurement referring to a low carbon manganese molybdenum electrode these authors constructed a C.C.T. diagram, showing that the ferrite structure started to form at 800°C. The bainitic structure at 650°C (it may be that these authors used the term bainite when referring to a structure commonly termed as acicular ferrite) and the martensitic structure at approximately 430°C. In the context of this work these results were used to explain the mechanisms of H.A.Z. hydrogen cracking but it is clear that this technique can be used to relate weld metal arc parameters, chemical composition and cooling cycle to the microstructure and properties, as it was done by Widgery (8). This author used a similar technique to Grangon (78) to interpret the transformation reactions occuring in metal inert gas arc weld deposits so as to gain a better understanding of the nature of the microstructural components of the weld metal.

In this case however, welding was interrupted during the temperature measurement because of arc interference in the measuring equipment. This author found, as Grangon (78) that two opposing effects were possible at the start of the transformation and that depending on the exact nature of the transformation and specimen geometry the cooling rate either decreased as the enthalphy of the transformation was released or increased because of the increase in thermal conductivity as the austenite transforms. If these two effects combine and are of similar magnitude then the resultant signal is attenuated and therefore difficult to interpret.

In Widgery's work (8) the first effect predominated and the start of the transformation reaction could be estimated, but this author noted that some degree of subjectivity was involved in precisely locating the start and finish of the transformation reaction.

Saunders (80) also used a similar thermal analysis technique to examine the effect of major alloying elements on the toughness properties of weld metals. This author, from the thermal analysis results, estimated the temperatures at which transformation reactions took place, but again found that accurate determination of the weld metal transformation characteristics was difficult.

In conclusion it is clear that the precise arc parameter affects the weld properties and predictions of the weld metal properties using the calculated heat input values can be misleading and although

there are analytical and empirical methods to calculate the weld thermo cycle from the arc parameters and therefore estimations of the weld properties can be made, it seems that these methods have only a limited application.

Consequently recording the actual weld metal cooling cycles for each weld run seems to be the most reliable method of obtaining accurate data to correlate arc parameters with cooling cycle and subsequent microstructure and properties.

Welding Flux Composition

Weld fluxes are used to provide an arc plasma giving a stable metal transfer, and also to give arc gas shielding and protective slag to prevent oxidation of the weld metal.

The composition of the weld metal flux has a large effect on the weld metal properties since different fluxes can provide different weld metal chemical composition, weld metal cooling rate and weld bead shape (14, 21, 25, 81).

Weld fluxes are generally composed of basic oxides such as CaO, MgO, BaO, $Na_2O$, $K_2O$, $CaF_2$ and acid oxides such as $SiO_2$, $AeO_3$, $tiO_2$, $ZrO_2$ etc. The "Basicity" of the flux is usually defined in terms of the ratio between the basic and acid ocides (21, 81).

The major differences between basic and acid fluxes lies in the low reactivity of the basic fluxes (81).

Because basic oxides are more thermodynamically stable than acid ones, the ratio between basic oxides and acid oxides present in the flux will have a determinant effect on the oxygen made available during welding and therefore basic fluxes lead to "cleaner" weld deposits (81).

However, the effects of flux composition on the weld properties is outside the scope of this work and therefore only one basic flux was used throughout all the welds. A basic flux was chosen because these fluxes are widely used and known to give a clean weld with good toughness properties.

Welding Electrode Composition

The chemical composition of the welding wire affects the weld metal composition and subsequently the properties (8, 14), and for this reason varying alloying additions of carbon, manganese, silicon, molybdenum, nickel, etc. are used in order to produce welds of desirable properties.

As in the case of weld fluxes in this work the effect of carying the welding wire alloying additions is outside the scope of this work, the same carbon manganese wire composition being used throughout this work.

## EQUIPMENT AND MATERIALS

### Welding Equipment

A Hagglunds type LSIT 1200 transformer rectifier rated at 84 K.V.A. corresponding to 1200 amp, 44 volts D.C. output was used for all welds.

The unit had a drooping static power characteristic and was used with a Hagglunds H.S.A. 150 voltage controlled wire feed system and head. The welding head was mounted on horizontal and vertical slides.

### Plate Material

The plate material used was in the as rolled condition and was a low sulphur, low phosphorous carbon-manganese microalloyed steel to B.S. 4360 : 50 D. The plate thickness was 40 mm. The plate chemical analysis (by Quantivac and vacuum fusion technique for oxygen and nitrogen) is shown in table 1.

### Welding Wire

The welding wire used was 4 mm diameter SD3 supplied by Oerlikon Ltd. The wire specification is shown in table 2.

### Welding Flux

All welds were made using a fully basic agglomerated flux commercially designated as OP41TT manufactured by Oerlikon Ltd. According to the manufacturers specification this flux contains mainly CaO, $CaF_2$ with less than 10% $SiO_2$ and is designed for direct current up to 900 amp.

### Temperature Measurement Equipment

The weld metal temperature measurements were made using 6% Rhodium-Platinum 30% Rhodium-Platinum thermocouples sheathed in 2.5 mm diameter twin bore recrystallized alumina insulators.

The pre-heat and interpass temperatures were measured using a Chromium Alumel thermocouple inplanted in the plate material. A multi channel U.V. recorder manufactured by S.E. Laboratories Ltd. Type 3006 was used to record the output from the thermocouples. A multipurpose digital voltmeter and a power source were used for calibration purposes.

### Thermal Analysis Equipment

Two different methods of determining the first derivative of the weld metal cooling curve were considered in detail.

One method consisted of electronic differentiation with respect to a time constant the voltage output from a thermocouple placed in the weld pool while welding was in progress. Both the

Table 1 Plate Material Chemical Composition in Wgt %

| C | Mn | Si | V | Nb | Al | P | S | Ni | Cr | Mo | Cu | Ti | B | Pb | SN | Co | O | N |
|---|---|---|---|---|---|---|---|---|---|---|---|---|---|---|---|---|---|---|
| 0.15 | 1.38 | 0.44 | 0.06 | 0.027 | 0.031 | 0.006 | 0.005 | 0.05 | 0.12 | 0.02 | 904 | 0.01 | 0.001 | 0.01 | 0.01 | 0.01 | 33.7 | 4 |

Table 2 Specification for the Oerlikon SD3 Welding Wire in Wgt %

| C | Mn | Si | S | P | Ti + Al + Zr | N |
|---|---|---|---|---|---|---|
| 0.08 - 0.12 | 1.50 - 1.80 | 0.25 - 0.40 | 0.015 max | 0.015 max | 0.07 - 0.15 | 0.012 max |

thermocouple voltage output and derivative trace were simultaneously recorded using a multi channel U.V. recorder. From the U.V. recorder trace of the thermocouple voltage output the weld metal cooling curve was obtained. The austenite phase transformation temperatures were obtained from the sharp change in slope of the weld metal cooling curve.

An alternative method consists basically of only recording the weld metal cooling curve from the thermocouple voltage output during the welding operation and subsequently calculating the cooling rate curve from the cooling curve. For this operation a computer is generally used.

In this work the method first described was used because of the moderate equipment requirements. However this method required a laborious and time consuming data processing stage and for future work the second method would probably be preferred.

The equipment used was developed in conjunction with the instrumentation department at C.I.T.

The circuit diagram of the equipment used is shown in figure 1.

Mechanical Testing

An Instron model TT-C tensile test machine was used for all tensile tests.

Charpy V notch impact tests were made on a Losenhausen machine capable of delivering a maximum energy of 294 J.

Hardness measurements were made on a normal Vickers hardness testing machine using a 30 kg load.

Metallographic Equipment

A Reichert model "Me F" projection microscope was used for all optical microscopy.

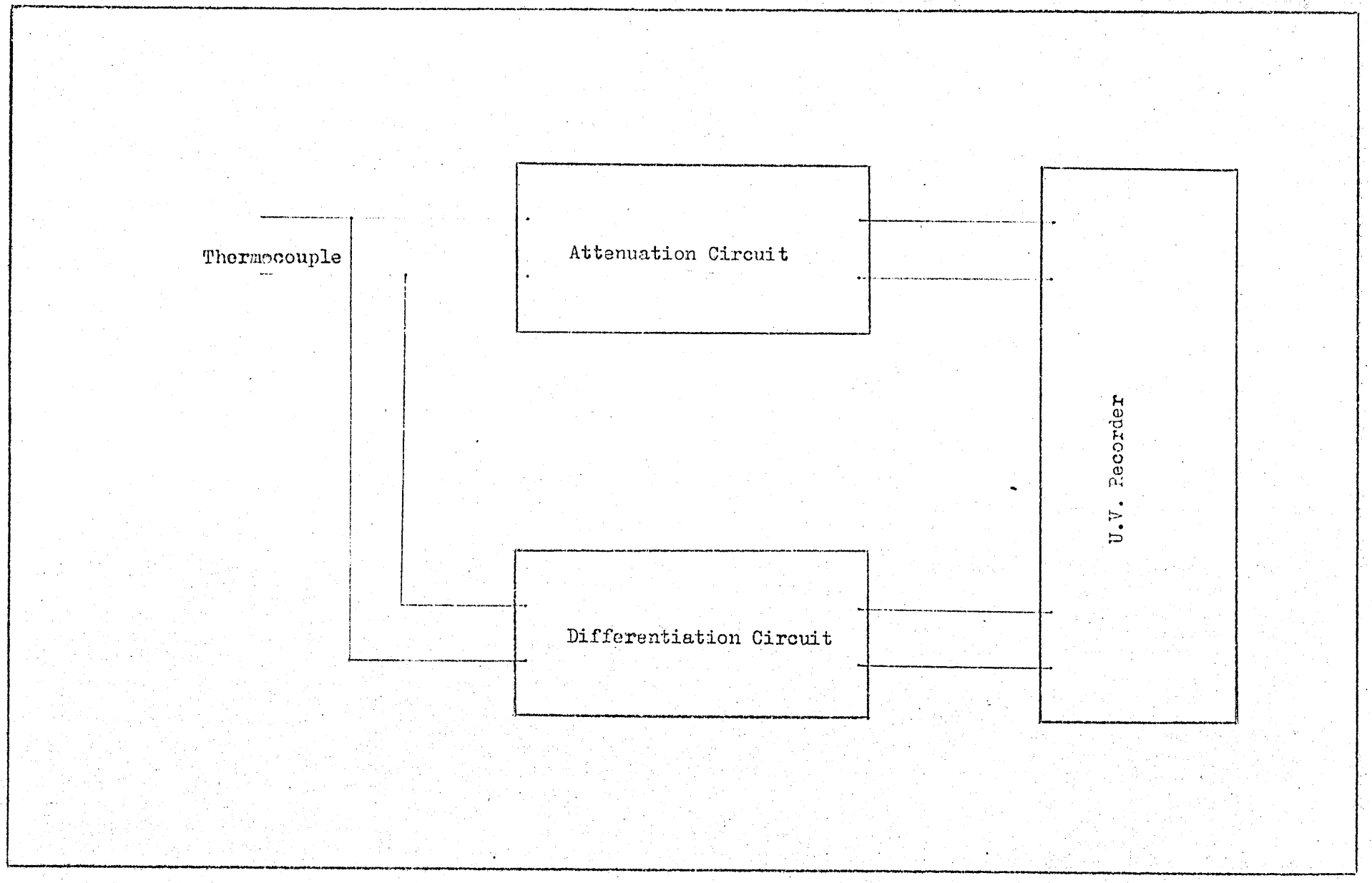


Figure 1 Diagram of the thermal analysis equipment.

## EXPERIMENTAL PROCEDURE

### Plate Preparation

All plates were flame cut to give a 90° single V edge preparation in conjunction with a 17 mm root face.

The cut surfaces were dressed smooth by grinding. The final plate dimensions were 660 mm long, 400 mm wide and 40 mm thick. Run on and run off tabs were used.

### Welding Procedure

All welds were made using a D.C. + ve setting. The welding direction was kept constant for all welds and no plate restraint was used. However, the plates were tuck welded together by means of a single continuous M.M.A. weld bead using a 4 gauge basic electrode "Bicito" Class 6 to B.S. E607H on the underneath of the plate.

Two weld series were made. For the first series the welding current was kept constant at 650 amp and the welding speed was varied from 200 mm/min to 300 mm/min and then to 400 mm/min. (The accuracy of measurement of the welding speed was within 1%). For the second series the welding speed was kept constant at 300 mm/min and the welding current was varied from 850 amp to 650 amp and then to 480 amp. The welding voltage was kept constant at 30 volts for all welds except for the 850 amp weld where 35 volts were used. The welding voltage and welding current were read from the welding head control panel meters. As the needle of the current and voltage meters oscillated (approximately 3%) during welding, the average needle reading was taken.

The pre-heat and interpass temperature used was 100°C. This temperature reading was taken from the central longitudinal remote plate edge surface and in the same relative position for all plates.

The heat inputs for the welding conditions used are shown in table 3 and were calculated by using the conventionally used formula

$$\text{Heat Input} = \frac{V \times A \times 60}{1000 \times \text{speed}}$$

H = K.J /mm
V = Arc voltage
A = Arc current
Speed = Table speed in mm/min.

### Temperature Measurements

The 6% Rhodium-Platinum and 30% Rhodium-Platinum thermocouples were, as stated previously, sheathed in twin-bore recrystallized alumina insulators.

The thermocouple joint was attached to one end of a 4 mm diameter cylindrical steel stub made from welding wire. The steel stubs were used in order to locate the thermocouple joint accurately in such a position as to measure the weld metal temperature, from above 1400°C to the inter-pass temperature but without permitting the thermocouple to intrude into the high temperature region of the weld pool immediately under the arc as this would destroy the thermocouple joint.

The steel stubs were made of various lengths according to the welding condition and weld bead location within the joint.

The steel stub and attached thermocouple was inserted in a cylindrical hole drilled through the plate in a direction perpendicular to the weld surface. The weld beads were then deposited above the steel stub and attached thermocouple.

The thermocouple position was found to be critical as in some cases the thermocouple would melt and not reunite. Therefore three thermocouples with slightly different stub lengths were used for each weld run.

Due to this method of placing a weld bead immediately over the thermocouples the weld metal temperature and cooling curves values obtained refer always to the lower fusion zone areas of the weld beads as shown in the schematic arrangement, figure 2.

The curves of the weld metal temperature and its first derivative were recorded on the U.V. recorder from the weld metal thermocouple output voltage, whilst welding was in progress.

Table 3 Welding conditions and Calculated Heat Input

| Welding Current amp. | Welding Voltage volts. | Welding Speed mm/min. | Calculated Heat Input KJ/mm |
|---|---|---|---|
| 650 | 30 | 200 | 5.8 |
| 650 | 30 | 300 | 3.9 |
| 650 | 30 | 400 | 2.9 |
| 850 | 35 | 300 | 5.8 |
| 650 | 30 | 300 | 3.9 |
| 480 | 30 | 300 | 2.9 |

After obtaining the weld metal cooling curve the thermocouples were kept in place to record the thermal cycles resulting from the subsequent weld beads.

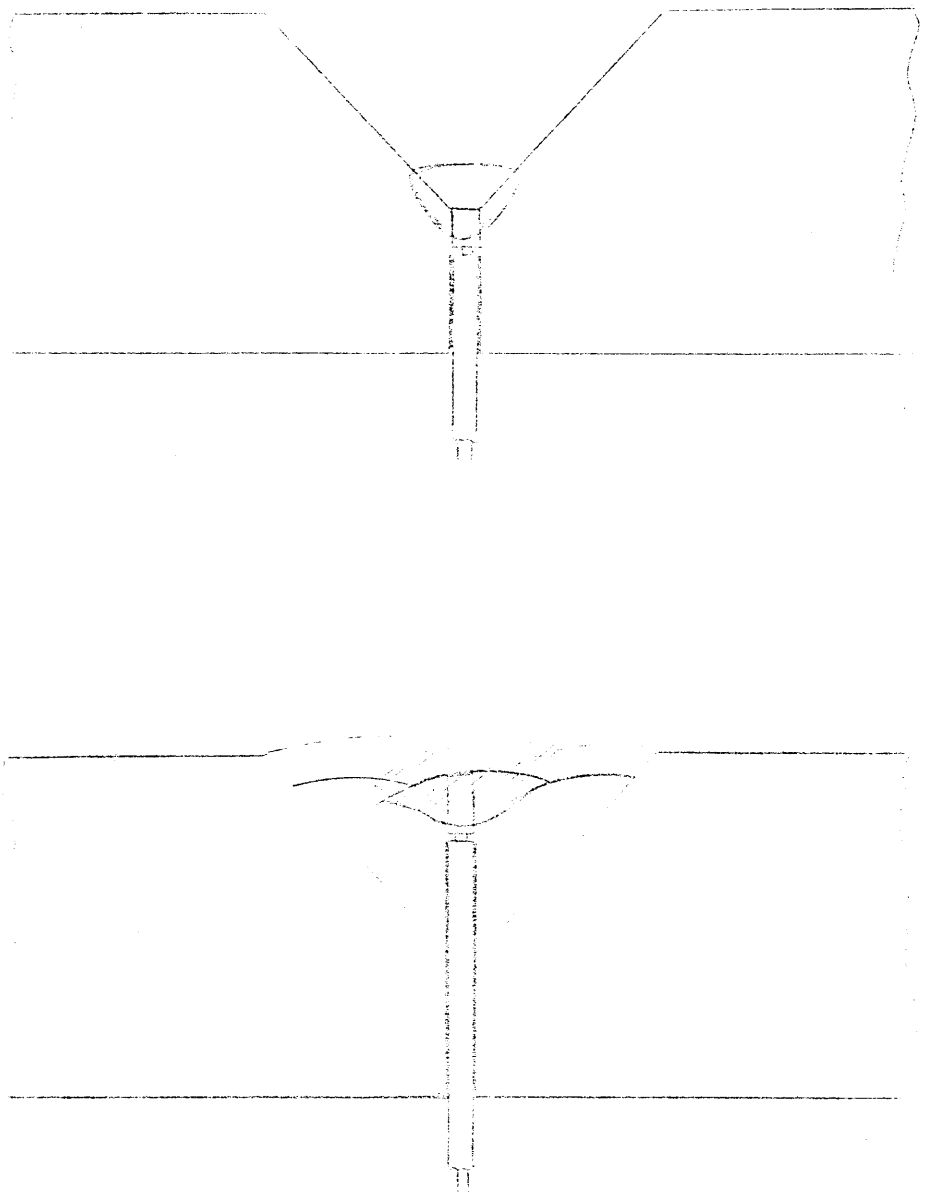

Figure 2 Thermocouple location in the weld head, root and sub-surface.

The U.V. recorder calibration was checked and if necessary adjusted prior to each weld run.

From the U.V. recorder chart the weld metal thermal curves were obtained. This operation involved accurately measuring the thermocouple voltage output from the U.V. record chart (a vernier was used for this purpose) at 1 sec. intervals for temperatures above approx. 400°C and at 5 sec. intervals for temperatures below 400°C.

From the voltage values and using a thermocouple calibration chart supplied by the thermocouples manufacturer, J.J. Matthews, the temperature values were obtained and the temperature time curves plotted.

Weld Bead Dimensions and Flux Consumption

For each weld joint the dimensions of the central sub-surface weld bead were measured from an etched macrosection, figure 3. The weld bead dimensions for the root areas could not be accurately determined because of the presence of subsequent weld runs.

An estimate for comparison purposes of flux consumption per unit length of weld metal was obtained by weighing the amount of slag removed from each weld bead.

Mechanical testing

Tensile Properties

Longitudinal tensile specimens (Hounsfield 13) were obtained from the sub-surface and root areas of all weld deposits, figure 5, and were tested at room temperature, at a cross head speed of 2.5 mm/min. One specimen was taken from each weld area.

Hardness Test

A hardness survey of the sub-surface and root areas was also carried out. Four impressions were made using a 30 Kg load for each area and the average value recorded.

Impact Tests

Standard Charpy V notch specimens (machined in accordance with BS 131 : Part 2) were taken from the sub-surface and root areas of all the weld deposits with the notch position at the centre of the weld bead, in a plane perpendicular to the plate surface and parallel to the welding direction, figure 4.

The Charpy tests were carried out at 30°C temperature intervals in the temperature range - 90°C to + 90°C. (For each test temperature three specimens were used).

For the high temperatures the specimens were immersed in hot oil, and for the low temperatures the specimens were immersed

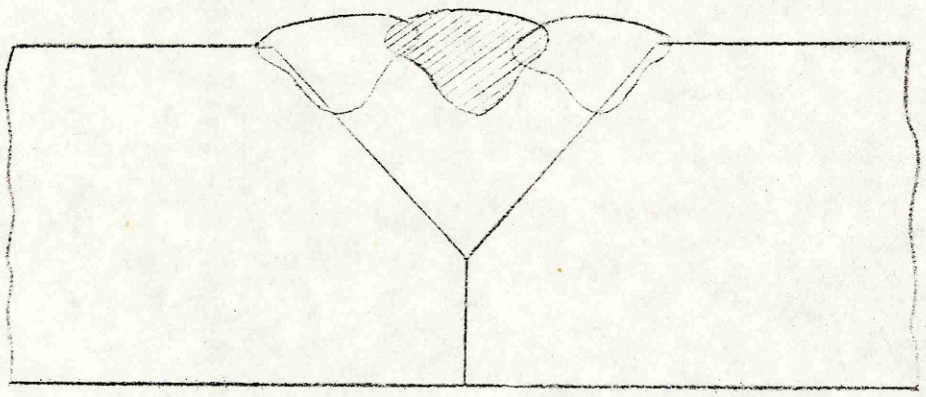

Figure 3 Location of the weld bead from which the bead dimensions were taken.

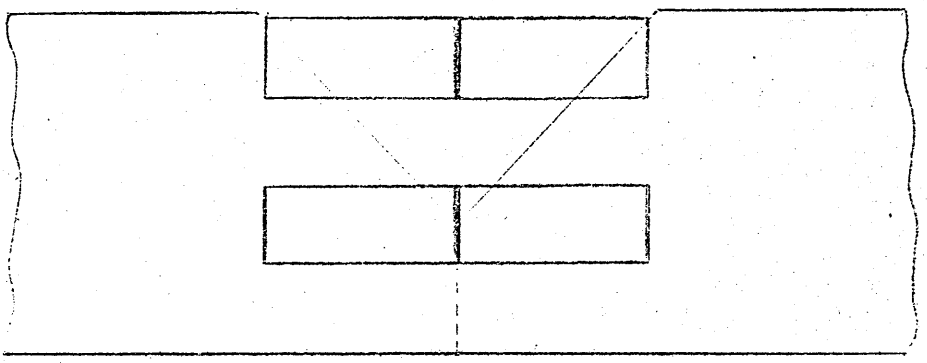

Figure 4 Location of the Charpy V Notch specimens, sub-surface and root.

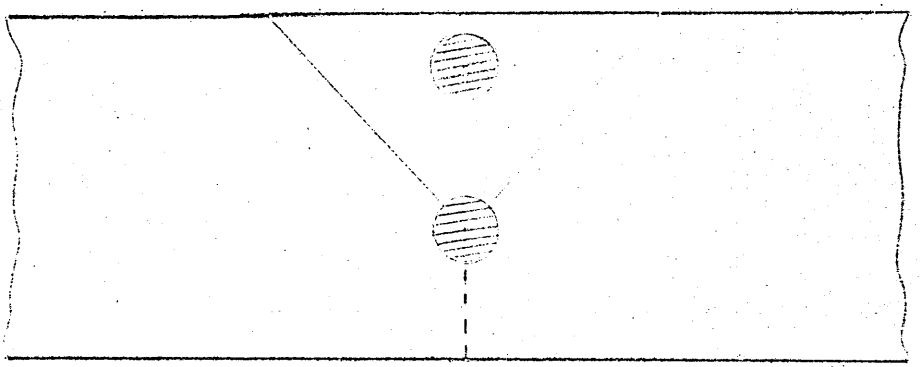

Figure 5 Location of the longitudinal tensile specimens sub-surface and root.
(Hounsfield 13)

in a mixture of metanol and liquid nitrogen. Specimens were held at the test temperature for 10 minutes prior to testing.

Metallographic Examination

Specimens from the sub-surface and root areas of each weld deposit as well as some broken Charpy V notch specimens were examined. The specimens were mounted in bakelite, wet ground and polished on rotating cloth pads using 6, 1 and $\frac{1}{4}$ micron diameter diamond dust paste.

The etchants used were 2% nitral, 4% picral and a saturated aquas solution of pricric acid and 1 grm of Vansa 5560.

Chemical Analysis

Weld metal analyses of the sub-surface and root areas of each weld were carried out by Quantovac for non-gaseous elements and by a vacuum fusion technique for oxygen and nitrogen.

## RESULTS

### General Welding Characteristics

The consumables used gave generally good weld bead shapes and easy slag detachability with the exception of the first root bead produced at the highest welding current (850 amps) where the slag detachability was poor. A macro section of each weld is shown in figures 6 and 7.

### Temperature Measurements

The thermal history of the weld bead or beads, in which the notch of the Charpy V specimen was placed were recorded in order to relate weld metal thermal histories and consequently arc parameters with weld metal properties. Unless otherwise stated only the central sub-surface and first root weld beads were described and compared as these two weld beads represent the two most extreme conditions within the welded joint.

The weld metal cooling rates for the temperature ranges 1400°C - 900°C, 900°C - 700°C and 700°C - 500°C were obtained in order to simplify the comparison between the cooling characteristics of different weld deposits.

In each case these cooling rates are quoted as mean cooling rates through the appropriate temperature range. It is important to note that for the 1400°C - 900°C temperature range a small difference in cooling time of 1 sec., can cause the calculated cooling rate to vary from 160°C/sec to 125°C/sec, and therefore variations in the cooling rate in this temperature range are not as significant as variations of the same magnitude in the lower temperature ranges.

### Weld Deposits made with a Welding Current of 650 amps

#### Sub-surface Weld Beads

The thermal analysis results for the sub-surface weld beads are shown in figure 8 and table 4. The results show that a successive reduction in welding speed from 400 mm/min. to 300mm/min. and then to 200 mm/min. led to a progressive reduction in the weld metal cooling rate.

#### Root Weld Beads

The thermal analysis results for the root weld beads are shown in figure 9 and table 4. As for the sub-surface the results showed that a successive reduction in welding speed led to a reduction in the weld metal cooling rate.

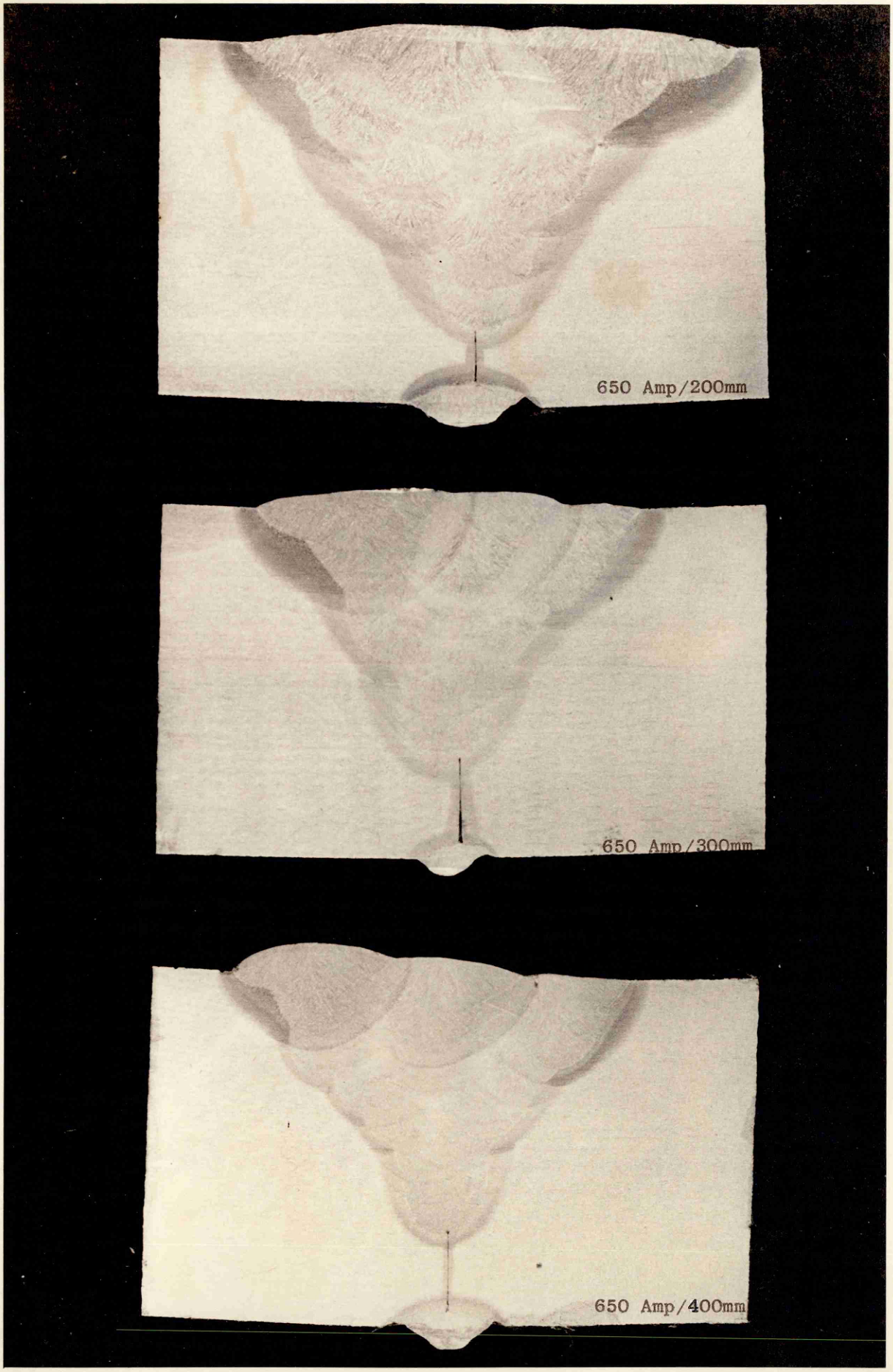


Figure 6. Weld Macrosections

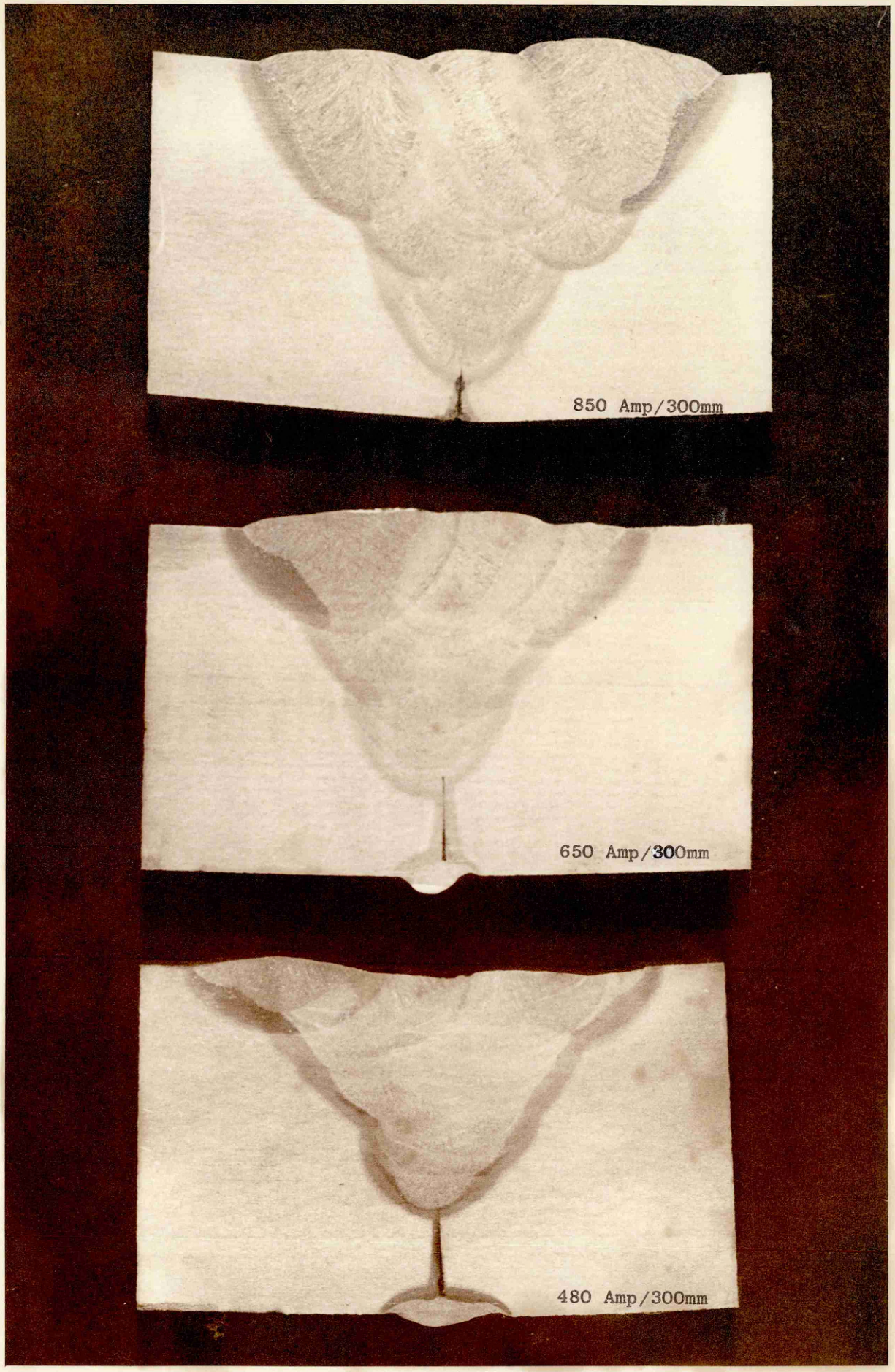


Figure 7. Weld Macrosections

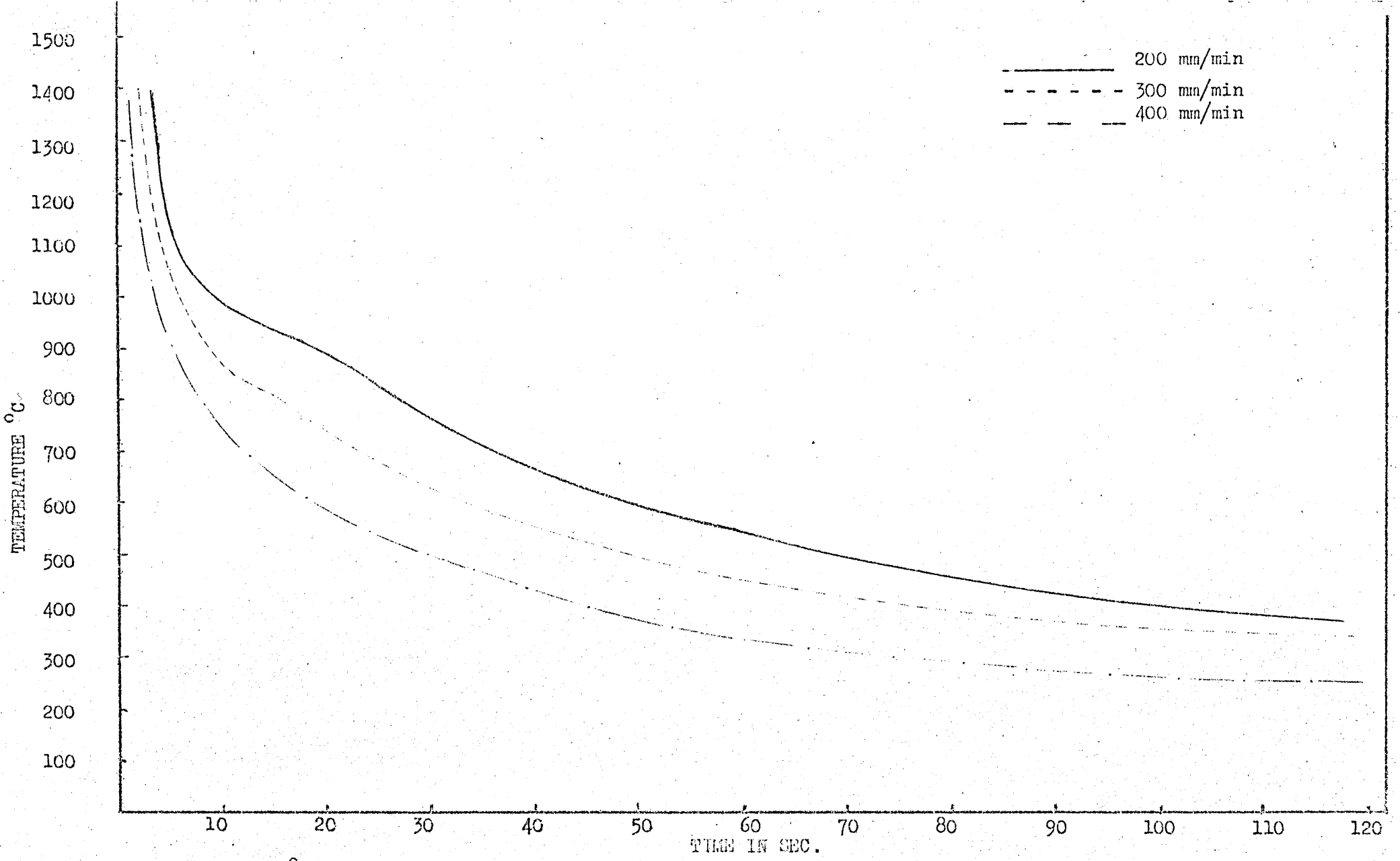


Figure 8 Continuous cooling curve for the sub-surface bead of the weld deposits, made at 650 amp. and 200 mm/min, 300 mm/min and 400 mm/min.

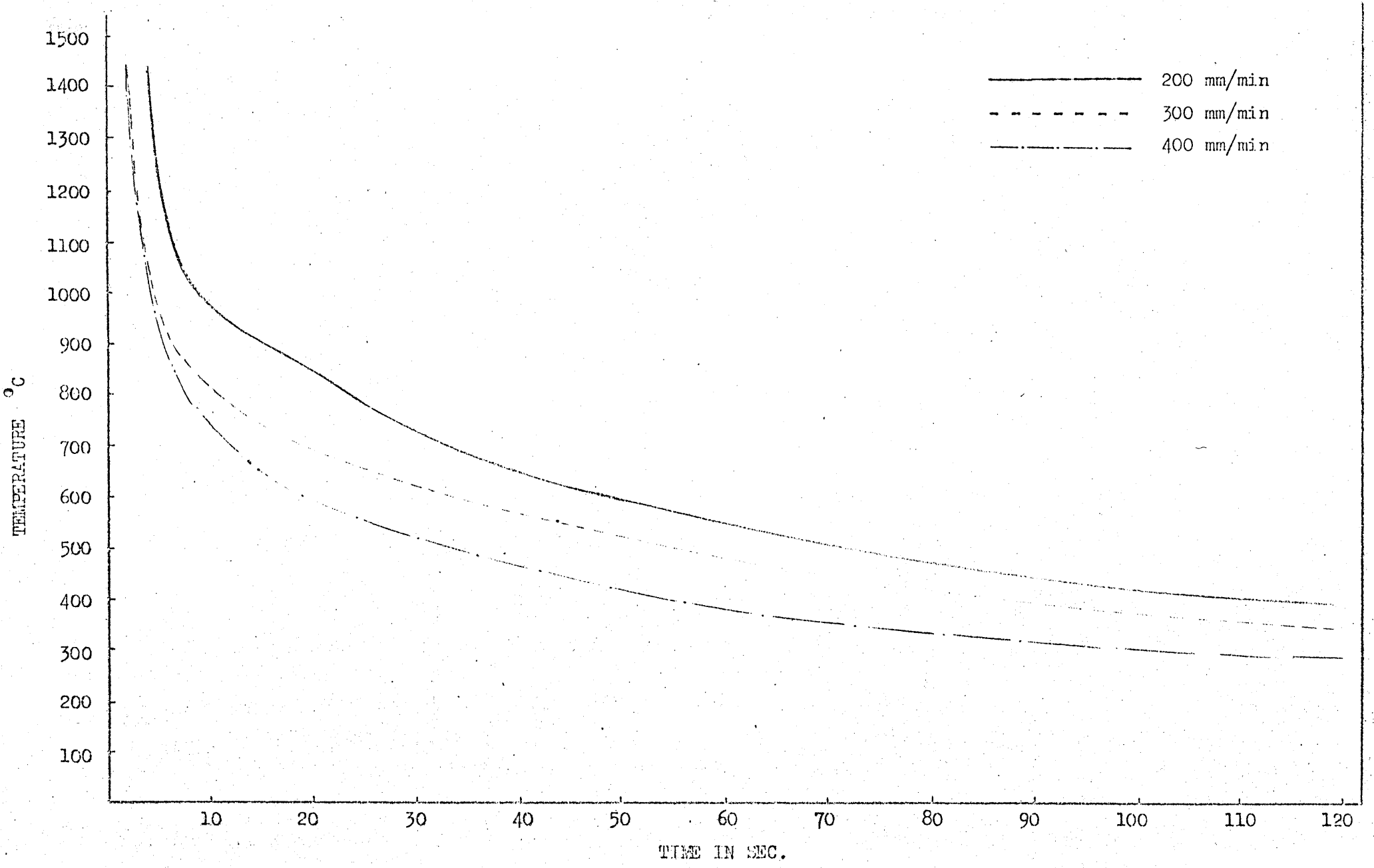


Figure 9 Continuous cooling curve for the root bead of the weld deposits, made at 650 amp. and 200 mm/min, 300 mm/min and 400 mm/min.

Table 4 Thermal Analysis Results

| Welding Conditions | Average Cooling Rate in °C/sec | | |
|---|---|---|---|
| | 1400°C - 900°C | 900°C - 700°C | 700°C - 500°C |
| 650 AMPS - 200 mm/min | | | |
| Sub-surface | 33 | 12.1 | 6.15 |
| Root | 45 | 11.1 | 5.6 |
| 650 AMPS - 300 mm/min | | | |
| Sub-surface | 66 | 14.8 | 7.5 |
| Root | 142 | 15.3 | 5.6 |
| 650 AMPS - 400 mm/min | | | |
| Sub-surface | 160 | 2.6 | 11.4 |
| Root | 142 | 30.7 | 8.8 |

Weld Deposits made with a Welding Speed of 300 mm/min.

Sub-Surface Weld Beads

The thermal analysis results for the sub-surface weld beads are shown in figure 10 and table 5.

The 850 amps - 300 mm/min and 650 amps - 300 mm/min weld beads had a similar cooling rate throughout the temperature range 1400°C - 650°C. For the temperatures below approximately 650°C the 850 amps - 300 mm/min had a lower cooling rate than the 650 amps - 300 mm/min. The 480 amps - 300 mm/min weld bead had a lower cooling rate than these two welds for the temperature range 1400°C - 900°C, but below this temperature this weld had the highest cooling rate of all three weld deposits.

Root Weld Beads

The thermal analysis results for the root weld beads are shown in figure 11 and table 5.

The results show that the weld made at 480 amps - 300 mm/min had the lowest cooling rate in the temperature range 1400°C - 900°C. Below 900°C the 850 amps - 300 mm/min weld had the lowest cooling rate, and the 480 amps - 300 mm/min weld the highest, with the 650 amp - 300 mm/min weld falling in between.

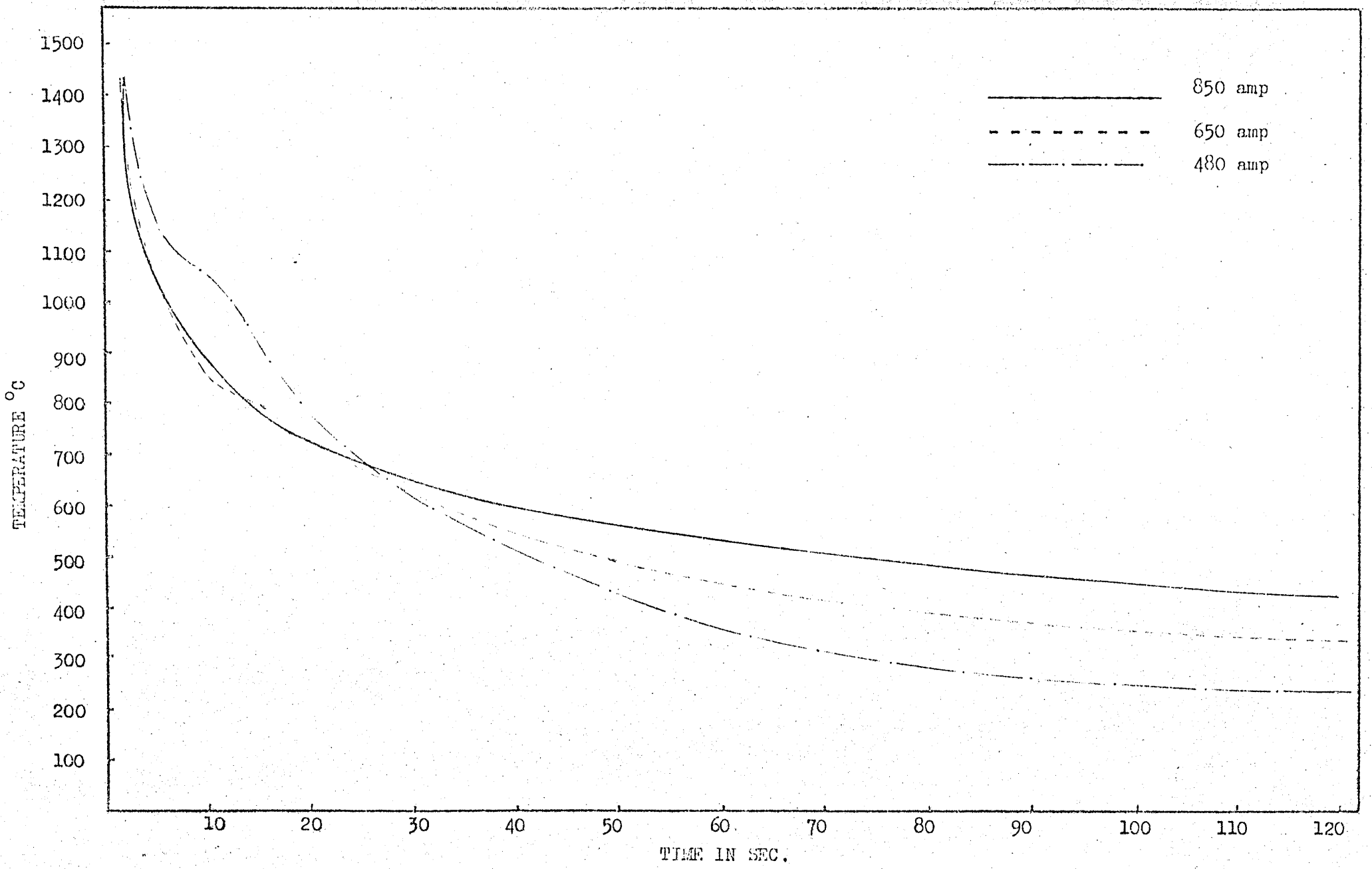


Figure 10 Continuous cooling curve for the sub-surface bead of the weld deposits made at 850 amp, 650 amp. and 480 amp and 300 mm/min.

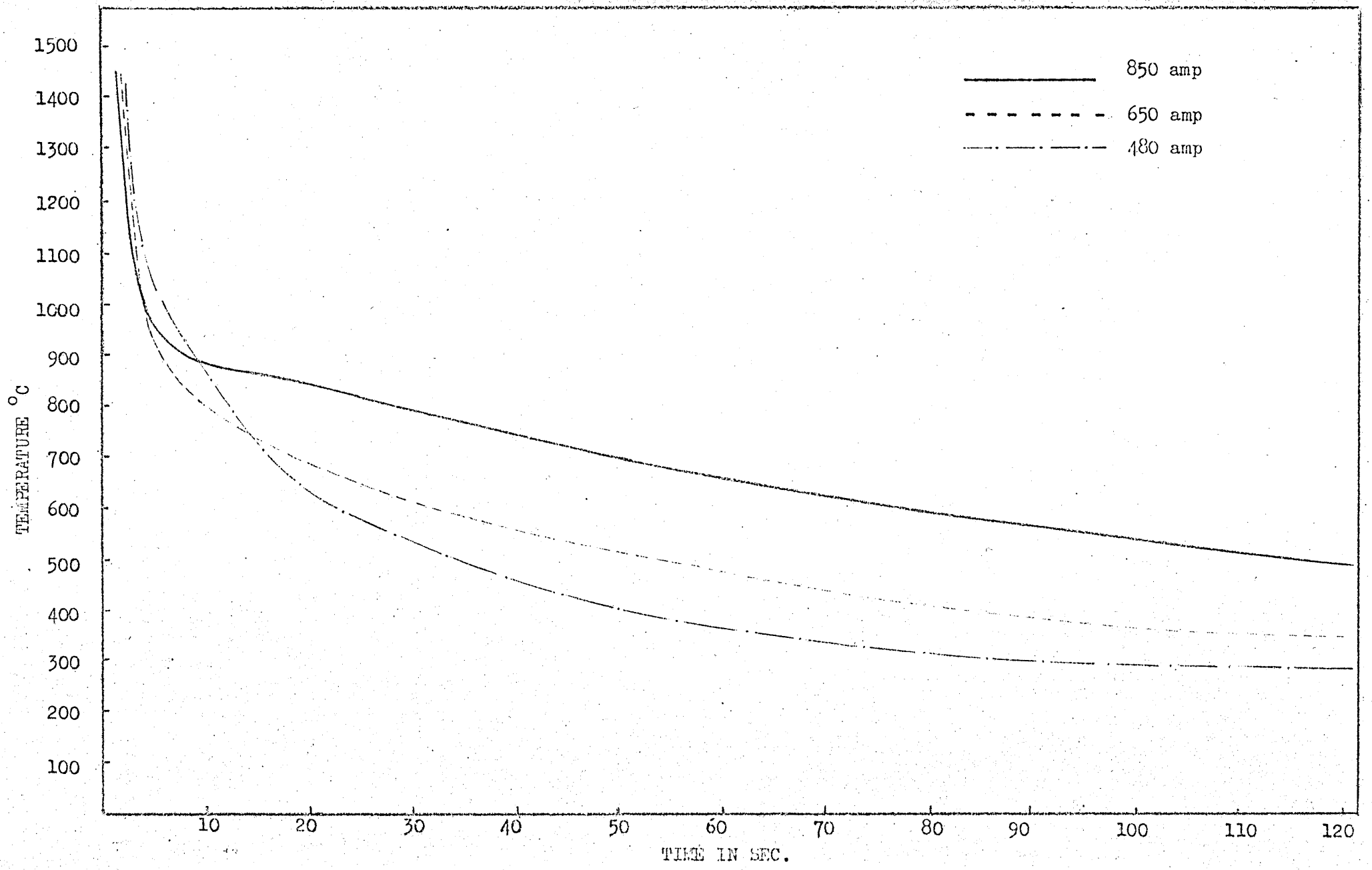


Figure 11 Continuous cooling curve for the root bead of the weld deposits made at 850 amp, 650 amp and 480 amp and 300 mm/min.

Table 5 Thermal Analysis Results

| Welding Conditions | Average Cooling Rate in °C/sec | | |
|---|---|---|---|
| | 1400°C - 900°C | 900°C - 700°C | 700°C - 500°C |
| 850 AMPS - 300 mm/min | | | |
| Sub-surface | 71 | 16.6 | 3.6 |
| Root | 100 | 4.7 | 3.2 |
| 650 AMPS - 300 mm/min | | | |
| Sub-surface | 66 | 14.8 | 7.5 |
| Root | 142 | 15.3 | 5.6 |
| 480 AMPS - 300 mm/min | | | |
| Sub-surface | 35 | 2.3 | 15.2 |
| Root | 76 | 28.5 | 10.5 |

Thermal Differences between the Sub-Surface and Root beads for the same welded Joint

The thermal histories at the sub-surface and root weld beads of the same weld were found to be considerably different.

These differences were due to two separate effects. Firstly, the initial weld metal cooling rate which was found to be different for the sub-surface and root regions and secondly the post-solidification thermal effects caused by the subsequent weld runs which affected the root beads.

An estimation of the post-solidification thermal histories for each of the welds deposits is shown in table

This table was obtained from the data in figure 12 to 36 and by summing the time at a given temperature for each weld run as a result of the subsequent ones. It is important to note that the values shown in table 6 refer to the thermal cycles experienced by the middle lower part of each individual weld bead as this was the thermocouple location.

Weld Deposit 650 amps - 200 mm/min

The sub-surface and root run cooling curves and average cooling rates are shown in figure 37 and table 7.

The results show that the root runs 1 and 2 had a slightly higher cooling rate than the sub-surface ($45^{\circ}C$/sec; $33.3^{\circ}C$/sec) for the temperature range of $1400^{\circ}C$ - $900^{\circ}C$.

For the temperature range of $900^{\circ}C$ - $700^{\circ}C$ and $700^{\circ}C$ - $500^{\circ}C$ the sub-surface had a marginally higher cooling rate than the root ($12.1^{\circ}C$/sec; $11.1^{\circ}C$/sec) and ($6.15^{\circ}C$/sec; $5.6^{\circ}C$/sec).

However weld run No. 3 did not follow the over all pattern and had a higher cooling rate for the $1400^{\circ}C$ - $900^{\circ}C$ and lower cooling rates for the $900^{\circ}C$ - $700^{\circ}C$ and $700^{\circ}C$ - $500^{\circ}C$ than all the other 5 weld runs.

These results show that for the above welding conditions the weld metal cooling rate in the $900^{\circ}C$ - $700^{\circ}C$ and $700^{\circ}C$ - $500^{\circ}C$ temperature ranges, decreased from run 1 to 3, and then subsequently increased. The average times at temperature for the root area was 30 sec at $600^{\circ}C$, 108 sec at $500^{\circ}C$ and 382 sec at $400^{\circ}C$, while the sub-surface never exceeded $400^{\circ}C$. Table 6.

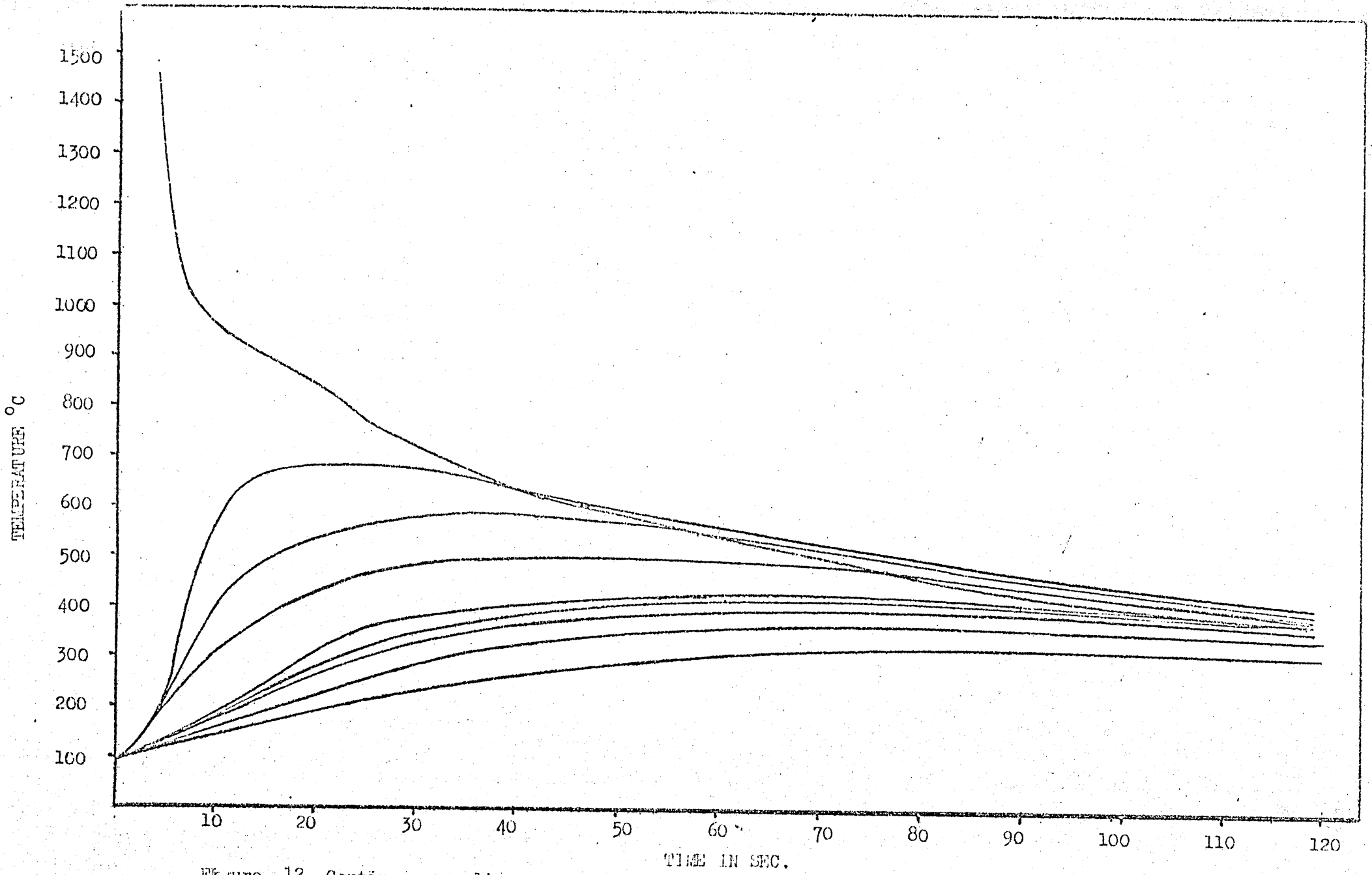


Figure 12 Continuous cooling curve and subsequent thermocycles for the first root bead of the weld deposits made at 650 amp, 200 mm/min.

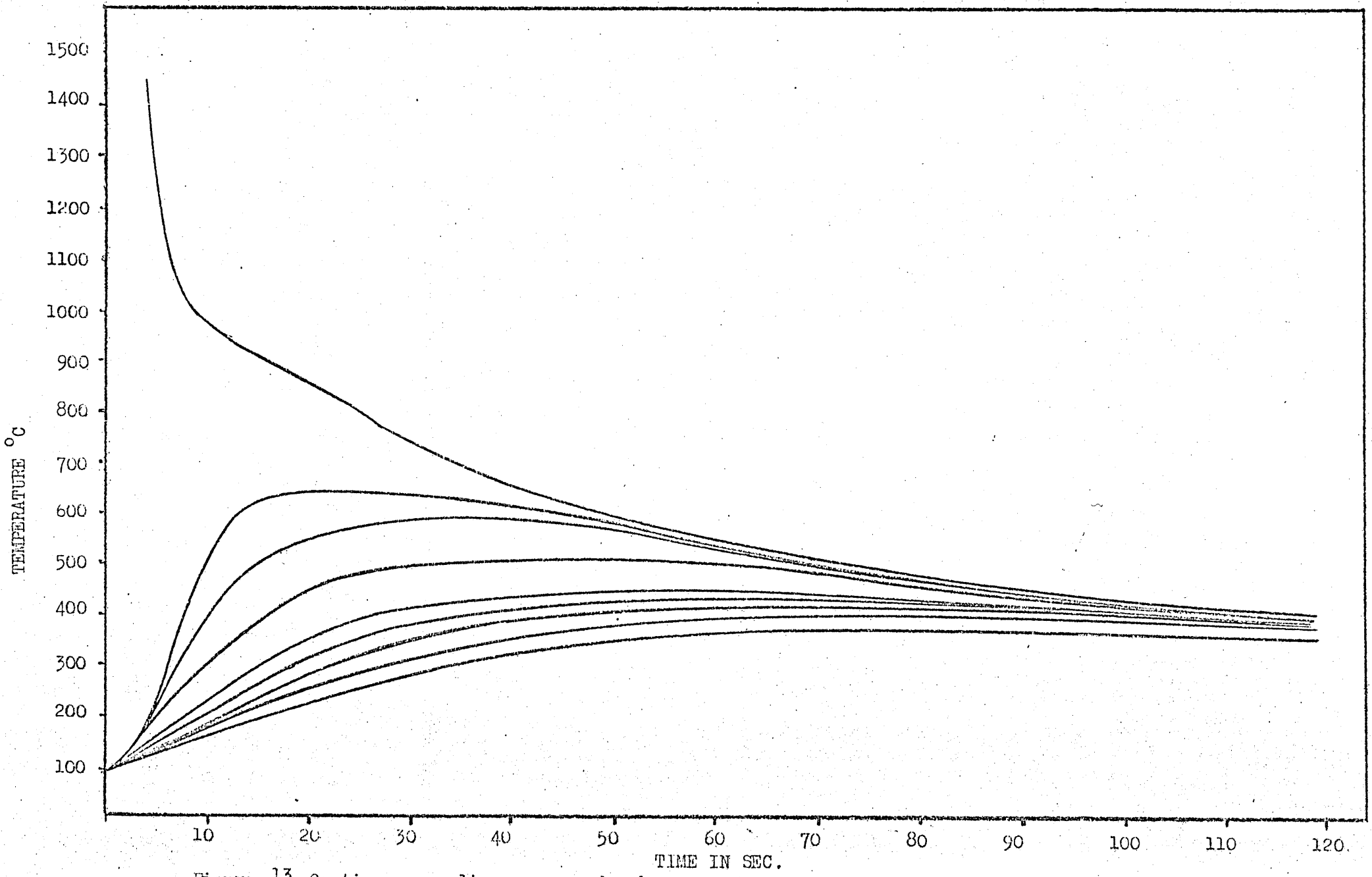


Figure 13 Continuous cooling curve and subsequent thermocycles for the second root bead at the weld deposit made at 650 amp - 200 mm/min.

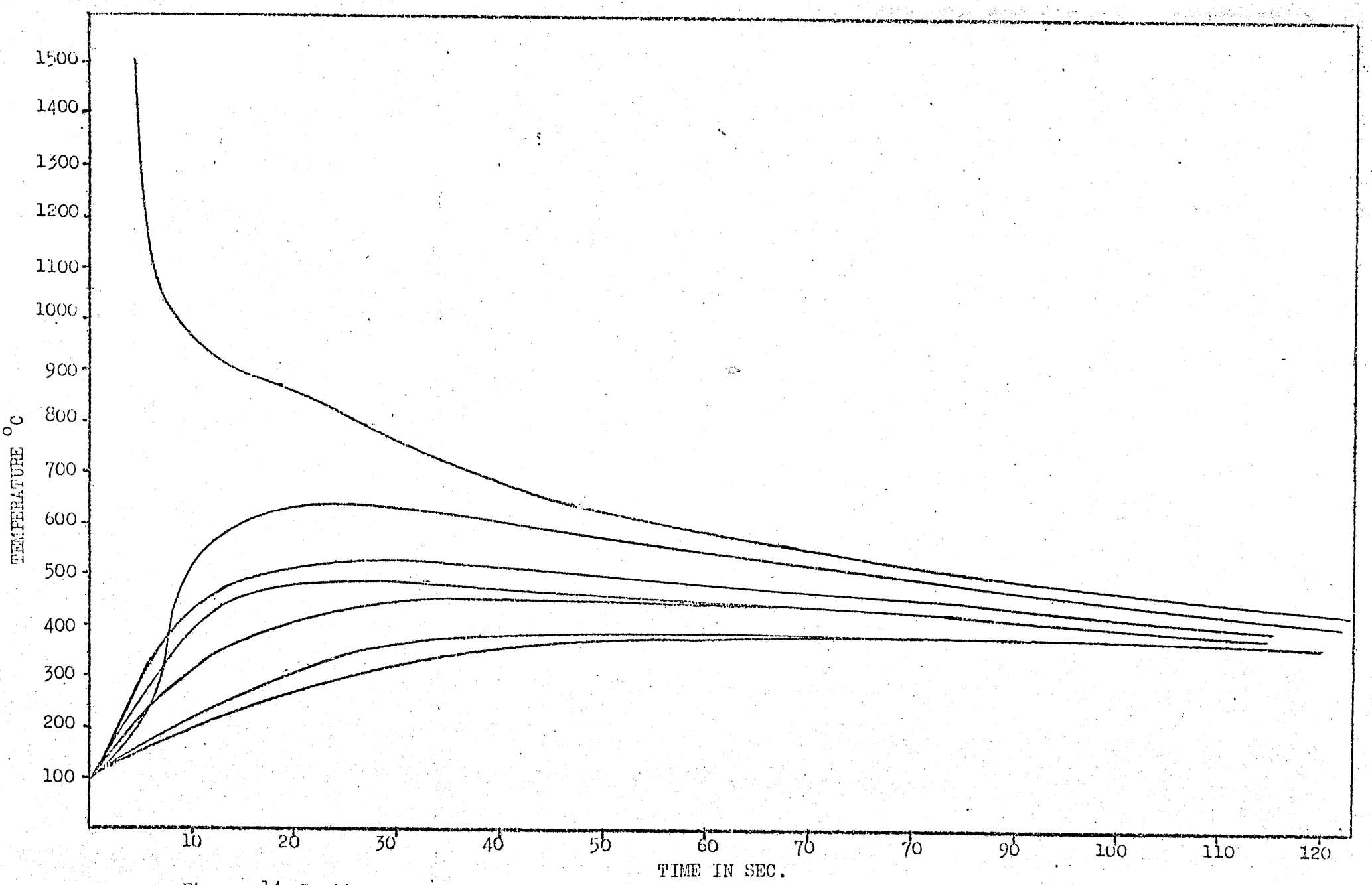


Figure 14 Continuous cooling curve and subsequent thermocycles for the third root bead of the weld deposit made at 650 amp - 200 mm/min.

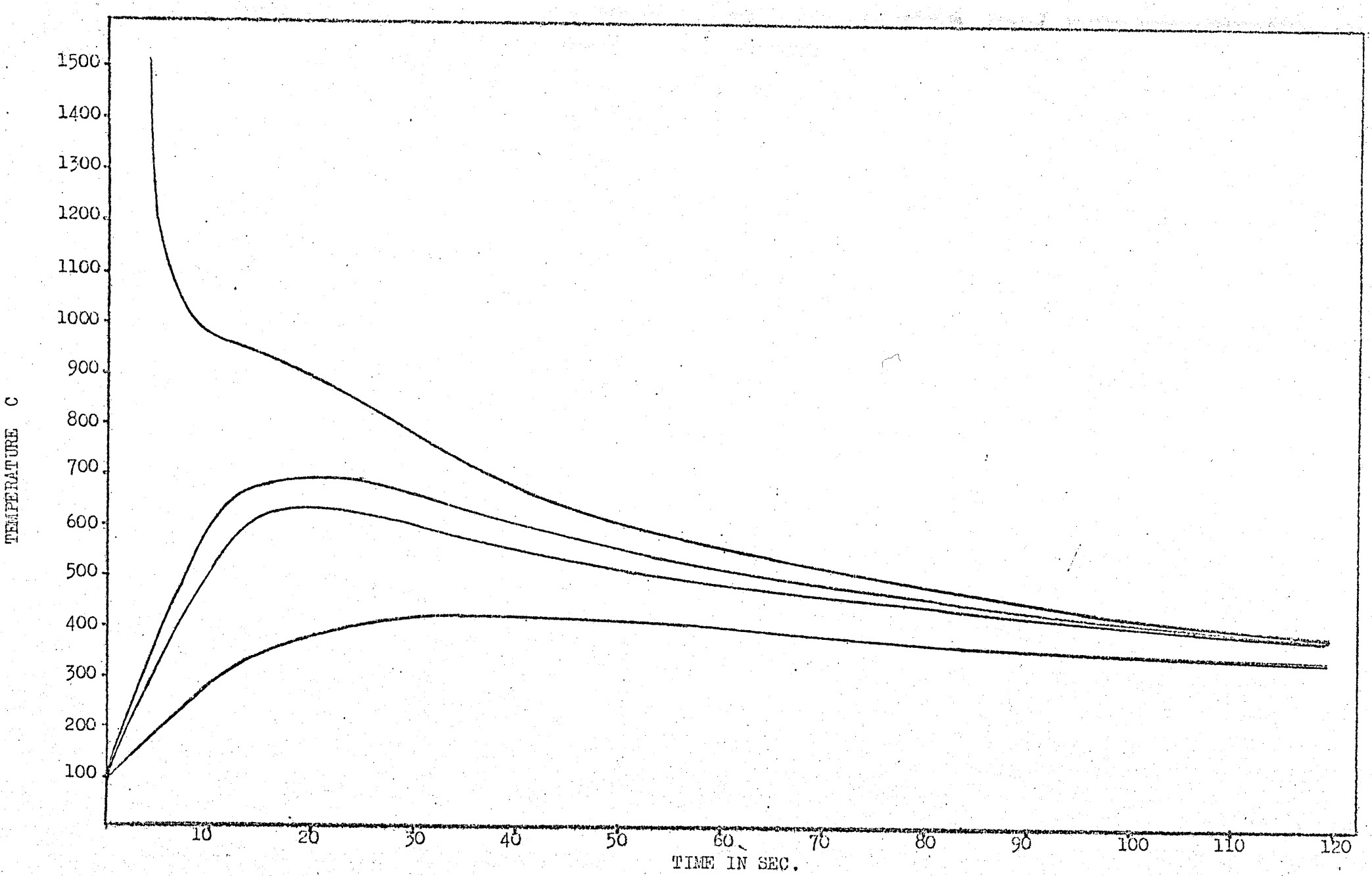


Figure 15 Continuous cooling curve and subsequent thermocycles for the seventh sub-surface bead of the weld deposit made at 650 amp - 200 mm/min.

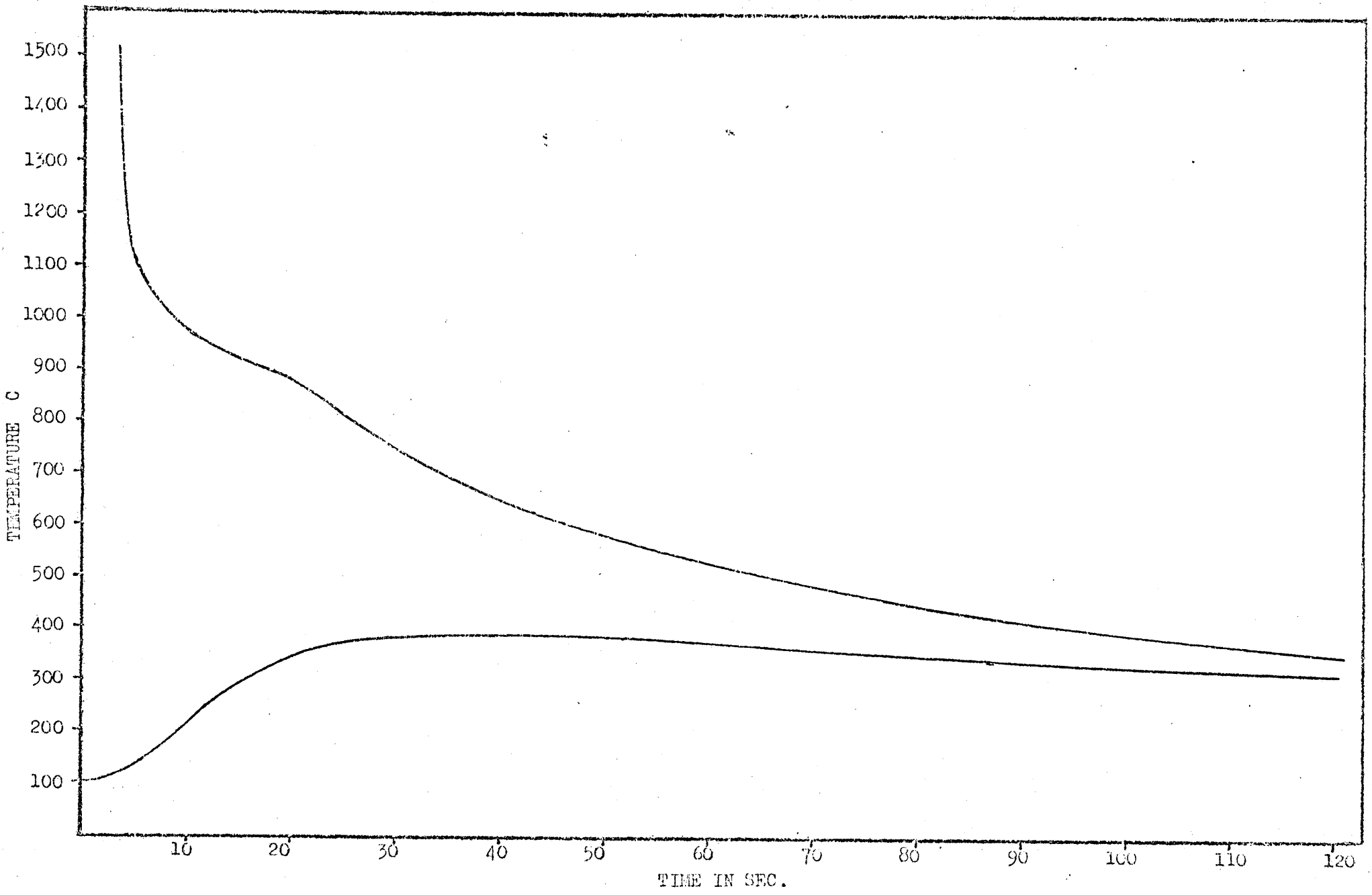


Figure 16 Continuous cooling curve and subsequent thermocycles for the ninth sub-surface bead of the weld deposit made at 650 amp - 200 mm/min.

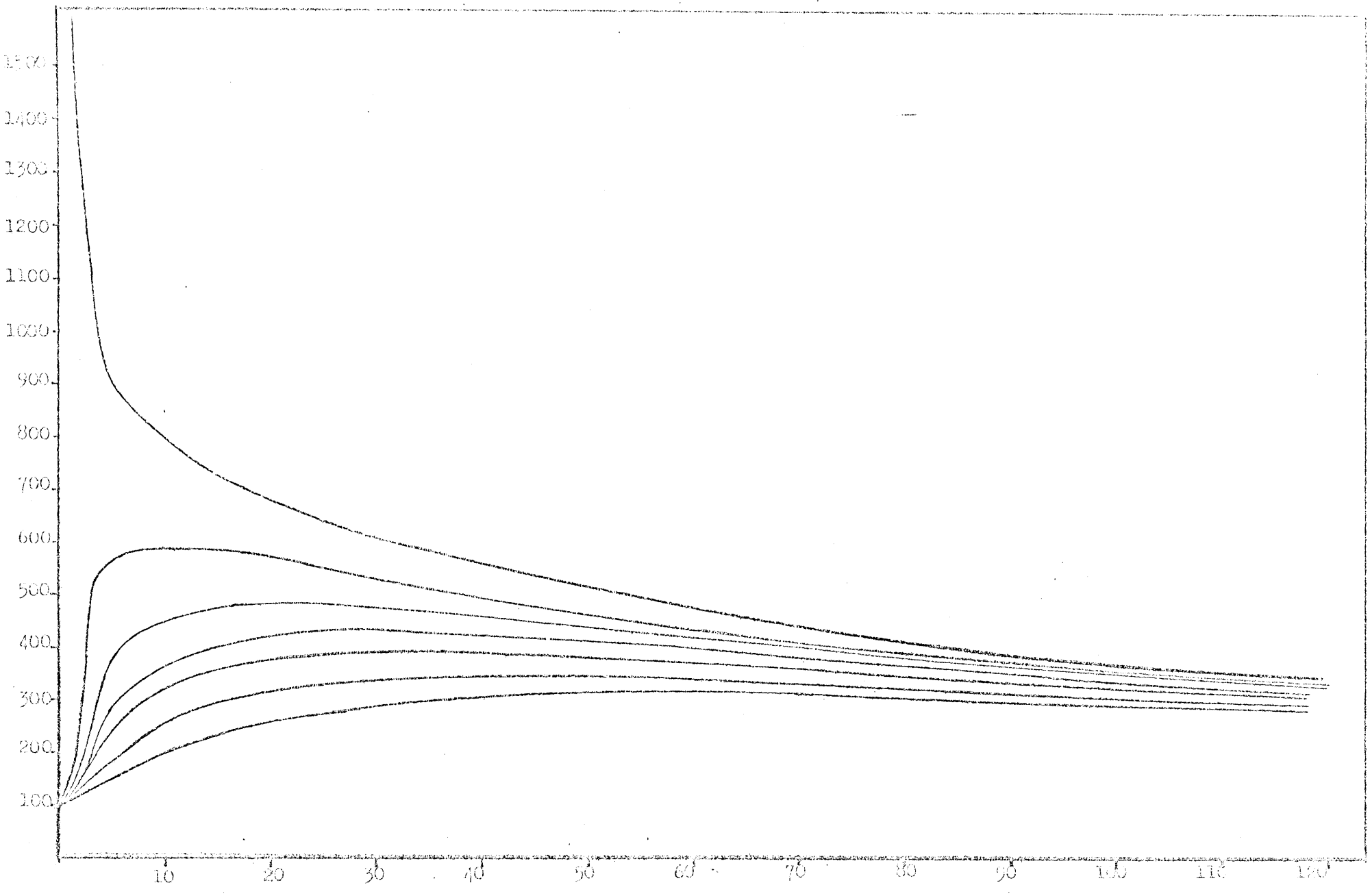


Figure 17 Continuous cooling curve and subsequent thermocycles for the first root bead of the weld deposit made at 650 amp - 30v ca/min.

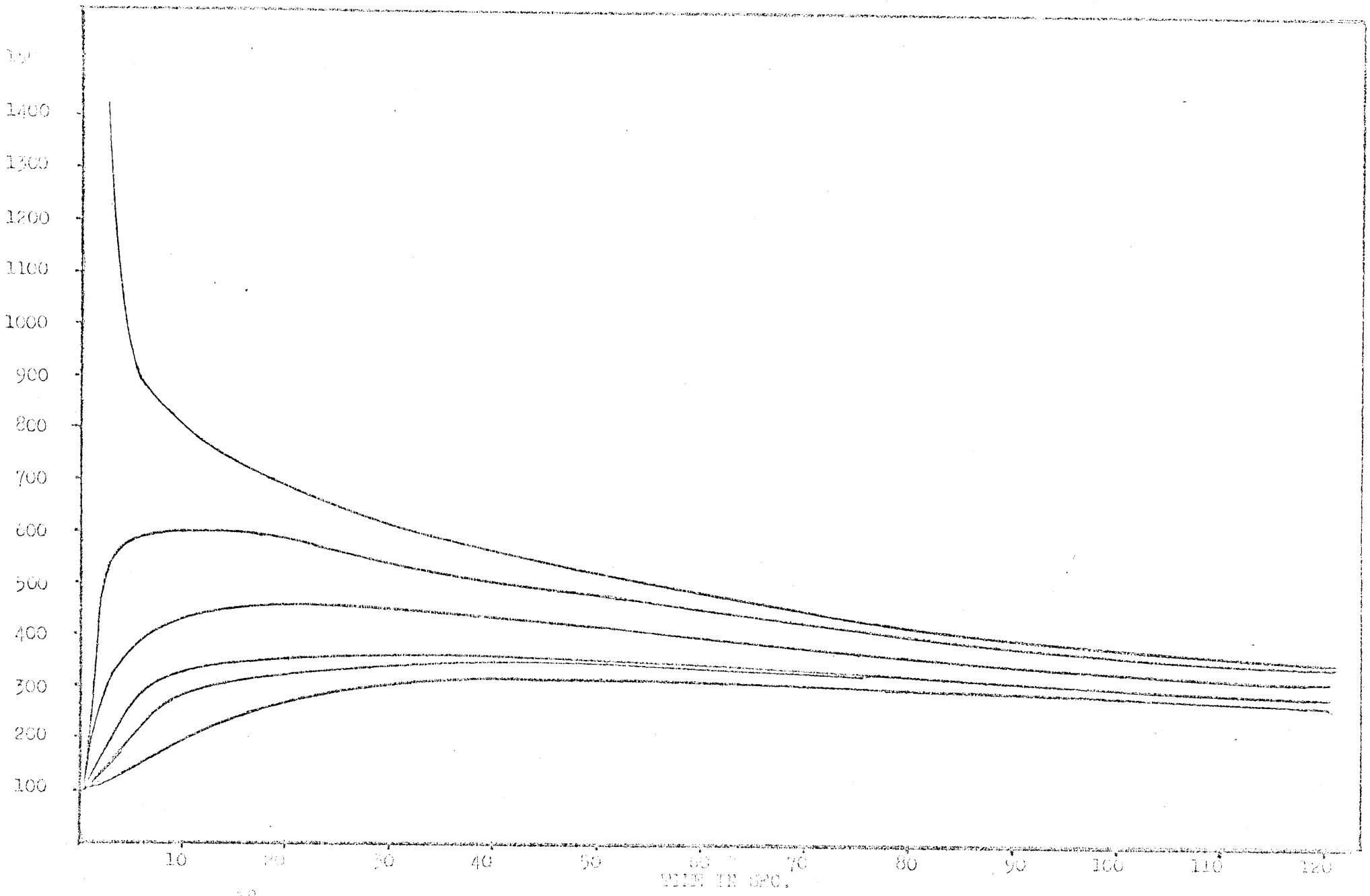


Figure 18 Continuous cooling curve and subsequent thermocycles for the second root bead of the weld deposit made at 450 amps - 30V travel.

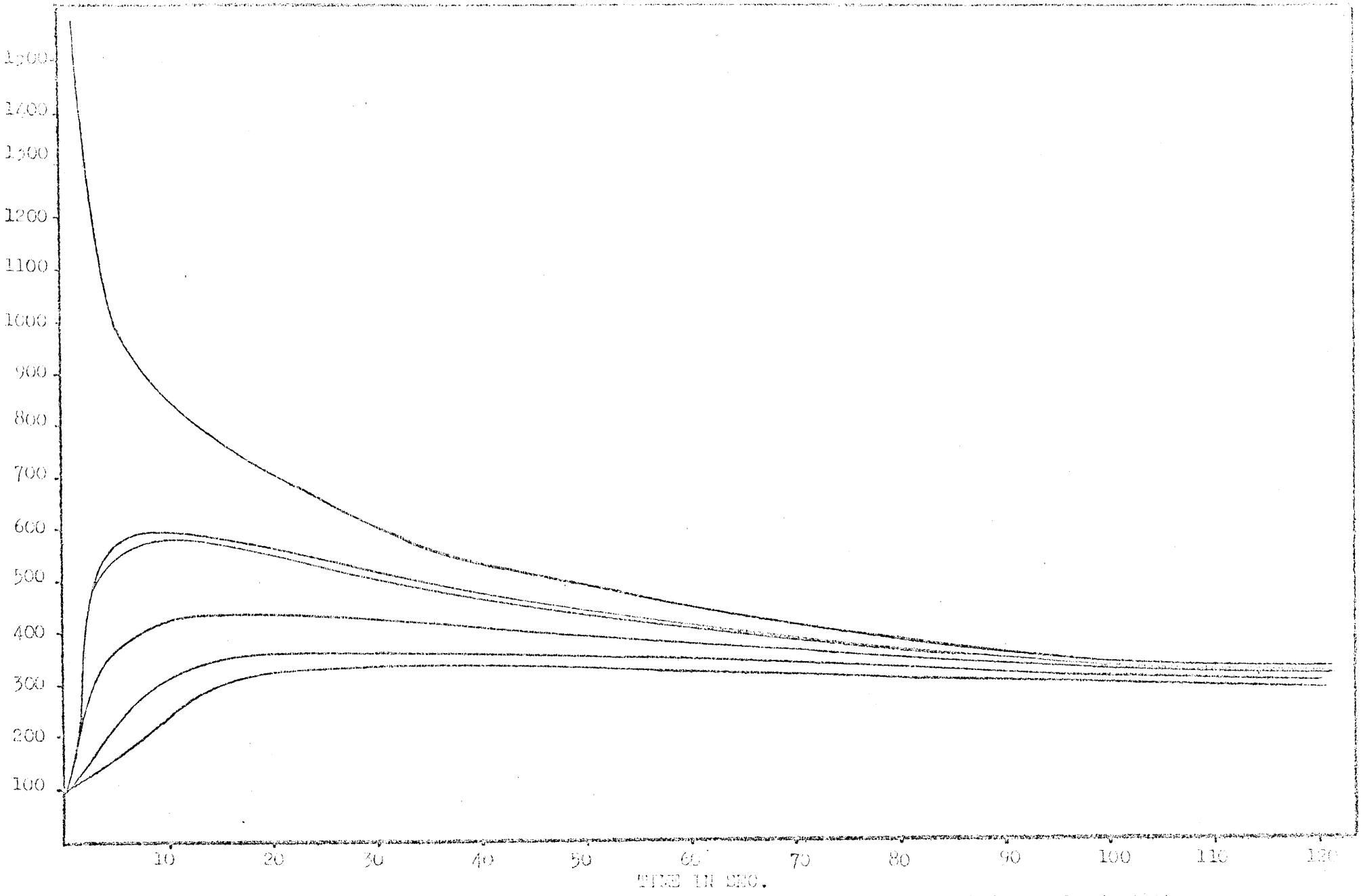


Figure 19 Continuous cooling curve and subsequent thermocycles for the third root bead at the weld deposit made at 650 amp - 300 mm/min.

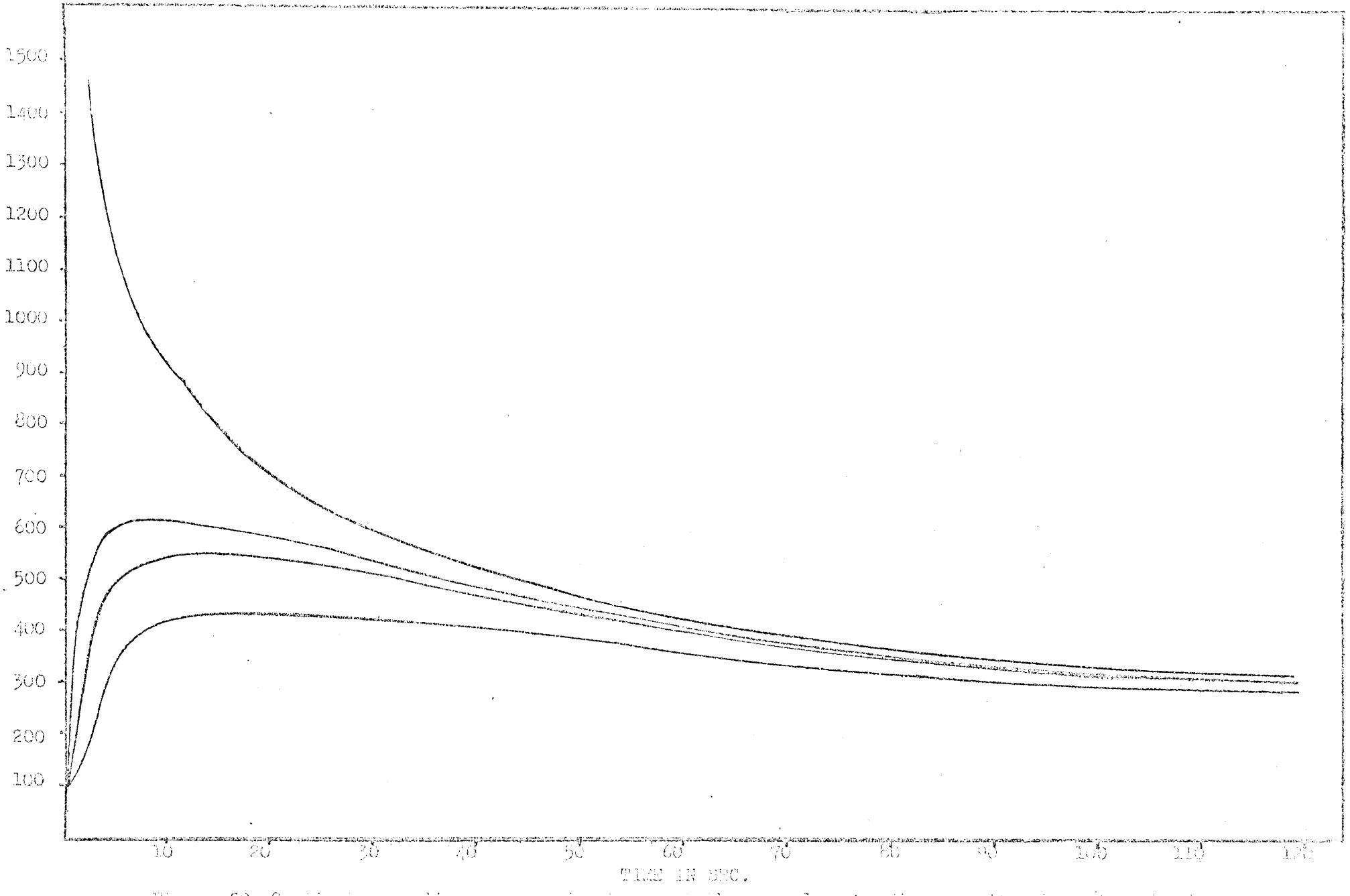


Figure 20 Continuous cooling curve and subsequent thermocycles for the seventh sub-surface bead of the weld deposit made at 650 amps - 700 m/min.

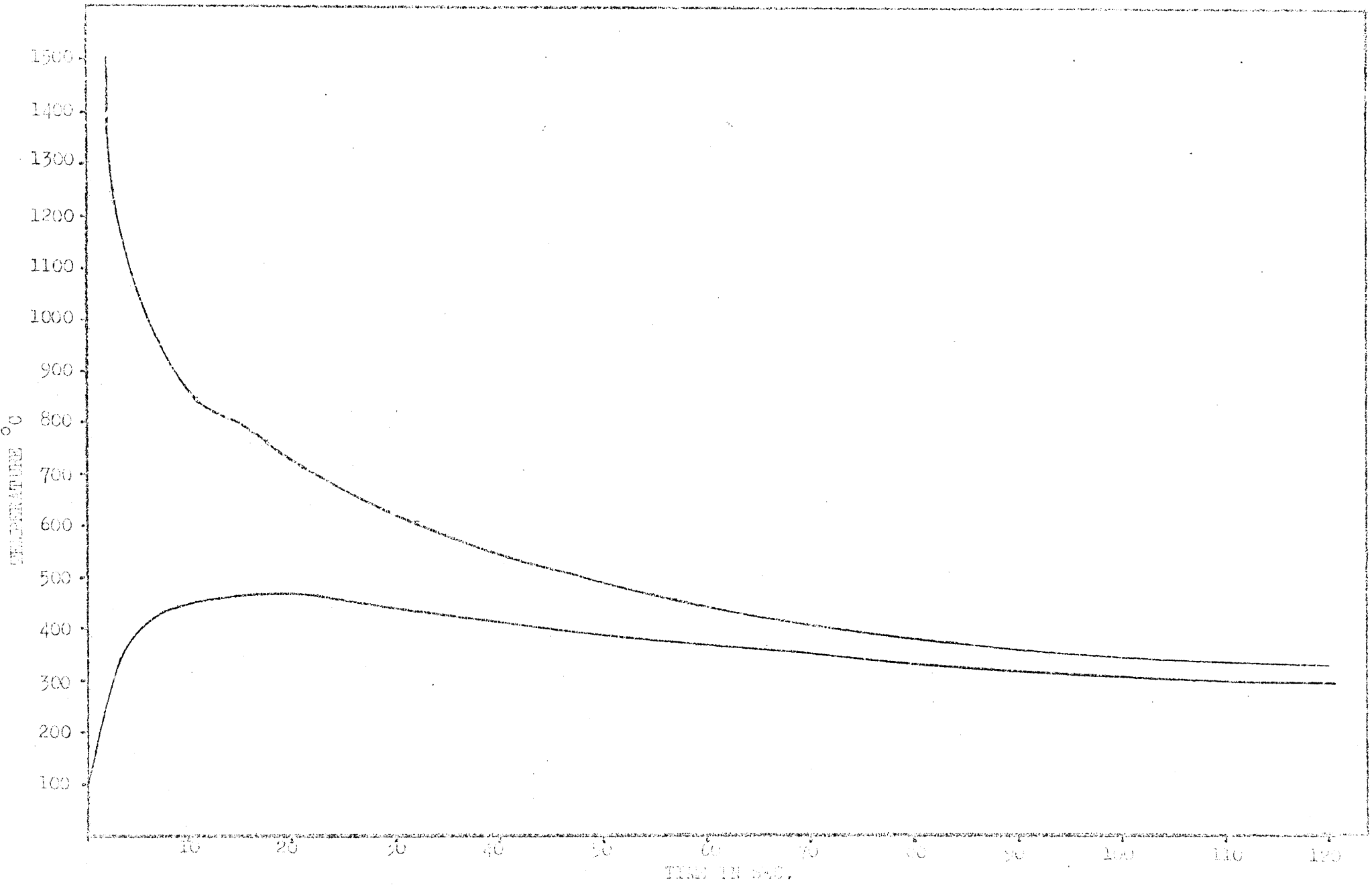


Figure 21 Continuous cooling curve and subsequent thermocycles for the eleventh sub-surface bead of the weld deposit made at 6% oxy - 3.5 cm/min.

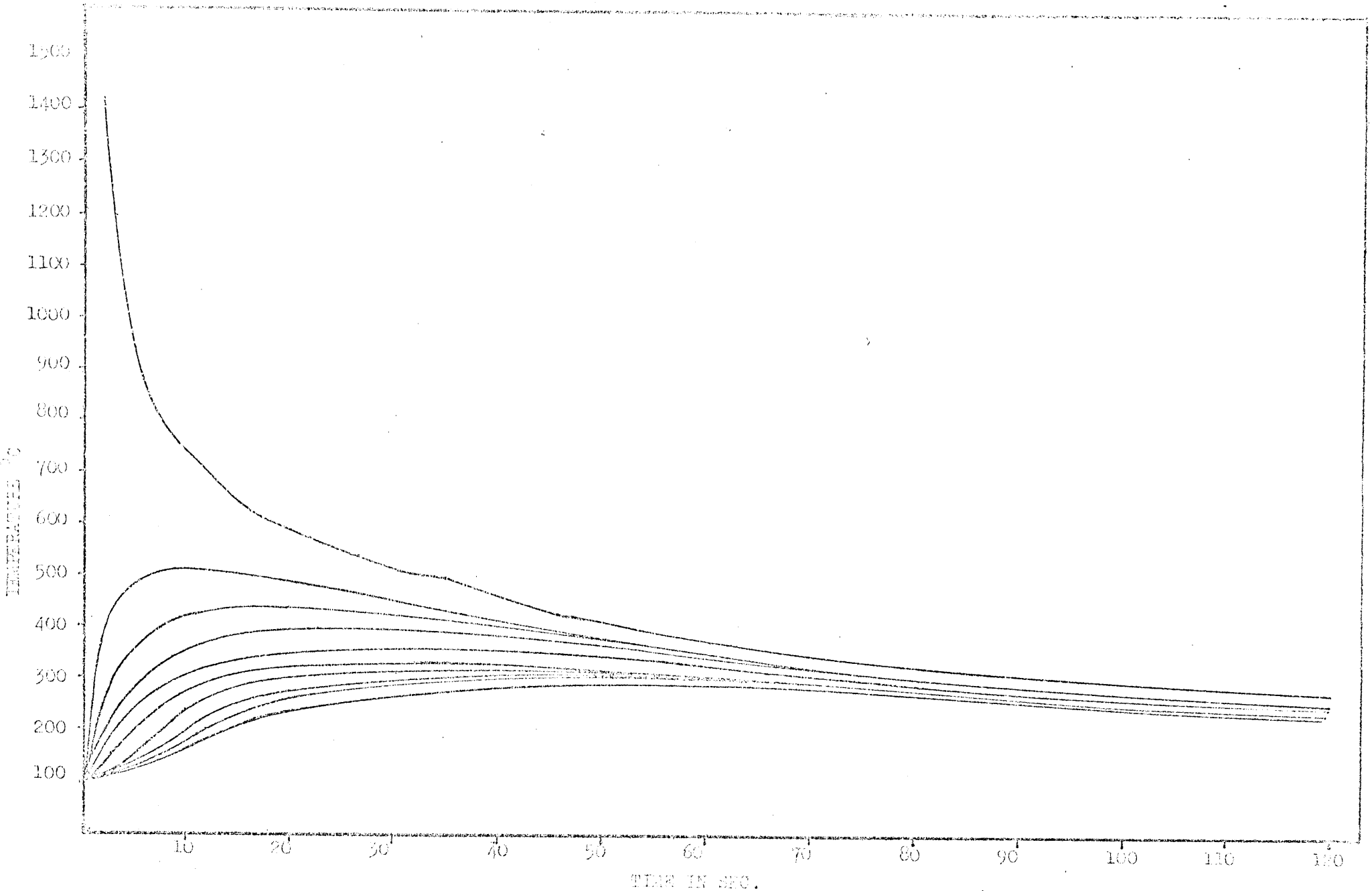


Figure 22 Continuous cooling curve and subsequent thermocycles for the first root bead of the weld deposit made at 650 amp - 400 mm/min.

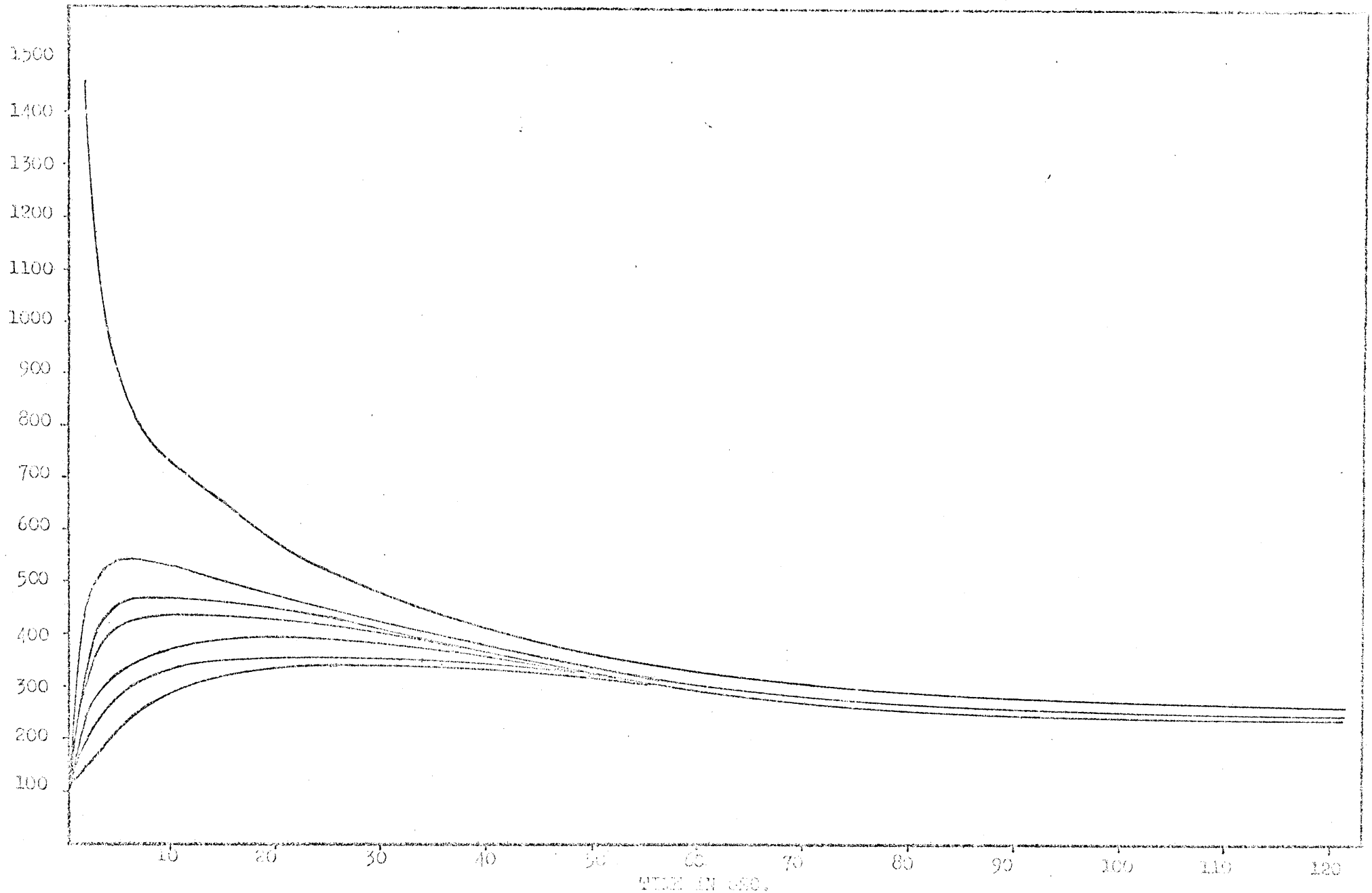


Figure26 Continuous cooling curve and subsequent thermocycles for the second root bead of the weld deposit made at 650 amp - 220 am/min.

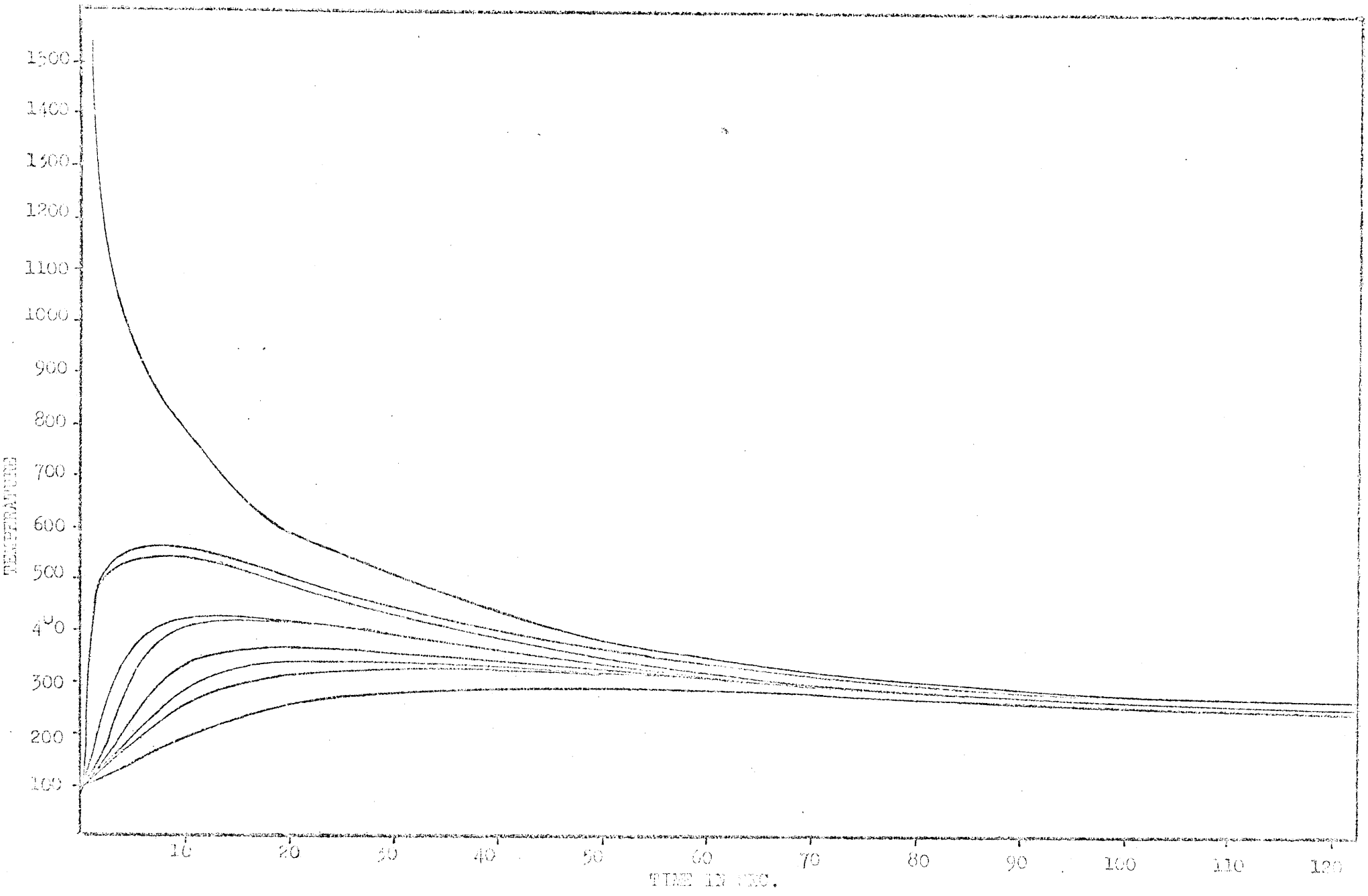


Figure 24 Continuous cooling curve and subsequent thermocycles for the third root bead of the weld deposit made at 650 amp - 400 mm/min.

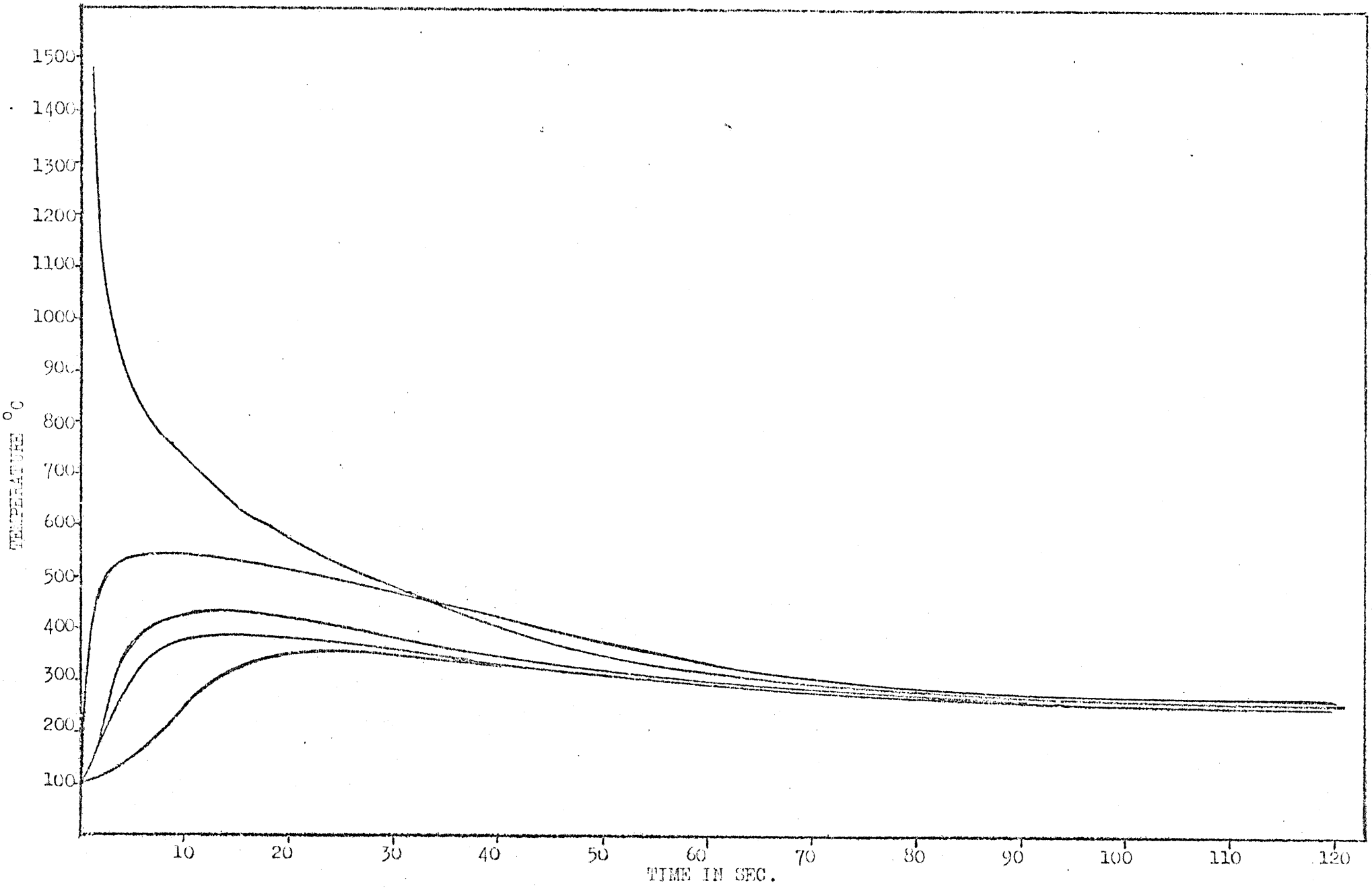


Figure 25 Continuous cooling curve and subsequent thermocycles for the eleventh sub-surface bead of the weld deposit made at 650 amp - 400 mm/min.

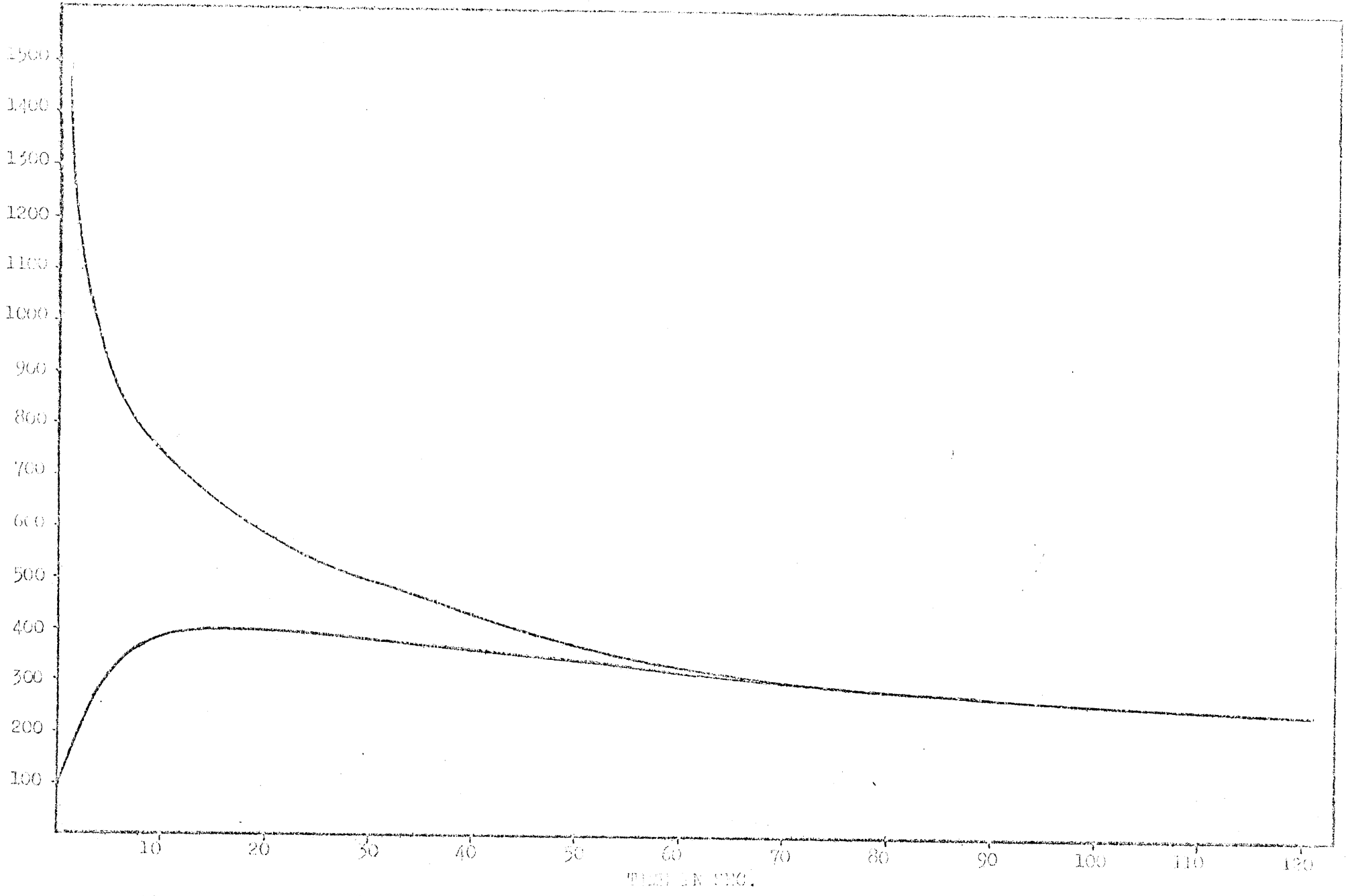


Figure 24 Continuous cooling curve and subsequent thermocycles for the 6th bead-on-plate bead of the weld deposit made at obr amp = 400 mm/min.

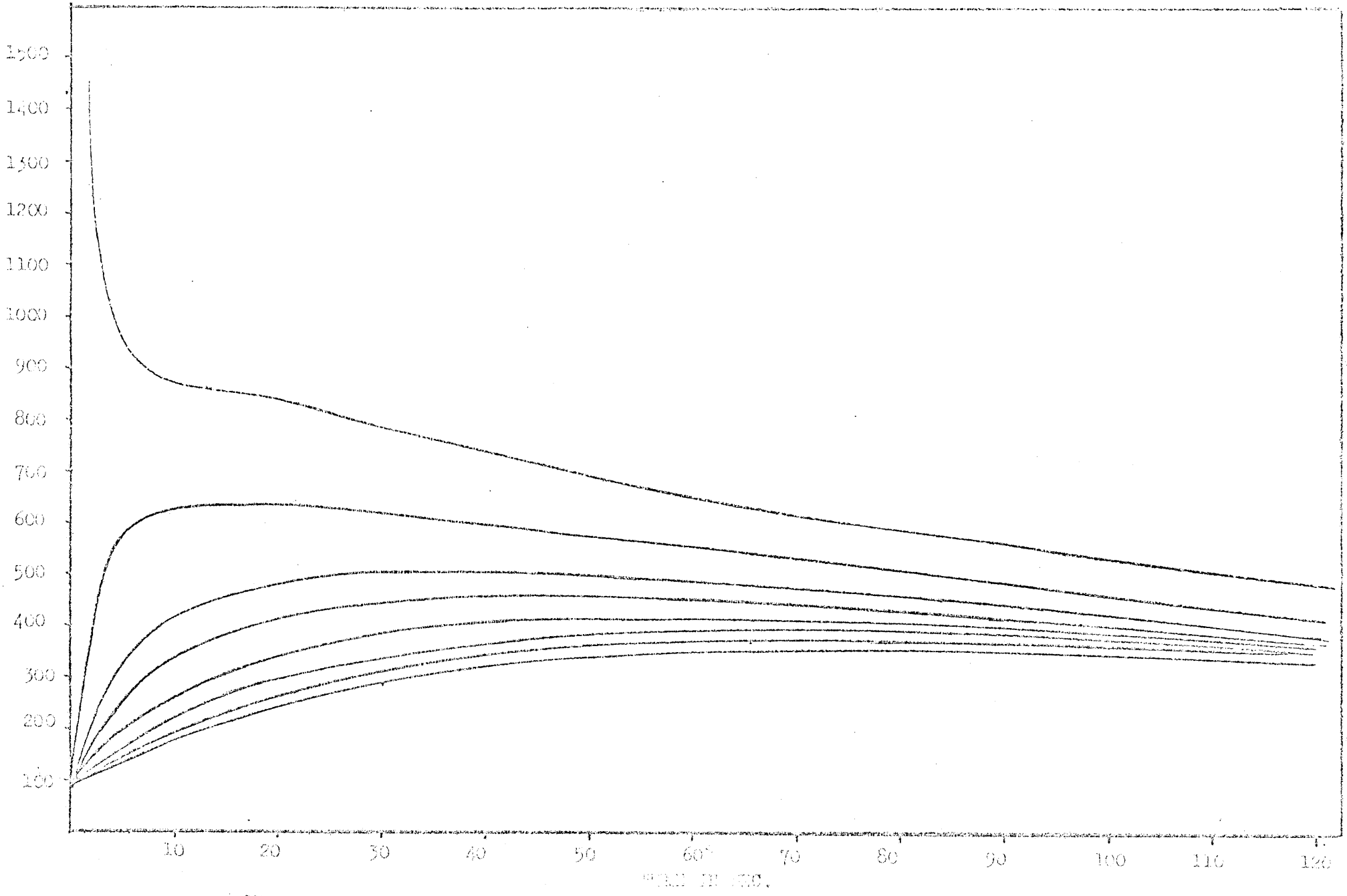


Figure 27 Continuous cooling curve and sub-grain diameters for the first weld bead of the weld deposit made at 500 amp - 300 mm/min.

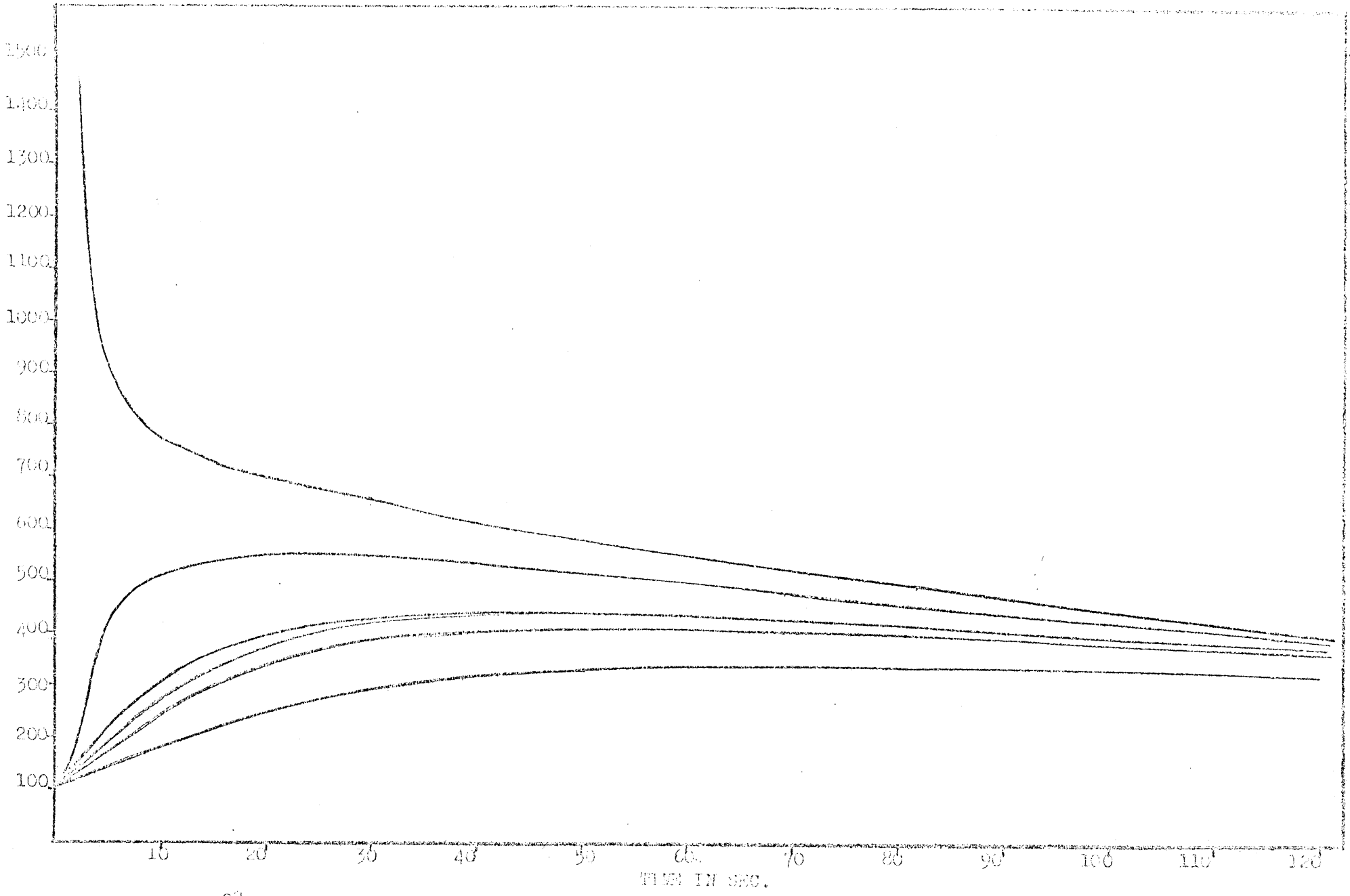


Figure 28 Continuous cooling curve and subsequent thermocycles for the second bead of the weld deposit made at 350 amp - 300 mm/min.

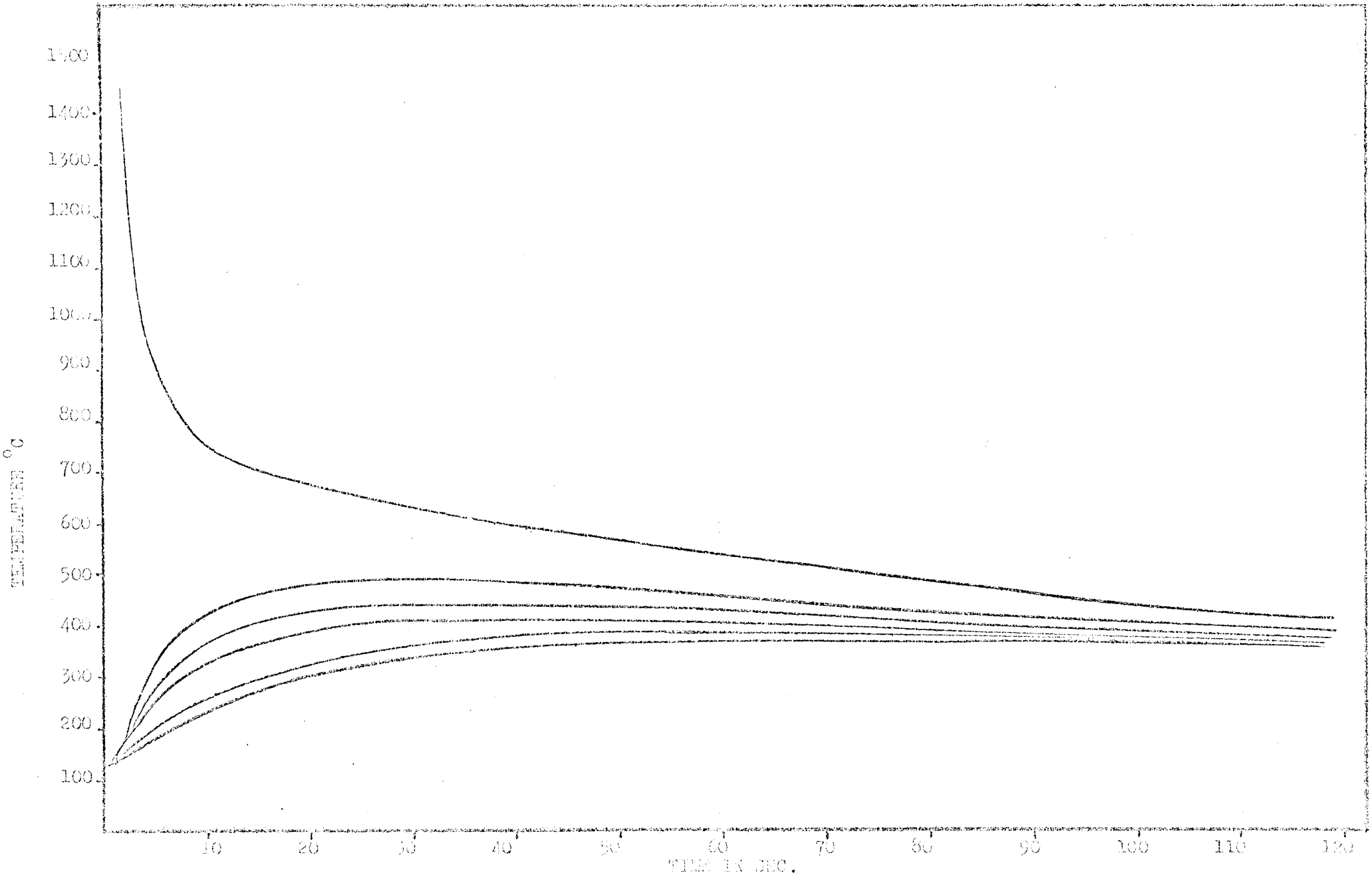


Figure 29 Continuous cooling curve and subsequent thermocycles for the third bead of the weld deposit made at 350 amp - 300 m/min.

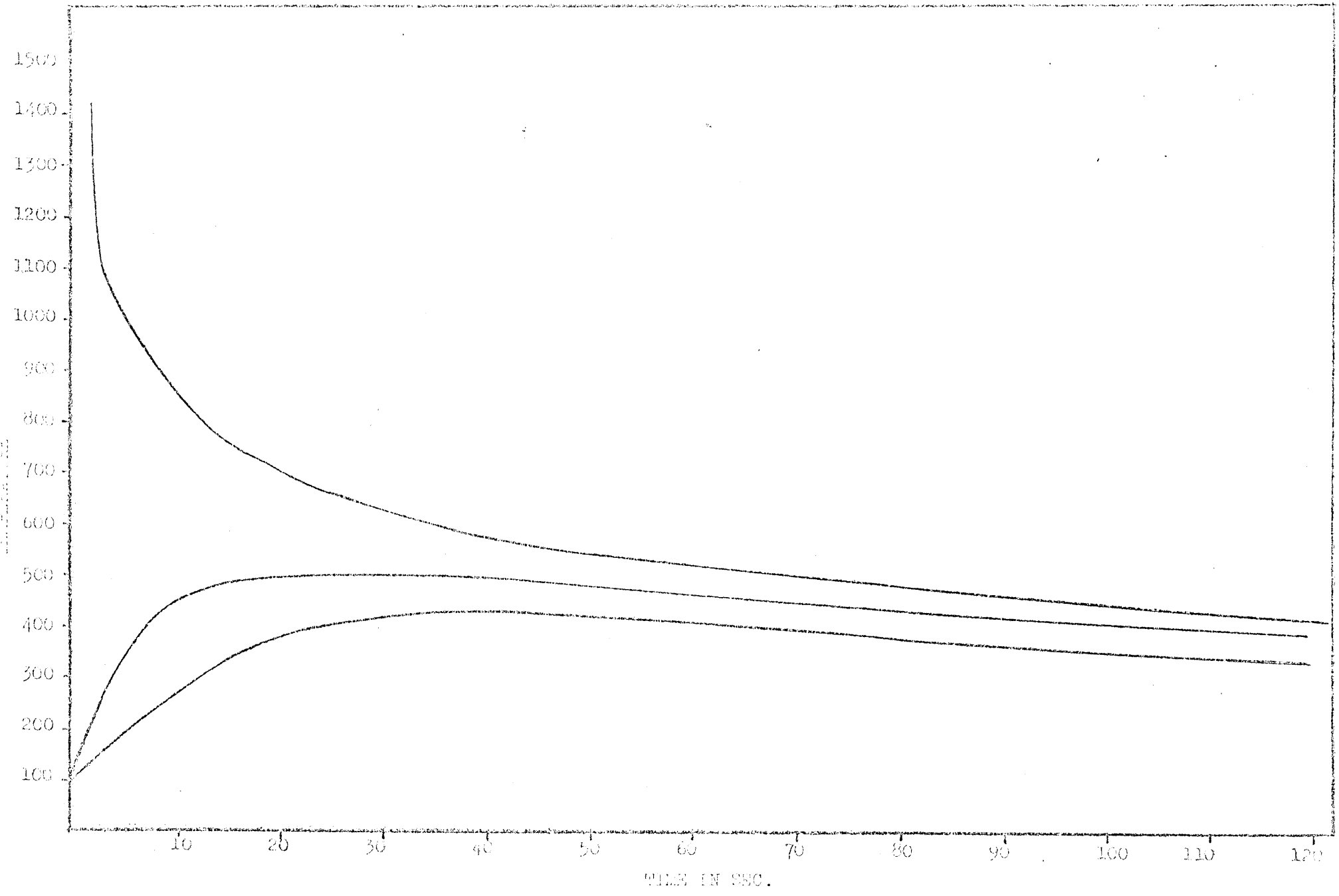


Figure 30 Continuous cooling curve and subsequent thermocycles for the sixth sub-surface bead of the weld deposit made at 850 amp - 300 mm/min.

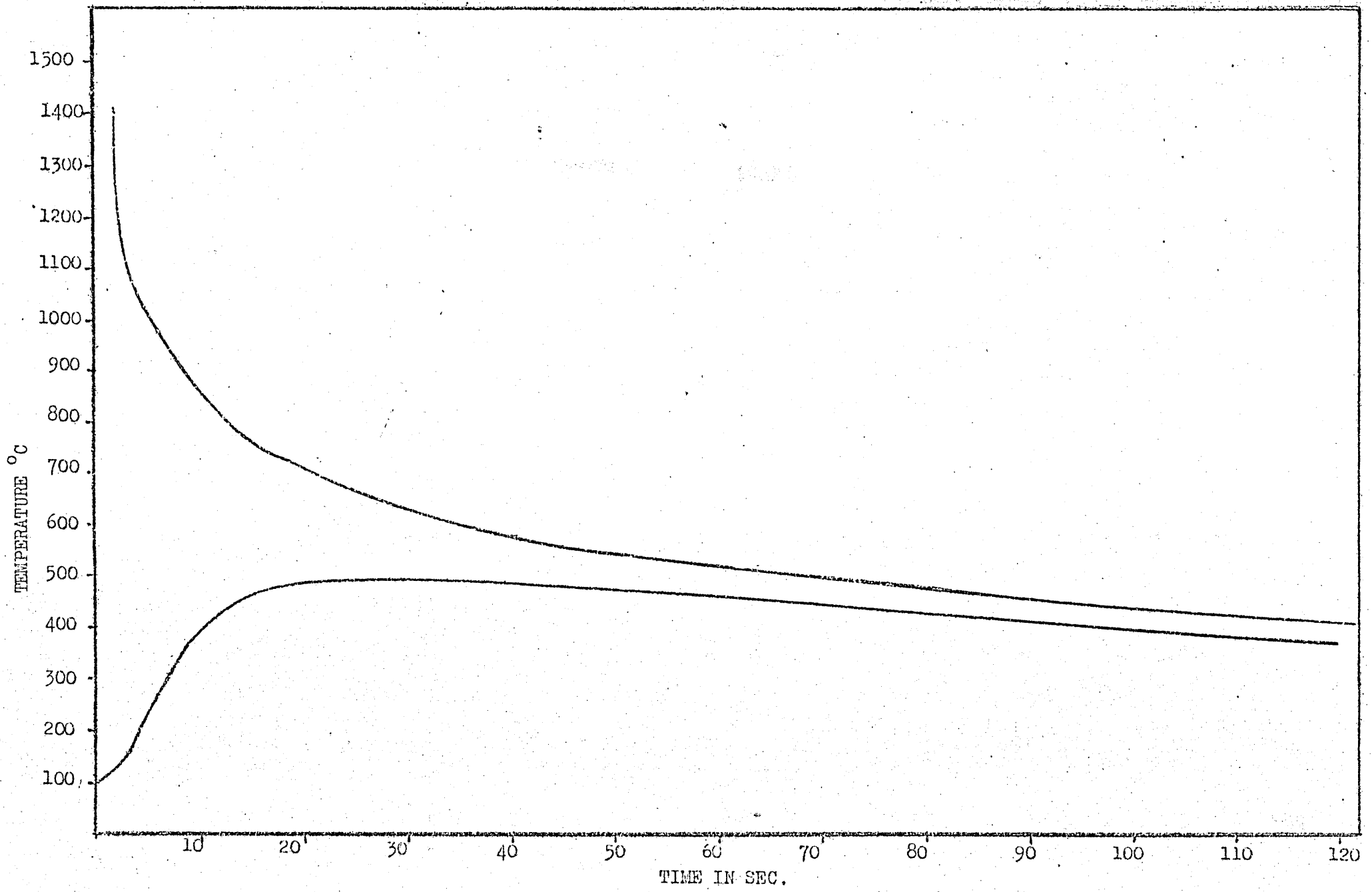


Figure 31 Continuous cooling curve and subsequent thermocycles for the eighth sub-surface bead of the weld deposit made at 850 amp - 300 mm/min.

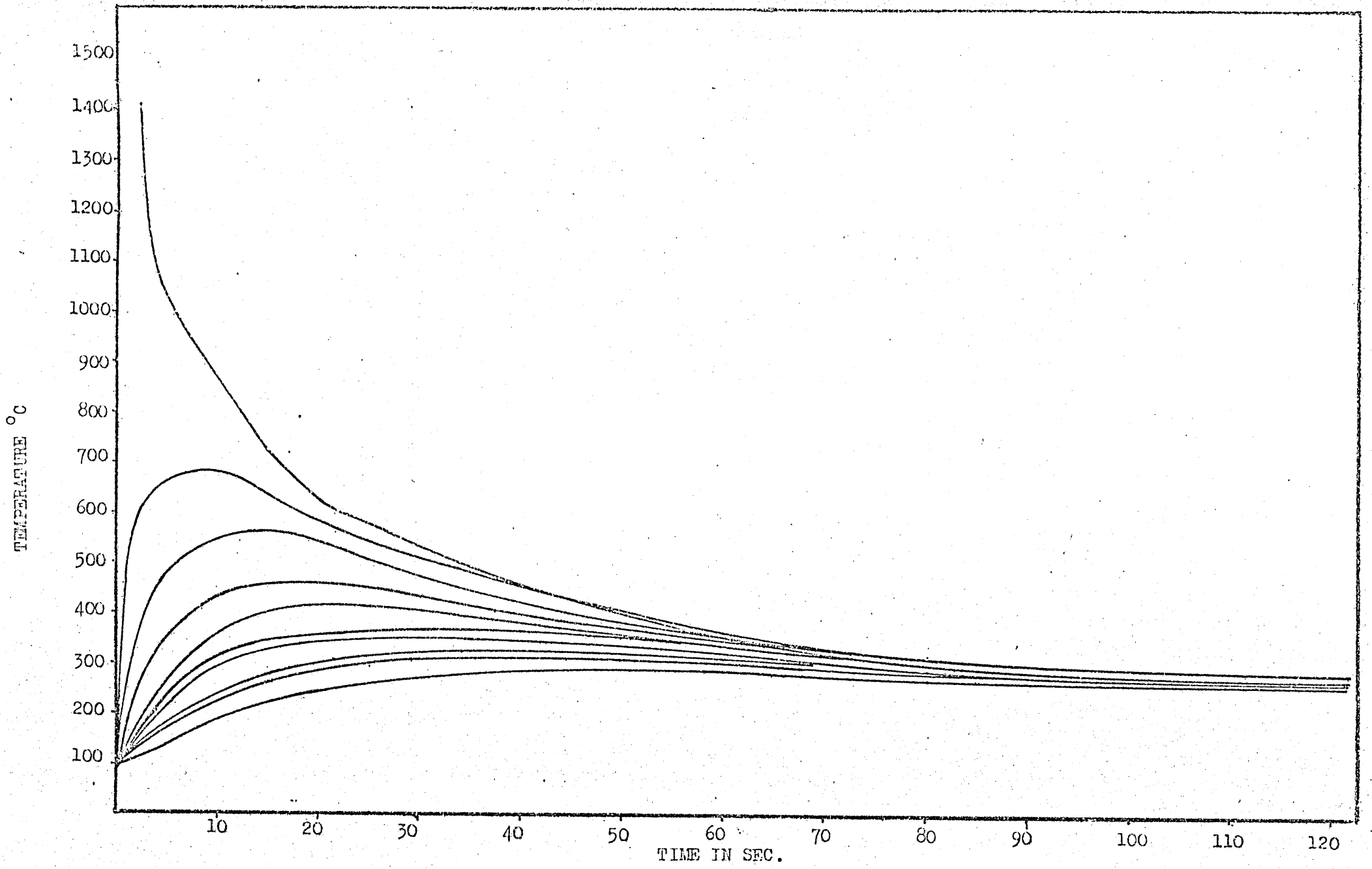


Figure 32 Continuous cooling curve and subsequent thermocycles for the first root bead of the weld deposit made at 480 amp - 300 mm/min.

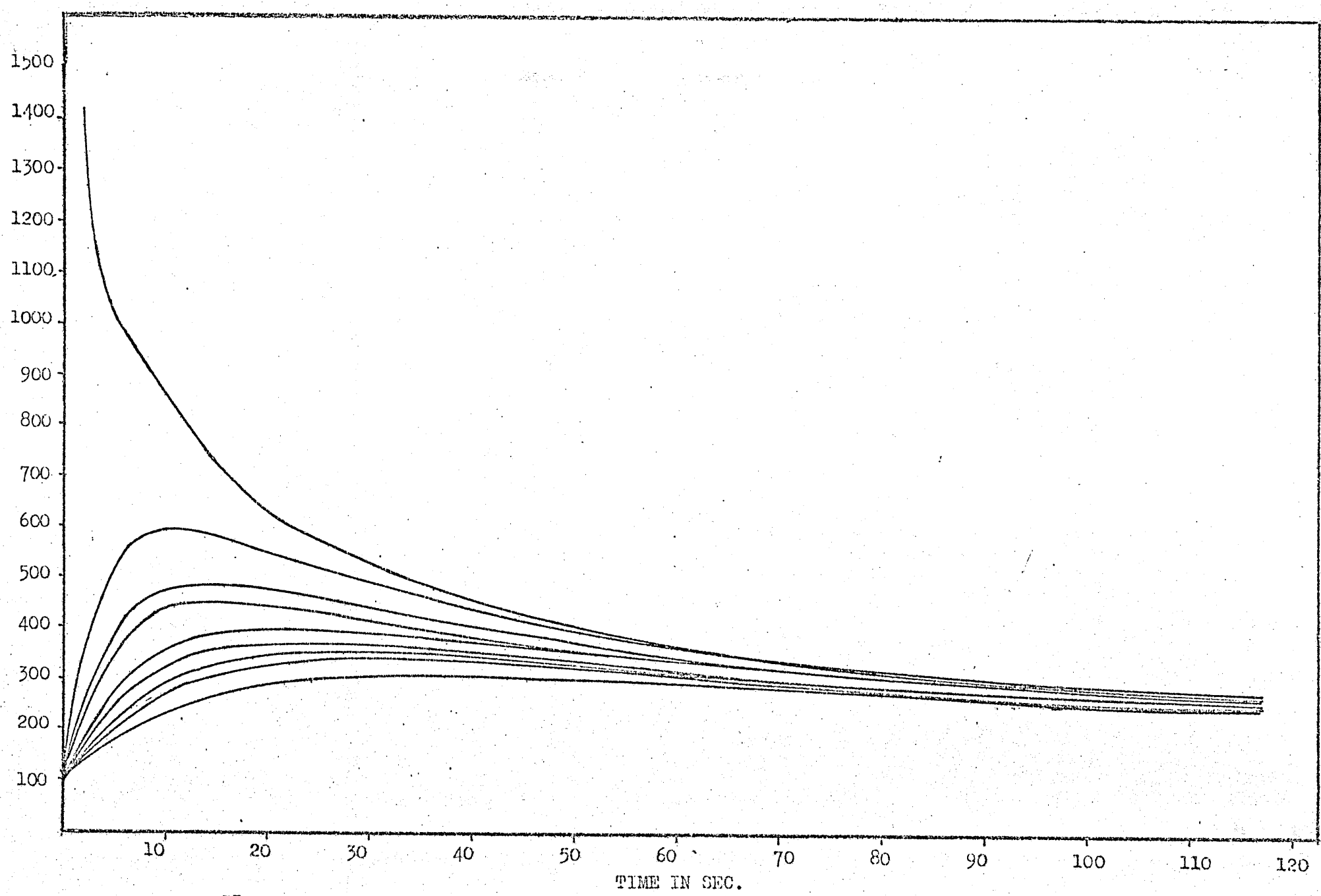


Figure 33 Continuous cooling curve and subsequent thermocycles for the second root bead of the weld deposit made at 480 amp - 300 mm/min.

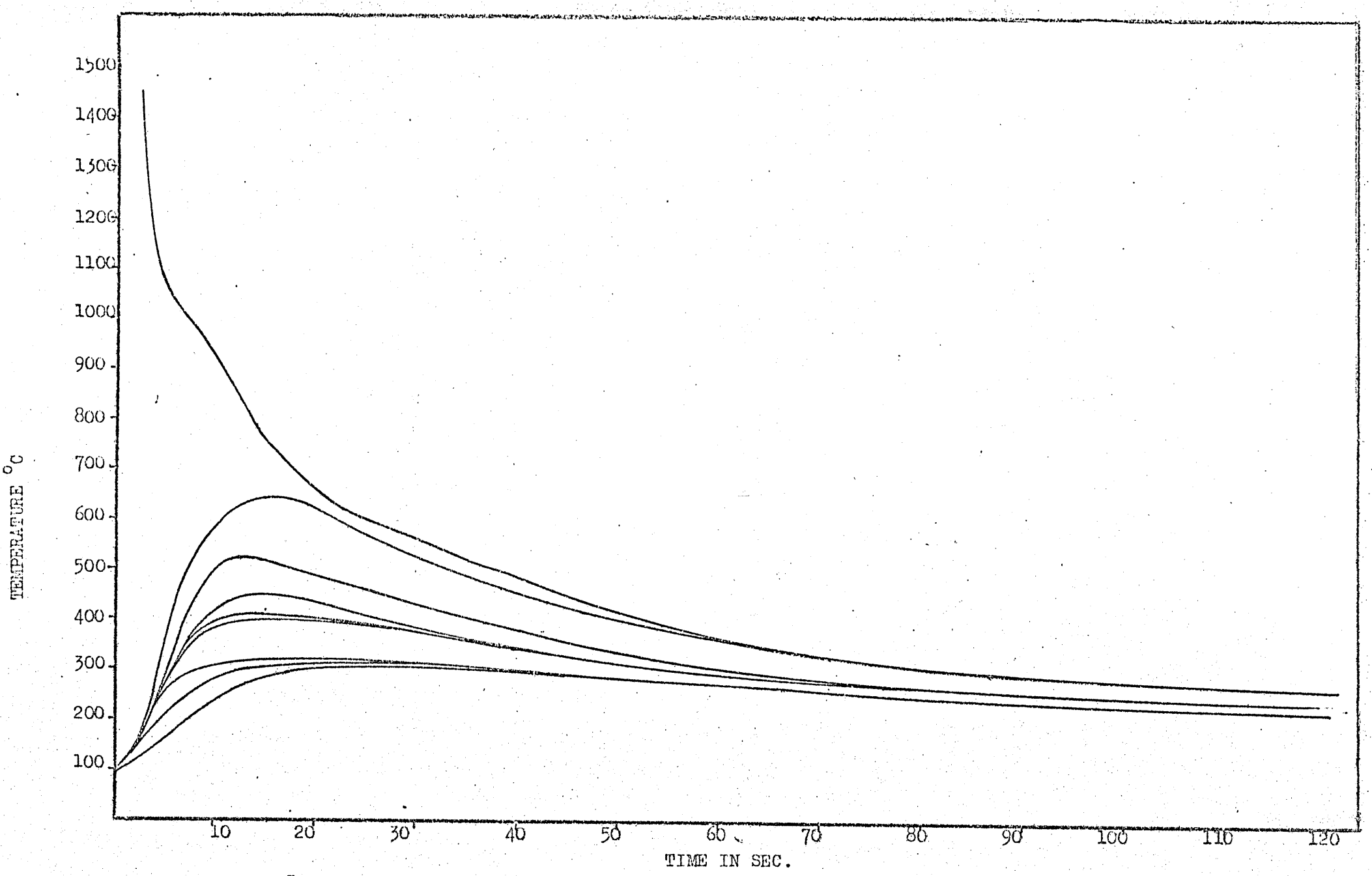


Figure 34 Continuous cooling curve and subsequent thermocycles for the third root bead of the weld deposit made at 480 amp - 300 mm/min.

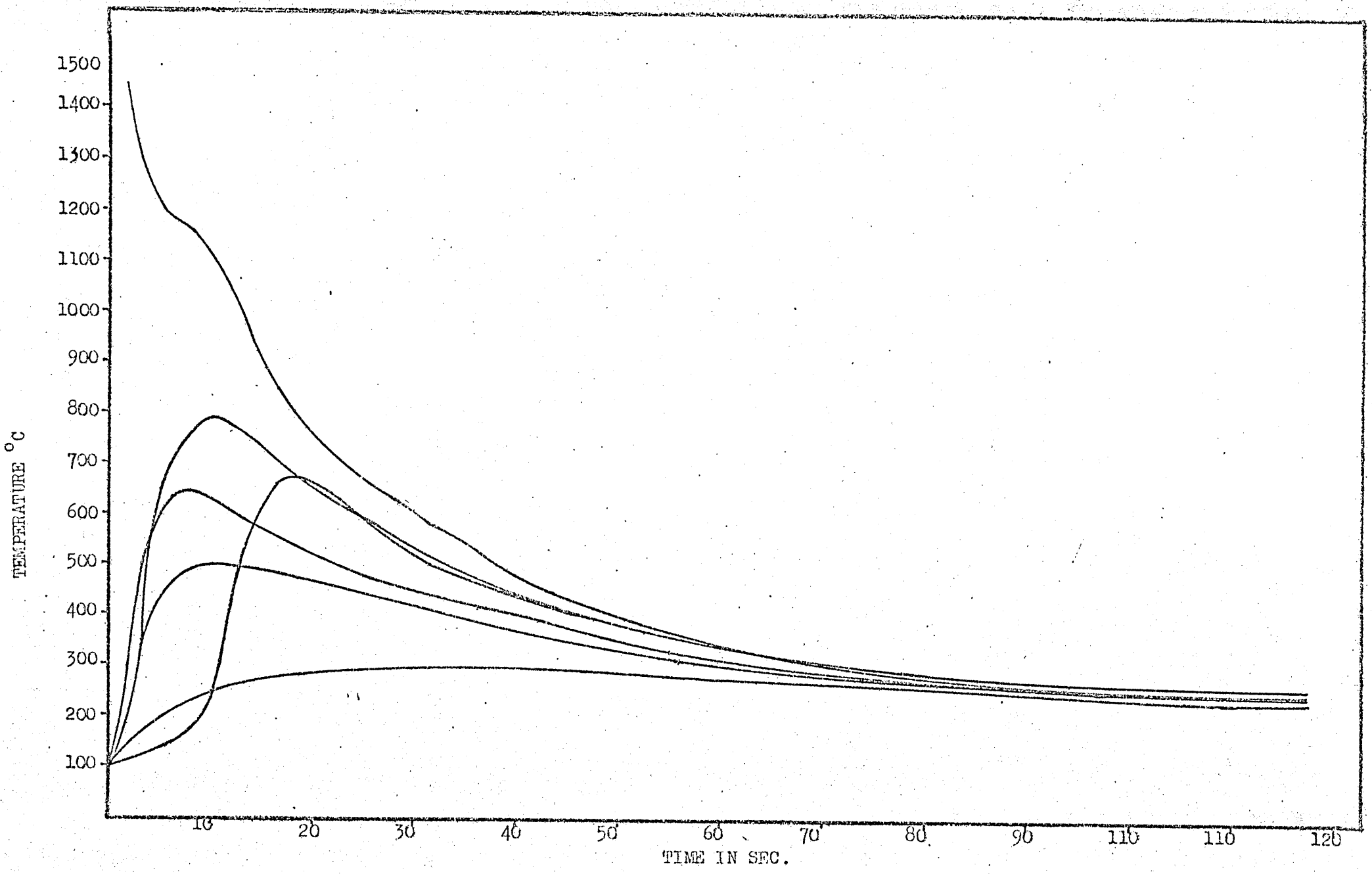


Figure 35 Continuous cooling curve and subsequent thermocycles for the eleventh sub-surface bead of the weld deposit made at 480 amp - 300 mm/min.

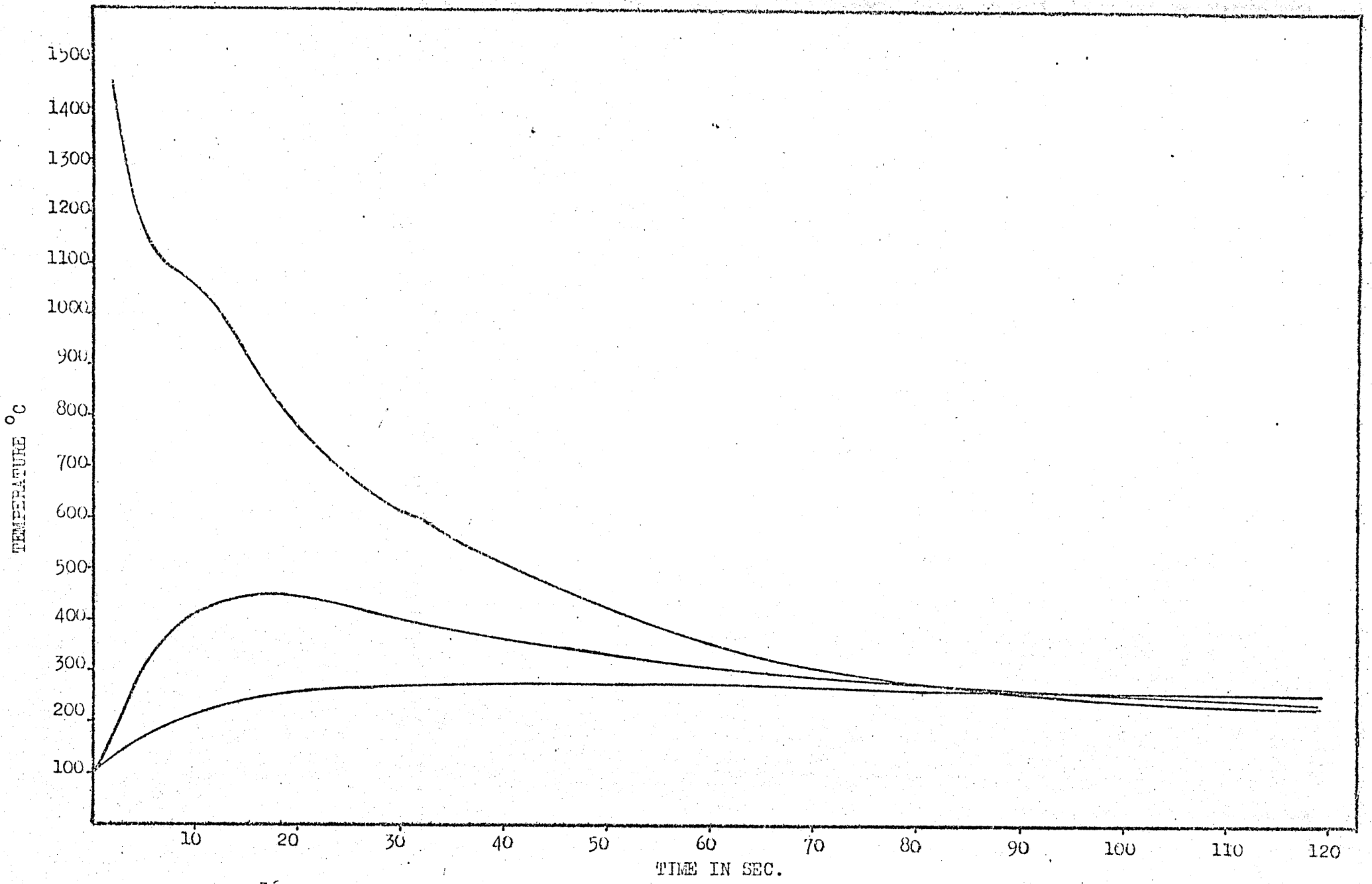


Figure 36 Continuous cooling curve and subsequent thermocycles for the fourteenth sub-surface bead of the weld deposit made at 480 amps - 300 mm/min.

Table 6 Weld metal Post-Solidification Thermal History Due to subsequent Weld Runs

| Welding Conditions | Run Number | CUMULATIVE TIME IN SEC. | | |
|---|---|---|---|---|
| | | Time at 600°C | Time at 500°C | Time at 400°C |
| 650 AMPS 200 mm/min | 1 | 36 | 127 | 387 |
| | 2 | 30 | 110 | 435 |
| | 3 | 25 | 87 | 325 |
| | 7 | 45 | 97 | 200 |
| | 9 | - | - | - |
| | Average of 1, 2, 3 | 30 | 108 | 382 |
| 650 AMPS 300 mm/min | 1 | - | 32 | 142 |
| | 2 | 5 | 37 | 125 |
| | 3 | - | 57 | 140 |
| | 7 | 7 | 61 | 61 |
| | 9 | - | - | 40 |
| | Average of 1, 2, 3 | 1.6 | 42 | 135 |
| 650 AMPS 400 mm/min | 1 | - | 10 | 67 |
| | 2 | - | 11 | 62 |
| | 3 | - | 32 | 105 |
| | 11 | - | 20 | 60 |
| | 14 | - | - | 12 |
| | Average of 1, 2, 3 | - | 17 | 78 |
| 850 AMPS 300 mm/min | 1 | 27.5 | 75 | 255 |
| | 2 | - | 50 | 250 |
| | 3 | - | - | 200 |
| | 6 | - | 12 | 100 |
| | 8 | - | - | 70 |
| | Average of 1, 2, 3 | 9 | 41 | 235 |
| 480 AMPS 300 mm/min | 1 | 17 | 50 | 120 |
| | 2 | 1 | 24 | 112 |
| | 3 | 11 | 35 | 77.5 |
| | 11 | 38.5 | 70 | 155 |
| | 14 | - | - | 22 |
| | Average of 1, 2, 3 | 9.6 | 36 | 103 |

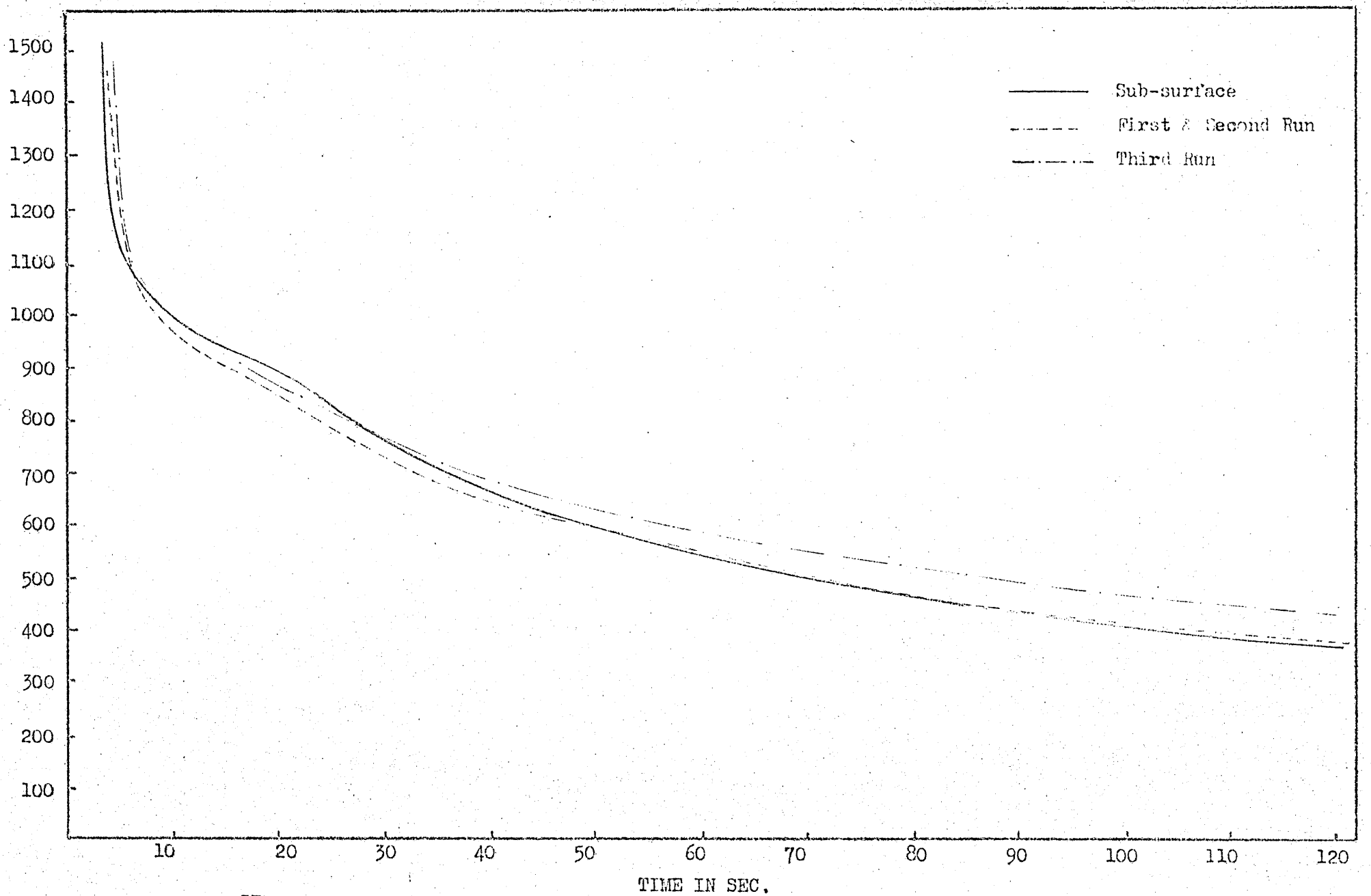


Figure 37 Continuous cooling curves for the first, second, third and sub-surface beads for the weld deposit made at 650 amp - 200 mm/min.

Table 7 Weld Deposit 650 Amps - 200 mm/min

| Weld Run | Average Cooling Rate in °C/sec. | | |
|---|---|---|---|
| | 1400°C - 900°C | 900°C - 700°C | 700°C - 500°C |
| 1 | 45 | 11.1 | 5.6 |
| 2 | 41.6 | 10.2 | 5.3 |
| 3 | 50 | 8.5 | 4.1 |
| 7 | 31.2 | 11.4 | 5.7 |
| 9 | 33.3 | 12.1 | 6.15 |

Weld Deposit 650 Amps - 300 mm/min

The sub-surface and roots run cooling curves and average cooling rates are shown in figure 38 and table 8.

These results show that the root weld bead had a higher cooling rate than the sub-surface (142°C/sec; 66.6°C/sec) for the temperature range 1400°C - 900°C.

For the temperature range 900°C - 700°C the sub-surface and root had similar cooling rates (14.8°C/sec; 15.3°C/sec). For the temperature range 700°C - 500°C the root had a lower cooling rate than the sub-surface (5.6°C/sec; 7.5°C/sec).

The weld run No. 7 did not follow the general pattern and had a lower cooling rate than all other weld runs for the 1400°C - 900°C temperature range but a higher cooling rate for the 900°C - 700°C and 700°C - 500°C.

The average times at temperature for the root area was 1.6 sec at 600°C, 42 sec at 500°C and 135 sec at 400°C while the sub-surface area did not exceed 500°C and was only 40 sec at 400°C. Table 6.

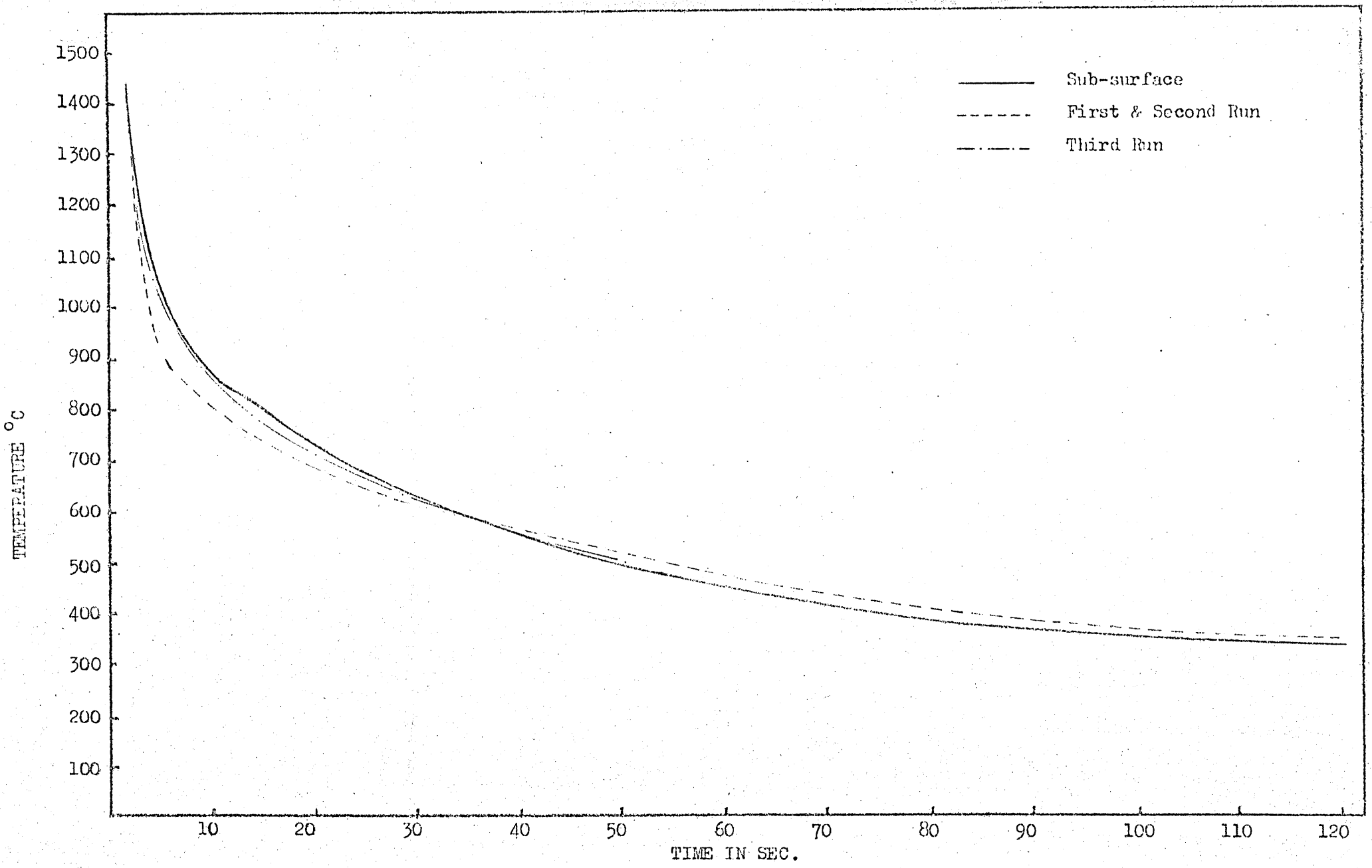


Figure 38 Continuous cooling curve for the first, second, third and sub-surface beads of the weld deposit made at 650 amp - 300 mm/min.

Table 8 Weld Deposit 650 amp. - 300 mm/min

| Weld Run | Average Cooling Rate in °C/sec. | | |
|---|---|---|---|
| | 1400°C - 900°C | 900°C - 700°C | 700°C - 500°C |
| 1 | 142 | 15.3 | 5.6 |
| 2 | 166 | 16 | 5.3 |
| 3 | 83 | 15.3 | 7.2 |
| 7 | 58.8 | 22.2 | 8.3 |
| 9 | 66.6 | 14.8 | 7.5 |

Weld Deposit 650 amp - 400 mm/min

The sub-surface and root run cooling curve and average cooling rates are shown in figure 39 and table 9.

The results show that the root had a marginally lower cooling rate than the sub-surface (142°C/sec; 160°C/sec) for the temperature range 1400°C - 900°C.

For the temperature range 900°C - 700°C the root had a higher cooling rate than the sub-surface (30.9°C/sec; 26°C/sec) but for the temperature range 700°C - 500°C the root had a lower cooling rate than the sub-surface (8.8°C/sec; 11.4°C/sec).

The average times at temperature for the root area were 17 sec at 500°C and 178 sec at 400°C while the sub-surface area did not exceed 500°C and was only at or above 400°C for 12 sec. Table 6 .

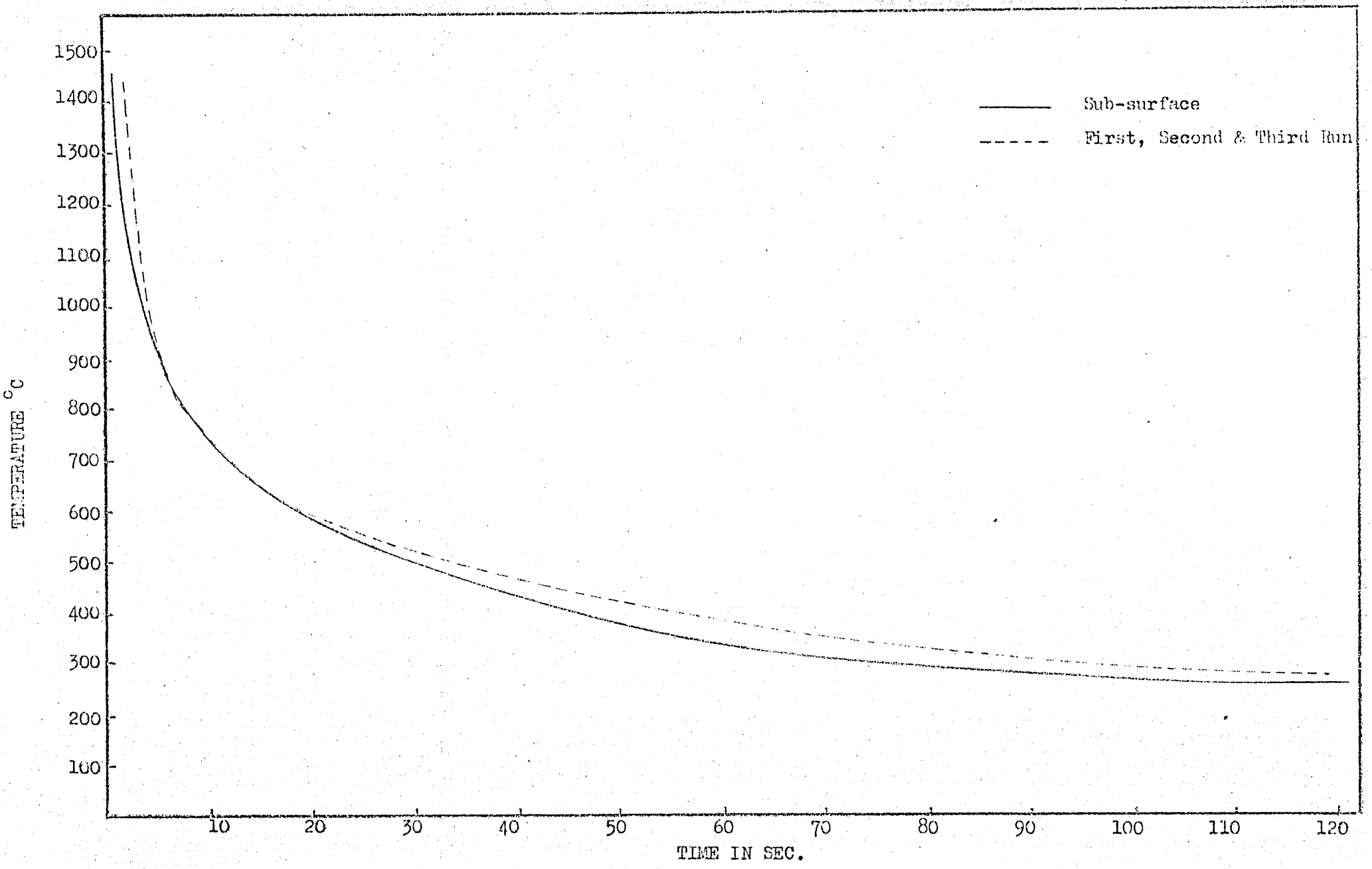


Figure 39 Continuous cooling curve for the first, second, third and sub-surface beads of the weld deposit made at 650 amp - 400 mm/min.

Table 9 Weld Deposit 650 amps - 400mm/min

| Weld Run | Average Cooling Rate in °C/sec. | | |
|---|---|---|---|
| | 1400°C - 900°C | 900°C - 700°C | 700°C - 500°C |
| 1 | 142 | 30.7 | 8.8 |
| 2 | 166 | 30.7 | 11.4 |
| 3 | 100 | 26.6 | 11.1 |
| 11 | 160 | 26 | 12.1 |
| 14 | 160 | 26 | 11.4 |

Weld Deposit 850 amp - 300 mm/min

The sub-surface and root run cooling curves and average cooling rates are shown in figure 40 and table 10.

For this welding condition as for all other weld deposits the weld metal cooling rate was different for the sub-surface and root runs, but a significant variation in the weld metal cooling rate was also found between the first three weld runs and in particular between the first and second run.

For the 1400°C - 900°C temperature range the variation between the first three weld runs was not large and only a marginal increase in cooling rate occured between the first and the other two runs, (100°C/sec; 166°C/sec and 142°C/sec). But for the 900°C - 700°C temperature range the cooling rate was found to vary considerably for each run (47°C/sec; 14.5°C/sec and 20°C/sec). For the 700°C - 500°C temperature range all three root runs had a similar cooling rate value (3.2°C/sec; 3.3°C/sec and 3.3°C/sec).

Comparing only the results for the root and the sub-surface run, as these two runs represent the two most extreme conditions, it was found that the root run had higher average cooling rate than the sub-surface (100°C/sec; 71°C/sec) for the temperature range 1400°C - 900°C.

For the temperature range 900°C - 700°C the situation reversed and the sub-surface weld run had a much higher cooling rate than the root bead (16.6°C/sec; 4.7°C/sec).

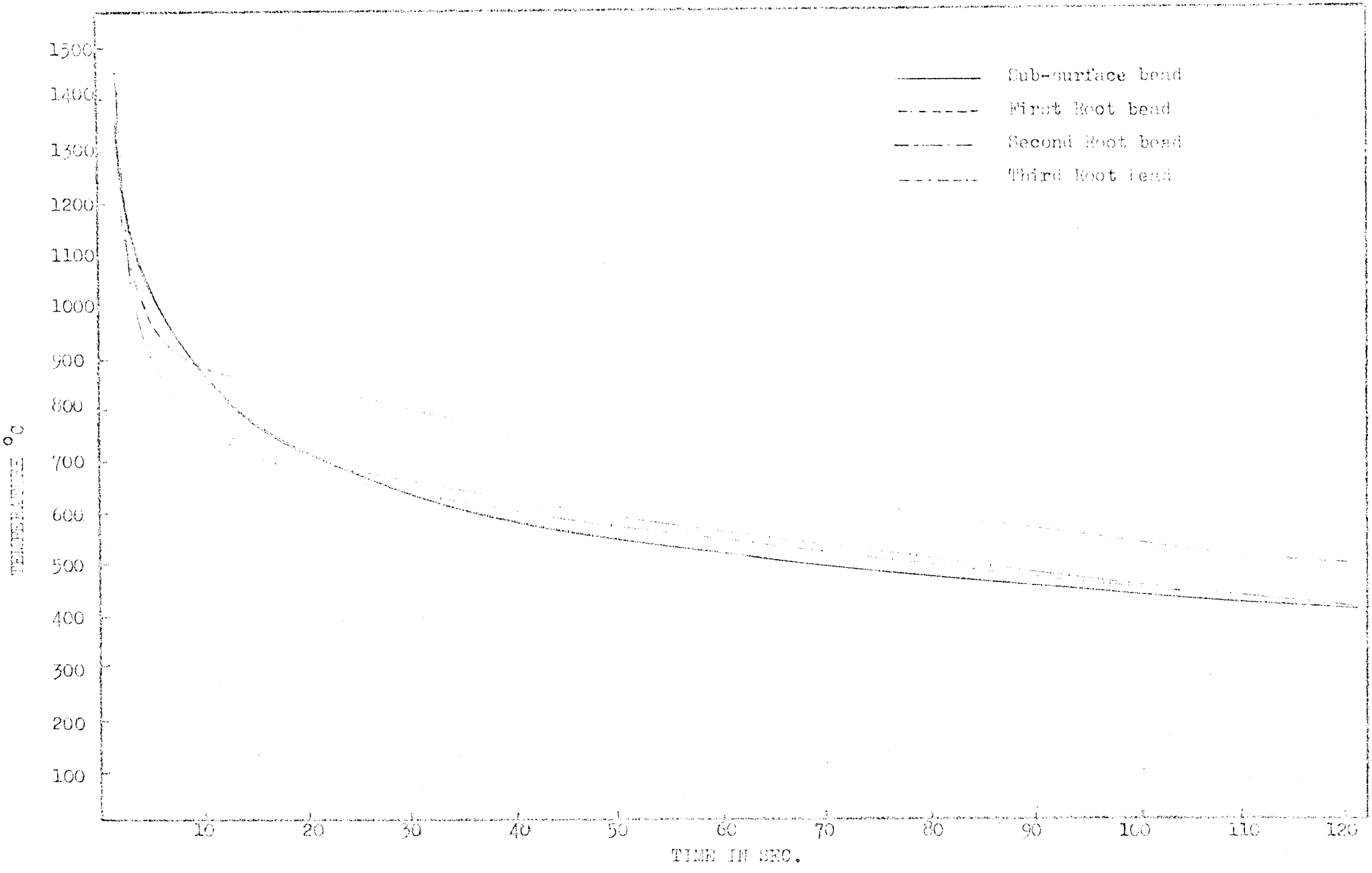


Figure 40 Continuous cooling curve for the first, second, third and sub-surface beads of the weld deposit made at 150 amp - 300 mm/min.

For the 700°C - 500°C both root and sub-surface weld runs had similar cooling rates (3.2°C/sec and 3.6°C/sec).

The average times at temperature for the root area was 9 sec at 600°C, 41 sec at 500°C and 235 sec at 400°C, whilst the sub-surface area did not exceed 500°C and was only at 400°C for 70 sec. Table 6.

Table 10 Weld Deposit 850 amps - 300 mm/min

| Weld Run | Average Cooling Rate in °C/sec. | | |
|---|---|---|---|
| | 1400°C - 900°C | 900°C - 700°C | 700°C - 500°C |
| 1 | 100 | 4.7 | 3.2 |
| 2 | 166 | 14.5 | 3.3 |
| 3 | 142 | 20 | 3.3 |
| 6 | 71 | 16.6 | 3.6 |
| 8 | 71 | 16.6 | 3.6 |

Weld Deposit 480 amps - 300 mm/min

The sub-surface and root run cooling curves and average cooling rates are shown in figures 41 and table 11.

The results show that the root had a considerably higher cooling rate than the sub-surface (76.9°C/sec; 35°C/sec) for the temperature range 1400°C - 900°C.

For the temperature range 900°C - 700°C the root had a marginally higher cooling rate than the sub-surface (28.5°C/sec; 25°C/sec).

For the temperature range 700°C - 500°C the situation reversed and the root bead had a slightly lower cooling rate than the sub-surface bead (10.5°C/sec; 15.2°C/sec).

The average times at temperature for the root region was 9.6 sec at 600°C, 36 sec at 500°C and 103 sec at 400°C whilst the sub-surface only reached the temperature of 400°C for 22 sec. Table 6 .

Table 11 Weld Deposit 480 amps - 300 mm/min

| Weld Run | Average Cooling Rate in °C/sec. | | |
|---|---|---|---|
| | 1400°C - 900°C | 900°C - 700°C | 700°C - 500°C |
| 1 | 76.9 | 28.5 | 10.5 |
| 2 | 76.9 | 26.6 | 11.4 |
| 3 | 58.8 | 28.5 | 9.5 |
| 11 | 35 | 24 | 12.9 |
| 14 | 35 | 23 | 15.2 |

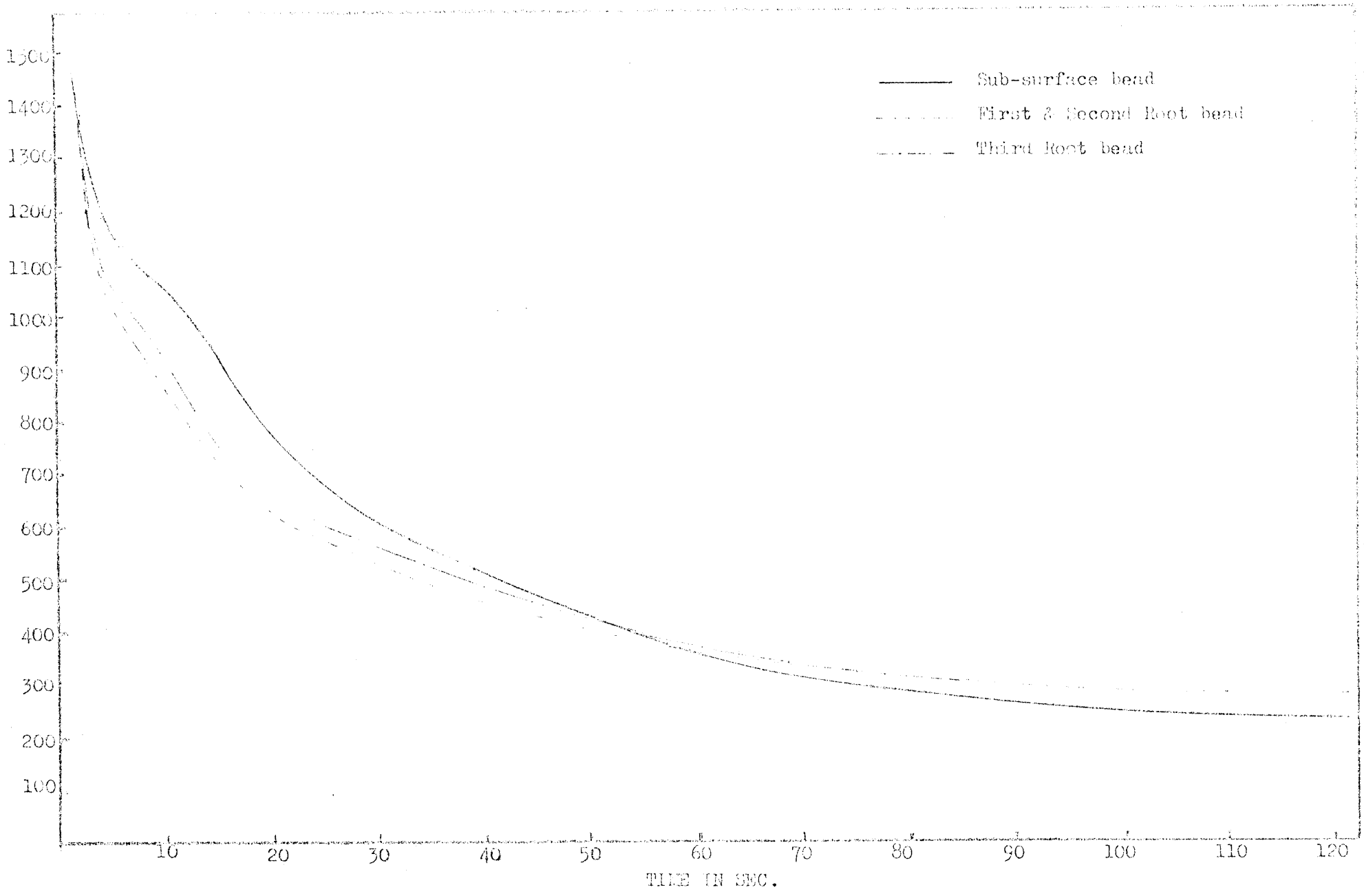


Figure 41 Continuous cooling curve for the first, second, third and sub-surface beads of the weld deposit made at 480 amp - 300 mm/min.

## Comparison between the Weld Deposits made at the same Calculated Heat Input

### Weld Deposits with a Calculated Heat Input of 5.8 KJ/mm

#### Sub-surface region

The cooling curves for the sub-surface region of the weld deposits made at 650 amps - 200 mm/min and 850 amps - 300 mm/min are shown in figure 42.

The weld deposit made at 650 amps - 200 mm/min had a much lower average cooling rate than the 850 amps - 300 mm/min weld. ($33^{\circ}C$/sec; $71^{\circ}C$/sec) for the temperature range $1400^{\circ}C$ - $900^{\circ}C$.

For the temperature range $900^{\circ}C$ - $700^{\circ}C$ the 650 amps - 200 mm weld had again a lower cooling rate than the 850 amps - 300 mm weld ($12.1^{\circ}C$/sec; $16.6^{\circ}C$/sec) but for the temperature range $700^{\circ}C$ - $500^{\circ}C$ the situation reversed and the 650 amps - 200 mm weld had a higher cooling rate than the 850 amps - 300mm/min weld. ($6.15^{\circ}C$/sec; $3.6^{\circ}C$/sec).

The average times at temperature were also different for these two weld deposits. The 850 amps - 300 mm weld exceeded $400^{\circ}C$ for 22 sec whilst the 650 amps - 300 mm/min did not reach $400^{\circ}C$. Table 6 .

#### Root region

The cooling curves for the root beads are shown in figure 43.

The 650 amps - 200 mm/min weld deposit had a lower average cooling rate than the 850 amps - 300 mm weld ($45^{\circ}C$/sec and $100^{\circ}C$/sec) for the temperature range $1400^{\circ}C$ - $900^{\circ}C$).

The situation reversed for the $900^{\circ}C$ - $700^{\circ}C$ and $700^{\circ}C$ - $500^{\circ}C$ temperature ranges. The 650 amps - 200 mm/min weld having a higher average cooling rate than the 850 amps - 300 mm/min weld ($11.1^{\circ}C$/sec; $4.7^{\circ}C$/sec) and ($5.6^{\circ}C$/sec; $3.2^{\circ}C$/sec).

The average times at temperature were again different for each weld: the 650 amps - 200 mm/min weld exceeded $600^{\circ}C$ for 30 sec, was at $500^{\circ}C$ for 108 sec and at $400^{\circ}C$ for 382 sec, whilst the 850 amps - 300 mm/min weld was only 9 sec at $600^{\circ}C$, 41 sec at $500^{\circ}C$ and 235 sec at $400^{\circ}C$. Table 6.

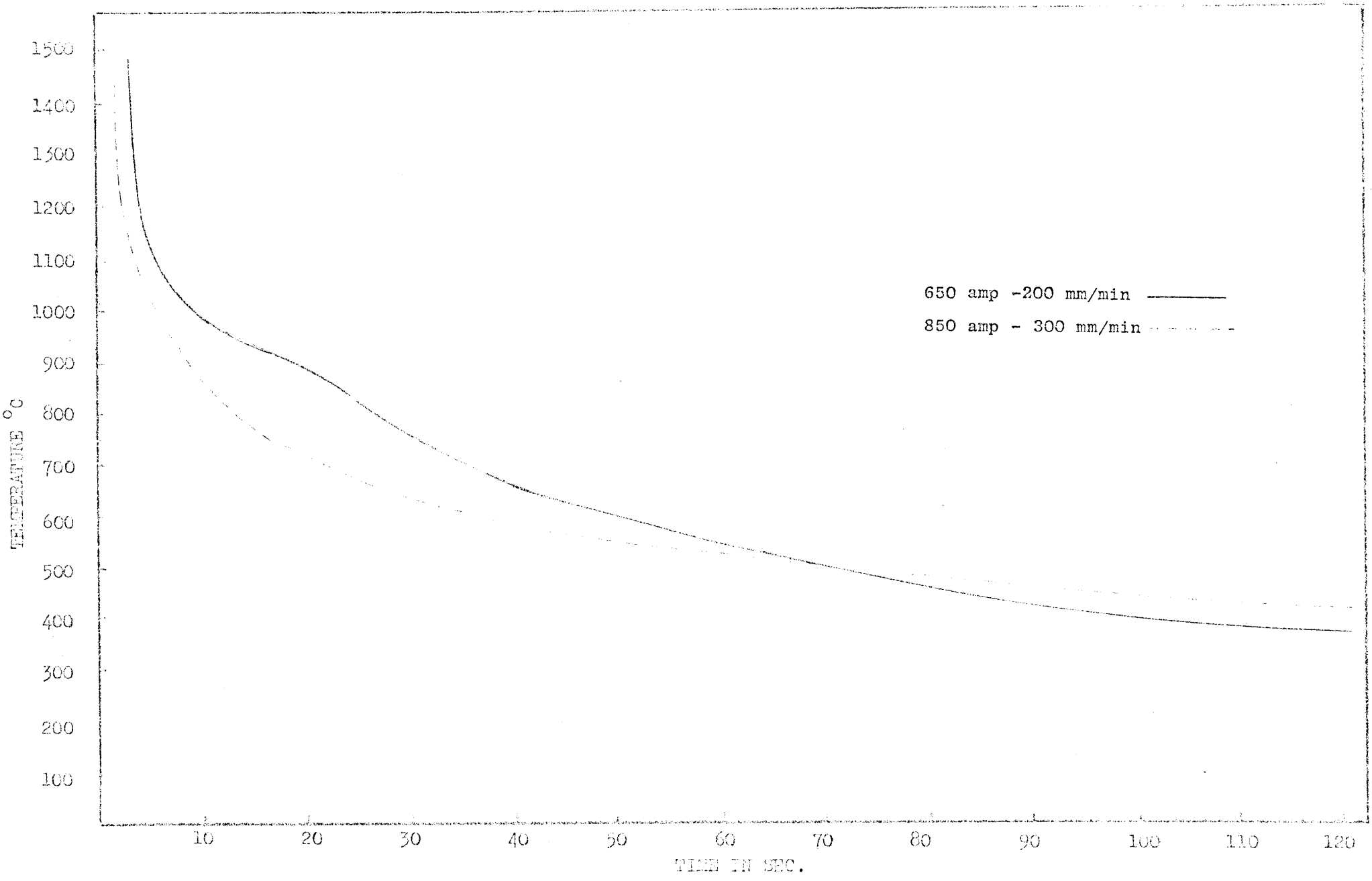


Figure 42 Continuous cooling curve for the sub-surface beads of the weld deposits made at 650 amp - 200 mm/min and 850 amp - 300 mm/min. (5.8 KJ/mm).

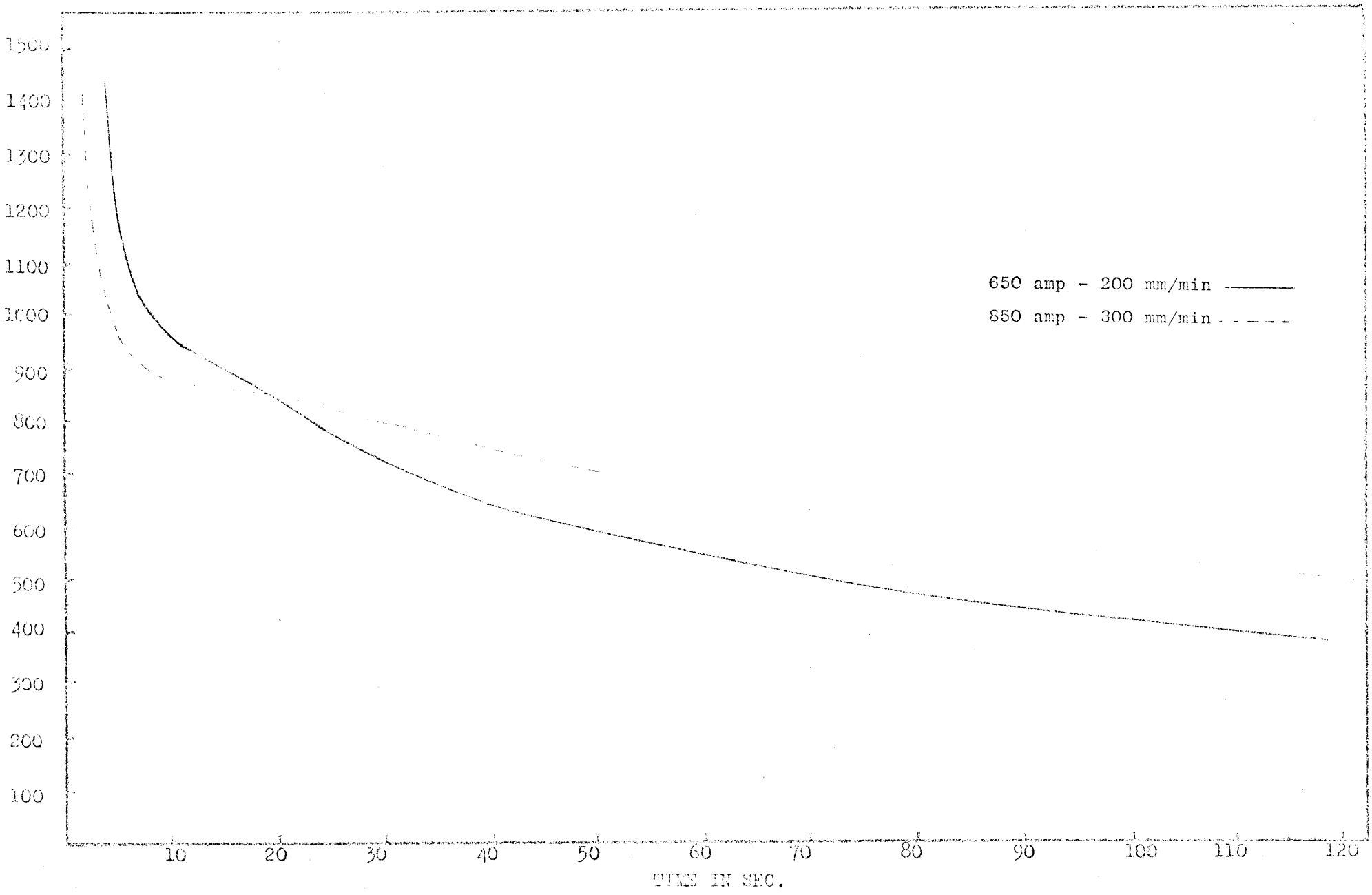


Figure 43 Continuous cooling curve for the first root beads of the weld deposits made at 650 amp - 200 mm/min and 850 amp - 300 mm/min. (5.3 KJ/mm).

Weld Deposits with a Calculated Heat Input of 2.9 KJ/mm.

Sub-surface region

The cooling curves for the sub-surface of the weld deposit made at 650 amps - 300 mm/min and 480 amps - 300 mm/min are shown in figure 44.

The weld deposit made at 650 amps - 400 mm/min had a much higher cooling rate than the 480 amps - 300 mm/min (160°C/sec; 35°C/sec) in the temperature range 1400°C - 900°C.

For the 900°C - 700°C temperature range the 650 amps - 400 mm weld had again a higher cooling rate than the 480 amps - 300 mm/min (26°C/sec; 23°C/sec), but for the 700°C - 500°C temperature range the situation reversed and the 650 amps - 300 mm/min weld had a lower cooling rate than the 480 amps - 300 mm/min (11.4°C/sec; 15.2°C/sec).

The average times at temperature were different for each weld deposit.

The 650 amps - 400 mm/min weld was 12 sec at 400°C whilst the 480 amps - 300 mm/min weld was 22 sec at 400°C.

It is important to note that due to the small bead size of the 480 amps - 300 mm/min weld bead (no. 11) which was directly beneath the central sub-surface one was possibly more representative of the Charpy specimen heat cycle, and in this case the weld bead reached a peak temperature of 800°C and was at 600°C for 38.5 sec, at 500°C for 70 sec and at 400°C for 155 sec. Table 6.

Root Region

The cooling curves for the root of the weld deposit made at 650 amps - 400 mm/min and 480 amps - 300 mm/min are shown in figure 45.

The 650 amps - 400 mm/min weld had a higher cooling rate than the 480 amps - 300 mm/min (142°C/sec; 76°C/sec) for the temperature range 1400°C - 900°C.

For the 900°C - 700°C temperature range again the 650 amps - 400 mm/min weld had a marginally higher cooling rate than the 480 amps - 300 mm/min weld (30.7°C/sec; 28.5°C/sec).

For the 700°C - 500°C temperature range the situation reversed and the 650 amps - 400 mm/min weld had a lower cooling rate than the 480 amps - 300 mm/min weld (8.8°C/sec; 10.5°C/sec).

The average times at temperature was also different for each weld deposit.

The 650 amps - 400 mm/min did not exceed a temperature of 600°C, was at 500°C for 17 sec and at 400°C for 78 sec, whilst

the 480 amps - 300 mm/ min weld was at 600°C for 9.6 sec, at 500°C for 36 sec and at 400°C for 103 sec. Table 6.

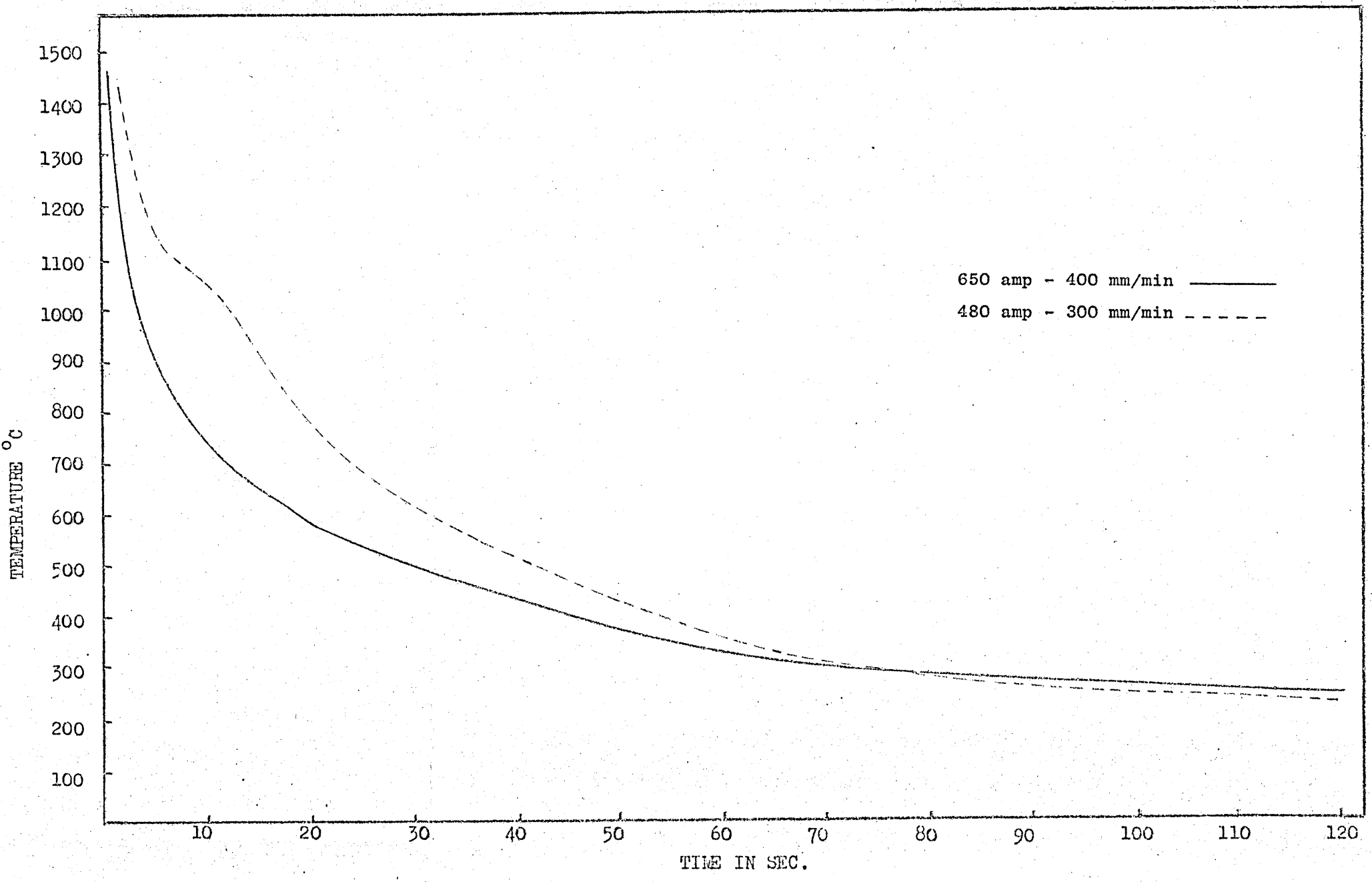


Figure 44 Continuous cooling curve for the sub-surface beads of the weld deposits made at 650 amp - 400 mm/min and 480 amp - 300 mm/min. (2.9 KJ/mm).

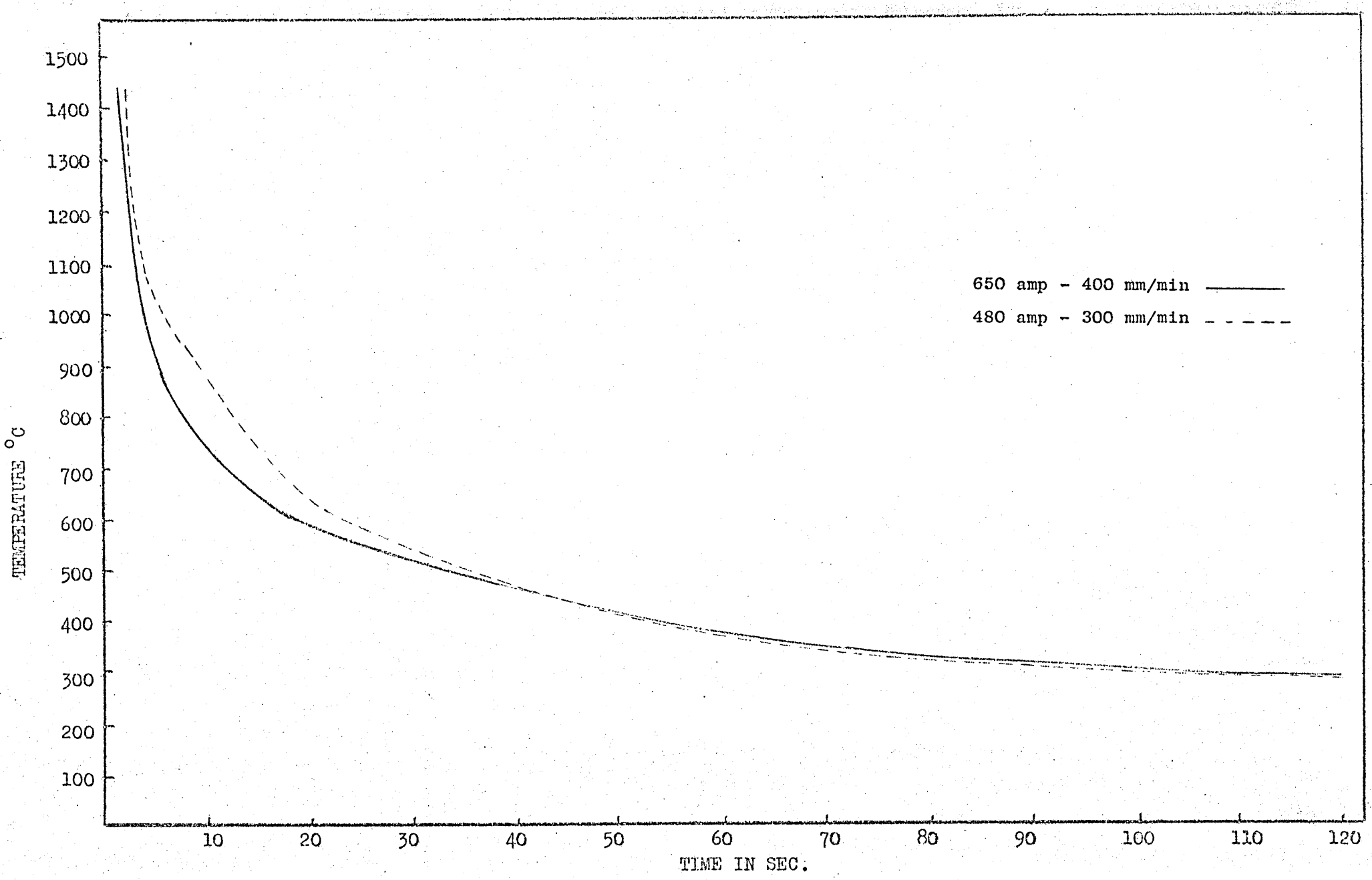


Figure 45 Continuous cooling curve for the first root bead of the weld deposits made at 650 amp - 400 mm/min and 480 amp - 300 mm/min. (2.9 KJ/mm).

Summary

The effects of welding speed and welding current variation on the weld metal cooling rate were found to be different as a decrease in welding speed led to a reduction in the weld metal cooling rate but an increase in welding current did not necessarily lead to a decrease in weld metal cooling rate.

For the same weld the cooling rates for the sub-surface and root beads were different. The root beads also had longer average times at temperature than the sub-surface beads.

The sub-surface beads had a lower cooling rate than the root beads for the temperature range 1400°C - 900°C but below 700°C the situation reversed.

For the temperature range 900°C - 700°C no systematic relationship between sub-surface and root bead cooling rates was found.

The magnitude of the differences between the cooling rate for the sub-surface and root beads was found to be highly dependent upon the welding parameters.

The results therefore show that a strict correlation between heat inputs as conventionally calculated and weld metal cooling rate and average time at temperature cannot be drawn.

## Thermal Analysis Results

### Introduction

The temperatures at which the austenite transformation occured were calculated from the first derivatives of the weld metal cooling curves which were recorded while welding was in progress.

Figure 46 shows that the derivative trace of the weld metal cooling curve had a small change in direction at point A. This point was associated with the start of transformation. From this point onwards the derivative decreased reaching point B. Point B indicated a point of low weld metal cooling rate and was associated with the maximum rate of transformation. After point B the derivative started to increase until it reached point C, which indicated the end of the transformation reaction.

For the high heat input weld deposit (650 amp - 200 mm/min, 5.8 KJ/mm) figure 46 the derivative trace showed clearly the thermal effect of the higher temperature transformation Points A, B, C, but the lower temperature transformation was not clearly defined C to $C_1$.

For the low heat input welds (650 amp - 400 mm/min, 2.7KJ/mm figure 47 the opposite occured and in this case it was the lower temperature transformation which was clearly shown by the derivative trace (A, B, C). The higher temperature transformation not being well defined ($A_1$ to A).

It is important to note that errors in the temperature measurement can occur due to the technique used (Master and Steim (92) Sing and Dybbs (93) ) and it is expected that the start of transformation could be in error by approx. 15% (Biss and Cryderman (27). However, as the measuring techniques remained unchanged throughout these test series this can be considered to be a standard error.

The derivative curve cannot be used to make a quantitative comparison of the amount of transformation between different welds as the gain of the derivative circuit was varied to best suit each particular welding condition.

### Thermal analysis results for the weld deposits made at 650 amp

The thermal analysis results for the welds made at 650 amp are shown in tables 12, 13, 14.

### Sub-Surface and Root

The results showed that an increase in welding speed led to an increase in weld metal cooling rate for both the sub-surface and root weld beads which in turn led to a lowering of the start of the austenite transformation.

For the high heat input weld 650 amp - 200 mm/min the higher temperature transformation was clearly indicated by the

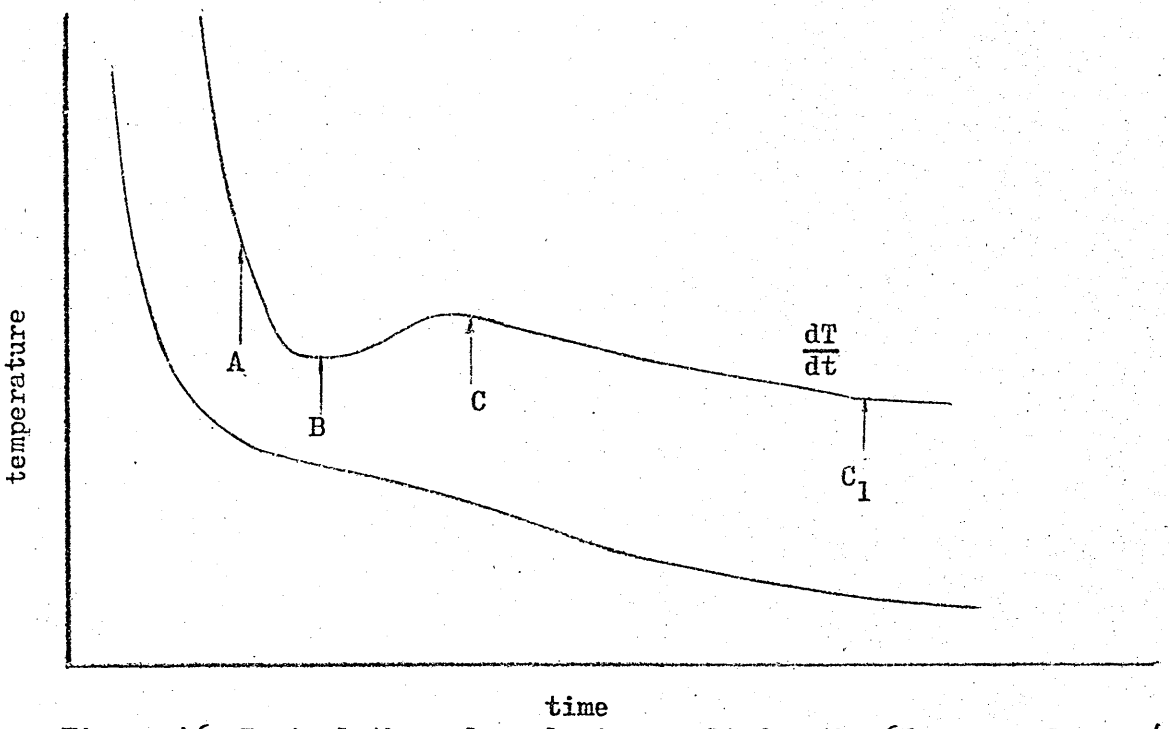


Figure 46 Typical thermal analysis result for the 650 amp - 200 mm/min weld.

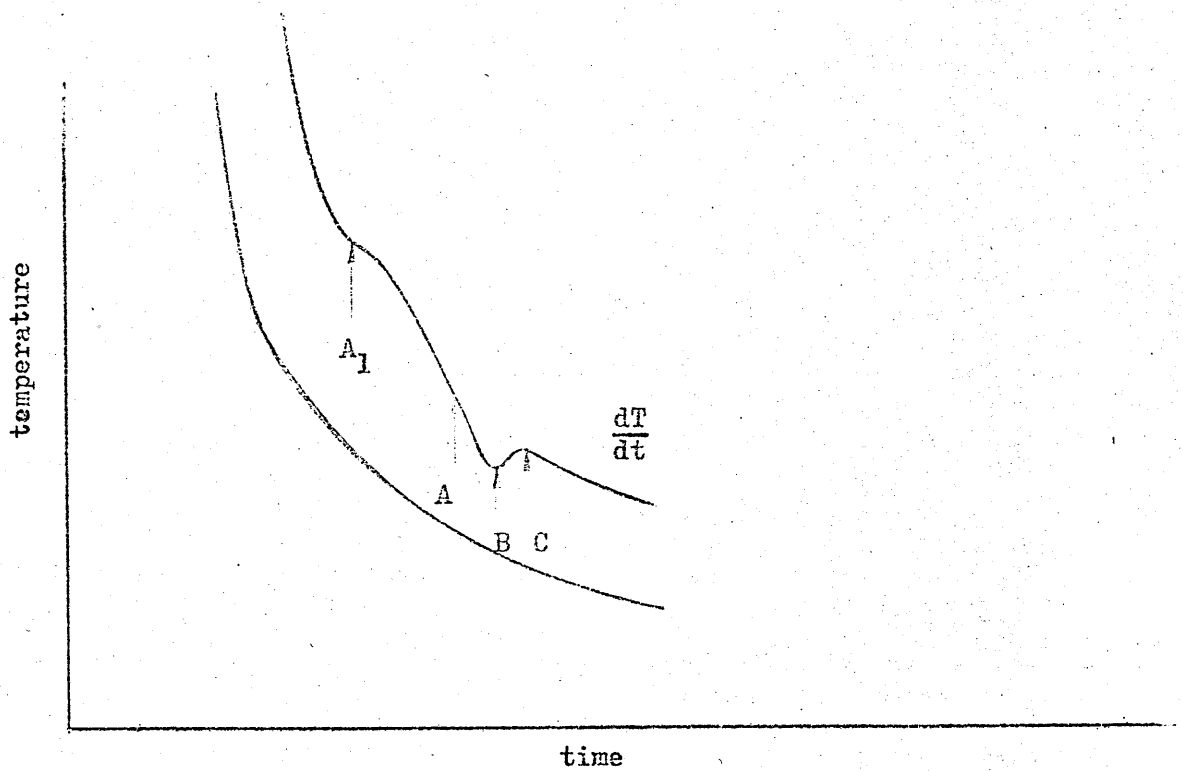


Figure 47 Typical thermal analysis trace for the 650 amp - 400 mm/min weld.

Table 12 Thermal Analysis Results
Weld 650 amps - 200 mm/min

| Weld Run | Estimated Transformation Temperature in °C | | | | | |
|---|---|---|---|---|---|---|
| | Pro-Eutectoid Ferrite | | | Acicular Ferrite | | |
| | Start | Max. | Finish | Start | Max. | Finish |
| 2 | 845* 810* | 780 | 720 | | | 590* |
| 3 | 890 | 840 | 770 | | | 625* |
| 9 | 880 | 850 | 760 | | | 610* |

* Not well defined.

Table 13 Thermal Analysis Results
Weld 650 amps - 300 mm/min

| Weld Run | Estimated Transformation Temperature in °C | | | | | |
|---|---|---|---|---|---|---|
| | Pro-Eutectoid Ferrite | | | Acicular Ferrite | | |
| | Start | Max. | Finish | Start | Max. | Finish |
| 1 | | | | 730 | 690 | 610 |
| 7 | | | | 750 | 690 | 620 |
| 9 | 820* | | | 730 | 690 | 640 |

* Not well defined.

Table 14 Thermal Analysis Results

Weld 650 amp - 400 mm/min

| Weld Run | Estimated Transformation Temperature in °C | | | | | |
|---|---|---|---|---|---|---|
| | Pro-Eutectoid Ferrite | | | Acicular Ferrite | | |
| | Start | Max. | Finish | Start | Max. | Finish |
| 1 | 730* | | | 620 | 580 | 540 |
| 2 | 745* | | | 640 | 595 | 570 |
| 3 | 760* | | | 650 | 600 | 580 |
| 11 | 760* | | | 640 | 585 | 544 |
| 14 | 758* | | | 620 | 595 | 550 |

* Not well defined.

derivative curve, but the lower temperature transformation could not be clearly defined.

The reverse occured for the medium and low heat input welds (650 amp - 300 mm/min and 650 amp - 400 mm/min). For these welds the lower temperature transformation was clearly defined but the higher temperature transformation was not always clearly indicated by the derivative trace.

Thermal Analysis Results for the weld deposits made using the welding speed of 300 mm/min.

The thermal analysis results for the welds made at 300 mm/min are shown in tables 13, 14, 16.

Sub-surface and Root

From the results for the sub-surface and root weld beads a relationship between welding current and the austenite transformation temperature range could not be obtained, as both the high heat input welds (850 amp - 300 mm/min and the low heat input deposit 480 amp - 300 mm/min had, for the sub-surface regions, very similar lower temperature transformations, (700°C - 585°C and 695°C - 585°C and the weld made at the intermediate heat input (650 amp - 300 mm/min) a slightly higher transformation temperature (730°C - 640°C).

For all welds, the derivative traces showed clearly the lower temperature transformation but the higher temperature transformation was not clearly indicated except for the root region of the 850 amp - 300 mm/min weld were the derivative trace only indicated the higher temperature transformation.

Thermal Analysis Differences between the Sub-surface and Root weld beads for the same Weld Joint

For the weld deposit made at 650 amp - 200 mm/min (Table 12) the higher temperature transformation had a lower estimated transformation temperature range for the root than the sub-surface. As the lower temperature transformation could not be accurately measured no comparison between the sub-surface and root transformation characteristics could be made.

For the weld deposits made at 650 amp - 300 mm/min and 650 amp - 400 mm/min (Table 13, 14) the range of the higher transformation temperature could not be accurately measured, but it was found that there was no appreciable difference in the lower transformation temperature range between the root and sub-surface.

For the weld deposit made at 850 amp - 300 mm/min (Table 15) it was found that the derivative trace referring to the root bead indicated the higher temperature transformation, whilst the derivative trace referring to the sub-surface bead indicated the lower temperature transformation.

Table 15 Thermal Analysis Results
Weld 850 amp - 300 mm/min

| Weld Run | Estimated Transformation Temperature in °C | | | | | |
|---|---|---|---|---|---|---|
| | Pro-Eutectoid Ferrite | | | Acicular Ferrite | | |
| | Start | Max. | Finish | Start | Max. | Finish |
| 1 | 870 | 830 | 790 | | | |
| 3 | | | | 700 | 675 | 620 |
| 8 | 810* | | | 700 | 615 | 585 |

* Not well defined.

Table 16 Thermal Analysis Results
Weld 480 amp - 300 mm/min

| Weld Run | Estimated Transformation Temperature in °C | | | | | |
|---|---|---|---|---|---|---|
| | Pro-Eutectoid Ferrite | | | Acicular Ferrite | | |
| | Start | Max. | Finish | Start | Max. | Finish |
| 1 | | | | 610 | 580 | 555 |
| 3 | | | | 655 | 590 | 560 |
| 11 | | | | 690 | 625 | 585 |
| 14 | 900* | | | 695 | 610 | 585 |

* Not well defined.

For the weld deposit made at 480 amps - 300 mm/min (Table 16 ) the high transformation temperature ranges cannot be compared as these temperatures could not be accurately measured, but the lower temperature transformation occured at a higher temperature range for the sub-surface than for the root beads.

Thermal differences between the Weld Deposits made at the same calculated heat imput of 5.8 KJ/mm.

Comparing the austenite transformation temperatures for the welds made at 650 - 200 mm/min and 850 amps - 300 mm/min, both with a calculated heat input of 5.8 KJ/mm, (Table 12 and 15), it was found that for the sub-surface, the derivative trace of the 650 amps - 200 mm/min weld indicated clearly only the higher temperature transformation, while only the lower temperature transformation was clearly indicated by the derivative trace for the 850 amps - 300 mm/min weld.

For the root regions it was found that the derivative traces of both welds only showed accurately the temperature associated with the higher temperature transformation. The 650 amps - 200 mm/min weld had a slightly lower transformation temperature range than the 850 amps - 300 mm/min weld.

Weld Deposits made at the same calculated heat imput of 2.7 KJ/mm

Comparing the austenite transformation temperature for the welds made at 650 amps - 400 mm/min and 480 amps - 300 mm/min with a calculated heat input of 2.7 KJ/mm (Table 14 and 16 ) it was found that only the lower temperature transformation could be compared between these two welds since the higher temperature transformation could not be accurately measured.

The lower temperature transformation occured at a higher temperature for the sub-surface beads of the 480 amps - 300 mm/min weld than for 650 amps - 300 mm/min weld, but at similar temperatures for the root beads of both welds.

Summary

The derivative traces indicated that a high and a low temperature transformation occured but for each weld only one of these transformation could usually be measured accurately.

An increase in welding speed caused a decrease in the transformation temperature range, but no systematic relationship between welding current and transformation temperature could be drawn.

For the same weld joint the root had a similar or lower transformation temperature range than the sub-surface, with the exception of the 850 amps - 300 mm/min weld where the opposite occured.

The weld deposits made at the same calculated heat input did not have the same transformation characteristics, except for the root regions of the low heat input welds (2.9 KJ/mm) which did have very similar transformation temperatures.

Weld Bead Size and Flux Consumption

The weld bead dimensions and estimated flux consumptions are given in Table 17 .

Both a decrease in the welding speed and an increase in the welding current caused an increase in the weld bead volume. It is also clear from these results that weld deposits made at the same calculated heat input did not necessarily have the same or similar weld bead volumes, therefore indicating that the weld bead volume is not a simple linear function of the heat input as conventionally calculated.

$$\frac{\text{Volts x Amps}}{\text{Speed x 1000}} = \text{Heat input}$$

For the sub-surface beads a decrease in the welding speed from 400 mm/min to 300 mm/min and then to 200 mm/min caused an increase in the width to depth ratio from 2.2 to 2.37 and then to 2.91, but an increase in welding current from 480 amps to 650 amps and then to 850 amps led to a decrease in the width to depth ratio from 4.8 to 2.37 and then to 1.5, Table 17.

A decrease in welding speed from 400 mm/min to 300 mm/min and then to 200 mm/min caused an increase in the estimated flux consumption from $1.68 \times 10^{-3}$ gm/mm$^3$ to $2.37 \times 10^{-3}$ gm/mm$^3$ and then to $3.65 \times 10^{-3}$ gm/mm$^3$.

An increase in welding current from 480 amps to 650 amps and then to 850 amps caused a decrease in the estimated flux consumption from $3.92 \times 10^{-3}$ gm/mm$^3$ to $2.37 \times 10^{-3}$ gm/mm$^3$ and then to $1.66 \times 10^{-3}$ gm/mm$^3$.

The estimated flux consumption for each weld joint was always lower for the root beads than for the sub-surface beads. (56% for the 650 amps - 200 mm/min weld, 42% for the 650 amps - 300 mm/min weld, 33% for the 650 amps - 400 mm/min weld, 21% for the 850 amps - 300 mm/min weld, and 26% for the 480 amps - 300 mm/min weld).

Due to the difficulty in accurately measuring the volume of the root weld beads as they were remelted by subsequent weld runs, the weld metal bead volume for each welded joint was assumed to be constant throughout the joint and the volume of the central sub-surface weld bead was used.

It was felt that errors in the estimated flux consumption due to the above assumption were very small and therefore not significant in this comparative study.

Table 17 Weld Shape and Flux Consumption

| Welding Conditions | Flux Consumption gm/mm | Bead Width mm | Flux Consumption $gm/mm^3$ | Weld bead cross-sectional area $mm^2$ | Width to Depth Ratio |
|---|---|---|---|---|---|
| 650 - 200 mm/min | | | | | |
| 1 | .44 | 29 | .0023 | | |
| 2 | .53 | 31 | .00277 | | |
| 3 | .535 | 32 | .00281 | | |
| 7 | .649 | 35 | .00339 | | |
| 9 | .75 | 35 | .00392 | 191 | 2.9 |
| Average of 7 & 9 | | | .00365 | | |
| 650 - 300 mm/min | | | | | |
| 1 | .276 | 16 | .00166 | | |
| 2 | .276 | 22 | .00168 | | |
| 3 | .33 | 23 | .00198 | | |
| 7 | .375 | 26 | .00225 | | |
| 9 | .415 | 28.5 | .0025 | 166 | 2.37 |
| Average of 7 & 9 | | | .00237 | | |
| 650 - 400 mm/min | | | | | |
| 1 | .18 | 17 | .00126 | | |
| 2 | .194 | 19 | .00136 | | |
| 3 | .207 | 21 | .00145 | | |
| 11 | .244 | 22 | .00171 | | |
| 14 | .237 | 22 | .00166 | 142 | 2.2 |
| Average of 11 & 14 | | | .00168 | | |
| 480 - 300 mm/min | | | | | |
| 1 | .28 | 20 | .00311 | | |
| 2 | .288 | 22 | .00320 | | |
| 3 | .3 | 22 | .00333 | | |
| 11 | .347 | 24 | .00385 | | |
| 14 | .36 | 24 | .0040 | 90 | 4.8 |
| Average of 11 & 14 | | | .00392 | | |
| 850 - 300 mm/min | | | | | |
| 1 | .41 | 21 | .00137 | | |
| 2 | .36 | 27 | .001204 | | |
| 3 | .459 | 28 | .001531 | | |
| 6 | .51 | 31 | .001705 | | |
| 8 | .489 | 30 | .00163 | 299 | 1.53 |
| Average of 6 & 8 | | | .00166 | | |

Summary

A decrease in welding speed and an increase in welding current caused an increase in weld metal bead volume, but the weld bead volume and weld bead shape of the weld deposits made at the same calculated heat input were different.

A decrease in welding speed caused an increase in the bead width and depth ratio as well as in the estimated flux consumption, but an increase in welding current led to a decrease in the bead width to depth ratio as well as in the estimated flux consumption.

For a given weld the root beads always had lower estimated flux consumptions than the sub-surface beads.

Chemical Analysis

The chemical analyses of all weld metal deposits are shown in table 18 .

All welds had the same basic chemical composition and no correlation between the welding variables (welding speed and welding current) and chemical composition variation could be drawn.

There was no significant variation in composition between welds made under the different conditions.

The only systematic compositional differences were those between root and sub-surface which resulted from the dilution effect of the parent plate.

The root regions of all welds were light in carbon (approx. 0.02%), silicon (approx. 0.04%), manganese (approx. 0.04%), niobium (approx. 0.002% - 0.005%) and aluminium (approx. 0.003%) than the sub-surface, but lower in phosphorous (approx. 0.003%). Oxygen and nitrogen levels, however, were very similar for both the sub-surface and root regions.

Table 18 Weld Metal Composition

| Welding Conditions | Chemical Composition of Weld Metals in wgt % (O.N. in p.p.m.) | | | | | | | | | | | | | | | | | | |
|---|---|---|---|---|---|---|---|---|---|---|---|---|---|---|---|---|---|---|---|
| | C | S | P | Si | Mn | Ni | Cr | Mo | V | Cu | Nb | Ti | Al | B | Pb | Sn | Co | N | O |
| 650 amp - 200 mm/min. | | | | | | | | | | | | | | | | | | | |
| Sub-Surface | 0.08 | 0.005 | 0.017 | 0.30 | 1.30 | 0.04 | 0.06 | 0.01 | 0.02 | 0.11 | 0.005 | 0.01 | 0.013 | 0.001 | 0.01 | 0.01 | 0.01 | 124 | 214 |
| Root | 0.10 | 0.005 | 0.014 | 0.34 | 1.34 | 0.05 | 0.07 | 0.01 | 0.02 | 0.09 | 0.007 | 0.01 | 0.016 | 0.001 | 0.01 | 0.01 | 0.01 | 106.25 | 259 |
| 650 amp - 300 mm/min. | | | | | | | | | | | | | | | | | | | |
| Sub-Surface | 0.08 | 0.005 | 0.015 | 0.35 | 1.38 | 0.05 | 0.07 | 0.01 | 0.02 | 0.10 | 0.006 | 0.01 | 0.014 | 0.001 | 0.01 | 0.01 | 0.01 | 116.2 | 240 |
| Root | 0.10 | 0.006 | 0.012 | 0.38 | 1.37 | 0.05 | 0.08 | 0.01 | 0.03 | 0.09 | 0.011 | 0.01 | 0.018 | 0.001 | 0.01 | 0.01 | 0.01 | 96.2 | 292 |
| 650 amp - 400 mm/min. | | | | | | | | | | | | | | | | | | | |
| Sub-Surface | 0.08 | 0.005 | 0.014 | 0.32 | 1.37 | 0.05 | 0.05 | 0.01 | 0.02 | 0.11 | 0.005 | 0.01 | 0.018 | 0.001 | 0.01 | 0.01 | 0.01 | 115 | 250 |
| Root | 0.11 | 0.005 | 0.011 | 0.37 | 1.36 | 0.05 | 0.08 | 0.01 | 0.03 | 0.08 | 0.011 | 0.01 | 0.021 | 0.001 | 0.01 | 0.01 | 0.01 | 83 | 207 |
| 850 amp - 300 mm/min. | | | | | | | | | | | | | | | | | | | |
| Sub-Surface | 0.10 | 0.005 | 0.014 | 0.33 | 1.39 | 0.04 | 0.06 | 0.01 | 0.02 | 0.10 | 0.009 | 0.01 | 0.012 | 0.001 | 0.01 | 0.01 | 0.01 | 99 | 244 |
| Root | 0.11 | 0.006 | 0.011 | 0.37 | 1.39 | 0.04 | 0.07 | 0.01 | 0.03 | 0.07 | 0.014 | 0.01 | 0.013 | 0.001 | 0.01 | 0.01 | 0.01 | 86 | 241 |
| 480 amp - 300 mm/min. | | | | | | | | | | | | | | | | | | | |
| Sub-Surface | 0.07 | 0.005 | 0.019 | 0.27 | 1.27 | 0.05 | 0.05 | 0.01 | 0.01 | 0.12 | 0.005 | 0.01 | 0.013 | 0.001 | 0.01 | 0.01 | 0.01 | 116 | 240 |
| Root | 0.10 | 0.005 | 0.014 | 0.34 | 1.32 | 0.05 | 0.06 | 0.01 | 0.02 | 0.09 | 0.008 | 0.01 | 0.017 | 0.001 | 0.01 | 0.01 | 0.01 | 101 | 207 |
| Parent Plate | 0.15 | 0.005 | 0.006 | 0.44 | 1.38 | 0.05 | 0.12 | 0.02 | 0.06 | 0.04 | 0.027 | 0.01 | 0.031 | 0.001 | 0.01 | 0.01 | 0.01 | 49 | 33.7 |

## OPTICAL MICROSCOPY

### Introduction

A qualitative and quantitative metallographic examination was made of the root and subsurface areas of all weld beads.

The microstructure of each of the welds showed primarily an acicular ferrite structure surrounded by pro-eutectoid ferrite in the as deposited part of each weld run.

Other microstructural phases were also present namely ferrite side plates, pearlite, and martensite - austenite microphases as described by Biss et al (27) and Garland et al (19). The microstructure of the reheated regions consisted of equiaxed polygonal ferrite grains.

Grain size measurements were made of the $\delta$ ferrite columnar and acicular ferrite grains using the mean linear intercept method (83). For the root regions of all welds the acicular ferrite structure in the root region was very irregular and therefore accurate grain size measurements could not be obtained. The proportion of acicular ferrite was measured for each weld but quantitative measurements of the amount of retained M.A. phases are not quoted because the very small (less than 5%) volume fraction of such phases made accurate measurement impossible.

### Quantitative Measurements

The quantitative measurements were made using the linear Intercept Method along 10 lines parallel to the plate surface and in an area representative of the Charpy V, notch location. These results are shown in table 19.

For each line 100 points were counted and therefore each result is the average of 1000 point readings. It is important to note that the value of grain size $\bar{d}$ shown in table 19 obtained using the M.L.I. (83) is less than the average diameter of the grains comprising the microstructure, D, which is in turn less than the maximum grain diameter $D_M$. The relationship between $\bar{d}$, $\bar{D}$ and $D_M$ depends on the grain shape assumed. Only the value of $\bar{d}$ was calculated since these results are only intended to be used for comparitive purposes between the weld deposits made in this work.

Great care was taken to make sure that as far as possible the metallographic sections were representative of the region from which the test pieces used in the mechanical test were taken in order to reduce errors associated with the inhomegeneity and anisotropy of the microstructure.

It is also important to note that for the root the notch of the Charpy V specimens had to be located through as deposited and reheated structure. The same occured for the 480 amp - 300 mm/min weld due to the fact that the bead depth was smaller than the Charpy V, notch length.

Table 19 Weld Metal Microstructure

| Welding Condition | Heat input KJ/mm | Ferrite grain size | Standard deviation | Columnar grain size | Standard deviation | Acicular Ferrite % | Standard deviation | Acicular Ferrite grain size | Standard deviation | Micro-phases |
|---|---|---|---|---|---|---|---|---|---|---|
| 650 amp - 200 mm/min. | | | | | | | | | | |
| Sub-Surface | 5.8 | 63 | 5.5 | 72 | 3.51 | 63.7 | 8 | 5.4 | 0.782 | 1 |
| Root | | 27 | 3.71 | 48 | 2.97 | 30.3 | 8.23 | - | - | 3 |
| 650 amp - 300 mm/min. | | | | | | | | | | |
| Sub-Surface | 3.9 | 45 | 2.87 | 60 | 4.9 | 69.9 | 7.48 | 5.9 | 0.898 | 2 |
| Root | | 24 | 1.73 | 49 | 4.79 | 28.8 | 5.41 | - | - | 3 |
| 650 amp - 400 mm/min | | | | | | | | | | |
| Sub-Surface | 2.9 | 37 | 5.83 | 45 | 3.4 | 71 | 4.99 | 3.6 | 0.332 | 3 |
| Root | | 19 | 1.09 | 40 | 2.42 | 58.9 | 7.34 | - | - | 3 |
| 850 amp - 300 mm/min. | | | | | | | | | | |
| Sub-Surface | 5.8 | 55 | 9.24 | 57 | 3.5 | 70.8 | 6.82 | 5.3 | 0.722 | 0 |
| Root | | 23 | 0.08 | 48 | 2.85 | 30.9 | 8.87 | - | - | 0 |
| 480 amp - 300 mm/min. | | | | | | | | | | |
| Sub-Surface | 2.9 | 29 | 1.39 | 76 | 4.7 | 71.8 | 3.42 | 4.0 | 0.517 | 2 |
| Root | | 19 | 0.02 | 40 | 6.22 | 40.8 | 11.96 | - | - | 1 |

**Microphases**

**0 - None**
**1 - Estimated at less than 1.5%**
**2 - Estimated at less than 3%**
**3 - Estimated at less than 5%**

## Weld Deposit made at the same Welding Current of 650 amps

### Sub-surface Beads

Typical microstructures of the sub-surface weld beads are shown in figures 50, 62, 74.

An increase in welding speed caused a decrease in the grain size of the $\delta$ ferrite, (63um, 45um, 37um) and columnar grain size (72um, 60um, 45um) figures 48, 60, 72, 49, 61, 73 , as well as a decrease in the amount of ferrite side plates present, but caused an increase in the percentage of acicular ferrite (63.7%, 69.9%, 71%

The acicular ferrite structure was similar for welds made at both 200 mm/min and 300 mm/min (5.4um and 5.9um) but an increase in welding speed to 400 mm/min led to a finer structure, (3.6 um), figures 51, 63, 75.

An increase in welding speed also led to an increase in the amount of M.A. microphases present, figures 53, 65, 77.

### Root Beads

Typical microstructures of the root weld beads are shown in figures 56, 68, 80.

An increase in welding speed caused a decrease in the $\delta$ ferrite grain size, (27um, 24um, 19um), figures 54, 66, 78. but the columnar grain size, acicular ferrite structure, percentage of acicular ferrite and ferrite side plates was similar for welds made at both 200 mm/min and 300 mm/min, figures 55, 67, 57, 69.

An increase in welding speed to 400 mm/min led to a decrease in the columnar grain size, to a finer acicular ferrite structure, and also to a decrease in the amount of ferrite side plates present, figures 79, 80, 81.

The same increase in welding speed led to an increase in the percentage of acicular ferrite, figure 80.

As for the sub-surface beads the amount of M.A. microphases present increased with an increase in welding speed, figures 59, 71, 85.

## Weld Deposits made at the same Welding Speed of 300 mm/min

### Sub-surface Beads

Typical microstructures for the sub-surface weld are shown in figures 86, 62, 98.

An increase in welding current caused an increase in the grain size of the $\delta$ ferrite (29um, 45um, 55um) but a decrease in the columnar grain size (76um, 60um, 57 um), figures 84, 60, 96, 85, 61, 97.

An increase in welding current from 480 amps to 650 amps led to an increase in the grain size of the acicular ferrite (4um to 5.9um), but to a decrease in the amounts of ferrite side plates. A further increase in welding current to 850 amps, did not affect significantly either of these structures, figures 87, 63, 99.

The proportion of acicular ferrite decreased with an increase in welding current from 480 amps to 650 amps, 71.8% to 69.9% but a further increase in welding current to 850 amps led to a small increase in the proportion of area occupied by this phase 70.8% figures 98, 62, 86.

M.A. microphases were not found in the 850 amps weld but were present in both the 650 amps and 480 amp welds.

The 650 amps weld having a more M.A. microphases present than the 480 amps weld, figures 89, 65, 101.

### Root Beads

Typical microstructures for the root beads are shown in figures 92, 68, 104.

An increase in welding current from 480 amps to 650 amps led to an increase in the $\delta$ ferrite grain size (19um, 24um) as well as to an increase in the acicular ferrite grain size, but a further increase to 850 amps had no significant effect on either of these structures. Figures 102, 66, 90, 105, 69, 93.

Again an increase in welding current from 480 amps to 650 amp led to an increase in the grain size of the columnar grain size, but a further increase to 850 amps, did not significantly alter the grain size of this structure, figures 103, 67, 91.

The percentage of acicular ferrite decreased with an increase in welding current, while the amount of ferrite side plates present increased with the same increase in welding current. 40.8%, 28.8%, 30.9%. Figures 92, 68, 104.

The M.A. microphases were not present in the 850 amps welds but were present in both the 650 amps and 480 amps welds. The 650 amps weld having more M.A. microphases present than the 480 amps weld, figures 95, 71, 107.

Microstructural Differences between the Sub-surface and the Root Bead for the same Welded Joint

For all weld deposits the sub-surface bead had a coarser ferrite grain size and a coarser columnar grain size than the root bead, but the acicular ferrite structure was generally finer.

The sub-surface beads also had a higher percentage of acicular ferrite than the root beads but a much smaller number of ferrite side plates, table 19.

Comparison between the Weld Deposits made at the same Calculated Heat Input

Weld Deposits made at 5.8 KJ/mm

Sub-Surface Beads

The 650 amp - 200 mm/min weld had a larger $\delta$ ferrite and columnar grain size than the 850 amp - 300 mm/min weld, but the acicular ferrite structure was similar for both weld deposits, figures 48, 84, 51, 87.

The 650 amp - 200 mm/min weld also had a lower percentage of acicular ferrite than the 850 amp - 300 mm/min weld, but showed a greater amount of ferrite side plates, figures 50, 86.

The M.A. microphases were only present in the 650 amp - 200 mm/min weld, figures 53, 89.

Root Bead

The 650 amp - 200 mm/min weld had a slightly larger $\delta$ ferrite grain size than the 850 amp - 300 mm/min weld and a similar columnar grain structure, figures 54, 90, 55, 91.

The acicular ferrite structure was similar in both welds, figures 57, 93.

The 650 amp - 200 mm/min weld had a higher percentage of acicular ferrite than the 850 amp - 200 mm/min weld as well as a smaller amount of ferrite side plates, figures 56, 92.

The M.A. microphases were only present in the 650 amp - 200 mm/min weld, figure 59.

Weld Deposits made at 2.9 KJ/mm

Sub-Surface Beads

The 650 amps - 400 mm/min weld had larger δ ferrite grains, but a much finer columnar grain size than the 480 amps - 300 mm/min, figures 72, 96, 73, 97.

The 650 amps - 400 mm/min weld also had a slightly larger acicular ferrite grain structure, as well as a marginally lower proportion of acicular ferrite than the 480 amp - 300 mm/min, but a smaller amount of ferrite side plates, figures 75, 99, 74, 98.

Both welds showed the presence of M.A. microphases, figures 77, 101.

Root Bead

Both weld beads had similar δ ferrite grain size and columnar grain size, but the 650 amp - 400 mm/min weld had a higher percentage of acicular ferrite than the 480 amps - 300 mm/min weld, but a smaller amount of ferrite side plates, figures 78, 102, 79, 103, 80, 104.

The 650 amp - 400 mm/min weld also had a finer acicular ferrite structure than the 480 amp - 300 mm/min, figures 81, 105.

Both welds showed M.A. microphases with the 650 amp - 400 mm/min weld, having a higher distribution of microphases than the 480 amp - 300 mm/min weld, figures 83, 107.

Summary

1. Generally all of the weld metal microstructures were composed of an acicular ferrite structure surrounded by pro-eutectoid ferrite and ferrite side plates.

   Martensite - Austenite microphases (19, 27 ) were also present in variable but very small amounts (estimated at less than 5%) in all but the weld made at 850 amp - 300 mm/min.

2. An increase in welding speed at a constant welding current led to a finer microstructure with an increase in the proportion of acicular ferrite and a decrease in the amount of ferrite side plates. It also led to an increase in the amount of the M.A. phases.

3. An decrease in welding current did not necessarily lead to a finer microstructure nor to a proportionat variation in the percentage of acicular ferrite, and ferrite side plates, but the M.A. microphases decreased with an increase in welding current.

4. For a given weld the differences in the microstructural features between the sub-surface and the root bead were significant. The sub-surface bead generally had larger $\delta$ ferrite and columnar grains, as well as a much higher percentage of acicular ferrite, than the root bead. The sub-surface bead also had a smaller amount of ferrite side plates than the root bead.

5. The two welds made at the same calculated heat input of 5.8 KJ/mm had different microstructures.

   The sub-surface bead of the 650 amp - 200 mm/min weld had larger $\delta$ ferrite and columnar grain, as well as a lower percentage of acicular ferrite, than the 850 amp - 300 mm/min weld.

   The 650 amp weld also had a larger amount of ferrite side plates than the 850 amp weld.

   The root beads had similar microstructures although the 850 amp weld had a slightly lower percentage of acicular ferrite, as well as a greater amount of ferrite side plates.

   M.A. microphases were only present in the welds made at 650 amp.

6. The two welds made at the same calculated heat input of 2.9 KJ/mm also had different microstructures.

   The sub-surface bead of the 650 amp - 400 mm/min weld had a larger $\delta$ ferrite grain size, smaller columnar grain size and a lower percentage of acicular ferrite than the 480 amp - 300 mm/min weld.

The 650 amp weld also had smaller amount of ferrite side plates than the 480 amp weld.

The root beads had similar $\delta$ ferrite and columnar grain size, but the 650 amp weld had a greater proportion of acicular ferrite than the 480 amp weld.

Contrary to the sub-surface beads the 650 amp weld had smaller amounts of ferrite side plates than the 480 amp weld.

In both sub-surface and root regions the 650 amp weld had more M.A. microphases than the 480 amp weld.

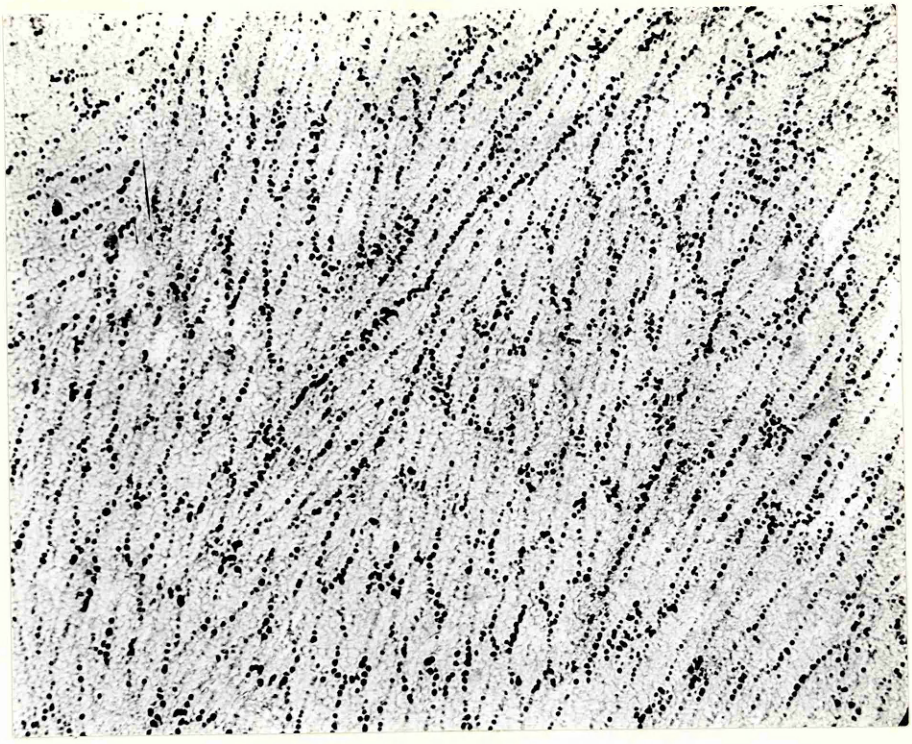

Figure 48 Weld 650 amp - 200 mm/min. Sub-Surface
δ Ferrite Structure x 50

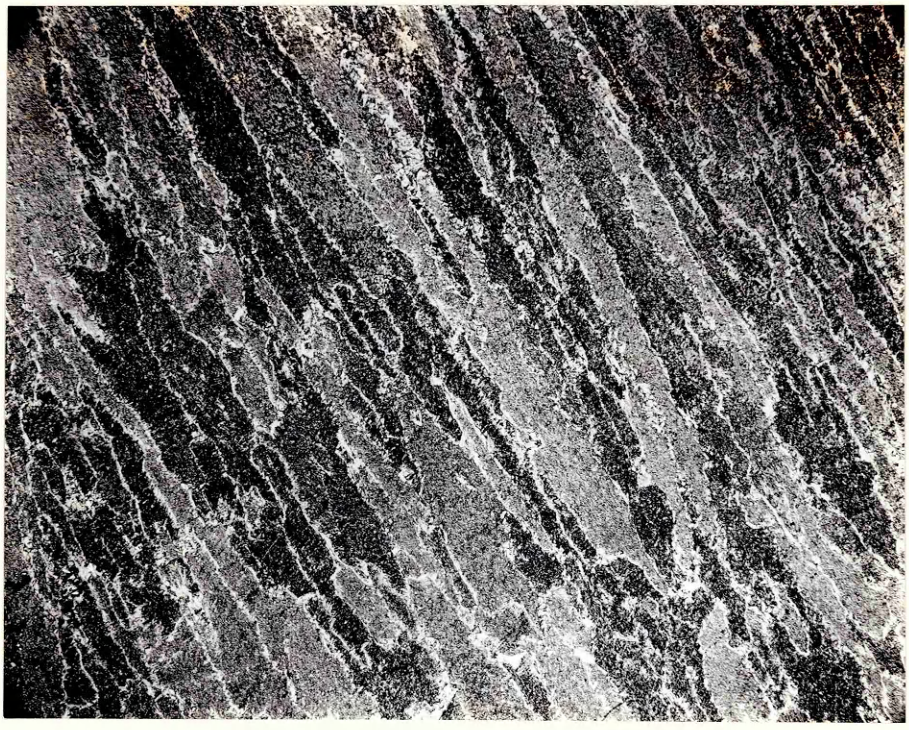

Figure 49 Weld 650 amp - 200 mm/min. Sub-Surface
Columnar Structure x 50

Figure 50 Weld 650 amp - 200 mm/min. Sub-Surface as deposited structure x 200

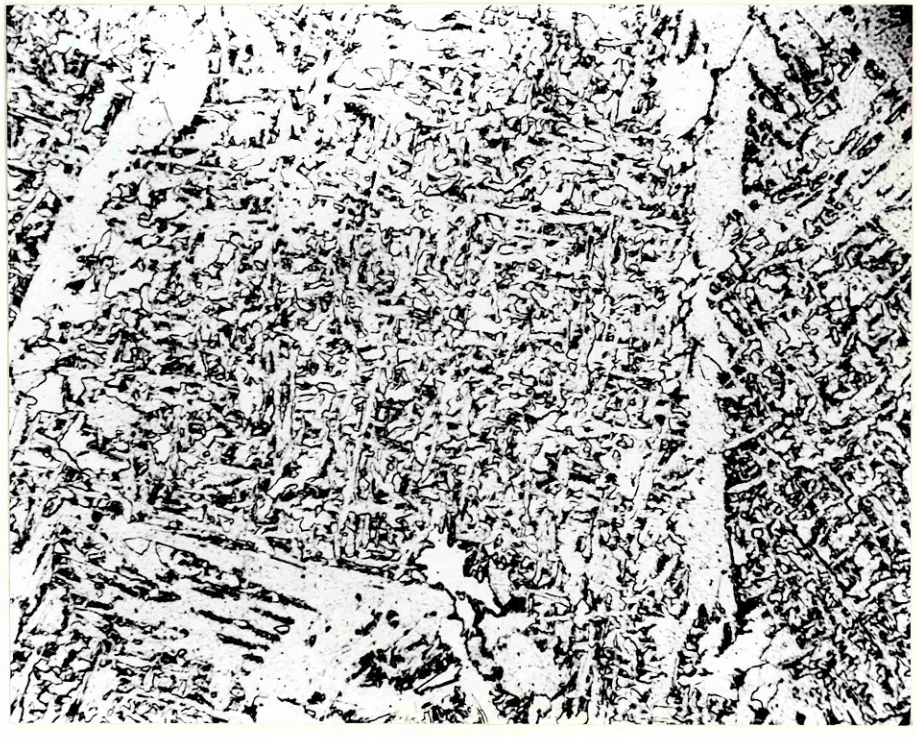

Figure 51 Weld 650 amp - 200 mm/min. Sub-Surface as deposited structure x 500

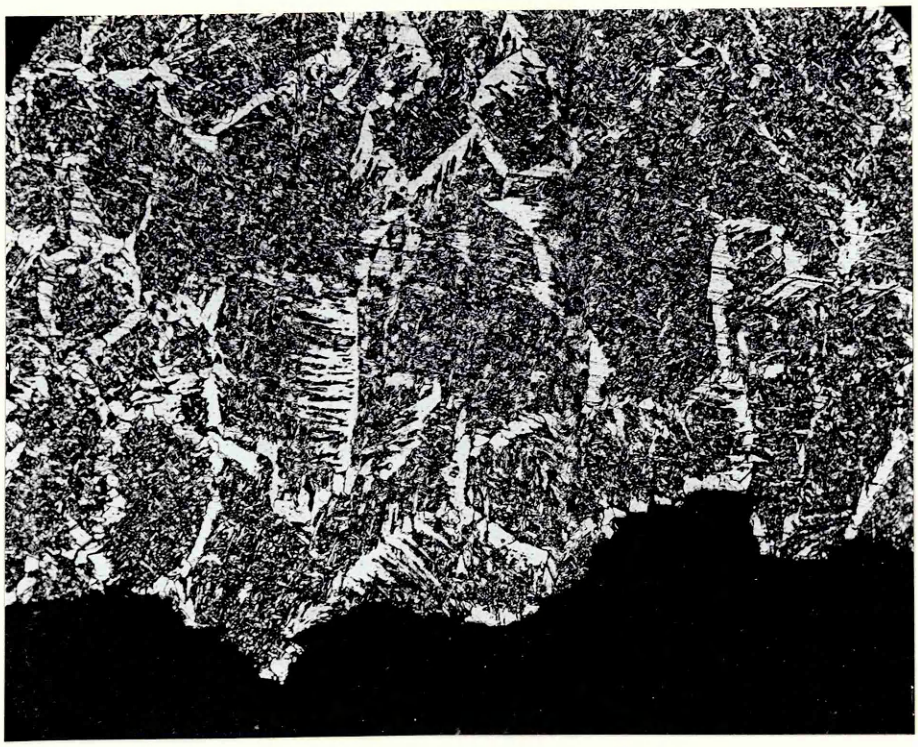

Figure 52 Weld 650 amp - 200 mm/min. Sub-Surface
Charpy V fracture path x 200

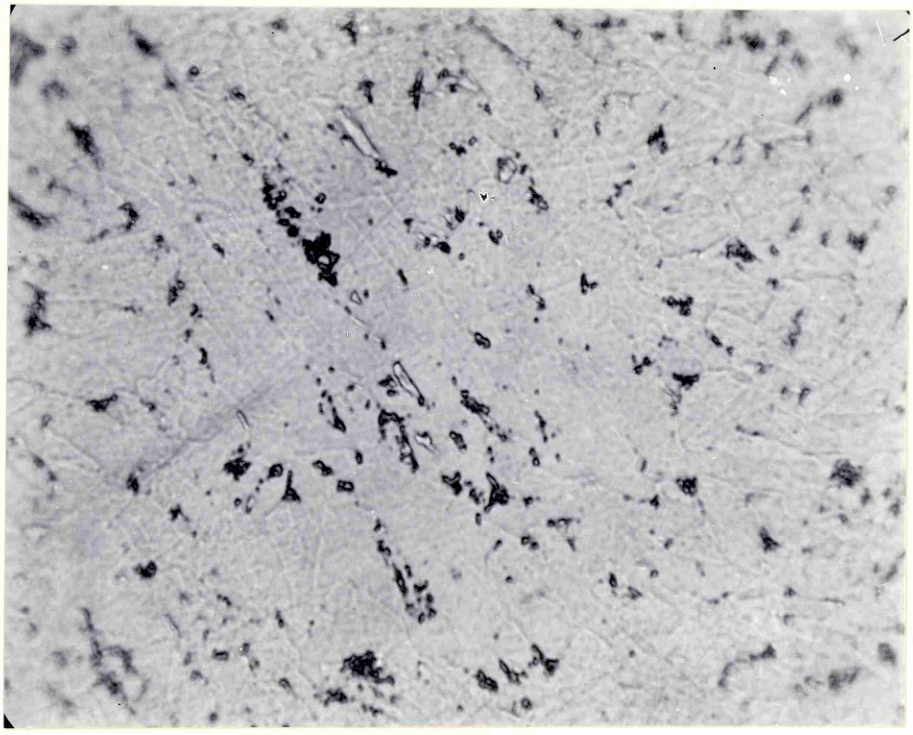

Figure 53 Weld 650 amp - 200 mm/min. Sub-Surface
M.A. Microphases x 2,000

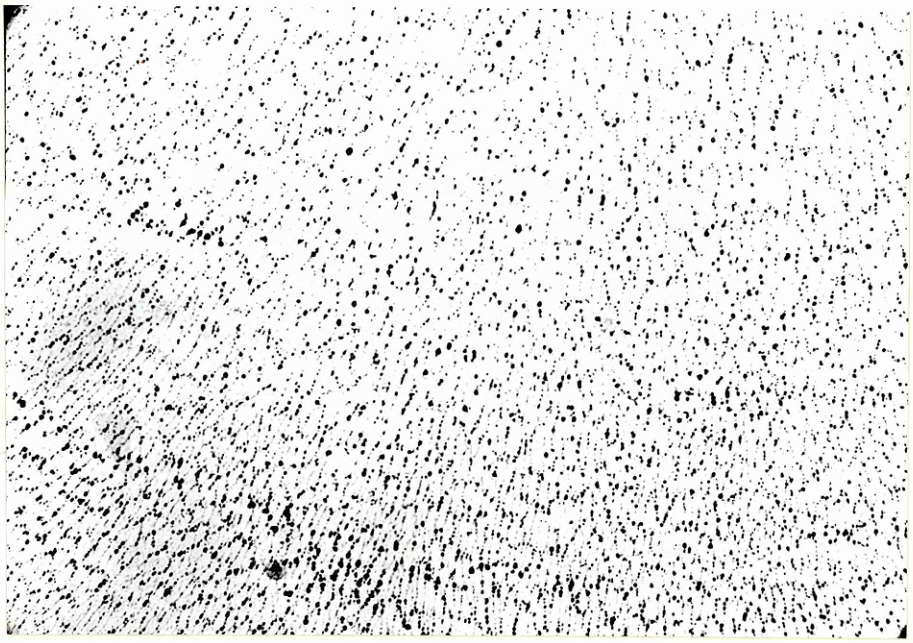

Figure 54 Weld 650 amp - 200 mm/min. Root δ Ferrite Structure x 50

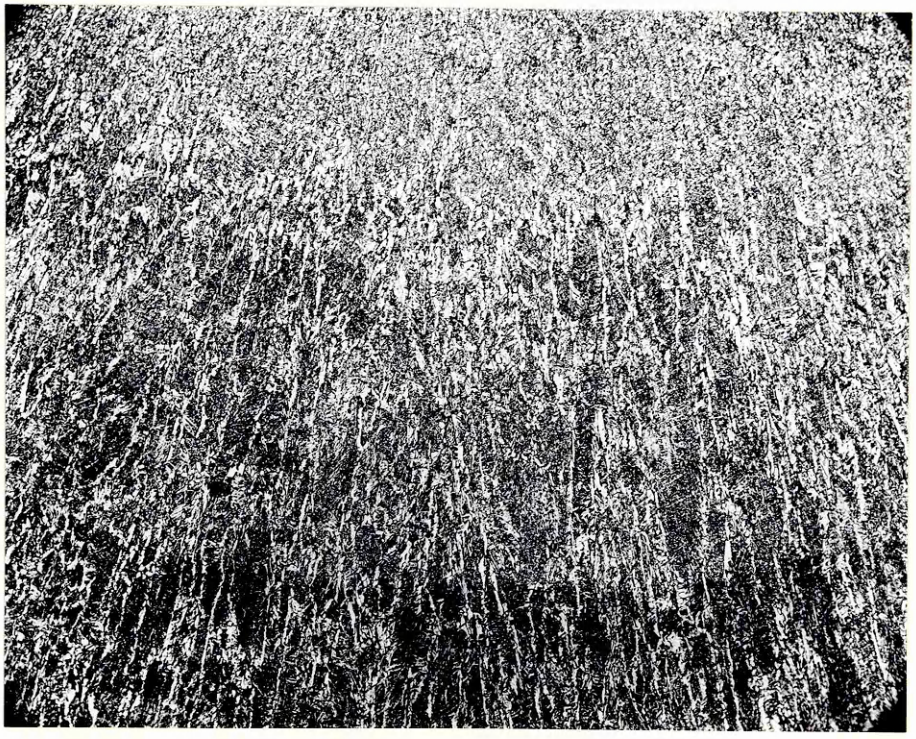

Figure 55 Weld 650 amp - 200 mm/min. Root Columnar Structure x 50

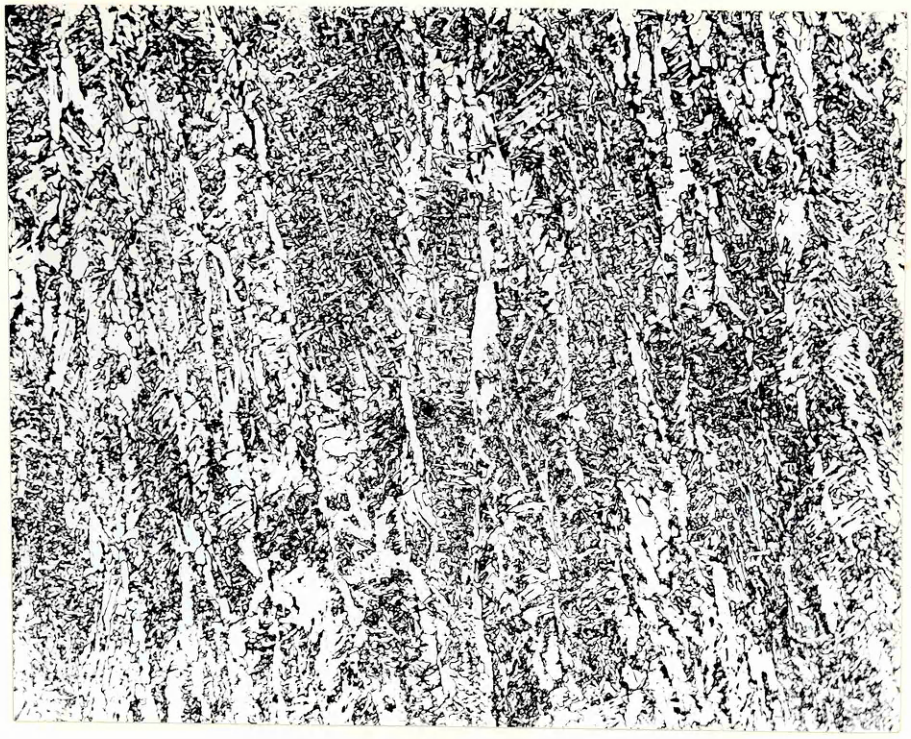

Figure 56 Weld 650 amp - 200 mm/min. Root as deposited structure x 200

Figure 57 Weld 650 amp - 200 mm/min. Root as deposited structure x 500

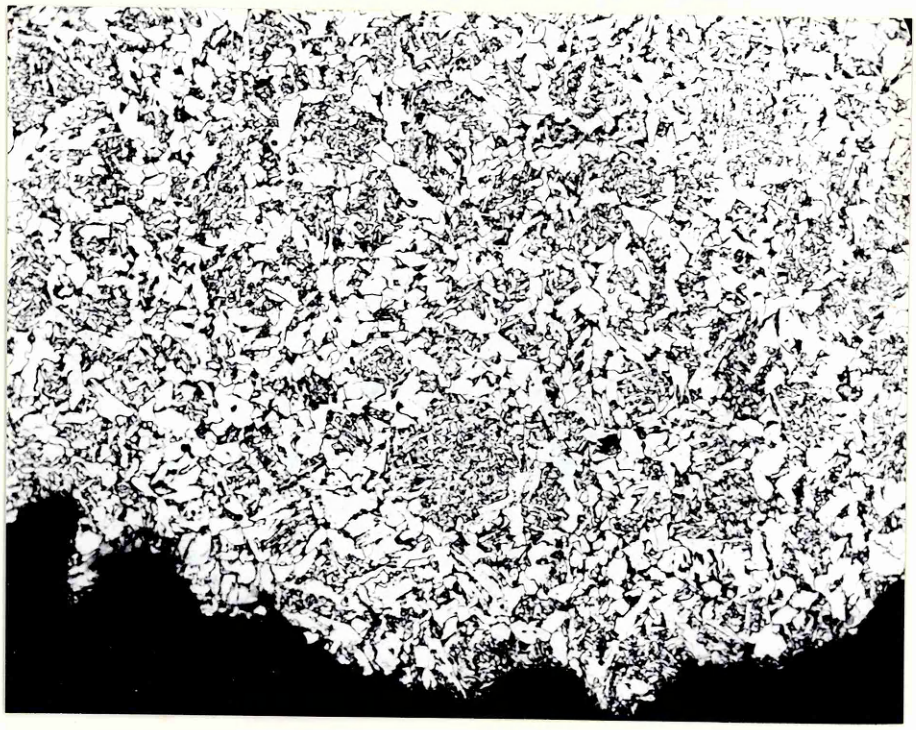

Figure 58 Weld 650 amp - 200 mm/min. Root Charpy V fracture path x 200

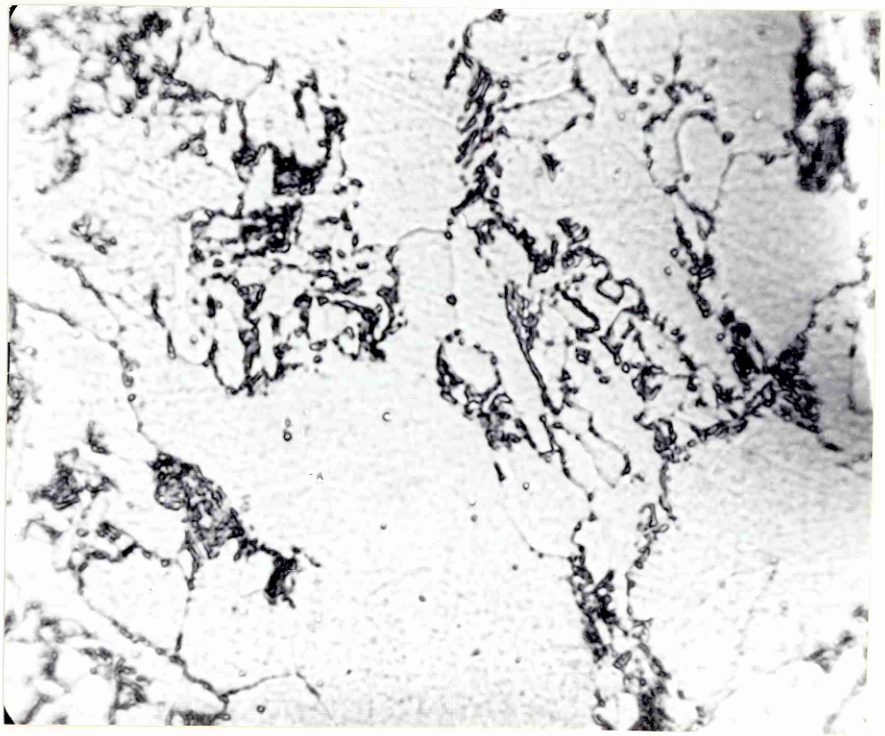

Figure 59 Weld 650 amp - 200 mm/min. Root M.A. Microphases x 2,000

Figure 60 Weld 650 amp - 300 mm/min. Sub-Surface δ Ferrite Structure x 50

Figure 61 Weld 650 amp - 300 mm/min. Sub-Surface Columnar Structure x 50

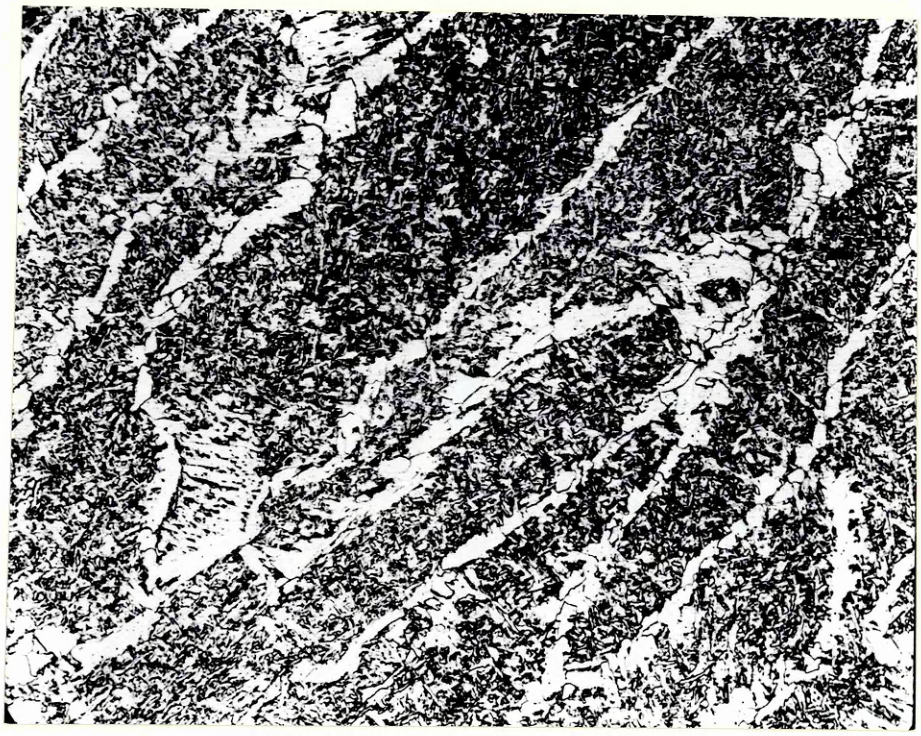

Figure 62 Weld 650 amp - 300 mm/min. Sub-Surface as deposited structure x 200

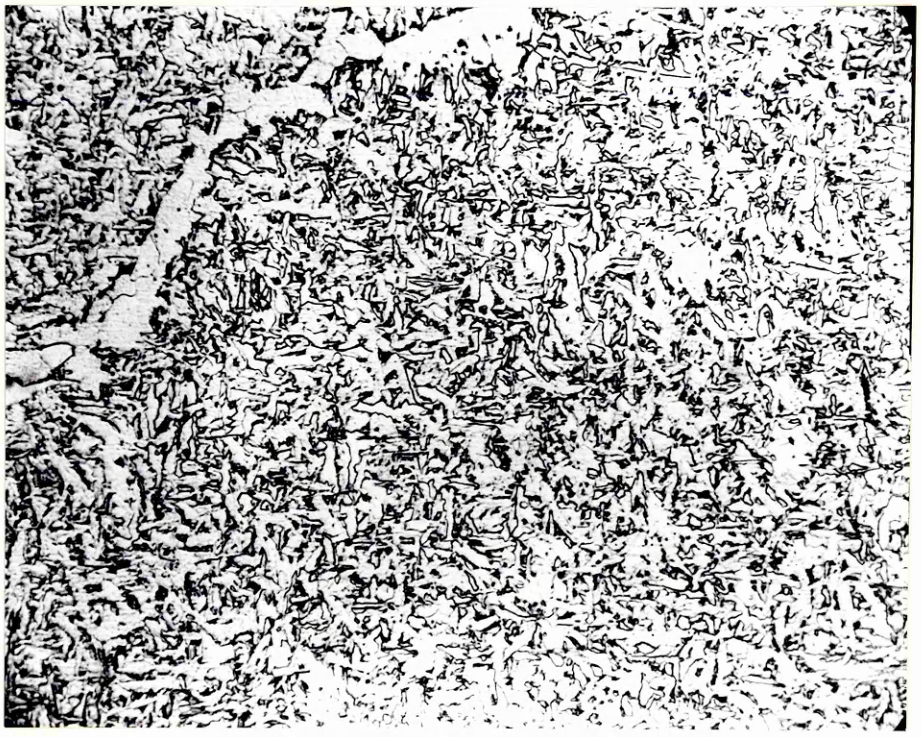

Figure 63 Weld 650 amp - 300 mm/min. Sub-Surface as deposited structure x 500

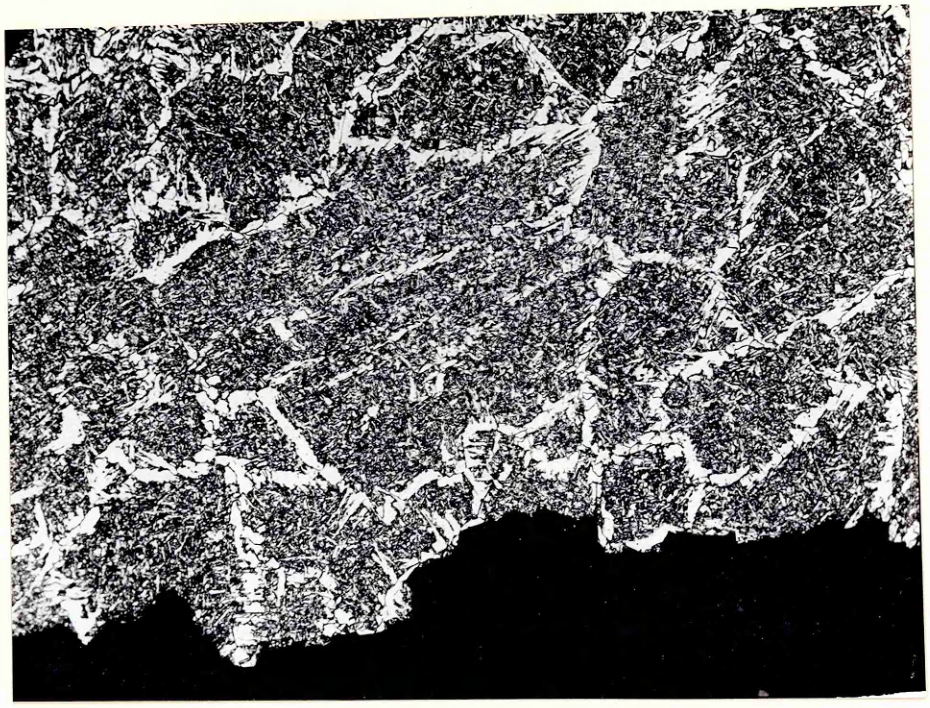

Figure 64 Weld 650 amp - 300 mm/min. Sub-Surface
Charpy V fracture path x 200

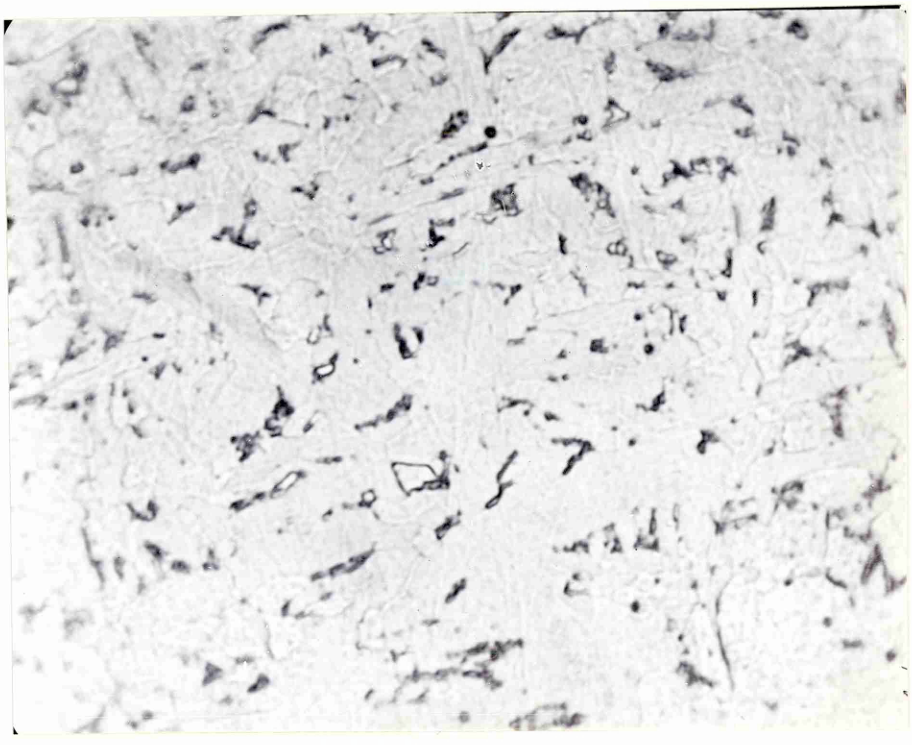

Figure 65 Weld 650 amp - 300 mm/min. Sub-Surface
M.A. Microphases x 2,000

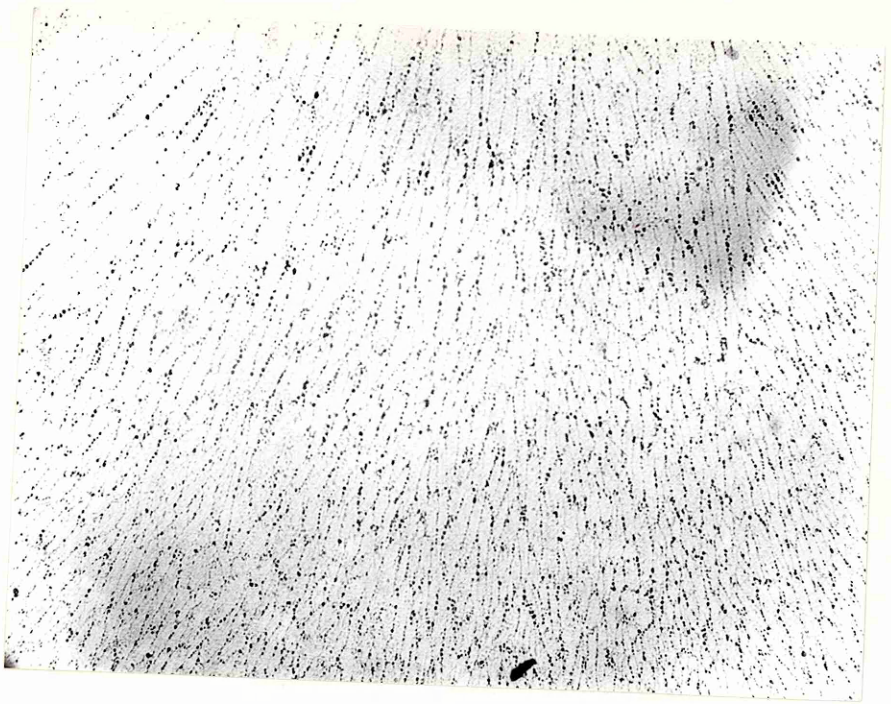

Figure 66 Weld 650 amp - 300 mm/min. Root δ Ferrite Structure x 50

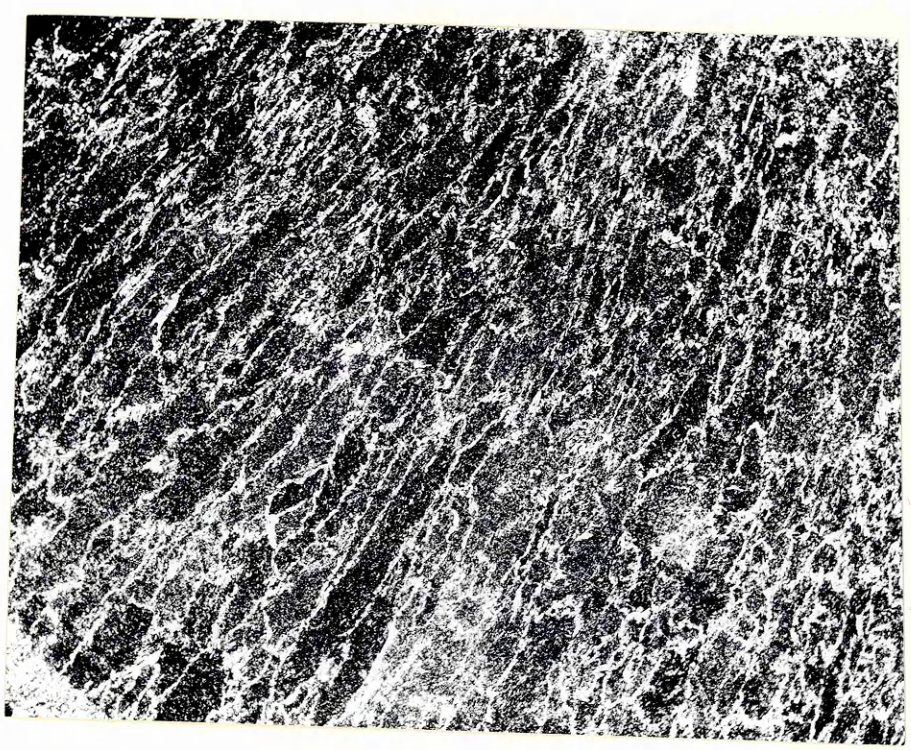

Figure 67 Weld 650 amp - 300 mm/min. Root Columnar Structure x 50

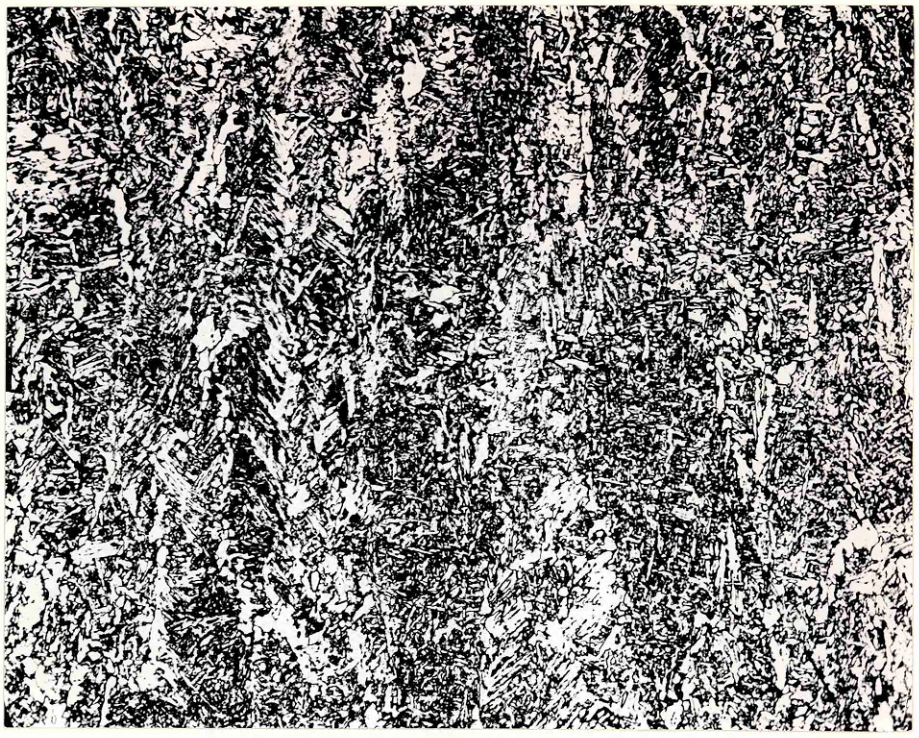

Figure 68 Weld 650 amp - 300 mm/min. Root as deposited structure x 200

Figure 69 Weld 650 amp - 300 mm/min. Root as deposited structure x 500

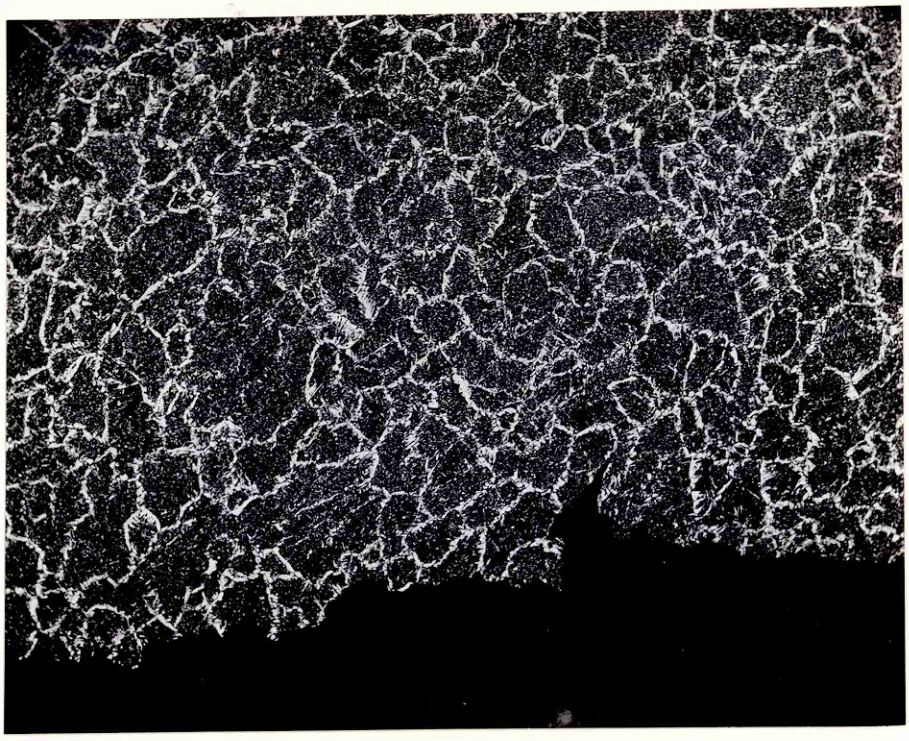

Figure 70 Weld 650 amp - 300 mm/min. Root Charpy V fracture path x 200

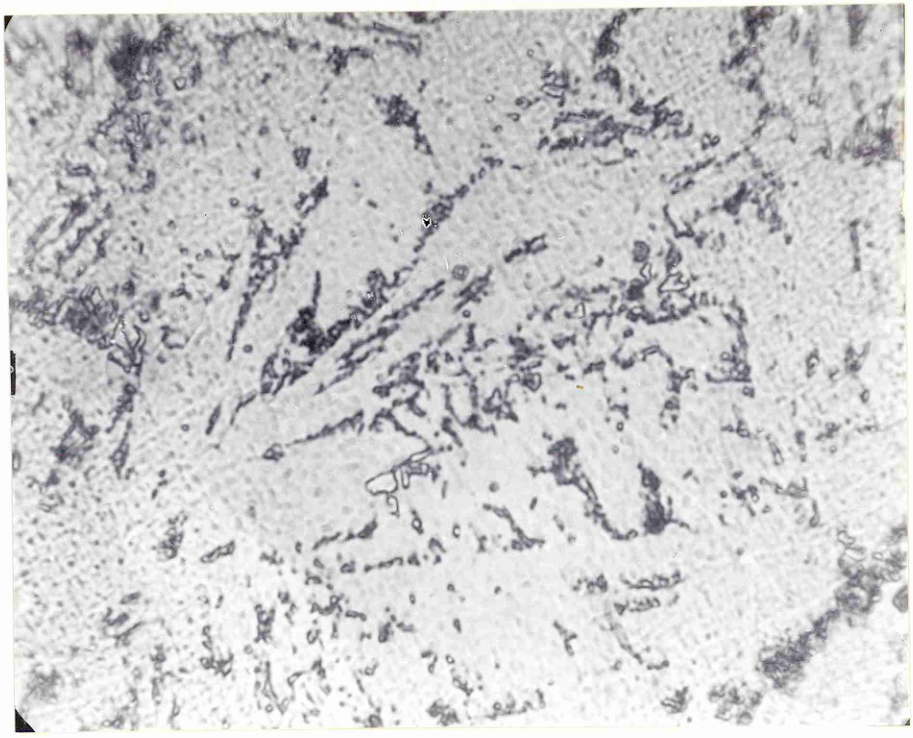

Figure 71 Weld 650 amp - 300 mm/min. Root M.A. Microphases x 2,000

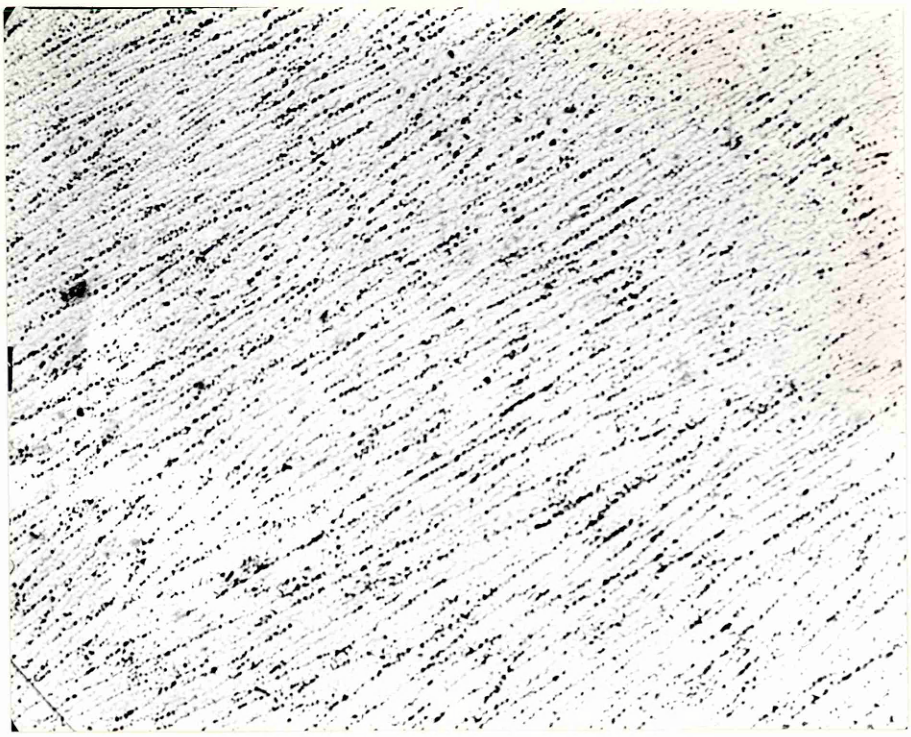

Figure 72 Weld 650 amp - 400 mm/min. Sub-Surface δ Ferrite Structure x 50

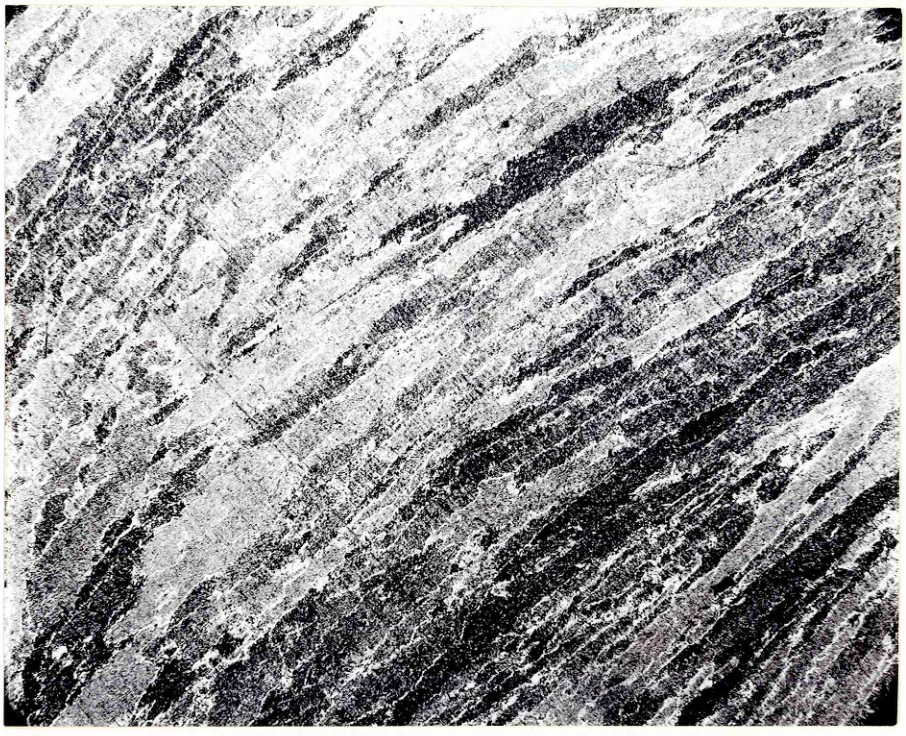

Figure 73 Weld 650 amp - 400 mm/min. Sub-Surface Columnar Structure x 50

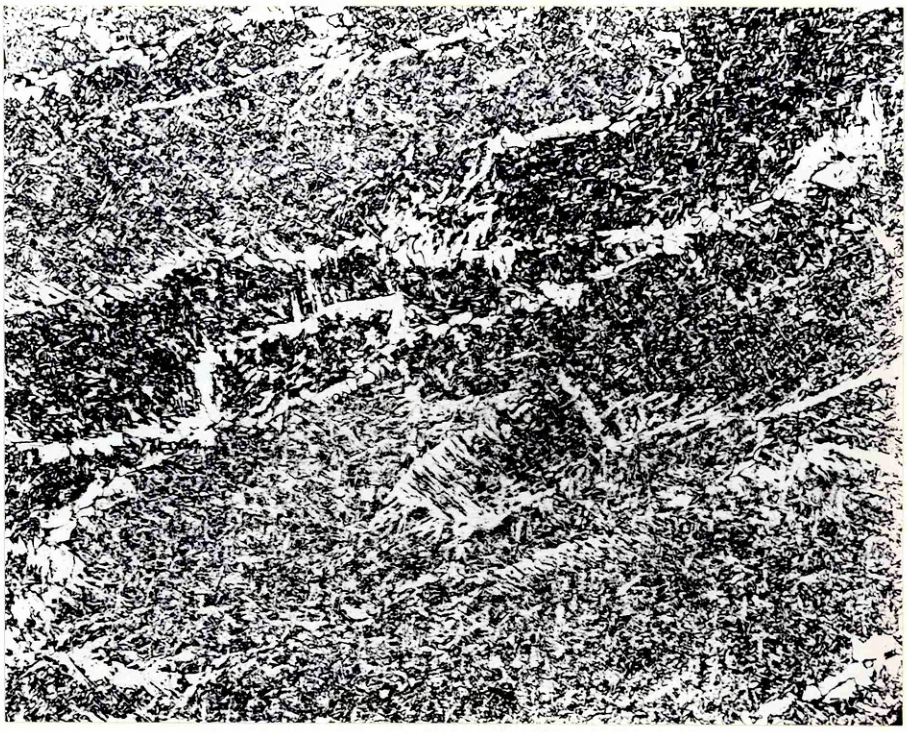

Figure 74 Weld 650 amp - 400 mm/min. Sub-Surface as deposited structure x 200

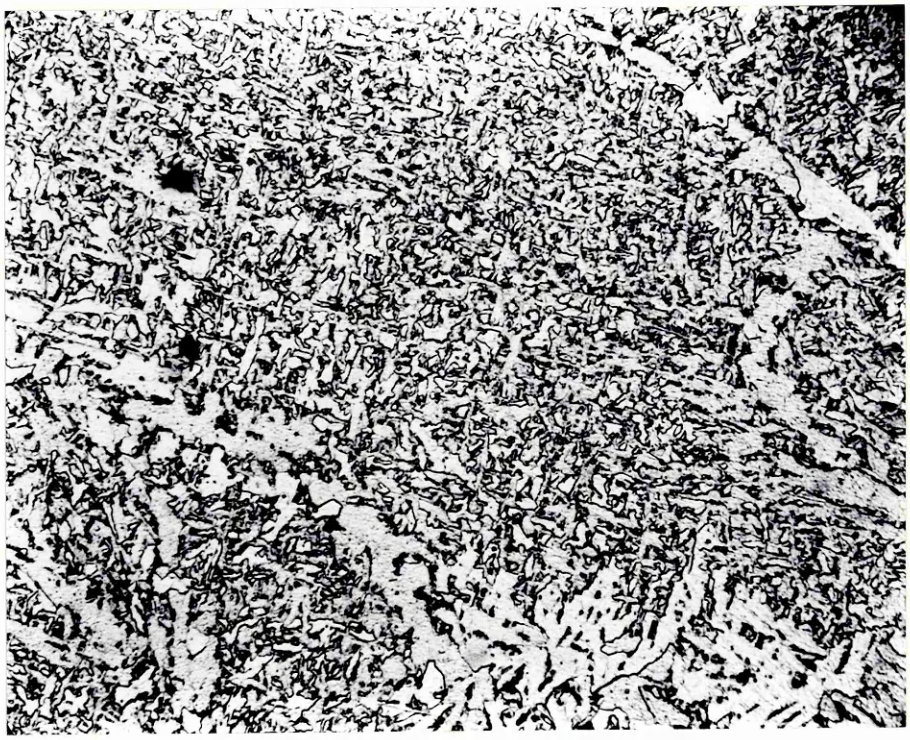

Figure 75 Weld 650 amp - 400 mm/min. Sub-Surface as deposited structure x 500

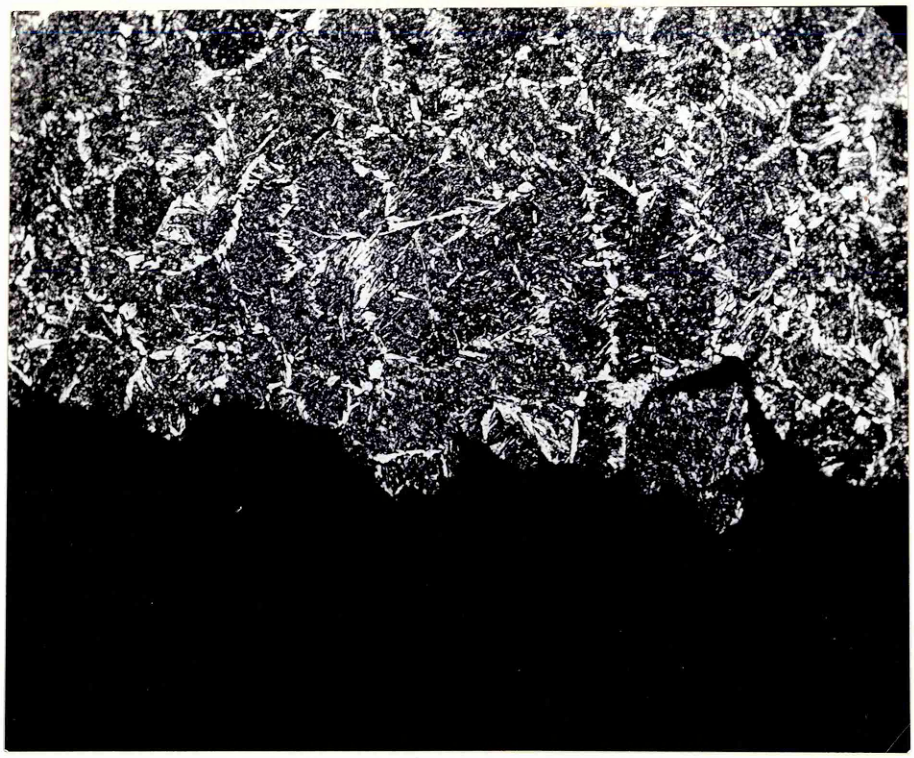

Figure 76 Weld 650 amp - 400 mm/min. Sub-Surface
Charpy V fracture path x 200

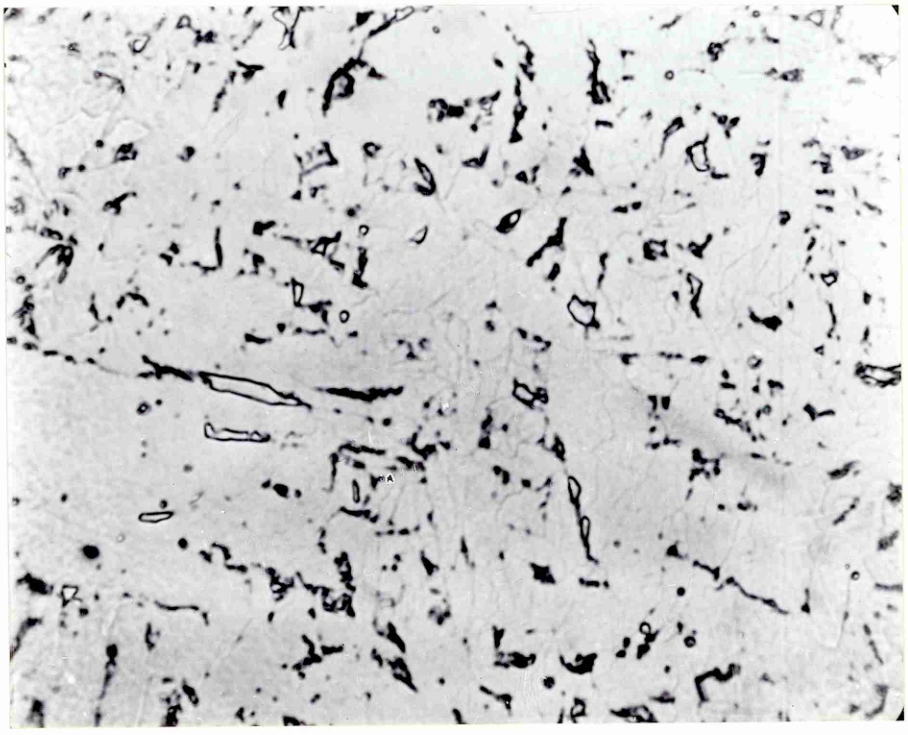

Figure 77 Weld 650 amp - 400 mm/min. Sub-Surface
M.A. Microphases x 2,000

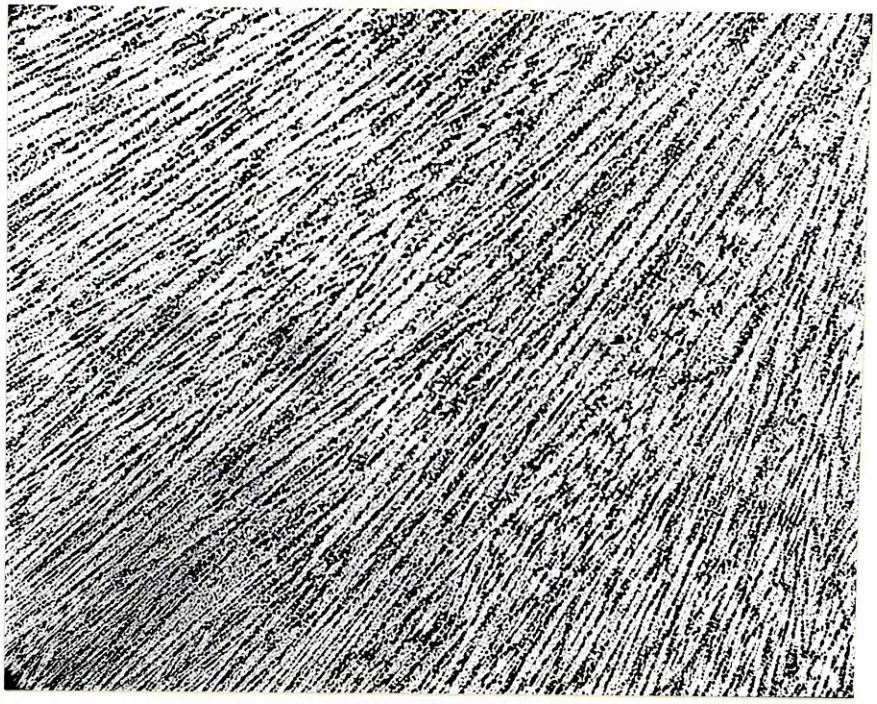

Figure 78 Weld 650 amp - 400 mm/min. Root δ Ferrite Structure x 50

Figure 79 Weld 650 amp - 400 mm/min. Root Columnar Structure x 50

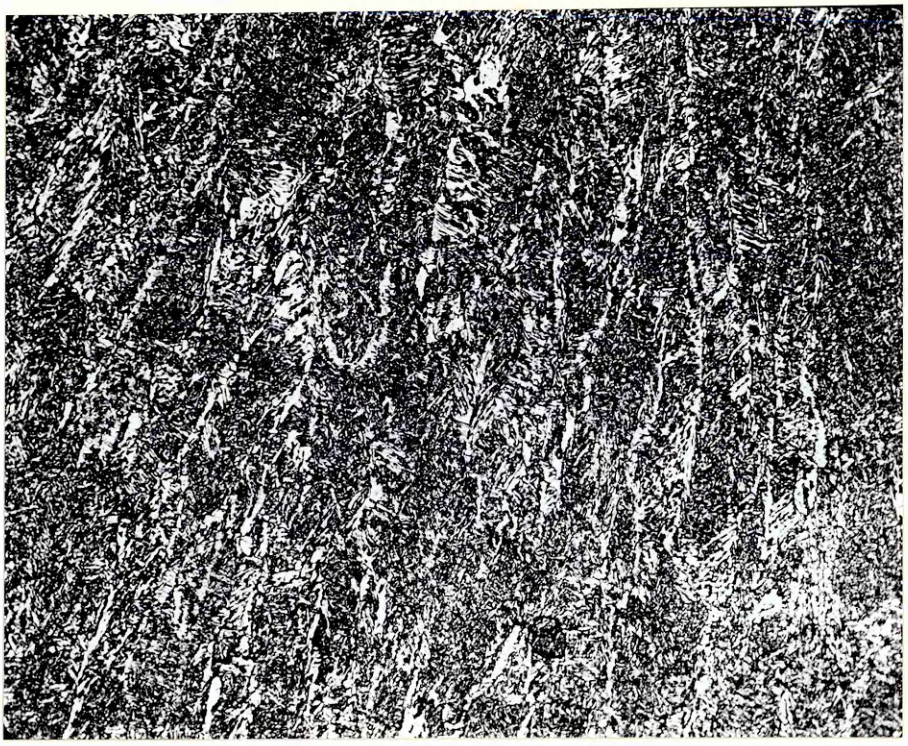

Figure 80 Weld 650 amp - 400 mm/min. Root as deposited structure x 200

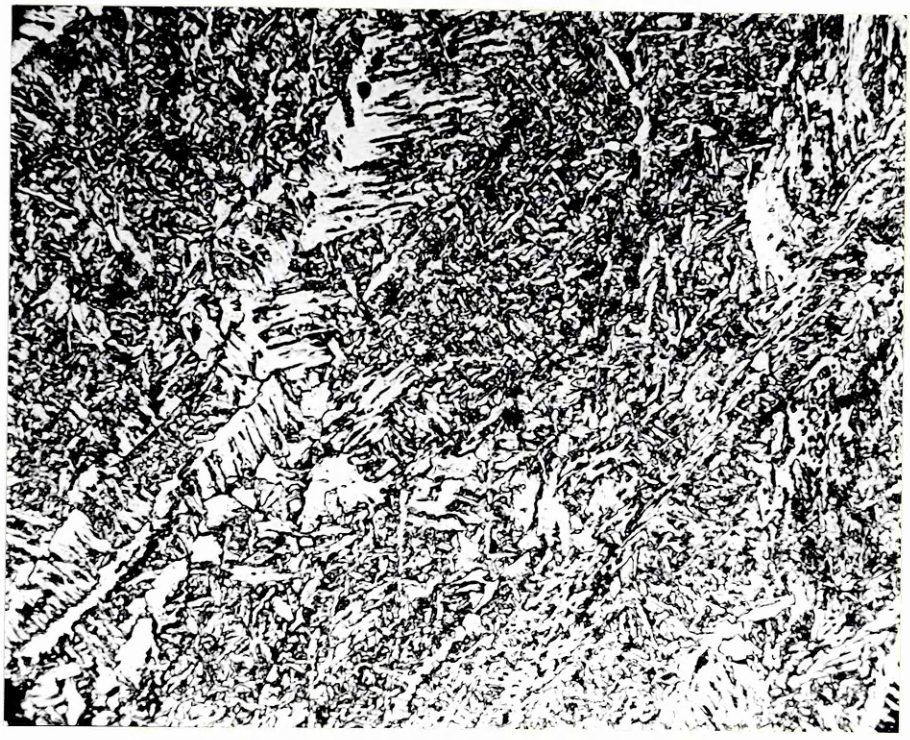

Figure 81 Weld 650 amp - 400 mm/min. Root as deposited structure x 500

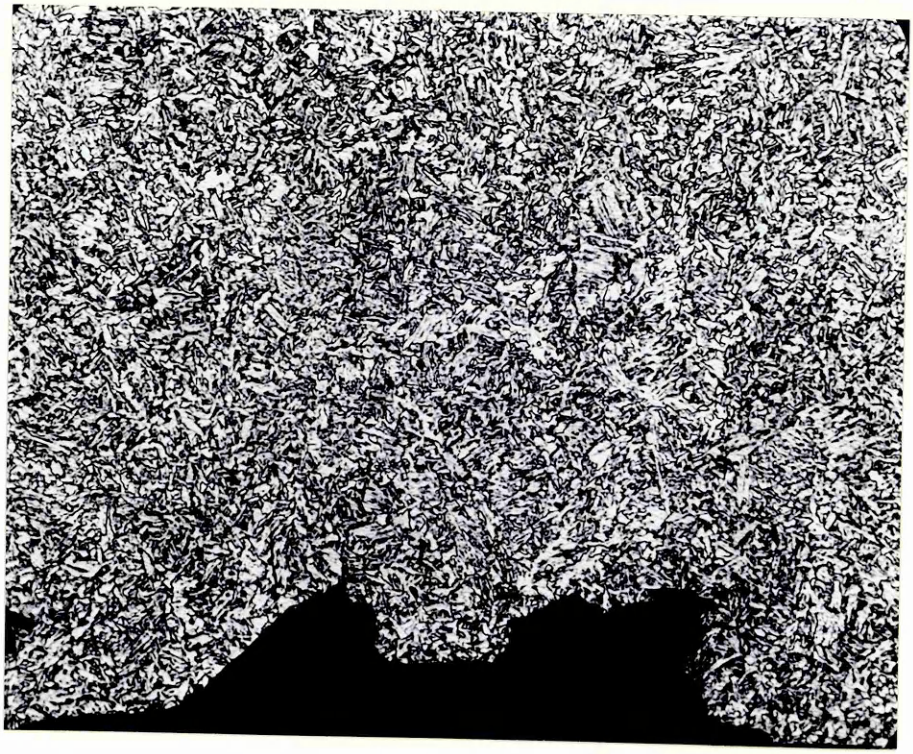

Figure 82 Weld 650 amp - 400 mm/min. Root Charpy V fracture path x 200

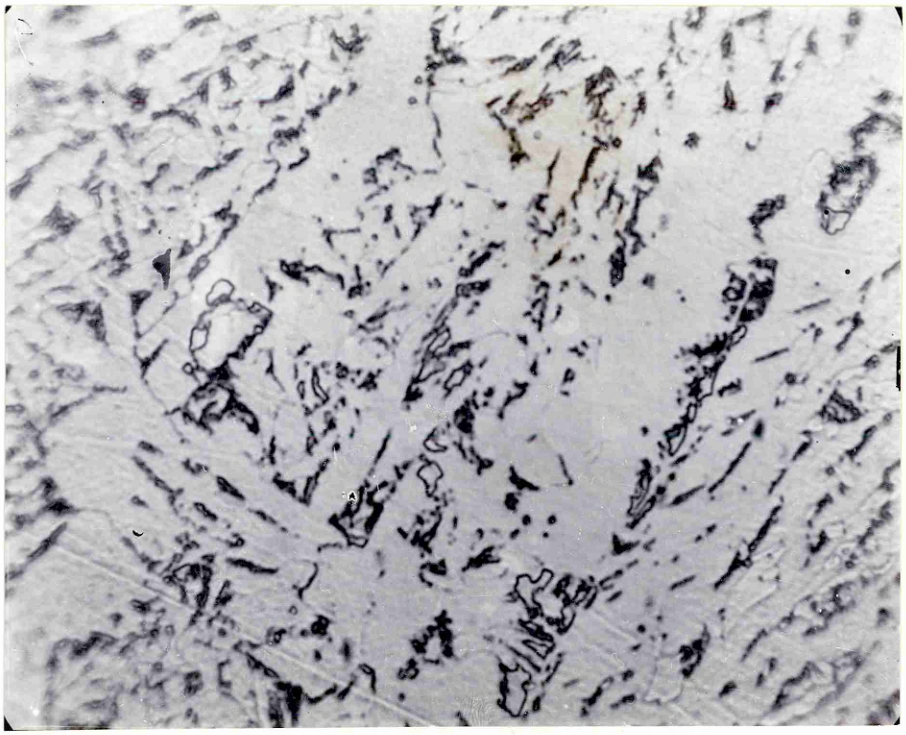

Figure 83 Weld 650 amp - 400 mm/min. Root M.A. Microphases x 2,000

Figure 84 Weld 850 amp - 300 mm/min. Sub-Surface δ Ferrite Structure x 50

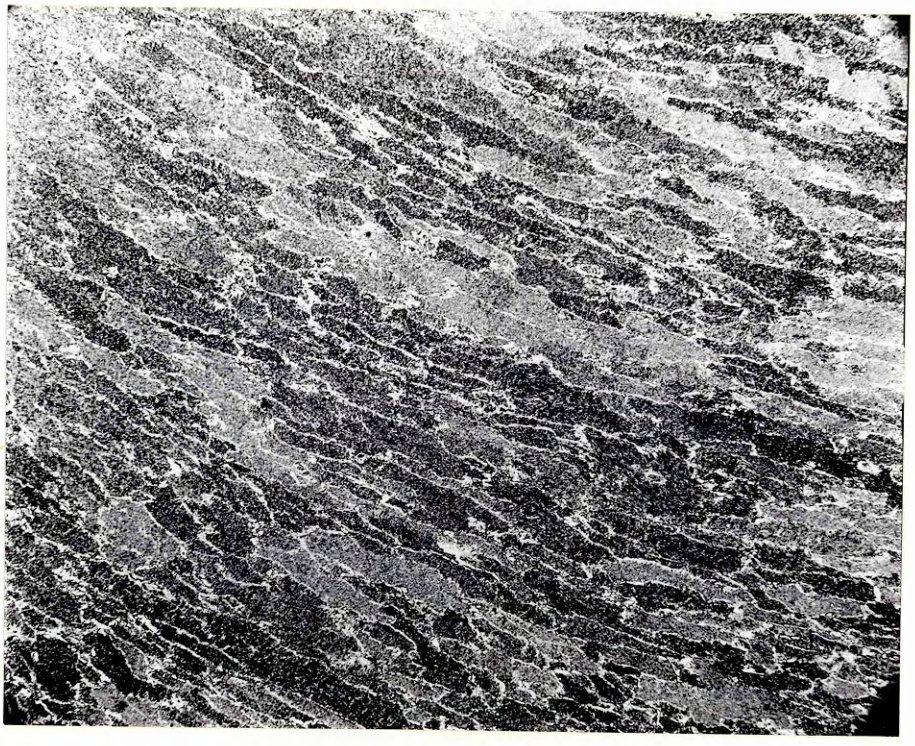

Figure 85 Weld 850 amp - 300 mm/min. Sub-Surface Columnar Structure x 50

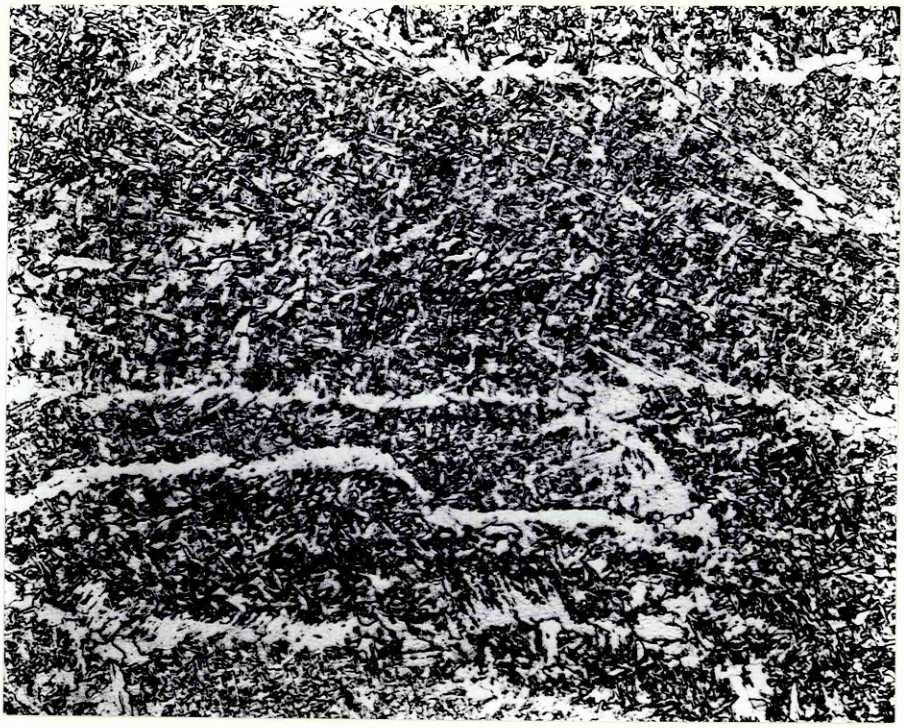

Figure 86 Weld 850 amp - 300 mm/min. Sub-Surface as deposited structure x 200

Figure 87 Weld 850 amp - 300 mm/min. Sub-Surface as deposited structure x 500

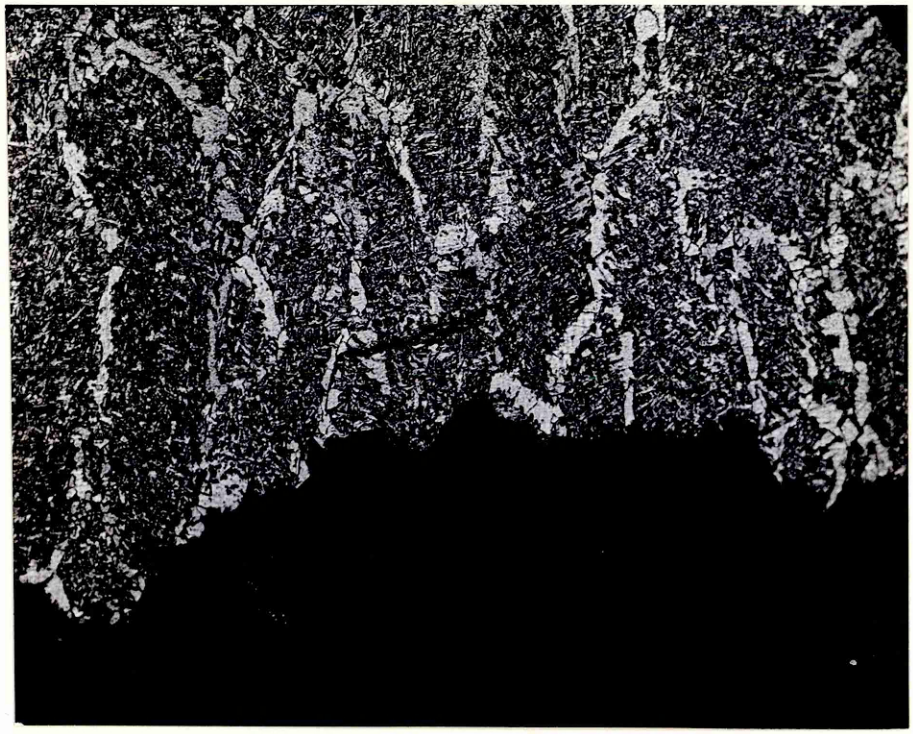

Figure 88 Weld 850 amp - 300 mm/min. Sub-Surface Charpy V fracture path x 200

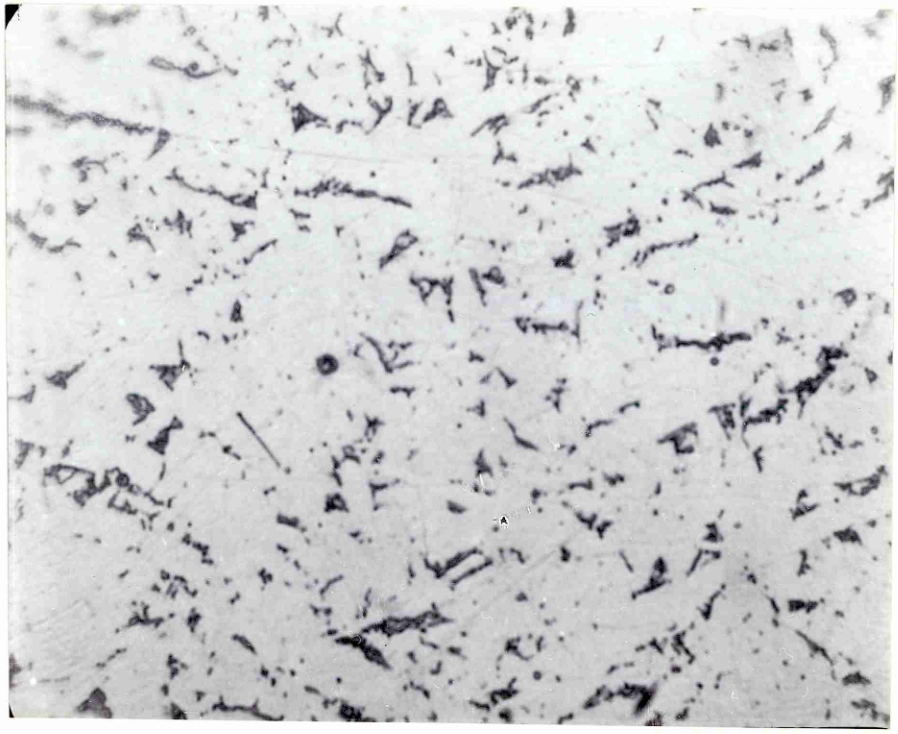

Figure 89 Weld 850 amp - 300 mm/min. Sub-Surface M.A. Microphases x 2,000

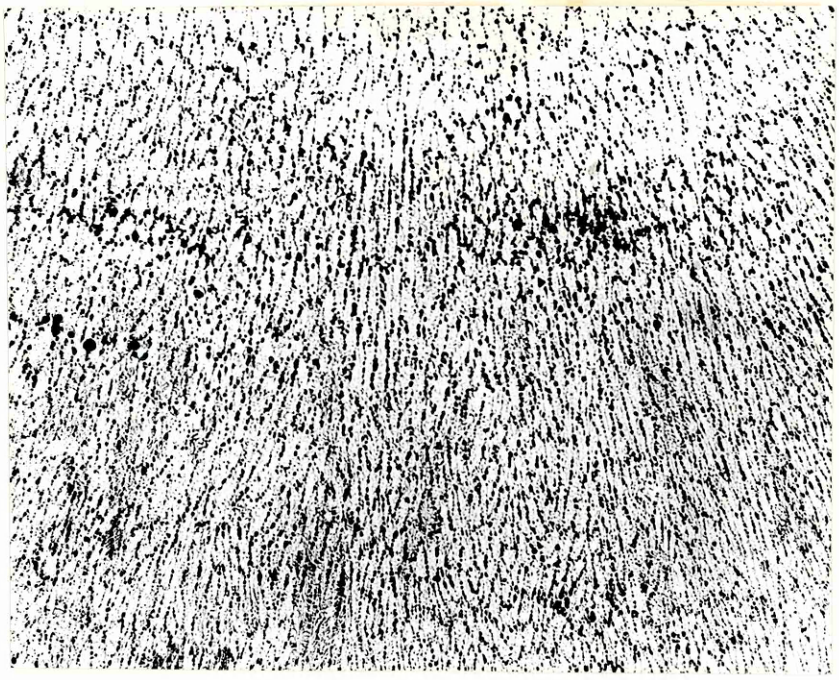

Figure 90 Weld 850 amp - 300 mm/min. Root & Ferrite Structure x 50

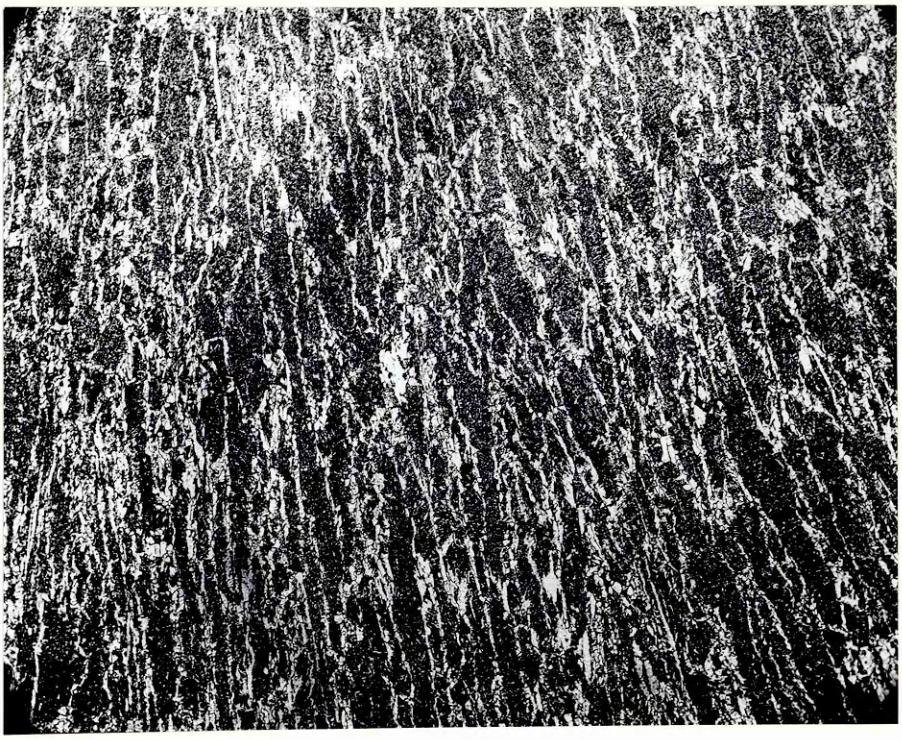

Figure 91 Weld 850 amp - 300 mm/min. Root Columnar Structure x 50

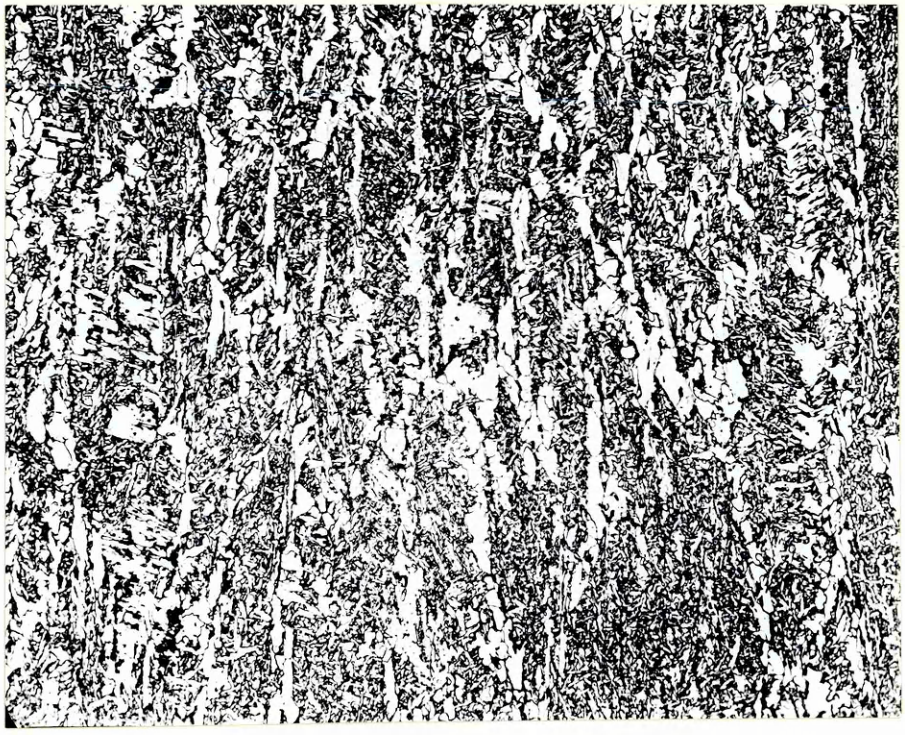

Figure 92 Weld 850 amp - 300 mm/min. Root as deposited structure x 200

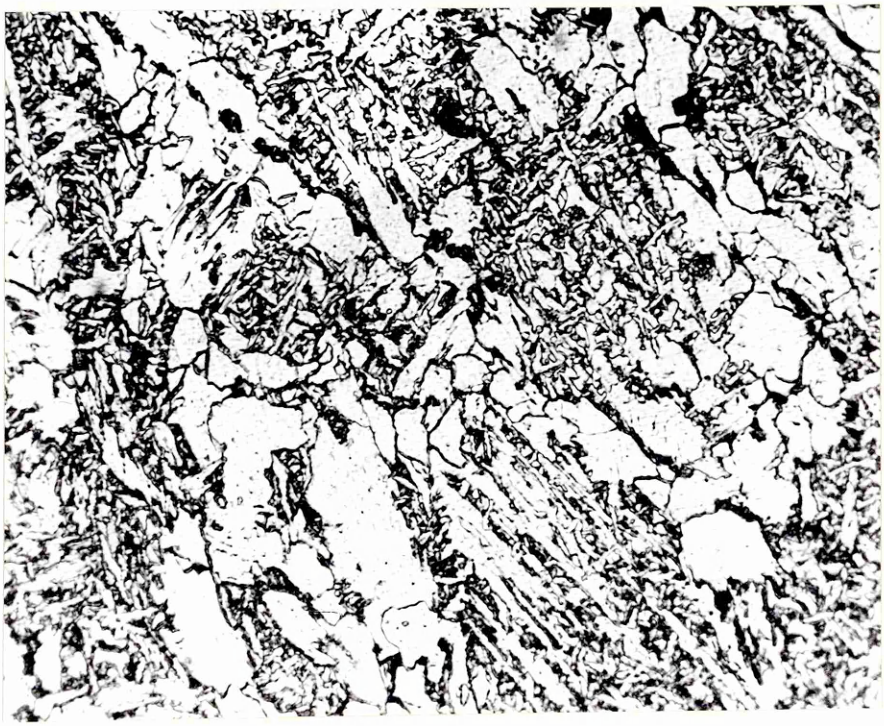

Figure 93 Weld 850 amp - 300 mm/min. Root as deposited structure x 500

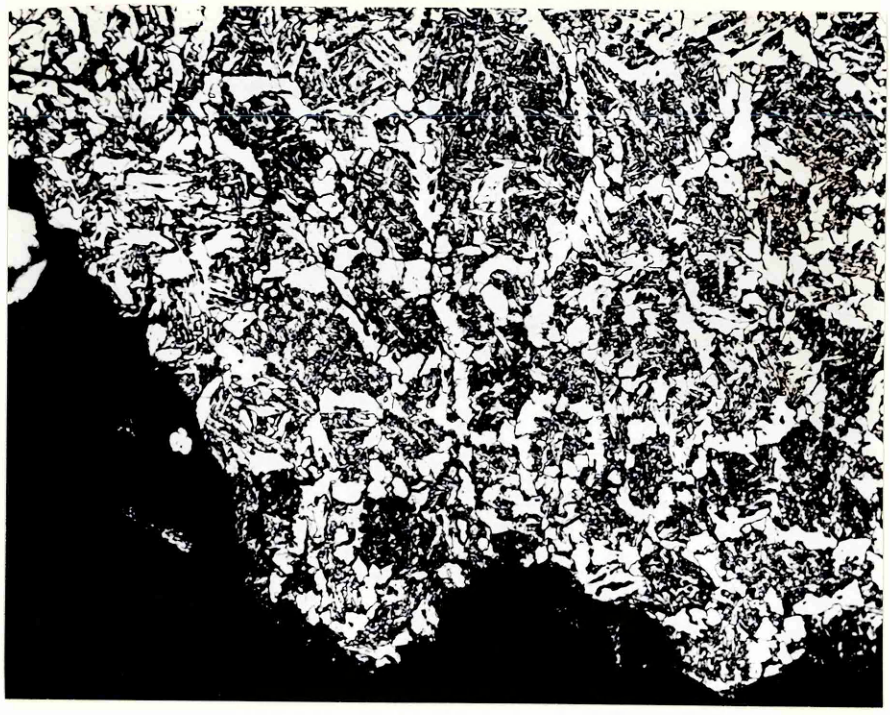

Figure 94 Weld 850 amp - 300 mm/min. Root Charpy V fracture path x 200

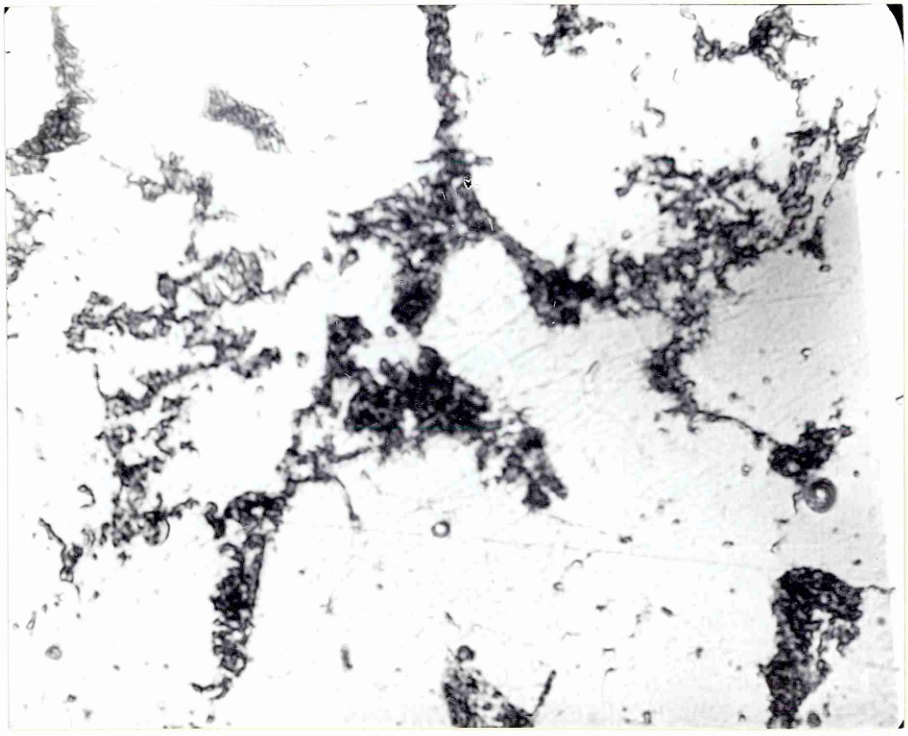

Figure 95 Weld 850 amp - 300 mm/min. Root M.A. Microphases x 2,000

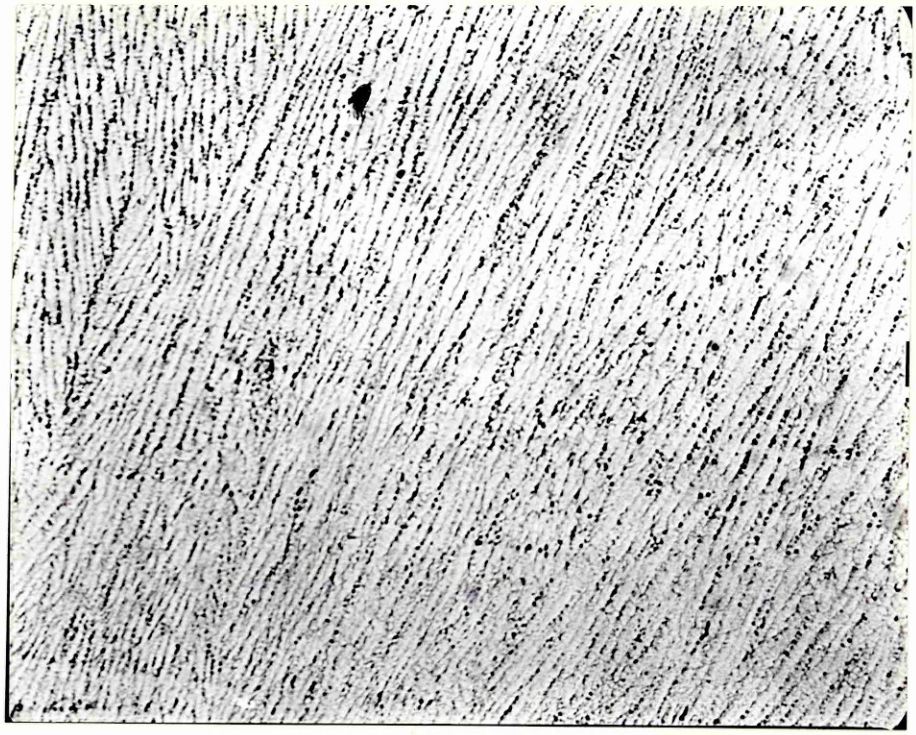

Figure 96 Weld 480 amp - 300 mm/min. Sub-Surface δ Ferrite Structure x 50

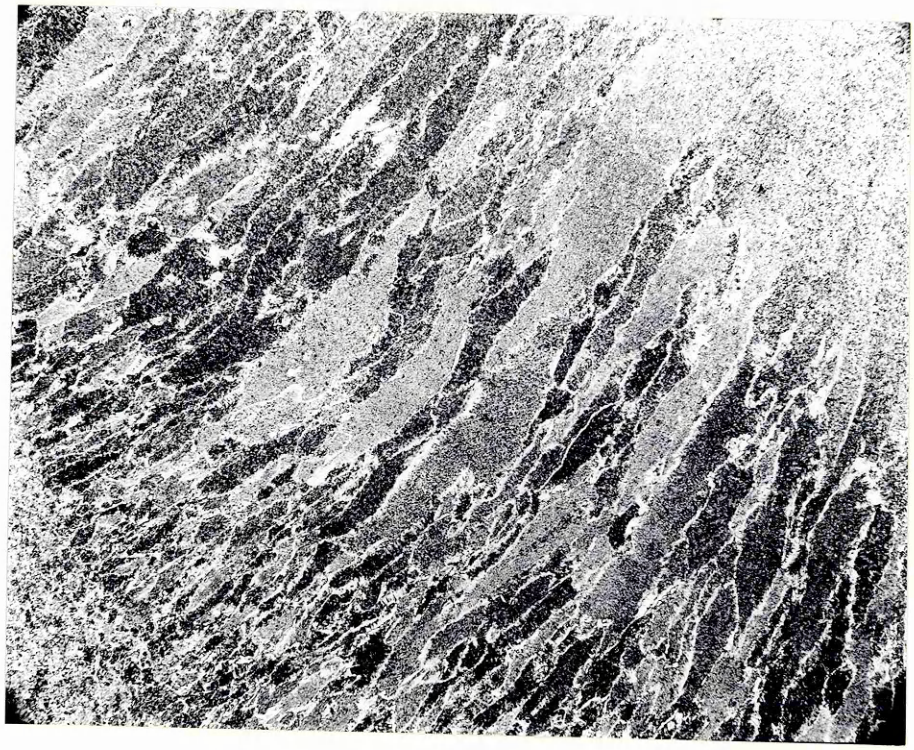

Figure 97 Weld 480 amp - 300 mm/min. Sub-Surface Columnar Structure x 50

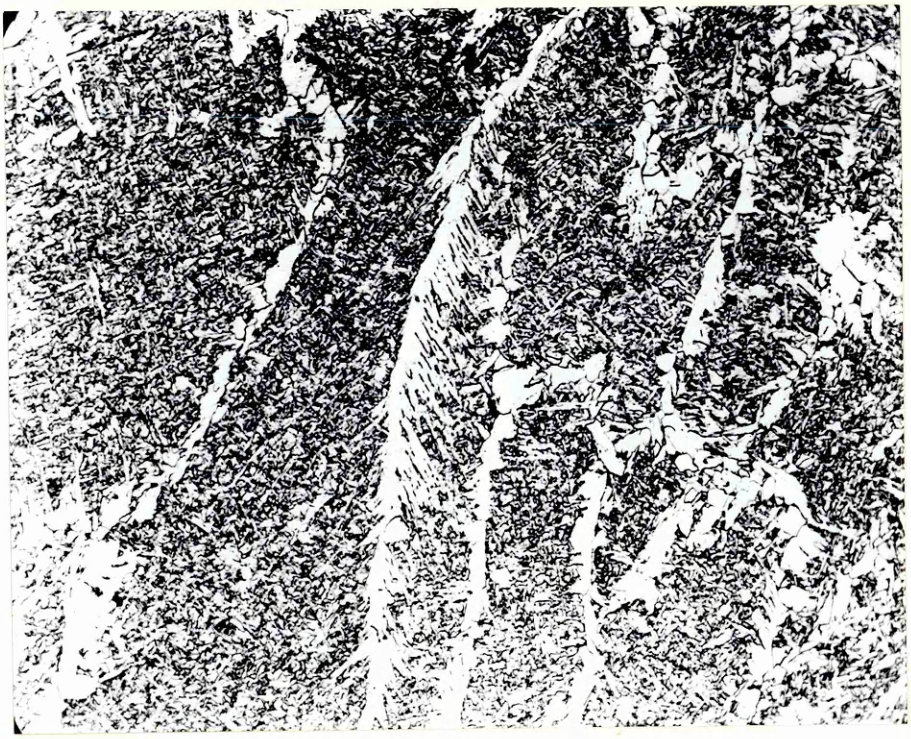

Figure 98 Weld 480 amp - 300 mm/min. Sub-Surface as deposited structure x 200

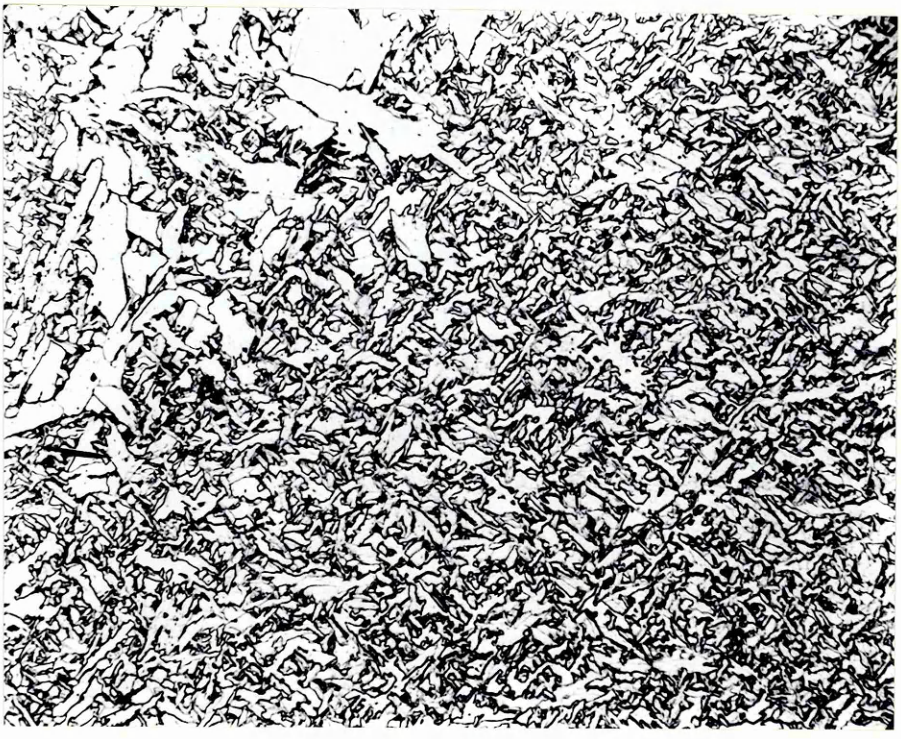

Figure 99 Weld 480 amp - 300 mm/min. Sub-Surface as deposited structure x 500

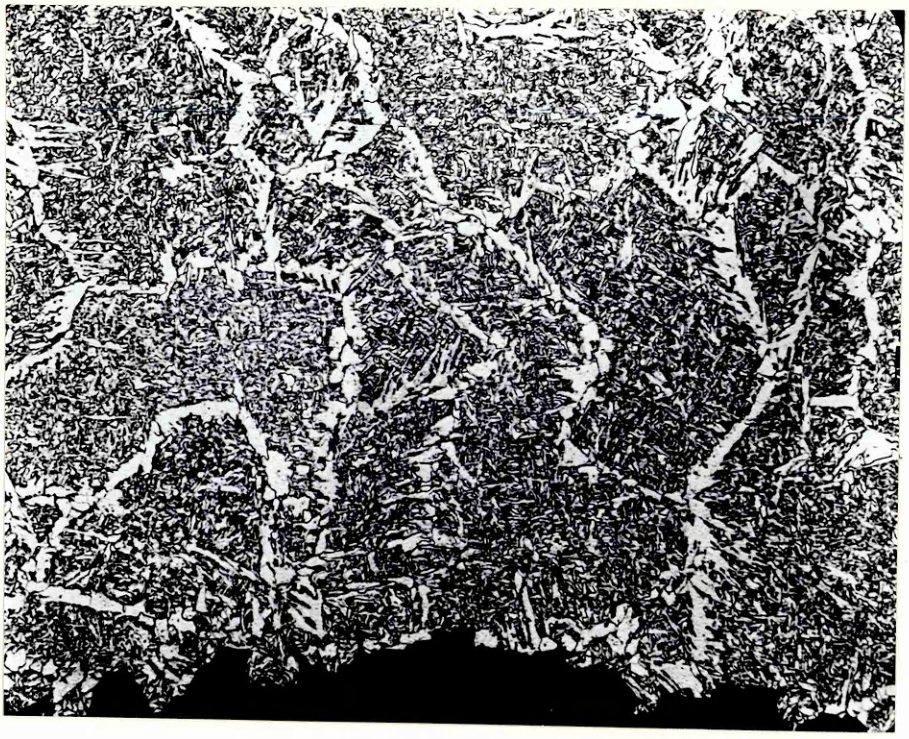

Figure 100 Weld 480 amp - 300 mm/min. Sub-Surface
Charpy V fracture path x 200

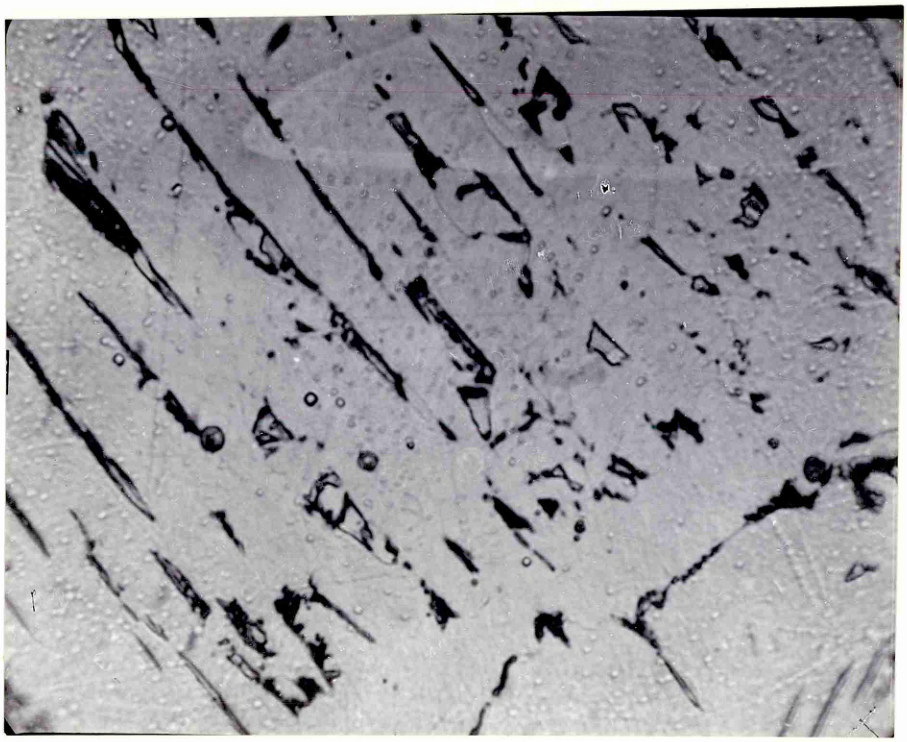

Figure 101 Weld 480 amp - 300 mm/min. Sub-Surface
M.A. Microphases x 2,000

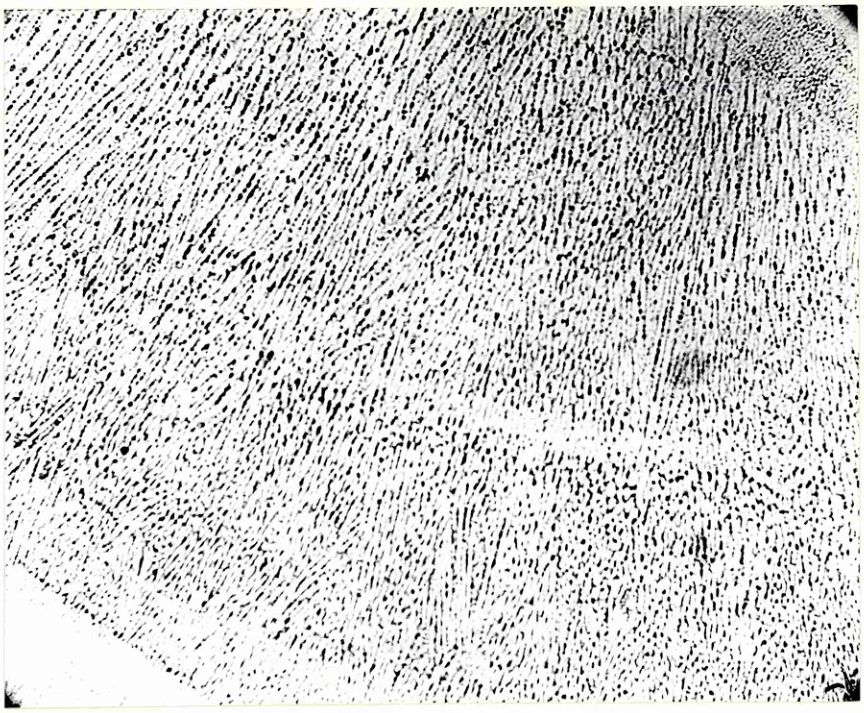

Figure 102 Weld 480 amp - 300 mm/min. Root & Ferrite Structure x 50

Figure 103 Weld 480 amp - 300 mm/min. Root Columnar Structure x 50

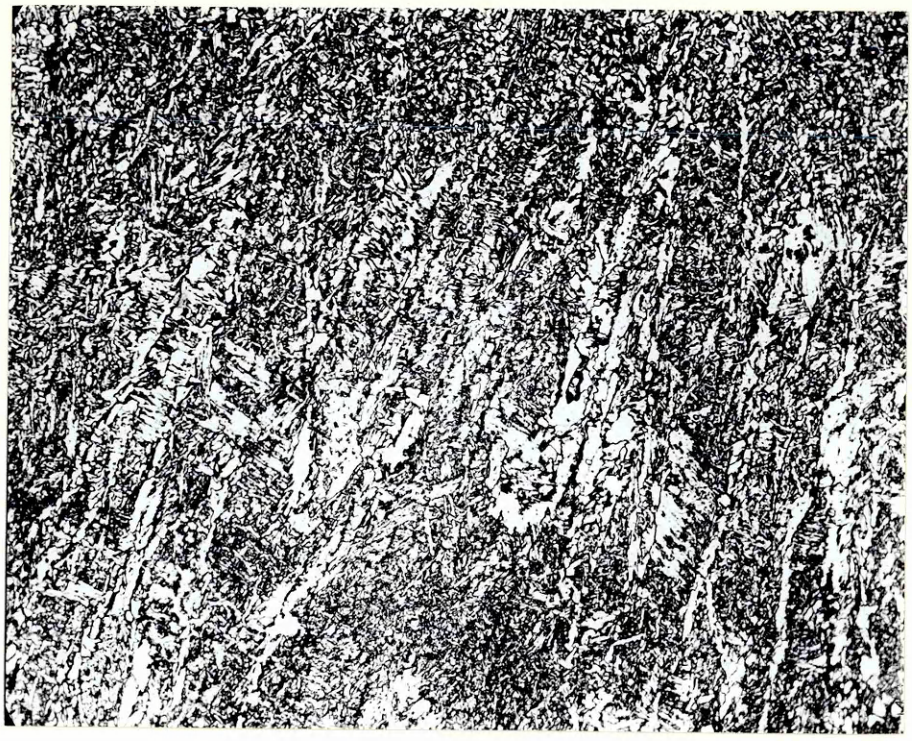

Figure 104 Weld 480 amp - 300 mm/min. Root as deposited structure x 200

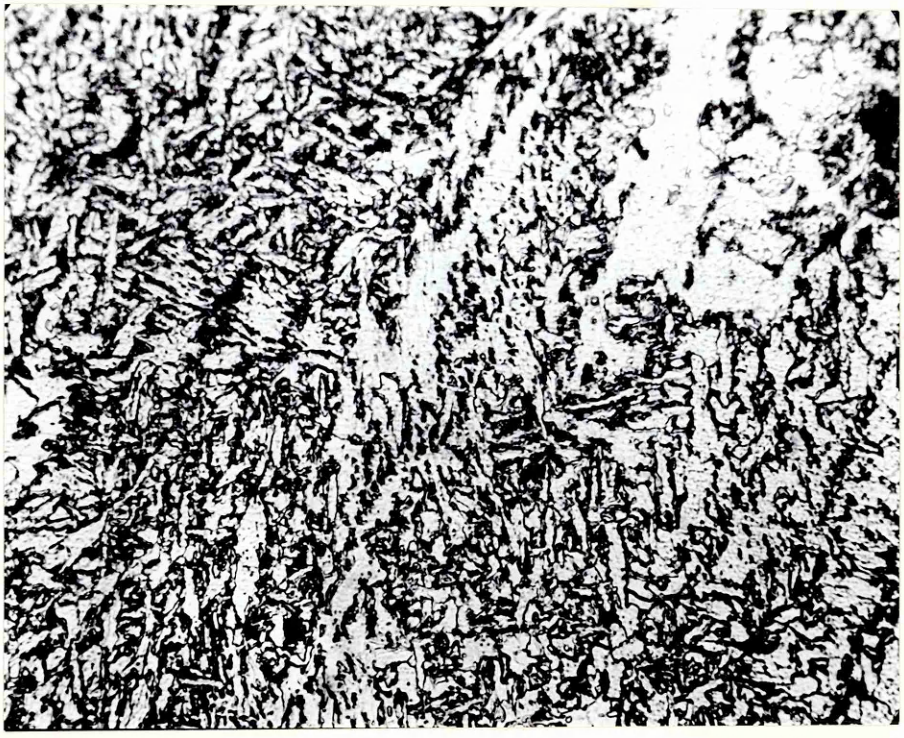

Figure 105 Weld 480 amp - 300 mm/min. Root as deposited structure x 500

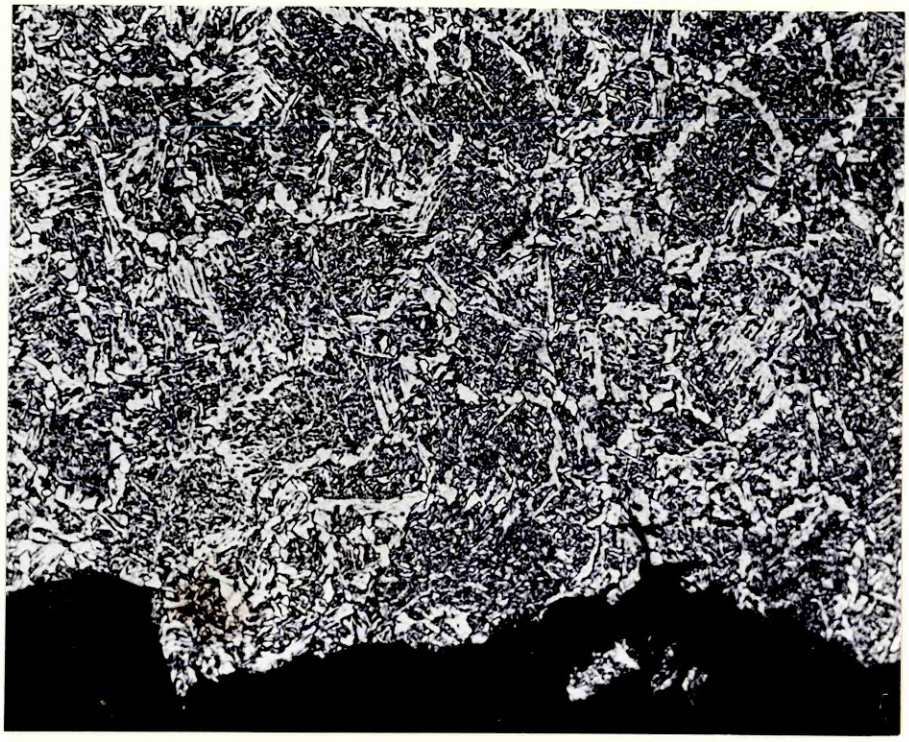

Figure 106 Weld 480 amp - 300 mm/min. Root Charpy V fracture path x 200

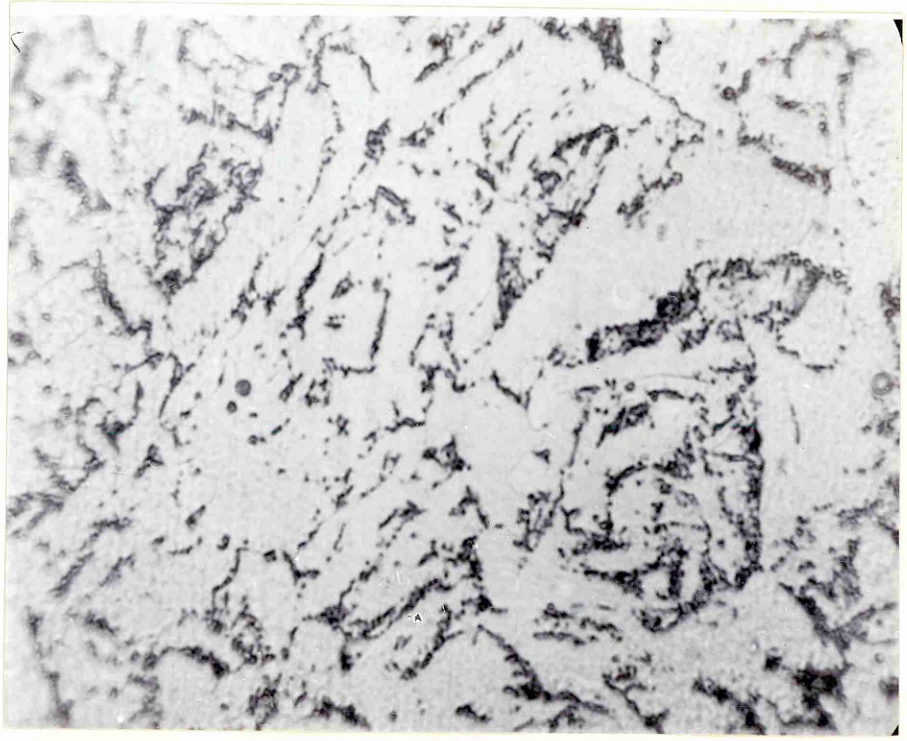

Figure 107 Weld 480 amp - 300 mm/min. Root M.A. Microphases x 2000

Tensile and Hardness Results

The tensile and Vickers hardness test results are shown in Table 20.

The sub-surface tensile results showed that an increase in welding speed from 200 mm/min to 300 mm/min led to a decrease of 8% in L.Y.S. and 4% in U.T.S. A further increase in welding speed from 300 mm/min to 400 mm/min led to an increase of 15% in L.Y.S. and 10% in U.T.S.

A decrease in welding current from 850 amps to 650 amps led to a decrease of 9% in L.Y.S. and 5% in U.T.S. but a further decrease in welding current to 480 amps led to an increase of 15% in L.Y.S. and 9% in U.T.S.

For the root areas an increase in welding speed from 200 mm/min to 300 mm/min led to an increase of 10% in L.Y.S. and 7% in U.T.S.

A further increase in welding speed from 300 mm/min to 400 mm/min caused a further increase of 9% in L.Y.S. and 6% in U.T.S.

A decrease in welding current from 850 amps to 650 amps and then to 480 amps had a very small effect (of the order of 2%) on the L.Y.S. and U.T.S.

Comparing the tensile results for the sub-surface and root areas of each joint it was found that the root areas had systematically higher L.Y.S. and U.T.S. values than the sub-surface. Table 21.

A systematic correlation was not found between ductility as measured by the reduction of area or elongation and the welding parameters but for each welded joint the sub-surface areas showed higher or equal ductility than the root areas.

The Vickers hardness results did not show a systematic correlation with the arc parameters but for all joints the sub-surface areas had lower hardness values, table 21 , than the root areas.

Table 20 Weld Metal Strength and Hardness

| Welding Conditions | LYS $N/mm^2$ | UTS $N/mm^2$ | E.L. % | R.A. % | Vickers Hardness |
|---|---|---|---|---|---|
| 650 A/200 mm Sub-surface | 468 | 563 | 34 | 71 | 200 |
| 650 A/200 mm Root | 495 | 588 | 34 | 72 | 226 |
| 650 A/300 mm Sub-surface | 428 | 548 | 33 | 72 | 217 |
| 650 A/300 mm Root | 548 | 631 | 28 | 70 | 227 |
| 650 A/400 mm Sub-surface | 495 | 602 | 31 | 70 | 221 |
| 650 A/400 Root | 602 | 669 | 28 | 68 | 245 |
| 850 A/300 mm Sub-surface | 468 | 575 | 31 | 68 | 212 |
| 850 A/300 mm Root | 535 | 642 | 30 | 64 | 232 |
| 480 A/300 mm Sub-surface | 495 | 602 | 34 | 70 | 212 |
| 480 A/300 mm Root | 535 | 616 | 28 | 70 | 245 |

Table 21 Differences between the Sub-surface and Root Strength and Hardness

| Welding Conditions | Difference between Sub-surface and Root Values | | | | |
|---|---|---|---|---|---|
| | L.Y.S. $N/mm^2$ | U.T.S. $N/mm^2$ | E.L. % | R.A. % | Vicker Hardness |
| 650A/200 mm | - 27 | - 25 | 0 | -1 | - 26 |
| 650A/300 mm | - 120 | - 83 | +5 | +2 | - 10 |
| 650A/400 mm | - 107 | - 67 | +3 | +2 | - 24 |
| 850A/300 mm | - 67 | - 67 | +1 | +4 | - 20 |
| 480A/300 mm | - 40 | - 14 | +6 | 0 | - 33 |

Summary

A correlation between L.Y.S. and U.T.S., and the welding arc parameters could not be found since an increase in welding speed or a decrease in welding current did not lead to a systematic variation in the strength.

All root weld beads had a higher L.Y.S. and U.T.S. but a lower ductility than the corresponding sub-surface beads.

Likewise, the root beads also had higher Vickers hardness values than the corresponding sub-surface beads, but no systematic correlation between welding arc parameter and hardness was found.

IMPACT TEST RESULTS

The Charpy V notch impact test results are shown in table 22 and figures 108, to 120.

Weld deposits made with a Welding Current of 650 amp

The results for the sub-surface region of the weld deposits made using the same arc current of 650 amps, figure 108, shows that for all three speeds (200 mm/min; 300 mm/min and 400 mm/min) very similar lower shelf energies and transition temperatures were obtained.

The upper shelf energies were different for each weld deposit. That made at a speed of 200 mm/min had the highest energy (approx. 190J) followed by the weld deposit made at 300 mm/min (approx. 175J) and then the weld deposit made at 400 mm/min (approx. 160J).

The results for the root regions of the three weld deposits showed similar lower and upper shelf energies (approx. 12J and 170J), but different transition temperatures. Figure 109.

The weld made at a welding speed of 200 mm/min had the highest transition temperature (approx. 100J at $0^{\circ}C$). The other two welds having similar, lower transition temperatures (approx. 100J at $-15^{\circ}C$).

Weld Deposits made with a Welding Speed of 300 mm/min

The results for the sub-surface region, figure 110, show that the lower shelf energies were similar for all three weld deposits but there was a large variation in both the transition temperature and upper shelf energies.

The weld deposit made at the highest welding current (850 amps) had the lowest transition temperature of the three welds, (approx. 100J at $-50^{\circ}C$) with the weld deposit made at a welding current of 650 amps. The highest transition temperature (approx. 100J at $-15^{\circ}C$).

The upper shelf energies were different for each weld deposit. The weld deposit made with a welding current of 480 amps had the highest value (approx. 220J) followed by the weld deposit made at 850 amps (approx. 195J). The weld deposit made at 650 amps had the lowest upper shelf energy (approx. 175J).

The results for the root regions of the weld deposits made at a welding speed of 300 mm/min show that all three weld deposits had, as for the sub-surface region, very similar lower shelf energies (approx. 10J). Figure 111. But in contrast to the sub-surface the weld made at a welding current of 850 amps had the highest transition temperature (approx. 100 at $+5^{\circ}C$) and the weld deposit made at 650 amps the lowest transition temperature (approx. 100J at $-10^{\circ}C$) with the weld made at 480 amps falling in between (approx. 100J at $-20^{\circ}C$).

The weld deposit made at 480 amps had the highest upper shelf energy of all three weld deposits (approx. 200J), the welds made at 850 amps and 650 amps being very similar (approx. 175J).

Table 22 Charpy V Notch Impact Results

| Welding Condition | Test Temperatures (Energy J) | | | | | | |
|---|---|---|---|---|---|---|---|
| | - 90°C | - 60 | - 30 | 0 | + 30 | + 60 | + 90 |
| 650 amp - 200 mm/min | | | | | | | |
| sub-surface | 8 | 21 | 56.7 | 129 | 182 | 197 | 190 |
| Root | 6.75 | 16.2 | 50.7 | 104 | 133 | 174 | 167 |
| 650 amp - 300 mm/min | | | | | | | |
| sub-surface | 9.4 | 31.8 | 60.7 | 136.3 | 152.2 | 170 | 159 |
| Root | 16.2 | 30.5 | 86 | 141 | 150 | 178 | 168 |
| 650 amp - 400 mm/min | | | | | | | |
| sub-surface | 13.5 | 16.2 | 72.9 | 140 | 144 | 155 | 162 |
| Root | 9.8 | 17.5 | 76.9 | 125 | 163 | 176 | 163 |
| 850 amp - 300 mm/min | | | | | | | |
| sub-surface | 10 | 51 | 149 | 187 | 207 | 198 | 194 |
| Root | 10 | 17 | 40 | 89 | 154 | 175 | 170 |
| 480 amp - 300 mm/min | | | | | | | |
| sub-surface | 13.5 | 28.2 | 103.9 | 166 | 198 | 228 | 240 |
| Root | 16.2 | 63.4 | 137.7 | 148 | | 202 | 220 |

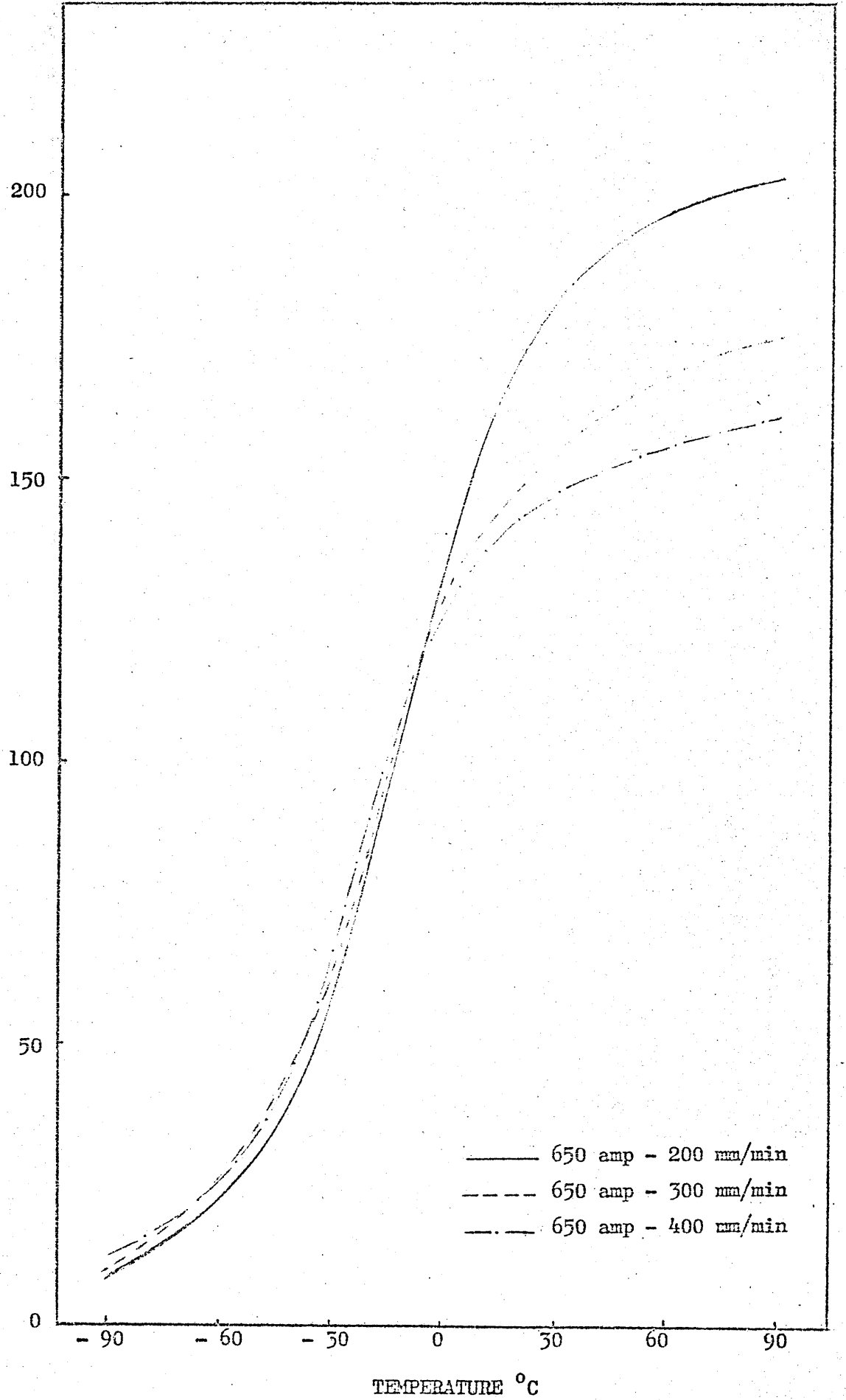


Figure 108 Weld metal impact properties for the sub-surface regions of the 650 amp - 200 mm/min, 300 mm/min and 400 mm/min welds.

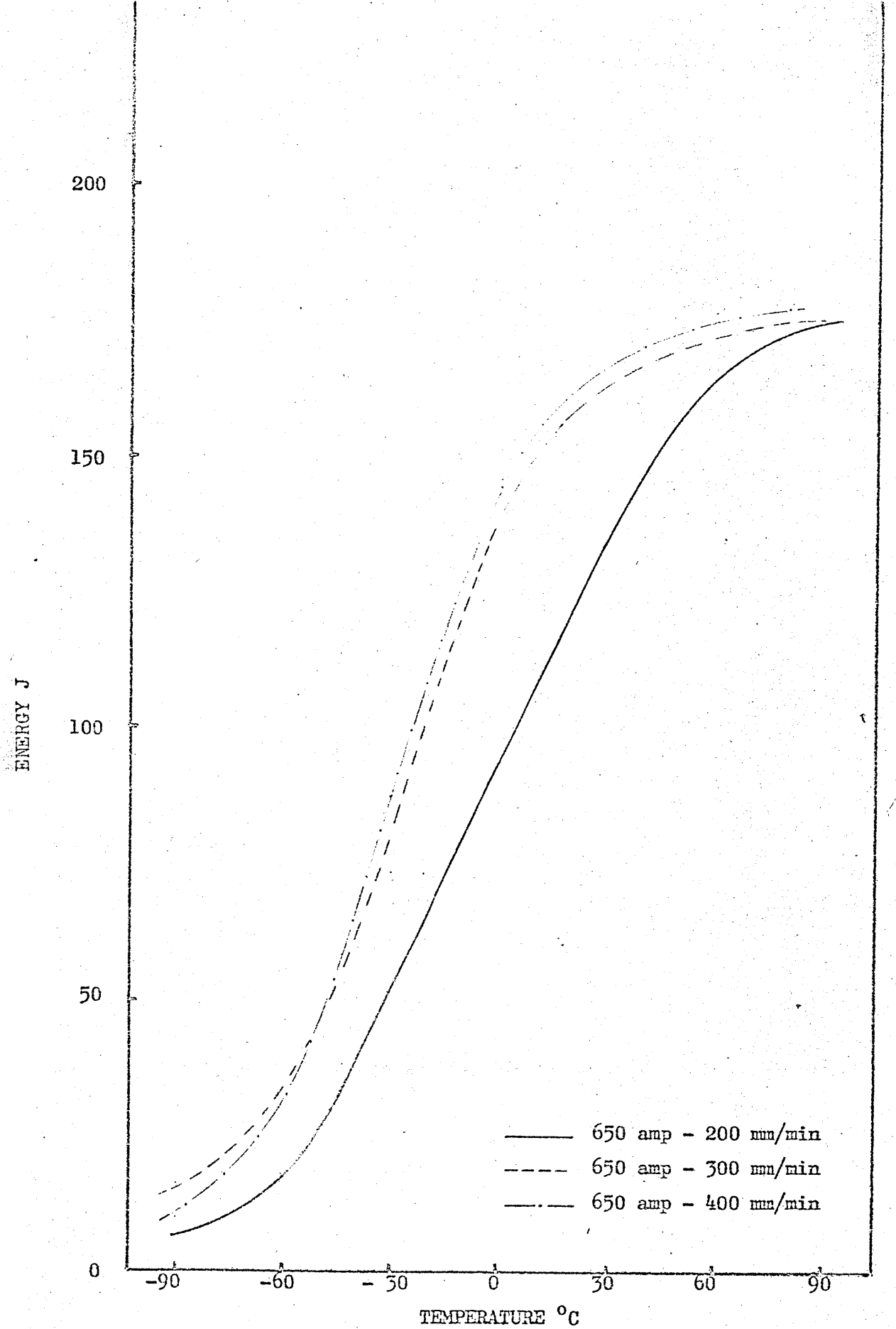


Figure 109 Weld Metal impact properties for the root regions of the 650 amp - 200 mm/min, 300 mm/min and 400 mm/min welds.

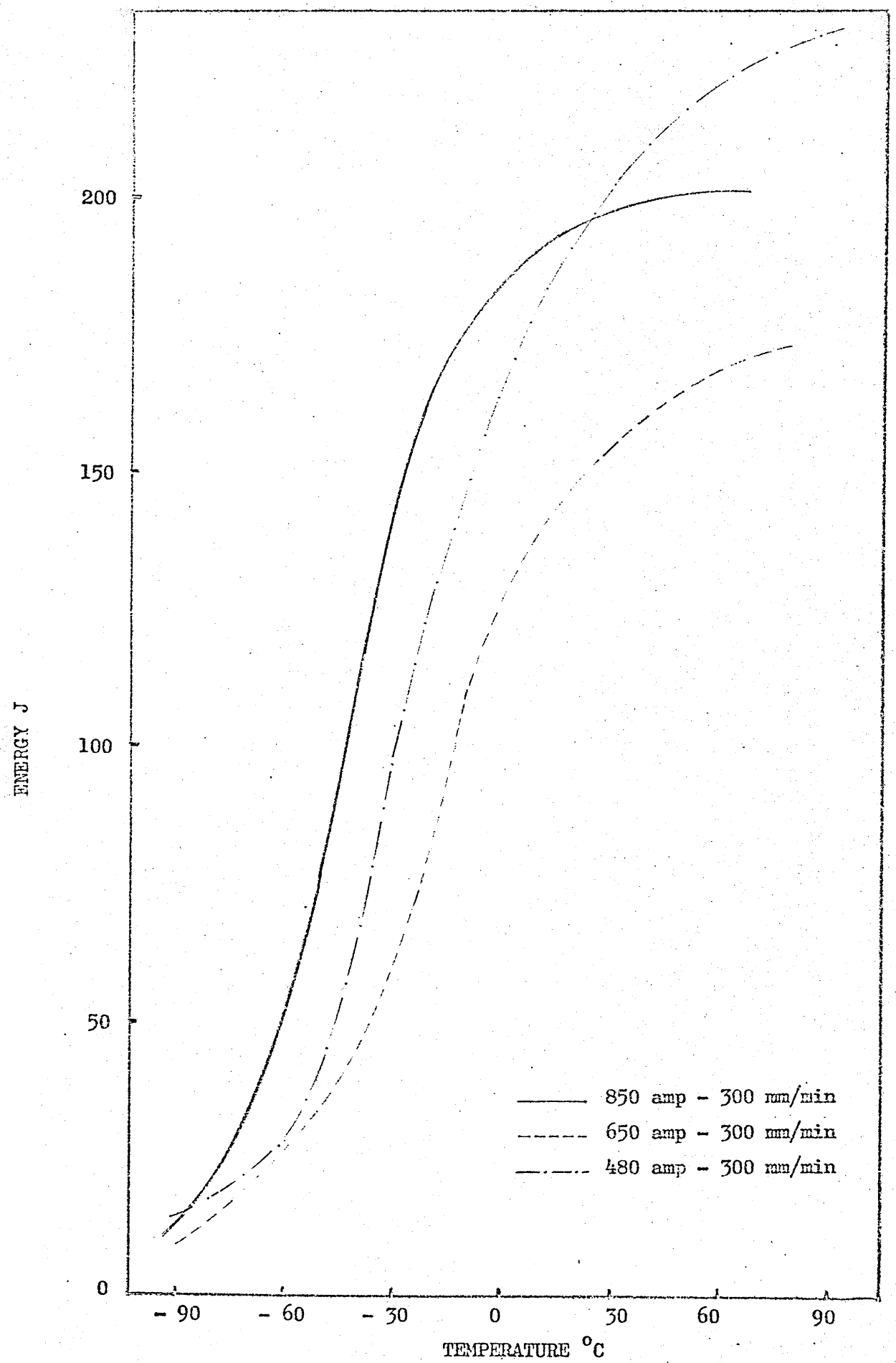


Figure 110 Weld metal impact properties for the sub-surface regions of the 850 amp, 650 amp and 480 amp - 300 mm/min welds.

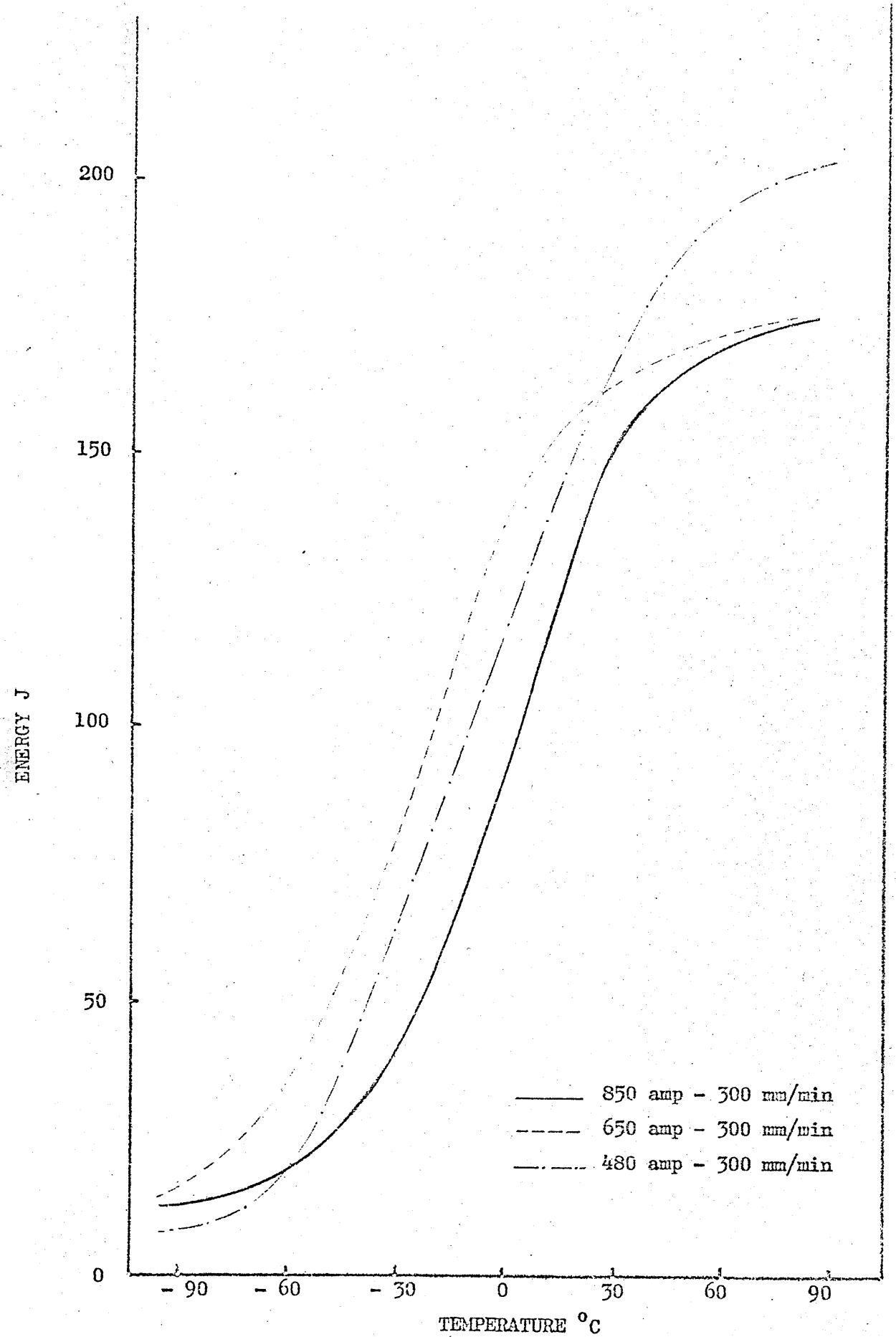


Figure111 Weld metal impact properties for the root regions of the 850 amp, 650 amp, 480 amp - 300 mm/min welds.

Through Thickness Toughness Variation

Weld Deposit 650 amps - 200 mm/min

The weld deposit made at a welding current of 650 amps and a welding speed of 200 mm/min had similar impact energies up to the temperature of - 30°C for both the sub-surface and root regions. Figure 112.

Above this the differences in toughness between sub-surface and root regions increased. The sub-surface had a higher energy reaching a maximum above that of the root region of approx. 50J at 0°C.

Weld Deposit 650 amp - 300 mm/min.

The weld deposit made at a current of 650 amp and a welding speed of 300 mm/min showed no significant difference in the Charpy curve between the root and the sub-surface. Figure 113.

Weld Deposit 650 amp - 400 mm/min

The weld deposit made at a current of 650 amp and a speed of 400 mm/min had slightly higher energy values for the root than for the sub-surface, a maximum difference of approx. 20J at 0°C. Figure 114.

Weld Deposit 850 amp - 300 mm/min

The weld deposit made at a current of 850 amp and a speed of 300 mm/min had similar root and sub-surface lower shelf energies. Figure 115.

Above the lower shelf the sub-surface had a considerably higher Charpy V energy than the energy values for the root regions reaching a maximum difference of approx. 100J at a temperature of 0°C.

Weld Deposit 480 amp - 300 mm/min

The weld deposit made at a current of 480 amp and a speed of 300 mm/min had higher sub-surface impact energy than the root region throughout the range, the maximum difference being approx. 50J at 0°C. Figure 116.

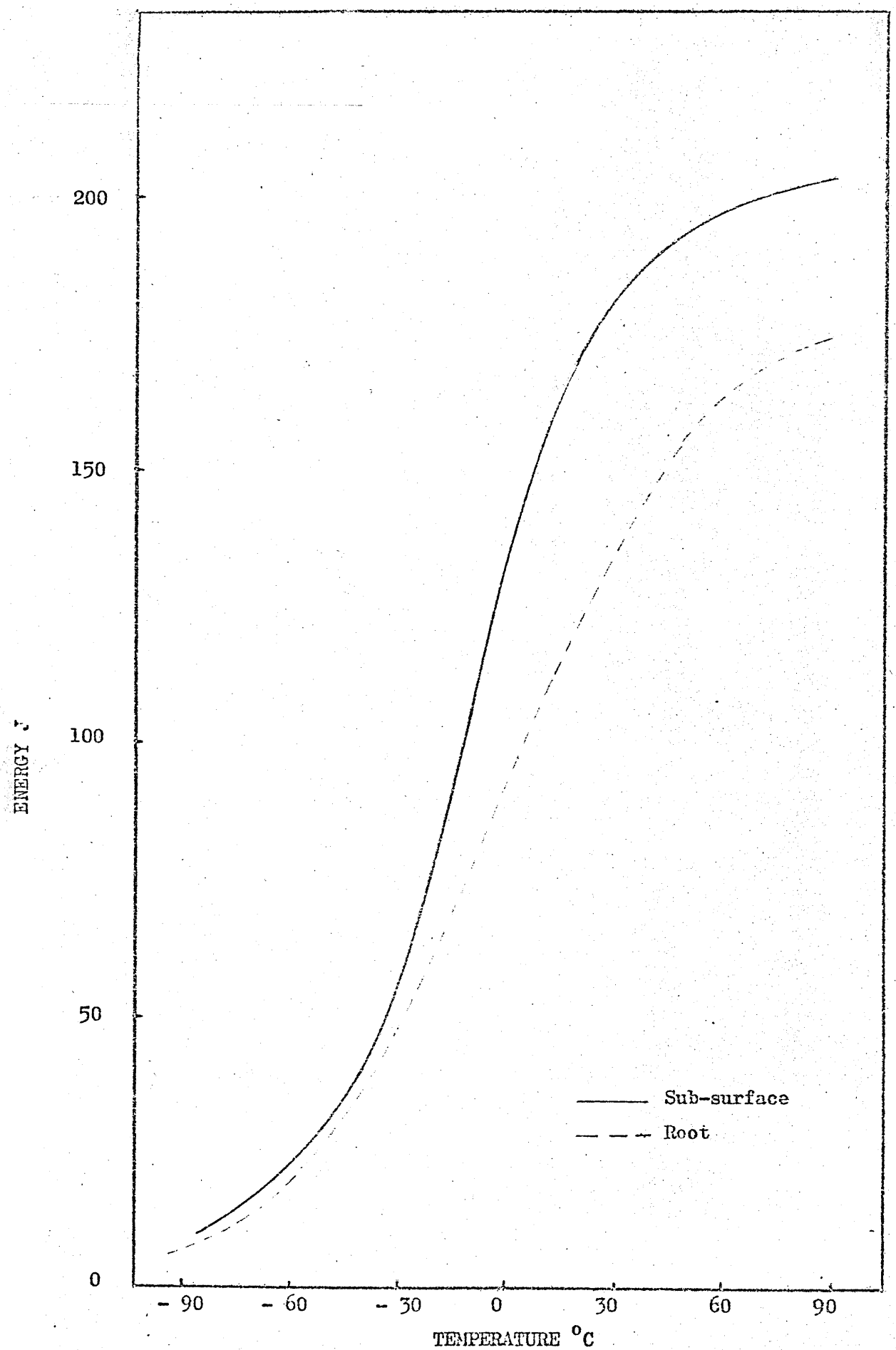


Figure 112 Weld metal impact properties for the sub-surface and root regions of the 650 amp - 200 mm/min weld.

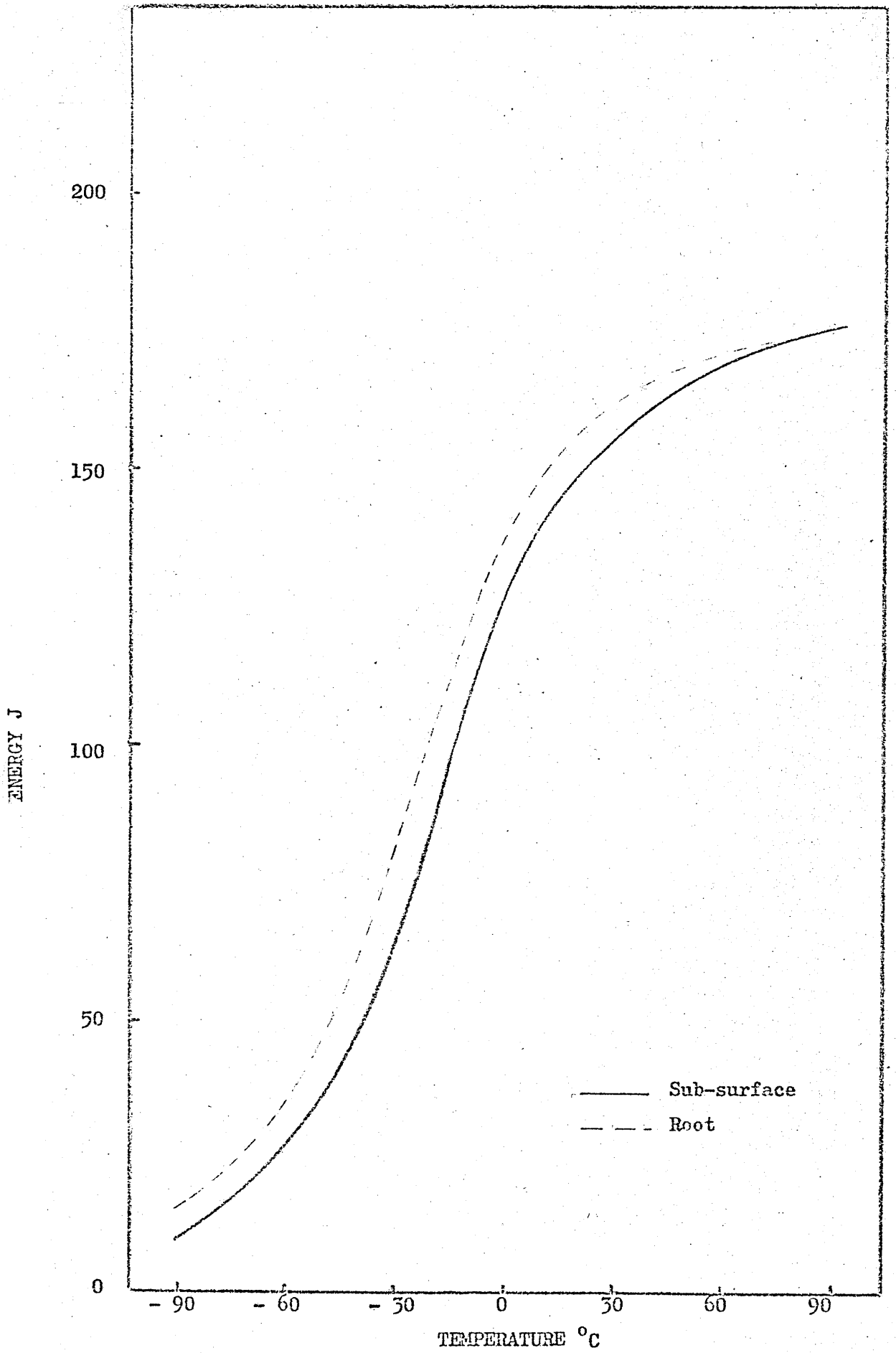


Figure 113 Weld metal impact properties for the sub-surface and root regions of the 650 amp - 300 mm/min weld.

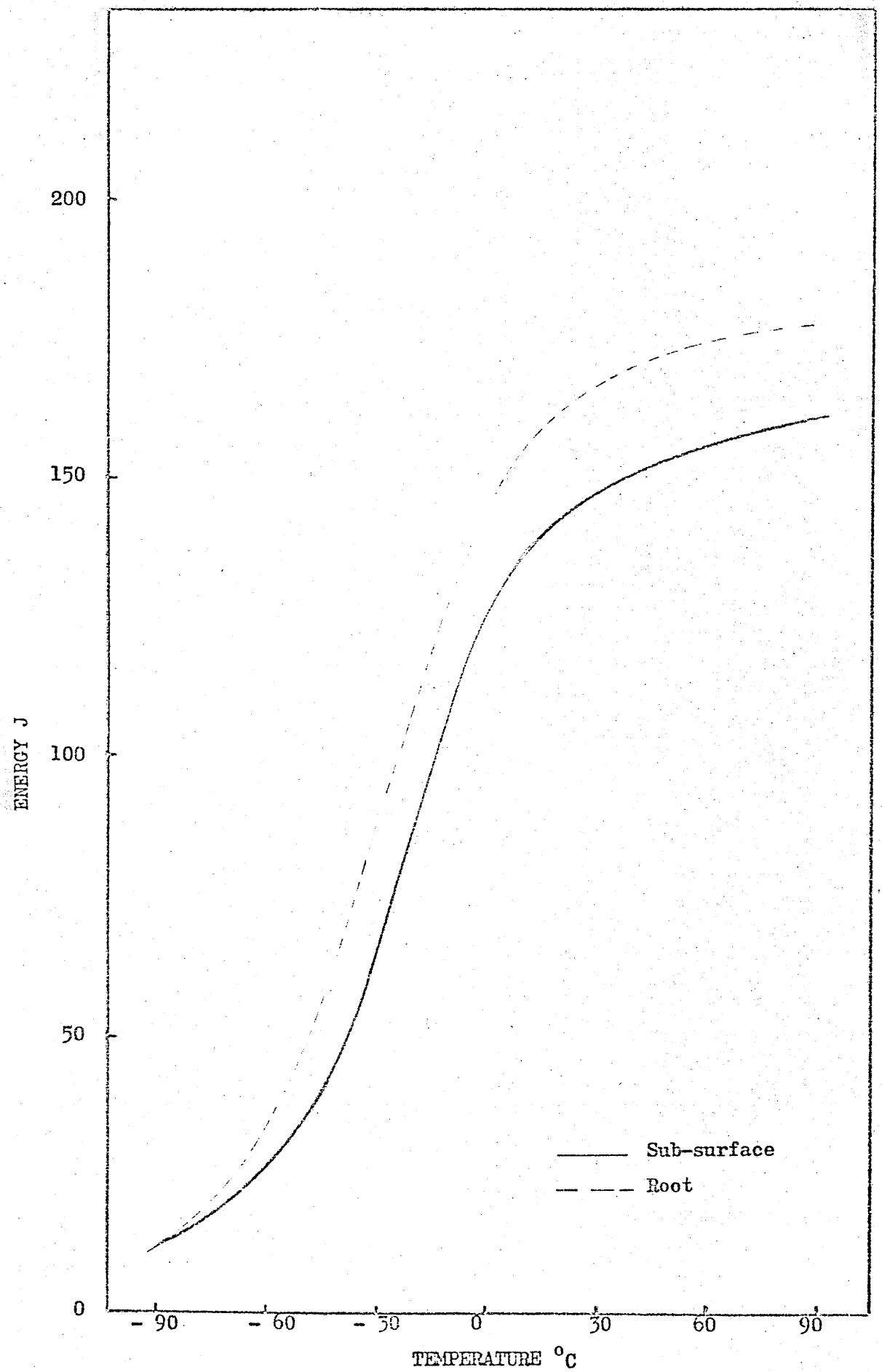


Figure 114 Weld metal impact properties for the sub-surface and root regions of the 630 amp - 400 mm/min weld.

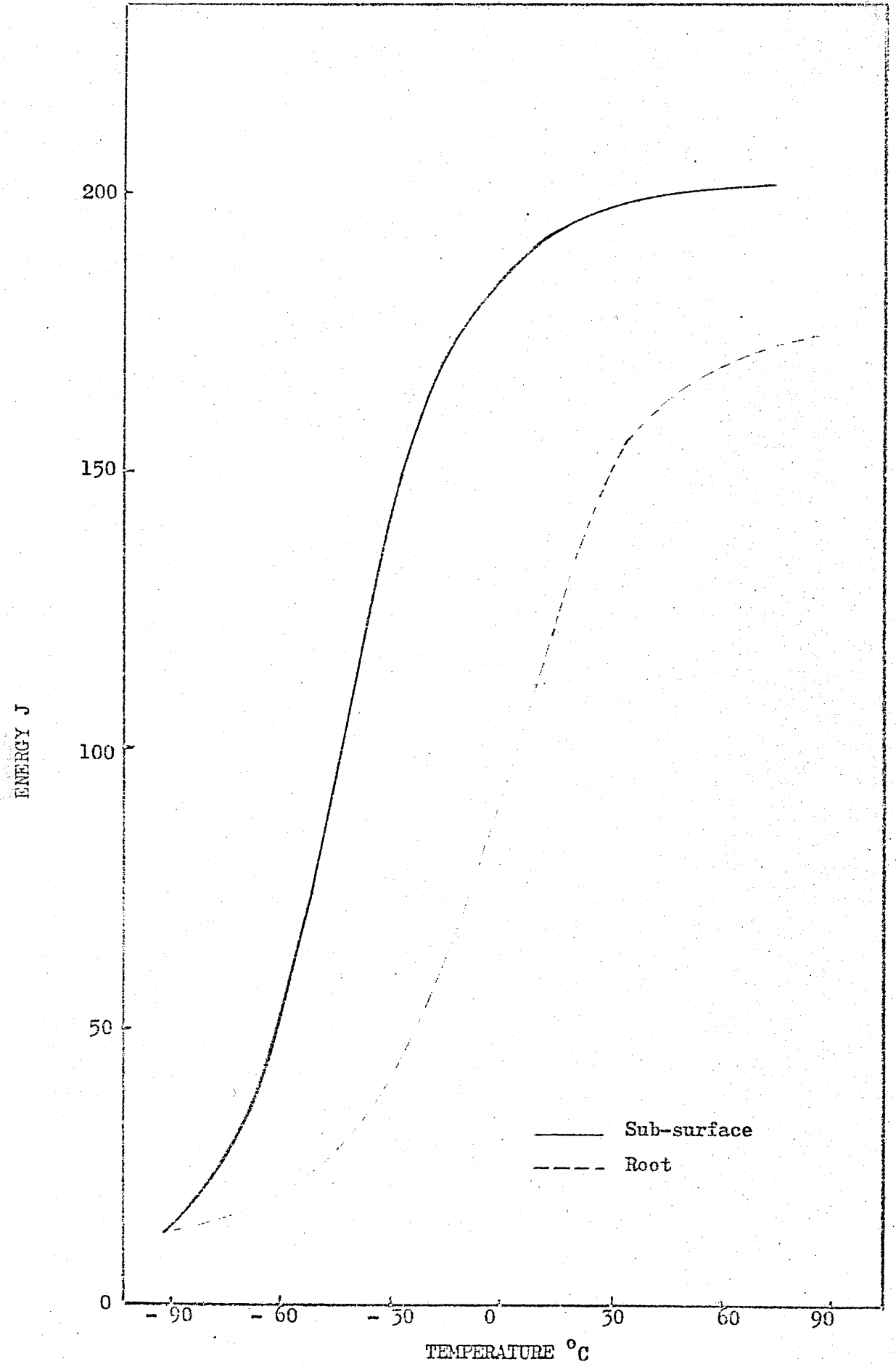


Figure 115 Weld metal impact properties for the sub-surface and root regions of the 850 amp - 300 mm/min weld.

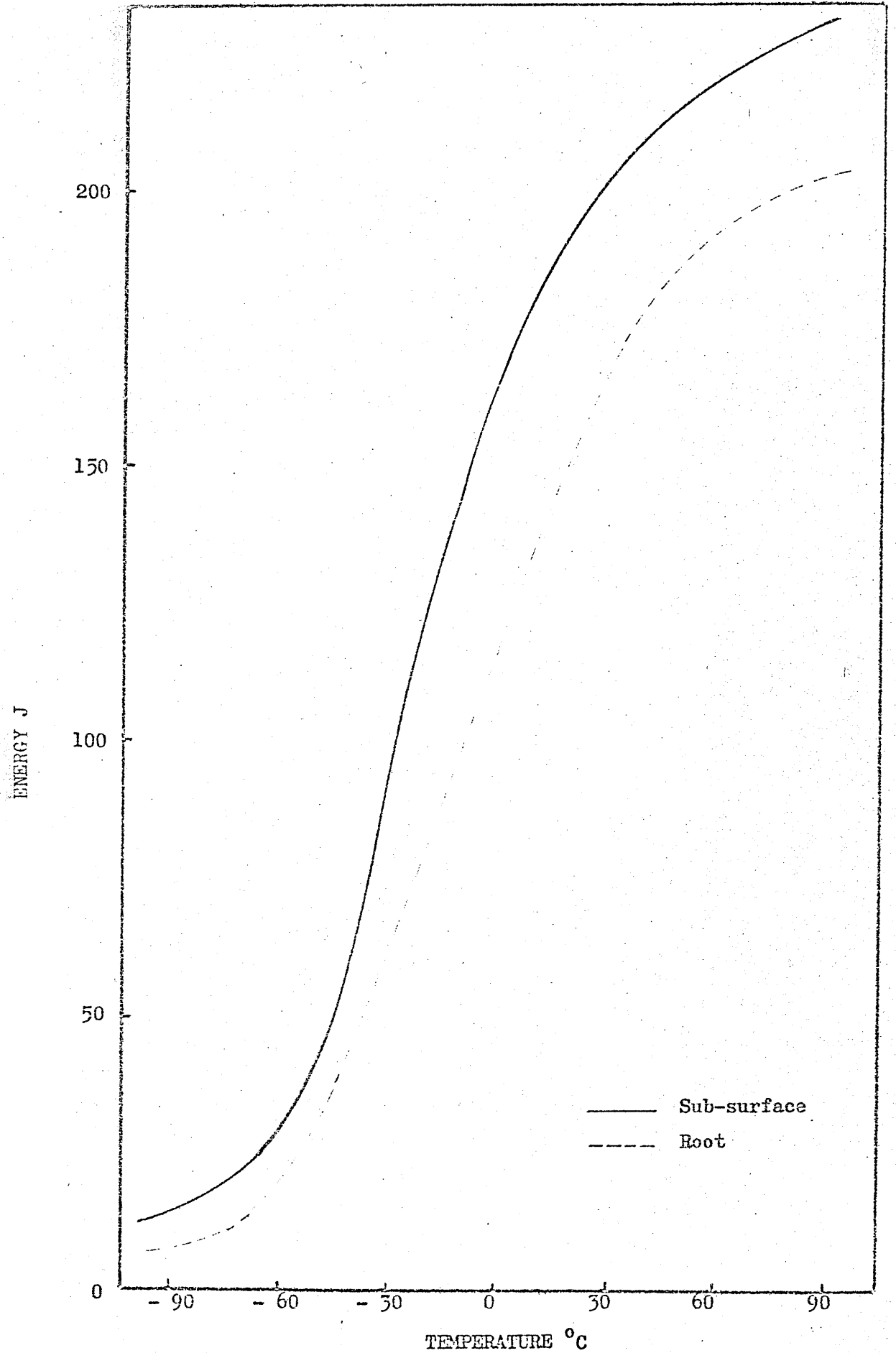


Figure 116 Weld metal impact properties for the sub-surface and root regions of the 480 amp - 300 mm/min weld.

## Comparison of Charpy V notch Toughness Results between Weld Deposits having the same calculated Heat Inputs

### Weld Deposits with a calculated Heat Input of 5.8 KJ/mm

#### Sub-Surface Region

Comparing the Charpy V energy values for the 650 amp - 200 mm/min and the 850 amp - 300 mm/min both conditions giving the same calculated heat input values of 5.8 KJ/mm, it was found that both welds had similar lower and upper shelf energies, but the transition temperatures were quite different, the 850 amp - 300 mm/min weld having a much higher energy value than the 650 amp - 200 mm/min weld, approx. 70 at $0^{o}C$. Figure 117.

#### Root Regions

The Charpy V energy values for the root region of the same two welds deposits did not show a significant difference. Figure 118.

### Weld Deposit with a Calculated Heat Input of 2.9 KJ/mm

The Charpy curves for the sub-surface regions of the weld deposit made at 650 amp - 400 mm/min and the weld made at 480 amp - 300 mm/min are shown in figure 119.

The weld deposit made at 480 amp had over all higher Charpy V energies (approx. 35J at $0^{o}C$ and 80J for the upper energy shelf) than the weld made at 650 amp.

The Charpy V curves for the root regions of the same two weld deposits are shown in figure 120. It was found that for the lower shelf and transition temperature the 650 amp - 400 mm/min weld deposit had higher energy values (5J at $-90^{o}C$ and 25J at $0^{o}C$) than the 480 amp - 300 mm/min. In the upper shelf region the 480 amp - 300 mm/min weld had a higher energy value (approx. 25J) than the 650 amp - 400 mm/min.

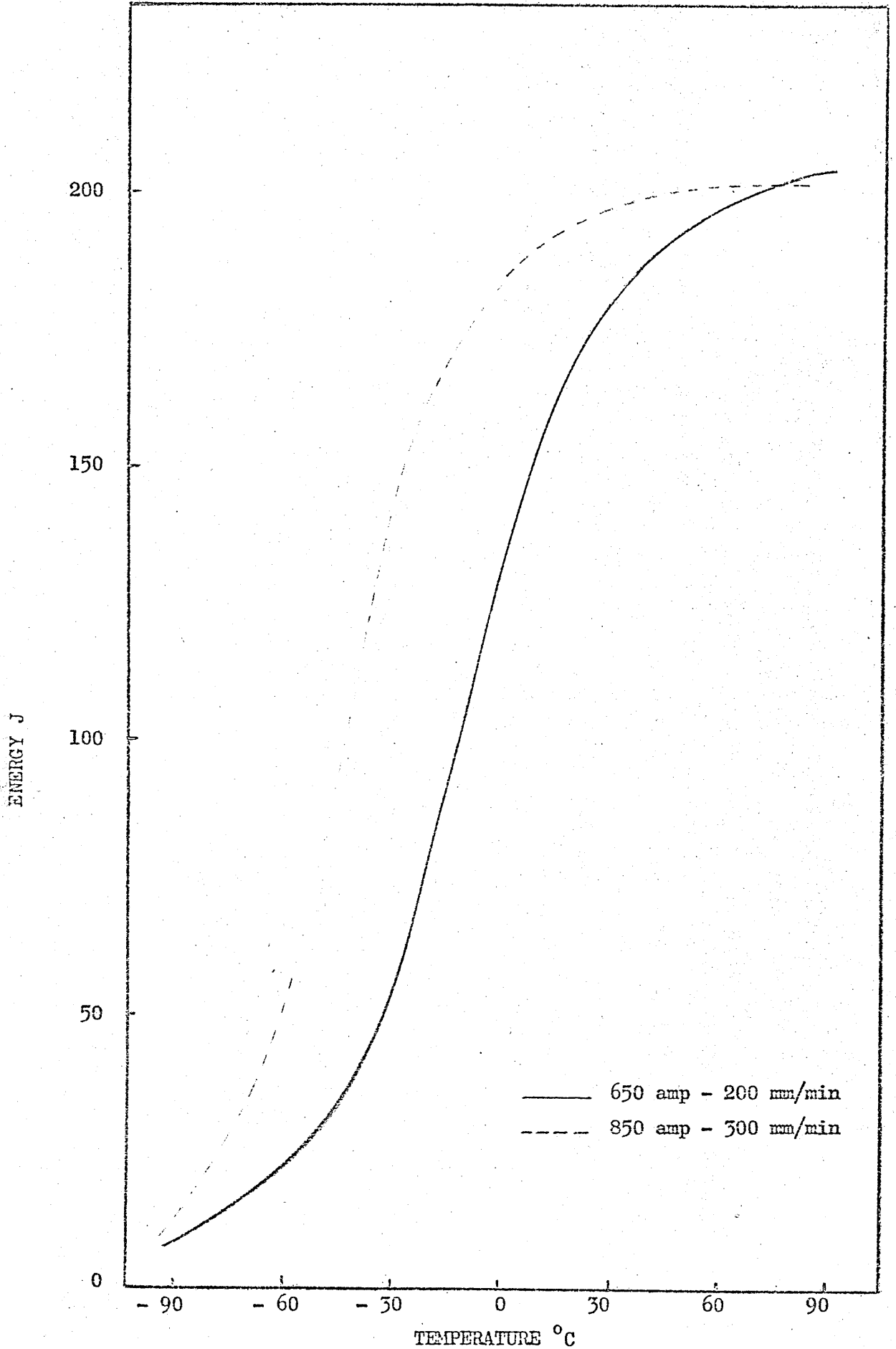


Figure 117 Weld metal impact properties for the sub-surface regions of the 650 amp - 200 mm/min and 850 amp - 300 mm/min welds. (5.8 KJ/mm).

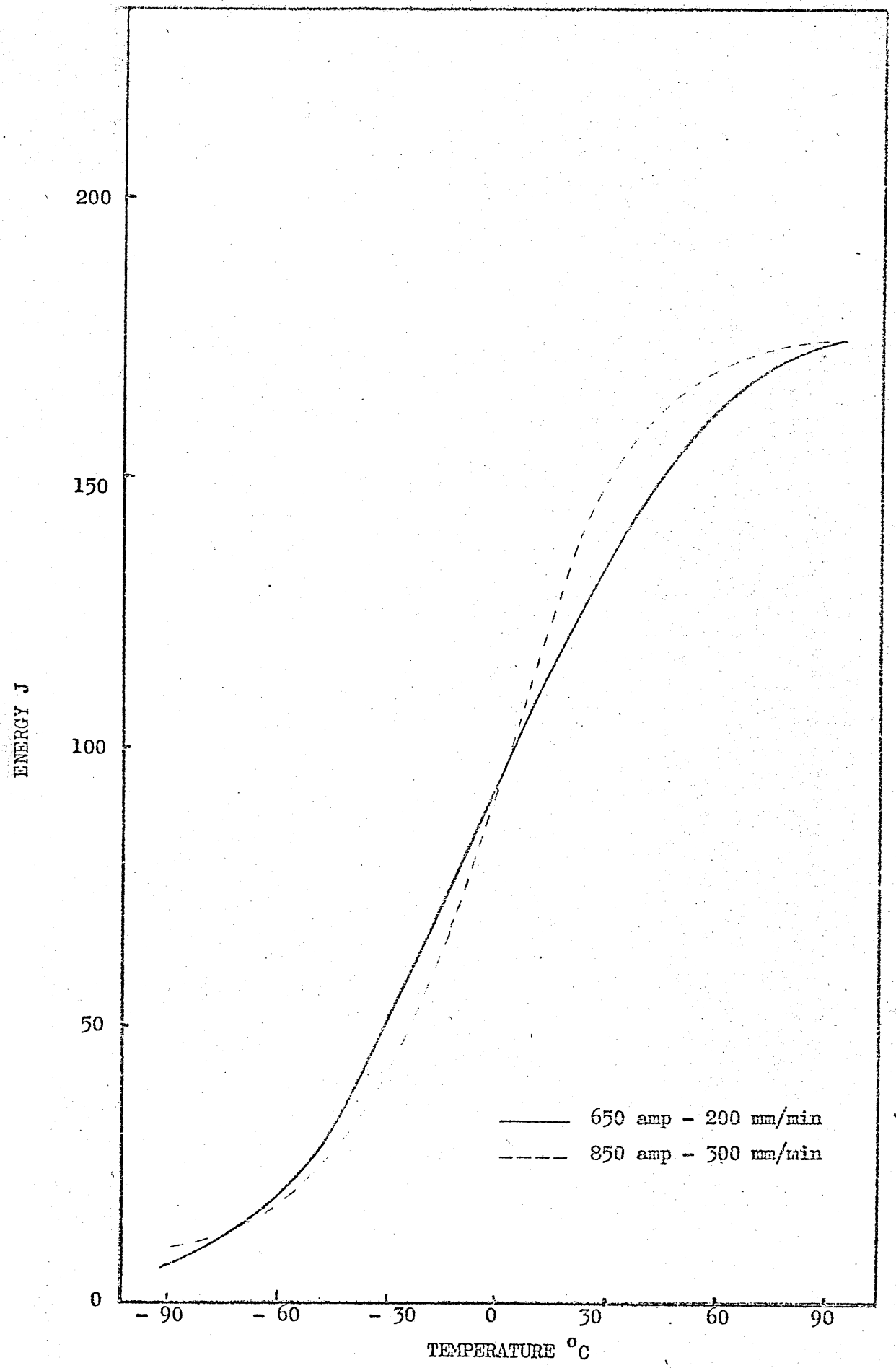


Figure 118 Weld metal impact properties for the Root regions of the 650 amp - 200 mm/min and 850 amp - 300 mm/min welds. (5.8 KJ/mm).

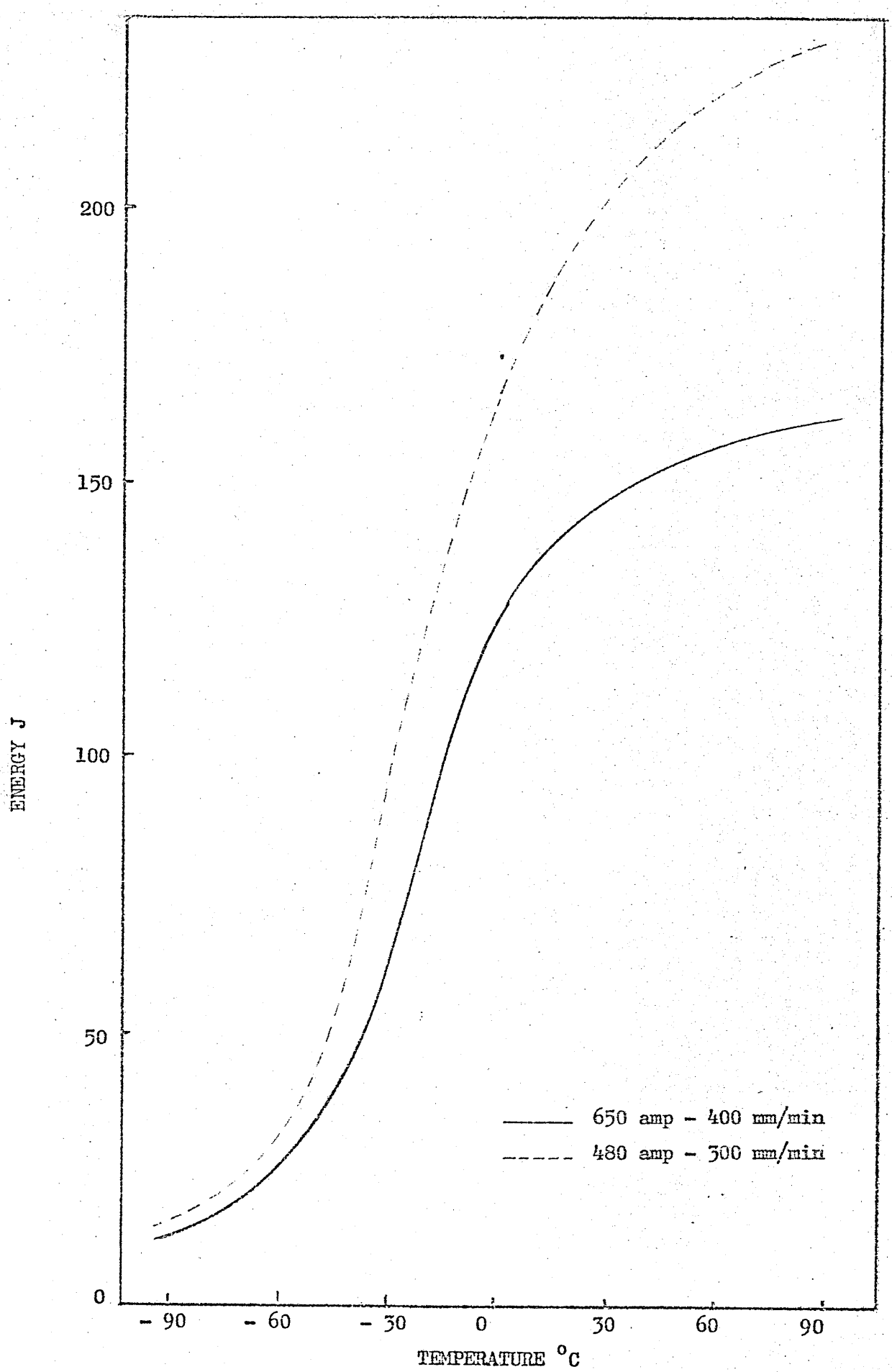


Figure 119 Weld metal impact properties for the sub-surface regions of the 650 amp - 400 mm/min and 480 amp - 300 mm/min welds. (2.9 KJ/mm).

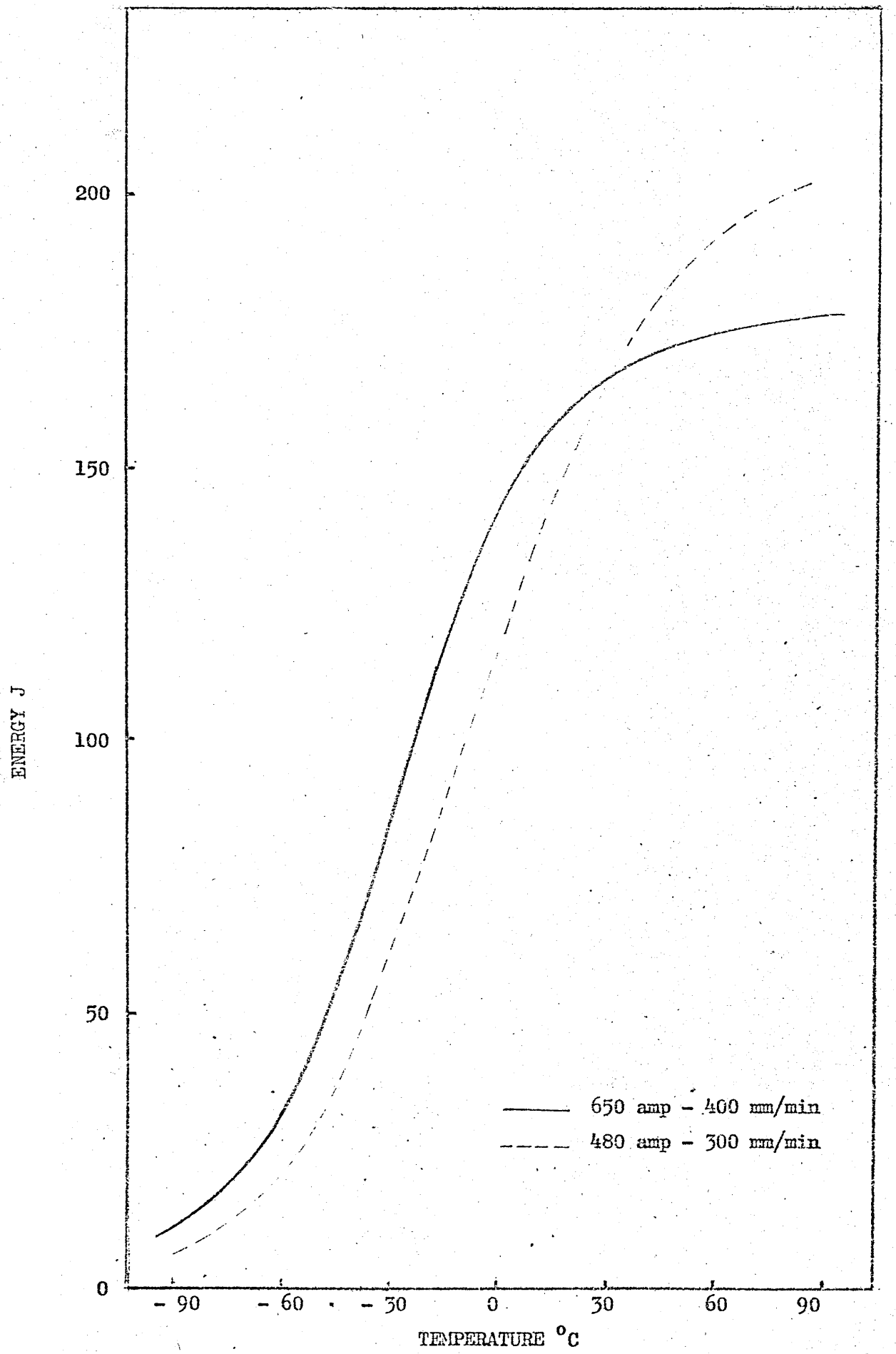


Figure 120 Weld metal impact properties for the root regions of the 650 amp - 400 mm/min and 480 amp - 300 mm/min welds. (2.9 KJ/mm).

SUMMARY

It was found that for most weld deposits the sub-surface had a higher toughness than the root region, the only exception being the 2.9 KJ/mm (650 amps - 400 mm/min) weld.

The through thickness toughness variation was found to be greater for the high heat input weld deposits than for the lower heat input weld deposits.

The results also showed that the weld deposits made with the same calculated heat input did not necessarily have the same toughness. Furthermore it was found that low heat input weld deposits did not necessarily have higher toughness than the high heat input weld deposits. This was clearly shown by the fact that the sub-surface of the weld deposit 850 amps - 300 mm/min with a calculated heat input of 5.8 KJ/mm showed the highest toughness properties of all the welds made in this work.

## DISCUSSION

### Sub-Surface Weld Beads

#### Introduction

As proposed in the introduction the two primary aspects to be examined in this work were :

The correlation between welding conditions measured in terms of weld metal heat input and impact toughness properties, and the through thickness impact toughness variations in microalloyed carbon manganese steels.

#### Effect of Heat input on the Weld Metal Properties

#### Weld Thermal Cycle

In this comparative study only the results referring to the sub-surface beads are discussed since it was important that all welds had similar chemical composition, table 18, and were made under similar heat flow condictions.(67)

The results referring to this series of welds showed that an increase in the weld heat input did not necessarily lead to a deterioration in the notch toughness properties and furthermore it was also found that different welds made at the same calculated heat input of either 2.9 KJ/mm or 5.8 KJ/mm had quite different Charpy energy values.

These results therefore suggest that weld deposits made at the same calculated heat input had different weld metal cooling cycles. This is because for welds with very similar chemical composition, which was the case for these five welds, table 18, it is the cooling cycle which determines the type of transformation reaction taking place during cooling which in turn determines the microstructure and consequently the properties.

As expected therefore, the thermal measurements, figures 8, 9, 10, 11, showed that weld deposits made at different heat inputs also had different cooling cycles and furthermore the welds made at the same heat input but at different welding conditions also had quite different cooling cycles, figures 42, 44.

The differences in weld metal cooling rate can be attributed to three main factors :-

(1) The weld bead cross-sectional area which is a function of the weld volume, and in turn is a measure of the calorific heat content of the weld (76).

(2) The weld bead shape measured in terms of width to depth ratio has an effect on the weld nugget area in contact with the metal plate through which the heat was conducted away (77).

(3) The weld flux consumption which can act as a heat source or just as an insulating blanket (17).

The magnitude of each of these factors was found to vary through the temperature range.

For the 1400°C - 900°C the weld deposit with high width to depth ratios and high estimated flux consumption per unit volume showed usually lower cooling rates irrespective of the calorific heat input measured in terms of the bead cross-sectional area, than the welds with low width to depth ratios and low estimated flux consumptions.

This effect is clearly indicated by the fact that the 480 amp - 300 mm and 650 amp - 200 mm welds had a lower cooling rate than the 850 amp - 300 mm weld.

The fact that weld beads with high width to depth ratios and high estimated flux consumptions also have a lower initial cooling rate than weld beads with low width to depth ratio and low estimated flux consumption, appears to be due to the fact that the weld bead with high width to depth ratio has a smaller weld nugget in contact with the weld metal through which the heat can be conducted away, therefore leading to a slower cooling rate. These weld beads also have a high flux consumption and therefore a larger weld bead area, covered by the solidified weld flux which should further contribute to a decrease in weld cooling rate.

As shown by Tuliani et al (17) during the weld cooling period the weld flux can be at a higher temperature than the weld bead and therefore the hot flux can act as a heat source, or just as an insulating blanket. However no attempt was made to assess independently the relative magnitude of the effects of the weld bead shape and flux consumption on the weld cooling rate.

The effect of the weld bead shape on the weld cooling rate has also been reported by Struck et al (77). These authors found using a G.M.A. welding process that the cooling rates of the individual passes made at the same welding condition were sensitive to their location relative to the bottom and side wall weld groove. These authors found that the average cooling rate of the weld upper half was approximately 25% less than that of the corresponding lower half. These differences in cooling rate were attributed to the fact that the root weld beads had a greater weld nugget area in contact with the metal plate through which the heat was conducted away.

For the temperature range of 900°C - 700°C the weld metal cooling rate it appears that both the weld metal bead shape, flux consumption and calorific heat content had similar magnitude effects.

For the temperature range of 700°C - 500°C the effect of the weld bead shape and flux consumption was very small and the weld metal calorific heat content was the determining factor.

The effect of the weld bead shape and flux consumption as determined by the welding parameters is therefore a critical factor controlling the weld thermal cycle during approximately the first 80 seconds of the cooling cycle.

It is important to note that since the weld metal cooling rate was found to vary considerably during the initial cooling time, it is therefore not possible to accurately define a cooling cycle by only determining the cooling rate value for a particular temperature range such as 800°C - 500°C.

These results also indicate the difficulty in the comparison of published results in which only the values of the calculated heat input are used to define the welding condition, since welds made at the same calculated heat input value may have quite different cooling cycles.

Thermal Analysis

To examine the effect of the weld metal cooling cycle on the weld transformation characteristics and therefore microstructure, measurements of the continuous cooling transformation behaviour in situ were made by monitoring the weld temperature during cooling and identifying the transformation temperature by the sudden change in cooling rate caused by the thermal reaction which takes place during transformation.

The advantages of this technique, which was developed by Lignon et al (84) and subsequently adapted and used by various workers (8, 78, 79, 80) over the conventional dilatometry technique have been pointed out by Saunders (80). This author noted that the dilatrometic measurements cannot be reliably applied to weld metal because reheating into the austenite region as done in conventional dilatometry breaks down the columnar grain structure and alters the transformation characteristics of the weld deposits.

The thermal analysis results, tables 12, 13, 14, and figures 46, 47, showed that two different transformation reactions took place during cooling. A high temperature transformation at approximately 850°C and a low temperature transformation at approximately 650°C.

From metallographic examination the high temperature transformation was identified with the formation of the pro-eutectoid ferrite phase and the lower temperature transformation with the formation of the acicular ferrite structure. Because of the relatively high temperature at which this structure was formed it appears that this phase is not a martensitic product as it has been suggested (13).

In order to show the effects of the weld cooling rate on the transformation of the austenite a C C T diagram was built using the thermal analysis results and measured from an assumed austenitizing temperature of 1400°C.

This temperature was chosen so that the effect of the weld metal cooling rate through the austenitic region was taken into account as this temperature gradient will determine the austenite grain size which can have a significant effect on the subsequent transformation structure (80).

For comparative purposes only the weld metal C C T diagram was plotted over the C C T diagram for a H.S.L.A. steel containing niobium, as a C C T diagram of a low alloy carbon manganese niobium free steel was not available. The chemical composition of this H.S.L.A. steel was 0.10% C, 1.33 Mn, 0.33 Si and 0.04% Nb. (85)

The weld metal C C T diagram, figure 121, shows, as expected, that a decrease in the weld cooling rate led to a depression in the transformation temperature of both the pro-eutectoid ferrite and acicular ferrite structure, therefore leading to a microstructure with a lower proportion of area occupied by the pro-eutectoid ferrite phase and a finer acicular ferrite structure.

Comparing both C C T diagrams for the steel and weld metal, it is clear that the weld metal transformation curves are shifted to the right in relation to the steel. This is confirmed by the fact that according to the C C T diagram for the steel the weld metal microstructure should be of a ferrite pearlite type structure which was clearly not the case. It appears therefore that this shift was due to the fact that the weld metal has a completely different austenite grain structure, which will alter the austenitic transformation characteristic, and therefore indicating the possible limitations of the conventional dilatometric measurement in which the weld metal is reheated into the austenitic region and therefore the columnar grain structure destroyed.

The fact that the chemical composition of weld metal and steel plate were slightly different, and the steel plate had a 0.04% niobium addition does not seem to invalidate this comparison.

Again, to investigate the effect of taking a weld metal austenatizing temperature of 1000°C instead of 1400°C and therefore indirectly excluding the possible effects on the subsequent transformations of the austenite morphology, another C C T diagram was constructed, figure 122.

Comparing these two diagrams, figures 121 and 122, it is clear that a greater amount of scatter in the results was found in the '1000°C' C C T diagram than on the '1400°C' diagram.

Although both C C T diagrams were obtained from a limited number of results, this comparison shows that the transformation characteristics are not only dependent upon the cooling rate below 1000°C, but also dependent on the cooling rate between 1400°C and 1000°C. This therefore again emphasizes the role played by the morphology of the columnar grain structure in altering the transformation characteristics of the subsequent structures, and therefore emphasizes the limitations of only using the value of a cooling rate through a particular narrow temperature range, e.g. 800°C to 500°C to define a weld metal cooling condition.

Weld Chemical Composition

As discussed in the literature survey, the weld metal chemical composition will determine the shape of the C C T diagram and therefore has an important effect on the weld microstructure and properties.

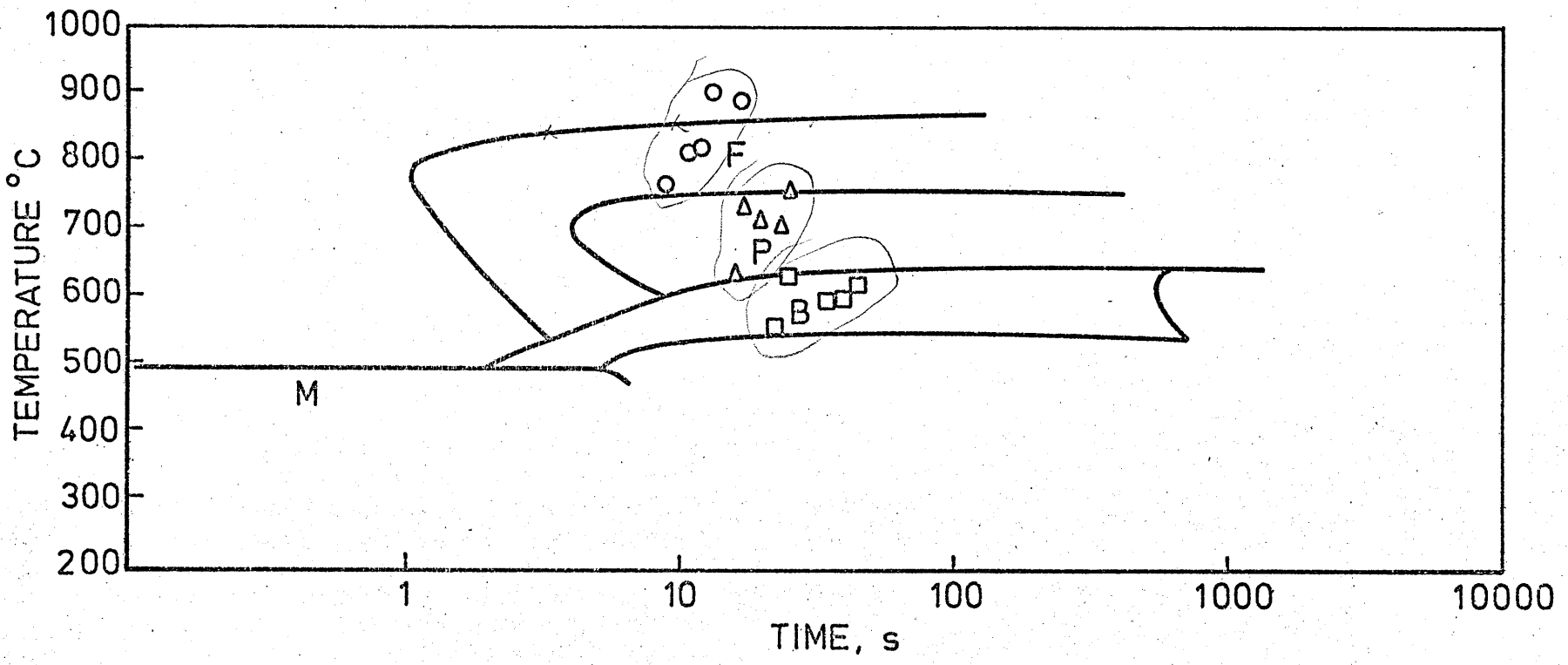


FIG. 121. C.C.T. DIAGRAM FOR HSLA STEEL CONTAINING Nb (85). 0.10% C, 1·33% Mn, 0.33% Si, 0.04% Nb AND C.C.T. DIAGRAM FOR THE SUB-SURFACE WELDS, USING AN AUSTENITISING TEMPERATURE OF 1400 °C.

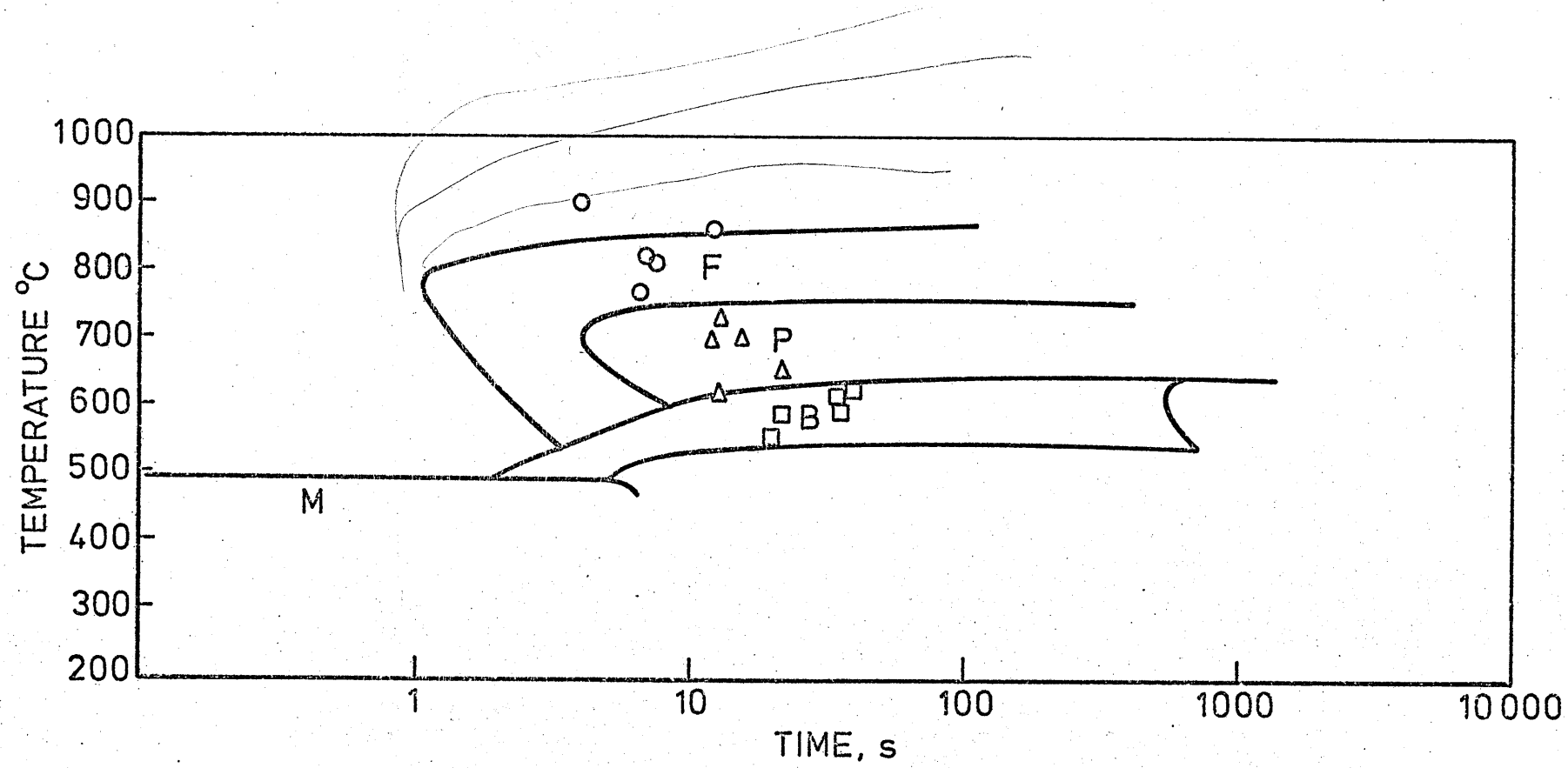


FIG. 122. C.C.T. DIAGRAM FOR HSLA STEEL CONTAINING Nb (85). 0.10% C, 1·33% Mn, 0.33% Si, 0.04% Nb AND C.C.T. DIAGRAM FOR THE SUB-SURFACE WELDS, USING AN AUSTENITISING TEMPERATURE OF 1000 °C.

Thus in this comparative study it was important to keep the chemical composition of all welds as similar as possible. This was achieved by only choosing for this study the central sub-surface weld beads of the 40 mm thick single V butt joint and therefore eliminating the plate/weld metal dilution effects. The chemical composition analysis for these welds is shown in table 18.

It is clear from this table that the chemical composition of all welds was very similar although a small variation of .03% carbon, 0.12% manganese and 0.7% silicon was found.

The effect of these small variations in the chemical composition on the weld metal transformation temperature, microstructure and properties is expected to be very small (19, 25, 38).

The manganese to silicon ratio was also similar for all welds, varying from 3.9 to 4.7. These high values of manganese to silicon ratios indicate, as noted by Tuliani et al (21), that the weld deposit had a low inclusion level and therefore the upper shelf energy should be above 100 lbf as was in fact the case.

Tuliani et al (21) also noted that whilst an increase in the manganese to silicon ratio to approximately 3, would lead to an increase in the ductile fracture energy, a further increase in the manganese to silicon ratio above 3, would lead to a decrease in the ductile fracture toughness. This author attibuted this drop in toughness to the increase in strength, presumably due to higher manganese levels, which would restrict the plastic deformation around the ductile voids.

In these present results however, no overall correlation was found between the ductile fracture toughness energy variations and the manganese to silicon ratios. This was possibly due to the fact that the differences in the manganese to silicon ratios were too small to have a significant effect.

It is interesting to note that contrary to what has been reported (14) the percentage of manganese marginally increased with an increase in the welding current. An increase in the welding current also led to a small increase in the percentage of carbon.

Since the welds with the higher percentage of carbon and manganese also had the lowest value of estimated flux consumption, it seems reasonable to assume that the variation in chemical composition was dependent on both the arc welding conditions and flux consumption.

Microstructure

In general terms the microstructures found in these welds can be considered in terms of five main features. The $\delta$ ferrite grain size, the austenite grain size, the percentage of pro-eutectoid ferrite, the grain size of the acicular ferrite and the presence of the M-A microphases, each of which were found to be closely correlated with the thermal history of the weld metal.

δ Ferrite Structure

Since the first structure to form was the δ ferrite it was of interest to examine the possible relationship between this structure and the subsequent austenite structure.

Grain measurements of these two columnar grain structures were compared and although the grain sizes estimates of the δ ferrite may have been slightly unreliable because of the difficulty in distinguishing between the columnar and the cell boundaries, these results consistantly indicated that the austenite grains were larger than those of the previous δ ferrite structure. This was particularly the case of the 480 amp - 300 mm weld which, after the fast solidification period, had a comparatively low cooling rate in the austenite temperature range. Figures 96, 97.

However the δ ferrite grain size may in some cases be larger than the subsequent austenite grains as it has been noted by Widgery (2). This was possibly due to the fact that Widgery (2) used a different welding process as well as a lower heat input welding condition, which in turn would have led to a much higher cooling rate through the austenitic region.

From the present results therefore, it appears that the δ ferrite structure and the austenite structure do not share the same grain boundaries, confirming the findings of Widgery (2), and it seems, as suggested by Widgery (2), that the austenite grains have grown across the δ ferrite columnar grains. This austenite growth mode being columnar because of the thermal gradient between the edge and the centre of the weld.

Although micrographic examination indicates that for these present welds the dominant austenitic growth mode was columnar, it is worth noting that another form of austenite nucleation and growth possibly occuring towards the centre of the weld pool can also occur (2).

In this case the austenite nucleation occurs ahead of the austenite columnar grains growing front, the austenite nucleating at the high angle δ ferrite grain boundaries.

Widgery (2) noted that in this growth mode the δ ferrite grain boundaries will only be preserved if the austenite grains only grow into an adjacent δ ferrite grain, but if the austenite grows into both adjacent grains the δ ferrite grain boundaries would be lost.

The practical significance of these results is to indicate that the δ ferrite structure does not seem to influence the subsequent austenite structure and therefore shows the limitations of attempting to alter the austenitic structure by alteration of the δ ferrite structure by, for example, changes in solidification conditions.

The austenite structure

The austenite columnar grain structure is often outlined by a more or less continuous band of ferrite, and, as expected, the grain size of this structure was found to correlate closely to the cooling rate through the austenite region.

For weld metals, the effect of the austenite grain size on the subsequent microstructure and therefore weld properties, has not generally been closely examined, but it is known (80) that the breaking down of the columnar grain structure and the formation of a different and generally finer austenite structure, which occurs when conventional dilatometric measurements are made, alters the austenite transformation characteristics.

The effect of the austenite grain size on the subsequent transformation structure was confirmed by the comparison between the two '1400°C' and '1000°C' C C T diagrams, which indicated that the scatter found in the 1000°C C C T diagram could be attributed to the effect of the different austenite grain structure which was not accounted for in the 1000°C C C T diagram.

Generally it is not necessary to individually examine the effects of the austenite grain size because the weld metal properties can be discussed in terms of the subsequent structures, e.g. pro-eutectoid ferrite, acicular ferrite etc., which indirectly account for the effects of the austenite structure.

However if it is found, as noted by Dolby (86), in H.A.Z. of electroslag welds, in C.Mn Steels and Bernard et al (9) for C.Mn welds, that a brittle crack can follow the pro-eutectoid ferrite band formed at the previous austenite grain boundary, then it seems that the size, and the orientation of the austenite columnar grains in relation to the direction of the crack propagation can have a dominant role in determining the fracture toughness of the material.

It was therefore of interest to examine the brittle fracture crack path through the Charpy V specimens representative of each weld condition. Figures 52, 58, 64, 70, 76, 82, 88, 94, 100, 106.

These figures show that although the crack propagated through a number of pro-eutectoid ferrite regions, which were formed at the austenite grain boundaries, it also, in cases, crosses the interior of the prior austenite grain. The moving crack had therefore to cross a number of structures which are known (13, 15, 33) to have different toughness properties, and consequently it was difficult to clearly assess the effects of the austenite grain size on the toughness properties.

However, it seems reasonable to assume that in a structure formed from large austenite grains the propagating crack will have to make large changes in direction in order to follow the pro-eutectoid ferrite band surrounding the austenite grains than in a structure formed from a smaller austenite grain size in which the moving crack is able to propagate easily with only a small change in direction through the inter connecting pro-eutectoid ferrite veins.

It seems therefore that a larger austenite columnar grain size is more desirable from a weld metal toughness point of view than a finer austenite structure.

Pro-eutectoid Ferrite - Ferrite Side Plates and Acicular Ferrite

All these structures were present in all the welds but the proportion of the area occupied by each of these phases varied according to the weld metal cooling conditions.

A pearlite structure may also have been present but because of the relatively high cooling rates of these welds, this structure if present, only occupied a very small area and was too fine to be resolved using a light microscope.

It seems reasonable therefore, to assume that this structure had no important effect on the properties of these welds.

The dominant structures were therefore the pro-eutectoid ferrite, the ferrite side plates, and the acicular ferrite whose effects on the weld properties have already been well documented (2, 13, 14, 15, 19, 21, 23).

For quantitative measurements the microstructural features were only divided into two types:

The acicular ferrite and the remaining structures which were mainly composed of pro-eutectoid ferrite and the ferrite side plates.

The fact that the pro-eutectoid ferrite and the ferrite side plates were for these measurement purposes considered to be as only one structure, should not affect the interpretation of the results since these two structures are known (2, 86) to have similarly poor notch toughness properties.

As expected, the percentage of area occupied by the acicular ferrite increased with an increase in the weld cooling rate in the 900°C - 700°C temperature range and generally the acicular ferrite grain size also decreased with an increase in the cooling rate in the 700°C - 500°C temperature range.

Weld deposits with a lower acicular ferrite transformation temperature also generally had a finer acicular ferrite structure.

M.A. Microphases

From micrographic examination it was found that the area occupied by these lower temperature transformation products as well as their form was related to the weld cooling rate in the temperature range below approximately 500°C.

An increase in the weld cooling rate in this temperature range led to an increase in the amount of M.A. microphases present which had a blocky or polygonal form. Figures 53, 65, 77, 101.

These variations in the amount and shape of the M.A. microphases with the weld metal cooling rate, were similar to the variations noted by Glover et al (87). These authors suggested that the M.A. microphases will nucleate only when insufficient "driving force" is available for carbide nucleation. The "driving force" for carbide nucleation was

considered by Glover et al (87) to come from both the thermodynamic supercooling effect associated with the austenite to carbide transformation and from the size of the carbon "spike", i.e. local carbon concentration that builds up in the austenite ahead of the growing ferrite lath.

The welds made in this work only showed a very small amount of microphases, less than 5%, and therefore no attempt was made to clearly identify the nature of these phases which could be either retained austenite or martensite in the twinned or lath form (19, 27, 60). Although the deleterious affects of these microphases in the fracture toughness of C.Mn welds and C.Mn steel have been reported (19, 27, 60), in this work the properties variations can be explained in terms of large microstructural differences, and therefore the effect of the M.A microphases on the weld properties, were difficult to isolate and quantify.

Weld Metal Strength and Hardness

The weld metal strength and hardness values were found to vary only within narrow limits as shown in table 20, and a clear relationship between the tensile and hardness properties with the weld cooling cycle could not be drawn.

Generally however, the weld deposits which had a high cooling rate in the 700°C - 500°C temperature range, and therefore a finer acicular ferrite structure, also had higher strength values than the welds which had a lower cooling rate in this temperature region but no correlation between the cooling cycle and the reduction of area and hardness values were found.

Although inclusion volume fraction measurements were not made the calculated inclusion volume fraction for the present welds using Widgery's suggested formula (92), are similar. This is because the oxygen and sulphur variation between welds was very small. Therefore it seems that the differences in the tensile measurement can not be attributed to variation in the inclusion level, and are due to matrix property variations.

Relationship between Microstructure and Toughness

The weld metal toughness properties are determined by the microstructural features and as discussed earlier the most relevant are:-

(1) The austenite grain size, since it appears reasonable to assume that larger austenite columnar grains are more desirable from a weld metal toughness point of view than a finer austenite structure.

(2) The pro-eutectoid ferrite, the ferrite side plates and the acicular ferrite because these structures are known to have large effects on the weld properties (2, 13, 14, 15, 19, 21, 23). The pro-eutectoid ferrite and the ferrite side plates being undesirable and the acicular ferrite desirable from a toughness point of view.

(3) The M.A. microphases which, if present, have a deleterious effect on the weld metal toughness properties (19, 17, 60).

(4) The heat treatment effect on the central sub-surface bead due to the subsequent weld run required to finish the weld joint. This heat treatment, although not very severe by comparison to a full typical heat treatment, should have beneficial effects on toughness since it has been shown that heat treatment of C.Mn steel improves the toughness properties (19, 62).

The discussion of the toughness results will therefore be based upon these main microstructural features.

It is important to note at this stage that the results for the 480 amp - 300 mm weld are not relevant to this discussion as only 30% of the impact specimens was formed by as deposited weld metal structure, due to the small size of these weld beads.

Of all the present welds the 850 amp - 300 mm weld had the lowest transition temperature. Figures 108, 110. This fact can be attributed to the large austenite grain structure, of this weld, as well as the large volume faction of acicular ferrite phase, and also the absence of M.A microphases. Figures 85, 86, 87, 89. The heat treatment effect on the sub-surface bead due to the subsequent weld run required to finish the weld joint was also the most severe of all these present welds (70 sec. at 400°C). Table 6.

As discussed earlier, all these factors will contribute to good notch toughness properties.

All other three welds had a similar but lower transition temperature than the 850 amp - 300 mm weld.

The poor toughness properties of these welds by comparison with the 850 amp - 300 mm weld were generally attributed to different microstructural aspects for each weld.

In the case of the 650 amp - 200 mm, the poor toughness properties can be attributed to the negative effect of the smaller volume faction of the acicular ferrite phase, as well as to the larger pro-eutectoid ferrite veins. Figures 50, 51.

The heat treatment effect of the subsequent weld run was also the lowest of all the welds. The temperature of 400°C was not reached.

These three factors, must have had a greater negative effect than the beneficial effect of the larger columnar grain size. Figure 49.

In the case of the 650 amp - 300 mm weld the poor notch toughness cannot solely be attributed to the size of the austenite grain structure which was similar for both welds nor to differences in the area occupied by the acicular ferrite which was only marginally smaller in the 650 amp - 300 mm than in the 850 amp - 300 mm weld, and therefore possibly not a very important factor.

The only microstructural difference between these two welds was that M.A. microphases were only present in the 650 amp - 300 mm weld and

the presence of these M.A. microphases are known (19, 27) to have a negative effect on the toughness properties, although the number of these M.A. microphases present appears to be too small to have a significant effect on the toughness properties.

The heat treatment effect of the subsequent weld run, was also lower than that of the 850 amp - 300 mm (40 sec. at 400°C). Table 6.

It seems that for this weld the poor notch toughness properties cannot be attributed to a dominant factor but are due to the cumulative effects of the lower volume faction of acicular ferrite, the presence of M.A. microphases and also the lower heat treatment effect due to the subsequent weld run.

In the case of the 650 amp - 400 mm weld, the poor notch toughness cannot be attributed to the differences in the volume faction of the acicular ferrite, but is possibly caused by the negative effect of the smaller austenite grain structure, and also by the presence of M.A. microphases which may cause a deterioration in the toughness properties. Figures 73, 74, 77.

The heat treatment effect caused by the subsequent weld run was also lower than that of the 850 amp - 300 mm (12 sec. at 400°C). Table 6.

Another important factor which may have affected the toughness properties was the orientation of the columnar grains in relation to the notch of the Charpy specimens, which is dependent on the cooling thermal gradient between the edge and the centre of the weld, and is therefore expected to be different for each welding condition.

This effect has been reported by Hipkins et al (91) but Bernal et al (9) using tensile and Charpy specimens with different orientations in relation to the weld bead, found that for C.Mn single bead submerged arc welds, the weld metal behaved in an isotropic manner.

The detailed examination of this effect was however outside the scope of this present work.

In all these welds the upper shelf energy values also varied, and as it has been shown by Farrar (56) and others (13, 21) this variation is a function of the size and distribution of the weld metal inclusions content as well as the matrix properties.

But since the calculated (92) inclusion volume faction was similar for all the present welds the upper shelf energy variation can be mainly attributed to differences in the matrix properties.

## Through thickness toughness variation

### Introduction

The toughness values for the sub-surface and root of each weld joint were found to be different.

The root of the 650 amp - 200 mm, 850 amp - 300 mm and 480 amp - 300 mm welds had lower toughness values than the sub-surface but for the 650 amp - 400 mm weld the root had a marginally higher toughness value than the sub-surface. In the case of the 650 amp - 300 mm both the root and the sub-surface had similar toughness values. Figures 112, 113, 114, 115, 116.

The results obtained from this present work indicate that the through thickness toughness variation can be partly attributed to the fact that the sub-surface had different thermal history from the root regions. The magnitude of these differences varying with the welding conditions which in turn would lead to different microstructural features and therefore properties.

The through thickness toughness properties can also be partly attributed to chemical composition variations between the sub-surface and the root region, caused by dilution effects.

### Weld thermal cycle

The thermal analysis results showed that for each weld joint the sub-surface weld beads had a slower initial cooling rate down to the temperature of approximately 700°C than the root beads. But below this temperature range the situation reversed and the root beads had a lower cooling rate than the sub-surfaces. Figures 37, 38, 39, 40, 41.

These differences in weld metal cooling rate between the sub-surface and root regions were found to be due to three main factors:

The weld bead shape, the weld flux consumption, and the geometry of the immediately surrounding plate.

The first two factors were found to be dominant for the higher temperature range, approximately 700°C, while the last one was only dominant for temperatures approximately below 700°C.

For the high temperature range, or initial cooling period approximately above 700°C the higher cooling rate of the root beads can be attributed to the fact that these beads had a higher depth to width ratio and lower flux consumption than the sub-surface beads. Table 17.

As already discussed, welds with higher depth to width ratios also have a larger area in contact with the metal plate through which the heat can be conducted away. (77) Lower flux consumption can also lead to a decrease in the weld cooling rate since the covering flux can act as a heat source or just an insulating blanket.

The effects of the weld bead shape and flux consumption on the weld bead cooling rate are clearly shown in the 480 amp - 300 mm weld. Figure 41.

In this weld, the root bead had a much higher cooling rate than the sub-surface bead. This effect was attributed to the high depth to width ratio and low flux consumption of the root weld bead in comparison with the sub-surface weld bead.

For the cooling period below 700°C the relationship between the weld bead size and the surrounding plate geometry was found to be important. Although the exact study of the differences in heat flow conditions between the root and the sub-surface of the same weld joint is complex and outside the scope of this work, these results suggest that at the weld root the heat flow condition varies from a nearly three dimensional type, if the weld bead is "small" in relation to the immediately surrounding plate, to a two dimensional type if the weld bead is "large" in relation to the immediately surrounding plate.

These variations in heat flow account for the lower cooling rate of the root bead in relation to the equivalent sub-surface bead for the temperatures below approximately 700°C. This effect was particularly emphasized on the 850 amp - 300 mm welds which had the largest weld bead volume of all the welds. Figure 40.

In this discussion it was assumed that for each weld condition the weld bead volume and therefore calorific heat input was the same for the sub-surface and root beads. It was possible however that the weld bead volume was slightly higher for the root than for the sub-surface, because of the fact that the root beads used less flux than the sub-surface beads, and therefore more energy was available to the weld.

This effect would further contribute to the slower cooling rate of the root beads by comparison with the sub-surface beads although it is reasonable to assume that these differences in weld bead volume were small and therefore this effect is not significant.

The post-solidification heat cycle caused by the subsequent weld runs was also different for the sub-surface and the root regions. Table 6.

Thermal analysis and Chemical Composition

The thermal analysis results show that the weld root bead, with the exception of the 850 amp - 300 mm weld, had a lower or a similar transformation temperature to the sub-surface bead. Tables 12, 13, 14, 15, 16. This fact can be attributed to the faster initial cooling rate of the root in relation to the sub-surface weld beads. In the case of the 850 amp - 300 mm weld the transformation temperature was higher for the root than for the sub-surface. This was due to the fact that the root weld bead had a slower cooling rate than the sub-surface weld bead below the temperature of approximately 900°C.

It is also possible that the slight chemical composition variation between the root and the sub-surface beads, the root beads having a marginally higher carbon and niobium value than the sub-surface also

contributed to the depression of the transformation temperature (85) Table 18.

Microstructure

The metallographic examination showed that the sub-surface beads had different microstructure from the root bead.

For the same weld joint the sub-surface bead showed a larger $\delta$ ferrite and austenite columnar grain structure than the root bead. Table 19.

The sub-surface bead also showed a much higher proportion of acicular ferrite than the root bead with the acicular ferrite structure being generally very irregular and therefore difficult to measure.

The finer $\delta$ ferrite and austenite columnar grain structure of the root bead can be attributed to the initially faster cooling rate of the root bead. ($1400^{o}C$ - $900^{o}C$).

The lower acicular ferrite volume fraction of the root bead is probably due to the finer prior austenite grain structure in which grain boundaries, the pro-eutectoid ferrite nucleate. This effect was also noted by Dolby (86) when examining the microstructures of H.A.Z. of electroslag welded C.Mn Steels, where a finer prior austenite grain structure lead to a greater volume fraction of pro-eutectoid ferrite.

The acicular ferrite structure of the root region was found to be very irregular and because of this, it was difficult to establish a correlation between the grain size of this phase and the welding conditions and cooling conditions.

For the same weld joint the volume fraction of the M.A. micro-phase was also found to be slightly different. These differences can again be attributed to differences in the weld metal cooling rate between the sub-surface and the root.

Weld Metal Strength and Hardness

The root tensile specimens had higher strength and hardness but lower ductility than the sub-surface tensile specimens. Table 20, 21.

The higher strength and hardness of the root bead may be partly attributed to strain ageing effects (62), although the higher carbon and niobium values of the root may have also contributed to the increase in strength of the root since these elements have a strong solid solution strengthening effect (89,26, 27).

The microstructural differences between the sub-surface area and the root, may have also contributed to the differences in strength and hardness values, although it is difficult to clearly establish these effects due to the irregular and variable type of microstructures present in the as deposited weld metal.

Relationship between Microstructure and Toughness

From the micrographic examination of the as deposited structures it was observed that the root beads had a smaller austenite columnar grain structure which in turn, as also noted by Dolby (86) creates more nucleating sites for the pro-eutectoid ferrite structure, leading to a reduction in the overall acicular ferrite volume fraction in the root weld beads. Table 19. Figures 49, 50, 55, 56, 61, 62, 67, 68, 73, 74, 79, 80, 85, 86, 91, 92, 97, 98, 103, 104.

In line with previous experience (13, 15, 17, 19) a decrease in the columnar grain size and volume fraction of acicular ferrite has a detremental effect on the toughness properties.

The volume fraction of the M.A. microphases was also found to be slightly different between the sub-surface and root weld beads in the case of 650 amp - 200 mm, 650 amp - 300 mm and the 480 amp - 300 mm, Table 19, but because the volume fraction of these M.A. phases was small, estimated at less than 5%, it was felt that the effect of this variation on the through thickness toughness was also small.

It is important to note that the Charpy V specimens for the root were composed of as deposited and refined structures and therefore, the toughness properties of the refined regions will also affect the overall toughness.

Although it is known that the grain size of the refined regions has an effect on the toughness properties (90) in this work no attempt was made to measure the grain size of the weld refined region because it was found that throughout this region the polygonal ferrite grain size varied.

This variation in grain size was caused by the non uniformity of the head treatment to which this "heat affected zone" was subjected, and therefore the polygonal ferrite grain size decreased with the increase in the distance away from the fusion zone.

Since the toughness properties of the root will be determined by both the refined and as deposited structures the Charpy energy values will be discussed in terms of the toughness contribution of these two structures.

The through thickness toughness variation for the 650 amp - 200 mm and 850 amp - 300 mm welds indicate that the poor toughness properties of the as deposited regions was not fully compensated for by the toughness of the refined regions. Therefore the sub-surface had better toughness properties than the root. Figures 112, 115.

In the case of the 650 amp - 300 mm and 650 amp - 400 mm the decrease in toughness properties of the as deposited region was over compensated by the higher toughness of the refined region and therefore the sub-surface had higher toughness properties than the root.

In the case of the 480 amp - 300 mm weld where both sub-surface and root Charpy V specimens were composed of approximately 70% of

refined weld metal, the toughness contribution of the refined region was similar for both the sub-surface and root. Therefore the drop in toughness must be mainly due to the drop in toughness of the as deposited region.

Although in the present series of welds the through thickness toughness variation was attributed only to large microstructural differences between the sub-surface and the root beads, it is important to note that the slightly higher carbon and niobium values of the root area may have had some deleterious effect on the toughness properties of the root area. Table 18.

However, the effects of niobium on the toughness properties was probably very small since it has been reported (44) that niobium additions below 0.02%, which was the case of the welds discussed, do not seem to affect the weld toughness properties. Also the weld metal toughness properties can be affected by strain ageing embrittlement, which can occur as a result of simultaneous straining and ageing (57).

Fick et al (62) has shown that for C.Mn submerged arc welds the thermo-mechanical effects caused by the subsequent weld runs on the root lead to an increase in yield strength and hardness, showing that a dynamic or, and static strain ageing and hardening reaction had taken place during the course of further welding. However, in spite of the increase in yield strength and hardness, the toughness of the "unbuttered" root runs improved, while the toughness of the "buttered" root runs decreased marginally.

These authors suggested that some opposing reaction occurred during the course of welding which was able to outweigh in one case and almost cancel in the other the detrimental strain ageing effects, suggesting therefore that for C.Mn welds strain ageing effects are not the main cause of poor weld root toughness.

The present results show that in C.Mn welded joints through thickness toughness variation can occur but the magnitude of this effect is mainly a function of the differences in the thermal history between the sub-surface and the root weld beads. These results also show that weld deposits made at the same calculated heat input can have different toughness properties.

SUMMARY

Sub-Surface Weld Beads

The results showed that for the sub-surface welds an increase in the weld heat input did not necessarily lead to a deterioration in the notch toughness properties and furthermore it was also found that welds made using different procedures but the same calculated heat input had quite different Charpy V energy values.

This was because a particular calculated heat input value does not define a precise weld metal cooling cycle, which, for the present welds of very similar chemical composition, determines the micro-structural features and therefore properties.

This work indicated that the weld metal cooling cycle was determined by three main factors which were themselves a direct consequence of the exact welding conditions. These factors are :-

(1) The weld bead cross-sectional area, which is a measure of the actual calorific heat input into the weld (76).

(2) The weld metal bead shape, which has an effect on the weld nugget area in contact with the metal plate through which the heat is conducted away (77).

(3) The weld flux consumption, since the fused flux covering the weld bead can act as a heat source or just as an insulating blanket (17).

The magnitude of these effects on the cooling rate varied through the temperature range.

For the high temperature range, approximately 1400°C - 900°C, the weld bead shape and flux consumption appear to be the dominant factors, while for the lower temperature range, below 700°C, it was the weld bead volume which showed a dominant effect.

It is also relevant to note that since the weld metal cooling ratio was found to vary considerably during the initial cooling time, (above 500°C), a particular cooling rate value for a relatively narrow temperature range, i.e. 800°C - 500°C, will not accurately define the overall cooling cycle.

To complement the thermal measurements the weld metal trans-formation temperatures were also determined, using an "in situ" measuring technique, from the same thermocouple which was used to measure the weld bead cooling cycle.

Two different transformations reactions were found to have taken place. A high temperature transformation at approximately 850°C and a low temperature transformation at approximately 650°C.

From metallographic examinations the high temperature trans-formation was identified with the pro-eutectoid ferrite transformation and the lower temperature transformation with the formation of the acicular ferrite.

As expected, the weld deposits which had a faster cooling cycle also had a microstructure showing a fine columnar grain structure. The faster cooling rate also led to a lower transformation temperature which in turn led to a lower volume fraction of pro-eutectoid ferrite and a finer acicular ferrite structure.

The present results indicate that from a weld metal toughness point of view a microstructure composed of a large columnar grain structure, with a high volume fraction of acicular ferrite is the most desirable structure.

Through Thickness Toughness Variation

The present results indicate that through thickness toughness variations can be mainly attributed to the fact that the sub-surface beads had a very different as deposited microstructure to the root bead, with the sub-surface beads showing larger prior austenite columnar grains and a higher volume fraction of acicular ferrite than the root beads, and also to the fact that the sub-surface Charpy specimens were only composed of as deposited weld metal while the Charpy specimens for the root were partly composed of refined equiaxed ferrite grains.

For the same welded joint the differences in the as deposited microstructure between the sub-surface and the root beads can be explained as a result of the differences in the thermal history between these two regions.

These differences in the weld metal thermal history were mainly attributed to :-

(1) The weld metal bead shape. The sub-surface bead had a higher width to depth ratio than the root beads. This affects the weld nugget area in contact with the metal plate through which the heat is conducted away (77) and therefore leads to the initial ($1400^{o}C$ - $900^{o}C$) higher cooling rate of the root in relation to the sub-surface beads. This in turn leads to a finer prior austenite columnar grain structure in the root beads, which possibly led to the lower volume fraction of acicular ferrite phase in the root beads. (86)

(2) The relationship between the weld bead size and the surrounding plate geometry. The present results suggest that at the weld root the heat flow conditions varied from a nearly three dimensional type, if the weld bead is "small" in relation to the immediately surrounding plate, to a two dimensional type if the weld bead is "large" in relation to the surrounding plate. These variations in heat flow account for the lower cooling rate of the root in relation to the equivalent sub-surface bead for the temperature below approximately $900^{o}C$ for both high heat input welds, (5.8 KJ/mm) and below approximately $700^{o}C$ for all other welds.

Therefore it seems that the lower volume fraction of acicular ferrite of the root beads can be attributed to both, the finer prior austenite grain size, caused by the initial ($1400^{o}C$ - $900^{o}C$) high cooling rate, and to the subsequent (below approximately $900^{o}C$) slower cooling rate of the root bead.

(3) The post-solidification heat cycle caused by the subsequent weld runs were also different for the sub-surface and the root beads. However in this work it was difficult to clearly establish the thermal effects on the weld properties.

Since the toughness properties of the root are determined by the contributions of both refined and as deposited structures it therefore appears that the through thickness toughness differences are a consequence of the exact balance between the loss in the toughness due to the poor as deposited structure, and the possible gain in toughness due to the high toughness properties of the refined region.

These results therefore indicate that through thickness toughness variation can occur, the magnitude of this effect being determined by the precise welding conditions.

## CONCLUSIONS

1. The weld metal heat input at conventionally calculated values does not define a precise weld metal cooling cycle.

2. The weld metal cooling cycle was found to be a function of the following factors :-

   (a) Weld bead volume

   (b) Weld bead shape

   (c) Weld bead flux consumption

   (d) The geometry of the "immediately" surrounding plate.

   All these factors are determined by the welding procedure.

3. The thermal analysis results show that during the weld metal cooling two transformations occured. These transformations were identified from metallugraphic examinations as the pro-eutectoid ferrite and acicular ferrite transformations.

   A decrease in the weld metal cooling rate led to a decrease in the transformation temperatures.

4. Generally the welds with a fast cooling cycle also had higher strength values than the welds which had a lower cooling cycle but no correlation was found between the cooling cycles and the reduction of area and hardness values.

5. From a toughness point of view the present results show that a welding parameter which gives a weld metal cooling rate which is "low" in the temperature range of 1400°C - 900°C, to give a "large" columnar grain structure followed by a "fast" cooling rate in the temperature range of 900°C - 500°C, leading to a microstructure with a large volume fraction of acicular ferrite phase, is the most desirable.

6. Through thickness toughness variations can occur. These toughness variations were attributed to the considerably different microstructural features between the sub-surface and the root beads. The sub-surface showed a larger prior austenite columnar grain size and a higher volume fraction of acicular ferrite than the equivalent root bead. Furthermore, the sub-surface Charpy specimens were only formed by as deposited weld metal while the root Charpy specimens were formed by as deposited and refined weld metal.

   These differences in the microstructural features can be explained in terms of differences in weld metal cooling cycles between the sub-surface and the root weld bead, caused by differences in the weld metal bead shape, the relationship between the weld bead size and the "immediately" surrounding plate geometry and the post-solidification heat cycle caused by the subsequent weld runs.

   The magnitude of the through thickness toughness variation is therefore determined by the precise welding condition and procedure.

REFERENCES


1. D.R. Milner & R.L. Apps — Introduction to Welding and Brazing. Pergamon Press.

2. D.J. Widgery — Microstructures in Steel Weld Metals. The Welding Institute Research Bulletin, October 1975.

3. F.A. Calvo, K.P. Bentley, R.G. Barker — Studies of the Welding Metallurgy of Steels. British Welding Research Association, Abington, 1963.

4. W.F. Savage, C.D. Lundin, A.H. Aronson — Weld Metal Solidification Mechanisms. Welding Research Supplement, April, 1965. 175-S.

5. W.F. Savage, A.H. Aronson — Preferred Orientation in the Weld Fusion Zone. Welding Research Supplement, February, 1966. 85-S.

6. J.H. Rogerson, J.C. Borland — Effects of the Shape of Intergranular Liquid on the Hot Cracking of Welds and Castings. Transactions of The Metallugical Society of A.I.M.E., Feb. 1963.

7. J.G. Garland — The Control of Weld Pool Solidification Ph.D. Thesis, University of Cambridge, 1972.

8. D.J. Widgery — De-oxidation Practice and the Toughness of Mild Steel Weld Metals. Ph.D. Thesis. Sidney Sussex College, Cambridge, 1974.

9. G. Bernard, B. Chevet — Aspects Metallurgique du Metal Fondu en Soudage Soux Flux. Soudage et Techniques Connexes. Jan, Feb. 1976.

10. G. Almquist, S. Palgary, C.H. Rosendahl, G. Valland. — Some Basic Factors Controlling the Properties of Weld Metal. Paper 16. International Conference in Welding Research Related to Power Plants. Southampton University, Nov. 1972.

11. B. Hemsworth, T. Boniszewski, N.F. Eaton. — Classification and Definition of High Temperature Welding Crack in Alloys. Metal Construction & British Welding Journal, February 1969.

12. J.C. Borland — Suggested Explanation of Hot Cracking in Mild and Low Alloy Steel Welds. British Welding Research Association Report, 1961.

13. L.G. Taylor, R.A. Farrar — Metallurgical Aspects of the Mechanical Properties of Submerged Arc Weld Metal Welding and Metal Fabrication. May 1975.

14. S.S. Tuliani, T. Boniszewski, N.F. Eaton — Carbonate Fluxes for Submerged Arc Welding in Mild Steel. Welding and Metal Fabrication, July, 1972.

15. R.E. Dolby — The Weldability of Low Carbon Structural Steels. Low Carbon Structural Steels for The Eighties, March 1977.

16. A.H. Cottrel — An Introduction to Metallurgy, Arnold.

17. R.E. Smallman — Morden Physical Metallurgy, Butterworth.

18. R.C. Cochrane — Weld Metal Microstructures and Terminology. Welding Institute Conference, October, 1977.

19. J.G. Garland, P.R. Kirkwood — Towards Improved Submerged Arc Weld Metal. Metal Construction, May 1975.

20. F.B. Pickering — The Structure and Properties of Bainite in Steels. Climax Molybdenum.

21. S.S. Tuliani, T. Boniszewski, N.F. Eaton — Notch toughness of Commerical Submerged Arc Weld Metal. Welding and Metal Fabrication, August, 1969.

22. R.E. Reed-Hill — Physical Metallurgy Principles. Van Nostrand Reinhold Comp.

23. D.J. Widgery — The influence of Microstructures on Fracture Initiation in Mild Steel Weld Metals. Welding Institute Report.

24. S.S. Tuliani — The Role of Manganese in Steel Submerged Arc Weld Metal. Paper 17 International Conference in Welding Research Related to Power Plants. Southampton University, November 1972.

25. R.A. Farrar, S.S. Tuliani, S.R. Norman — Relationship between Fracture Toughness and Microstructure of Mild Steel Submerged Arc Welding. Welding and Metal Fabrication, 1974.

26. G.E. Dieter — Mechanical Metallurgy, McGraw-Hill.

27. V. Biss, R.L. Cryderman — Martensite and Retained Austenite in Hot-Rolled Low-Carbon Bainitic Steels. Metallurgical Transactions, Vol. 2. August 1971. 2267.

28. J.M. Wheatley, R.G. Baker — Mechanical Properties of a Mild Steel Weld Deposit by the Metal Arc Process. British Welding Research Association Report.

29. W.E. Duckworth — Metallurgy of Structural Steels - present and future possibilities. Strong Tough Structural Steels Proceedings APRIC 1967 Iron and Steel Institute.

30. K.J. Irvine, F.B. Pickering — Relationship between Microstructure and Mechanical Properties of Mild Steel Weld Deposits. British Welding Journal, 1960.

31. J.I.J. Fick, J.H. Rogerson — The Effect of Post-Solidification Metallurgical Reactions on the Toughness of Weldments in Thick Structural Steel Plate. Low Carbon Structural Steels for the Eighties, March 1977.

32. P. Colvin & A.F. Bush — Multipass Submerged Arc Welding of High Yield Strength Notch Ductile Ferritic Steels. Iron and Steel, Dec. 1969.

33. P. Colvin — Weld Metal Toughness Basic Fluxes Development - Applications. Welding and Metal Fabrication, November, 1974.

34. N.E. Hanmerz, J.F. Lowery — Influence of Micro Slag Distribution on MIG-MAG Weld Metal Impact Properties. Metal Construction, Jan. 1975.

35. D.J. Widgery — Measuring Inclusions in Weld Metal. The Welding Institute Research Bulletin, Jan. 1975.

36. S.S. Tuliani — Carbonate fluxes for Submerged Arc Welding of Mild Steel. Ph.D. Thesis, Southampton University, May 1973.

37. S. Nicholson, P.F. Rogers — Controlling Weld Metal Toughness in Manual Metal Arc Welds. Welding in Offshore Structures. International Conference Feb. 1974.

38. S.S. Tuliani, R.A. Farrar — The Effects of Silicon in Submerged Arc Weld Metals at Low Concentrations. Welding & Metal Fabrication, September 1975.

39. J. Malcolm Gray, W.G. Wilson — Effect of Processing Variables on the Properties of a Low Carbon Columbium Steel Proposed for Artic Pipelines. Molybdenum Corporation of America, Pittsburg, Pensilvania.

40. T. Boniszewki, S.E. LeDieu, H.F. Tremiett — Sulphur Behaviour during Deposition of Mild Steel Weld Metals British Welding Journal, Sept. 1966.

41. T. Boniszewki — Titanium in Steel Wire for $CO_2$ Welding. Metal Construction and British Welding Journal, May, 1969.

42. K. Masubuchi, R.E. Monroe, D.C. Martin — Interpretive report on Weld Metal Toughness. Project S-R 170-SSC 169.

43. D.J. Kotecki, R.A. Moll — A Toughness Study of Steel Weld Metal from Self-Shielded Flux Covered Electrode. Welding Research Supplement April 1970, March 1972.

44. P. Colvin, A.F. Bush — Notch Toughness Properties of Single Pass Submerged Arc Welding Quality Steels. Welding and Metal Fabrication, February 1971.

45. K.E. Dorschu, R.D. Stout — Some Factors Affecting The Notch Toughness of Steel Weld Metal. Welding Journal, 1961.

46. H. Sakaki — Effect of Alloying Elements on Notch Toughness of Basic Weld Metals. Report 1 - 7 A Welding Institute Translation.

47. J.M. Sawhill, M.P. Bussel — Welding of Acicular Ferrite Mn-Mo Nb Steels. Low Carbon Structural Steels for The Eighties, May 1977.

48. A.M. Sage, D.W. Eans — Vanadium Structural Steels High Weld Steel and Vanadium Corp. Ltd., London.

49. N.E. Hannerz, B.M. Jonsson-Holmquist — Vanadium in Mild Steel Weld Metal. Metal Construction and British Welding Journal, February 1974.

50. P.R. Kirwood, J.G. Garland — The Influence of Vanadium on Submerged Arc Weld Metal Toughness. Welding Metal Fabrication, January, February 1977, March 1977.

51. H.I. Kaplan, D.C. Hill — Thermodynamic of Air Operation Flux Cored Electrodes and an Analysis of Weld Toughness. Welding Research Supplement 13-S, January 1976.

52. J.D. Baird — Strain Ageing of Steels. Aceytical Review Iron and Steel May 1963.

53. N. Jemkins, SM. Stevens. — Nitrogen in Ferrous Welding. The Welding Institute Research Bulletin, January 1977.

54. P.R. Kirkwood — New Observations on Microstructural and Toughness Control in Low Carbon Weld Metal. Low Carbon Structural Steels from The Eighties, March 1977.

55. J. Gurland, J. Plateaux — Mechanism of Ductile Rupture in Metal Containing Inclusions. Transactions of A.S.M. Volume 5, 1963.

56. R.A. Farrar — The Role of Inclusions in the Ductile Fracture of Weld Metals. Welding and Metal Fabrication, October 1976.

57. M.G. Dawes — Fracture Initiation in Weld Metals. Welding and Metal Fabrication, March 1972.

58. J.B. Bair — Strain Ageing of Steel - A Critical Review, Iron and Steel, May 1963.

59. F.M. Burdekin, M.G. Dawes, C.L. Archer, F. Bonomo, G.R. Egen. — Selection of Weldments to Avoid Fracture Initiation. British Welding Journal, December 1968.

60. R.C. Cochrane, P. Terry, J.G. Garland — Root-run Toughness in Multi-pass Manual Metal-Arc Welds. Welding and Metal Fabrication, May 1976.

61. J.L. Robinson — The Problem of Weld Root Areas. Welding Institute Conference, October 1977, Paper 4.

62. J.I.J. Fick, J.H. Rogerson — Root Toughness of Multipass Submerged Arc Welds in Microalloyed Steels. Department of Materials Report, Cranfield Institute of Technology.

63. R.C. Cochrane — Private Communication.

64. D.J. Widgery — Factors Controlling Fracture by Microvoid Coalescence in As Deposited Weld Metal. Welding Institute Conference, Paper 3.

65. D. Rosenthal, R. Schmerber — Thermal Study of Arc Welding Experimental Verification of Theoretical Formulas. Welding Research Supplement, April 1938.

66. D. Rosenthal — Mathematical Theory of Heat Distribution During Welding and Cutting. Welding Research Supplement, May 1941.

67. E.G. Signes — A Simplified Method for Calculating Cooling Rates in Mild and Low Alloy Steel Weld Metals. Welding Research Supplement, October 1972.

68. P. Jhaveri, W.G. Moffatt, C.M. Adams — The Effect of Plate Thickness in Radiation on Heat Flow in Welding and Cutting. Welding Research Supplement, January 1962.

69. K.E. Dorschu — Control of Coding Rates in Steel Weld Metal. Welding Research Supplement, February, 1968.

70. M. Clyde, J.R. Adams — Cooling Rates and Peak Temperatures in Fusion Welding. Welding Research Supplement, May 1958.

71. D.E. Schillinger, I.G. Betz, H. Markus — Simplified Determination of Thermal Experience in Fusion Welding. Welding Research Supplement, September 1976.

72. A.P. Bennet — Effect of Heat Input in Automatic Welding. Welding and Metal Fabrication, Sept. 1969.

73. A. Clark, M.J. George, P.R. Kirwood — Development of automatic welding procedures to meet toughness requirements for Offshore Structurs. Welding Offshore Structures Information Conference, Feb. 1974.

74. J.G. Garland, P.R. Kirkwood — The Notch Toughness of Submerged Arc Weld Metal in Micro-Alloyed Structural Steels. IIW DOC IX 892-74.

75. J.E.B. Wilson, R.S. Brown, R.L. Apps — Influence of the Number of Runs on the Properties of Submerged Arc Welds. Welding and Metal Fabrication, December 1965.

76. B.L. Shultz, C.E. Jackson — Influence of Weld Bead Area on Weld Metal Mechanical Properties. Welding Research Supplement, January 1973.

77. S.S. Strunck, R.D. Stout — Heat Treatment Effects in Multipass Weldments of a High Strength Steel. Welding Research Supplement, October 1972.

78. H. Granjon, R. Gaillard — Possibilities offertes par l'analyse thermique "in situ" pour l'etude des transformations de l'acier au cours du soudage. Hemoire Scientifique Revue Metallorgique. LXIV N4 1967.

79. H. Granjon, S. Debiez, R. Gaillard — Resultats obtenue et nouvelles possibilites offertes par la methode des implants pour l'etude de la soudabilite des acier. Soudage et techniques connexes No. 3/4 Mars - Avril, 1968. PP. 109 -

80. G.G. Saunders — Effect of Major Alloying Elements on the Toughness of High Strength Weld Metal. Welding Research International Volume 7, 1977, Number 2.

81. P. Colvin — Weld Metal Toughness Basic Fluxes Development Applications. Welding and Metal Fabrication, November 1974.

82. R.L. Cryderman, A.P. Coldren, Y.E. Smith, J.H. Mihelich — The Development of a High Strength Hot-Rolled Mn-Mo-Cb Steel. Climax Molybdenum Company.

83. F.B. Pickering — The Basic of Quantitative Metallurgy Institute of Metallurgists Technicians 1976.

84. R. Lignon, H. Cuyot — Procede d'analyse thermique des systemes solides en evolution rapide. Memoire Scientifique Revue Metallurgique LVIII No. 8, 1961.

85. M.K.H. Shorshorov, E.A. Demin, V.V. Belov — Phase Transformations during Continuous Cooling of Low Alloy Steels from Sub-solidus Temperatures. Metals Science Heat Treatment, 1973, page 598.

86. R.E. Dolby — The Haz Toughness of Electroslag Welds in C-Mn Steels. Welding Research International, Volume 7, 1977, number 4.

87. A.G. Cilover, J.T.McGrath, M.J. Tinkler, G.C.Weatherby — The Influence of Cooling Rate and Composition on the Weld Metal Microstructure in a C.Mn and H.S.L.A. Steel. Welding Research Supplement 267-S, September, 1977.

88. D.V. Dorling, P.E.L.B. Rodrigues, J.H. Rogerson — A Comparison of the Toughness of Self-shielded Arc and Submerged Arc Weld Metals in C.Mn - Nb Steels. Weld and Metal Fabrication, July/August and September, 1976.

89. A.M. Sage — Properties and Applications of present day products. Low Carbon Structural Steels for the Eighties, Conference, March 1977.

90. N.J. Petch — The Cleavage Strength of Poly Crystals. Journal of Iron Steel Institute (London) Volume 173, 1953.

91. M.G. Hipkins, F.S. Dickinson — Influence of Notch Orientation and Position on the Notch Ductility of Automatic and Manual Welding in Mild Steel. Welding and Metal Fabrication, May 1965.

92. T.I. Masters, S. Stein — Effect of an Axial Cavity on the Temperature History of a Surface Heat Slab. The Review of Scientific Instruments, Volume 27, Number 12, December 1956.

93. B.S. Singh, A. Dybbs — Error in Temperature Measurements due to Conduction along the Sensor Leads. Journal of Heat Transfer, Volume 98, 491, 1976.

ACKNOWLEDGEMENTS

The author wishes to thank Mr. J.H. Rogerson for his supervision during the preparation of this thesis, and Mr. B. Moffit for the design and construction of the electronic measuring equipment used in this work.

Messrs. K. Nelson, S. Batchelor, R. Hardwick, P. Cook and C. Matthews are acknowledged for their assistance during the experimental work.

Thanks are also due to the Library Staff.

Special thanks is due to Mrs. Prudden for her organisation of the typing of this thesis.